

# **Role of epigenetic biomarkers and IDH1 mutation in anticancer drug resistance of high-grade gliomas**

## **Dissertation**

Zur Erlangung des Grades

Doktor der Naturwissenschaften

am Fachbereich Biologie

der Johannes Gutenberg-Universität in Mainz

vorgelegt von

Olivier Switzeny

geb. am 24.12.1981 in Bregenz / Österreich

Mainz, August 2017

**Institut für Toxikologie**

**Johannes Gutenberg-Universität Mainz**

**Dekan:**

**1. Berichterstatter:**

**2. Berichterstatter:**

**Tag der mündlichen Prüfung: 05.12.2017**

Die vorliegende Arbeit wurde in der Zeit von Januar 2013 bis August 2017 am Institut für Toxikologie der Universitätsmedizin Mainz angefertigt und wird am Fachbereich Biologie der Johannes Gutenberg Universität (D77) eingereicht.



## **Erklärung**

Ich erkläre, dass ich die vorgelegte Doktorarbeit selbständig, ohne unerlaubte fremde Hilfe und nur mit den Hilfen angefertigt habe, die ich in der Doktorarbeit angegeben habe. Alle Textstellen, die wörtlich oder sinngemäß aus veröffentlichten oder nicht veröffentlichten Schriften entnommen sind, und alle Angaben, die auf mündlichen Auskünften beruhen, sind als solche kenntlich gemacht. Bei den von mir durchgeführten Untersuchungen habe ich die Grundsätze guter wissenschaftlicher Praxis, wie sie in der Satzung der Johannes-Gutenberg-Universität Mainz zur Sicherung guter wissenschaftlicher Praxis niedergelegt sind, eingehalten.

---

Olivier Switzeny



# Table of contents

<b>1. Introduction .....</b>	<b>5</b>
1.1. Epigenetic modifications .....	7
1.1.1. DNA methylation.....	7
1.1.2. Histone modification.....	10
1.1.3. Other epigenetic mechanisms .....	11
1.2. High-grade astrocytoma.....	13
1.2.1. Isocitrate dehydrogenase 1 and Isocitrate dehydrogenase 2 mutations....	15
1.2.2. Alkylating agents in malignant glioma therapy .....	20
1.2.3. Ionizing radiation in malignant glioma therapy.....	22
1.2.4. Artesunate in malignant glioma therapy .....	22
1.3. DNA repair pathways and their epigenetic regulation .....	27
1.3.1. Direct Reversal of DNA Alkylation Damage .....	27
1.3.1.1. <i>O</i> <sup>6</sup> -alkylguanine-DNA alkyltransferase – MGMT .....	28
1.3.1.2. Oxidative Dealkylation by AlkB .....	29
1.3.2. Base excision repair – BER .....	32
1.3.3. DNA mismatch repair – MMR.....	33
1.3.4. DNA double-strand break repair.....	35
1.3.4.1. Non-homologous end joining – NHEJ.....	35
1.3.4.2. Homologous recombination – HR.....	36
1.4. Aim of the work.....	39
<b>2. Material and Methods.....</b>	<b>41</b>
2.1. Chemicals and Consumables.....	41
2.2. Wet laboratory equipment .....	41
2.3. Software .....	42

2.4.	Solutions.....	43
2.5.	Cell culture .....	44
2.6.	Patients and treatments.....	48
2.7.	Methylation quantification assays .....	49
2.7.1.	DNA extraction.....	49
2.7.2.	DNA standards .....	49
2.7.3.	Bisulfite treatment.....	50
2.7.4.	Analysis of the MGMT promoter methylation by MSP .....	50
2.7.5.	Analysis of the MGMT promoter methylation by high-resolution melt (HRM) curve analysis.....	50
2.7.6.	Analysis of the MGMT promoter methylation by pyrosequencing.....	51
2.7.7.	Analysis of the <i>ATM</i> , <i>BRCA1</i> , <i>BRCA2</i> , <i>EGFR</i> , <i>LINE1</i> , <i>MBD4</i> , <i>MLH1</i> , and <i>RAD51c</i> promoter methylation by high-resolution melt (HRM) curve analysis .....	53
2.8.	SNP detection by pyrosequencing .....	53
2.8.1.	<i>IDH1</i> R132H mutation detection by pyrosequencing.....	53
2.8.2.	<i>BRAF</i> V600E mutation detection by pyrosequencing.....	54
2.9.	Primer sequences.....	54
2.10.	Cell survival assays.....	57
2.10.1.	Evaluation of cell viability using the MTT assay.....	57
2.10.2.	Propidium iodide staining .....	58
2.10.3.	Annexin V-FITC/Propidium iodide double-staining.....	59
2.10.4.	iCELLigence real-time cell analysis system.....	59
2.11.	Protein analysis.....	60
2.11.1.	Total protein extraction by sonication .....	60
2.11.1.	Protein extraction using RIPA buffer.....	60
2.11.2.	Protein extraction using cracking buffer .....	60



2.11.3.	Protein concentration determination .....	61
2.11.4.	Semi-quantitative measurement of protein concentration .....	61
2.11.5.	Sodium dodecyl sulfate polyacrylamide gel electrophoresis.....	61
2.11.6.	Immunoblotting .....	62
2.11.7.	Antibodies .....	63
2.11.8.	Immunofluorescence .....	63
2.11.9.	MGMT enzyme activity assay.....	64
2.12.	DNA adduct measurements .....	65
2.12.1.	South-western slot-blot analysis.....	65
2.12.2.	Fpg-modified alkaline comet assay.....	65
<b>3.</b>	<b>Results .....</b>	<b>67</b>
3.1.	Epigenetic regulation of DNA repair genes.....	67
3.1.1.	DNA methylation of the <i>MGMT</i> promoter .....	67
3.1.1.1.	Cell line based studies .....	67
3.1.1.2.	<i>MGMT</i> promoter methylation in high-grade glioma samples.....	74
3.1.1.2.1.	Univariate Kaplan-Meier survival analysis.....	80
3.1.1.2.2.	Accuracy of outcome prediction evaluated by receiver-operating characteristics (ROC) curve .....	82
3.1.1.2.3.	Multivariate Cox proportional hazards model .....	83
3.1.2.	DNA methylation of the <i>MLH1</i> promoter .....	85
3.1.2.1.	Cell line based studies .....	85
3.1.2.1.	<i>MLH1</i> promoter methylation in high-grade glioma samples.....	86
3.1.3.	DNA methylation of the <i>RAD51c</i> promoter.....	88
3.1.3.1.	Cell line based studies .....	88
3.1.3.1.	<i>Rad51c</i> promoter methylation in high-grade glioma samples .....	89
3.1.4.	DNA methylation of the <i>ATM</i> , <i>BRCA1</i> , <i>BRCA2</i> , and <i>MBD4</i> promoter .....	89

## Introduction

3.1.5.	DNA methylation of the <i>LINE1</i> promoter .....	90
3.1.6.	<i>BRAFV600E</i> mutational status in HGA patients .....	90
3.1.7.	Association between <i>IDH1R132H</i> mutational status and <i>MGMT</i> promoter methylation in high-grade astrocytoma (HGA) patients .....	92
3.2.	Metabolic regulation of DNA repair enzymes.....	95
3.2.1.	Effect of DNA alkylation in LN229 IDH1wt and mt cells .....	95
3.2.2.	Effect of DNA alkylation in LN319 IDH1wt and mt cells .....	103
3.2.3.	Cytotoxic effect of artesunate in LN319 IDH1wt and mt cells .....	114
3.2.4.	Influence of 2-HG on ART induced cell death .....	118
3.2.5.	Effect of DNA alkylation and ART in ALKBH2 knock-out cells.....	119
3.2.1.	Exogenous $\alpha$ -KG rescues higher ART induced toxicity in IDH1mt cells .....	129
<b>4.</b>	<b>Discussion.....</b>	<b>131</b>
4.1.	Improved <i>MGMT</i> promoter methylation quantification by HRM .....	132
4.2.	Promoter methylation of other DNA repair genes .....	134
4.3.	IDH1 mutation related 2-HG drives cells ART sensitive due to ALKBH2 impairment 137	
<b>5.</b>	<b>References.....</b>	<b>145</b>
<b>6.</b>	<b>Supplementary information .....</b>	<b>167</b>
<b>7.</b>	<b>Abbreviations .....</b>	<b>169</b>
<b>8.</b>	<b>Summary .....</b>	<b>173</b>
<b>9.</b>	<b>Curriculum Vitae .....</b>	<b>175</b>

## 1. Introduction

Both genetic and epigenetic changes contribute to the development of human cancer. Before the concept of epigenetic regulation has been stated, it was emphasized that gene regulation in cancer cells is the key driver for uncontrolled growth, invasiveness, and metastasis. The term epigenetics was first introduced by the British embryologist and geneticist Conrad Hal Waddington in 1940 and meant the “causal analysis of development” (Slack 2002). In 1975, two key papers independently suggested that methylation of cytosine in the context of CpG dinucleotides could serve as an epigenetic mark in vertebrates (Holliday and Pugh 1975; Riggs 1975). These papers proposed that DNA could be methylated *de novo*, that this methylation marks could be inherited through somatic cell division, and that this methyl groups could be interpreted by DNA binding enzymes to silence genes. In 1979 a study first revealed a connection between DNA methylation and gene expression (Taylor and Jones 1979). Today, epigenetics refers to the study of heritable changes in gene expression without a change in gene sequence.

The discovery of mutations in oncogenes that lead to cellular transformation (Shih and Weinberg 1982) accentuated the genetic reason for the key drivers of cancer cells. The invention of the polymerase chain reaction (PCR) method in 1983 was the basis for the rapid genetic testing of tumor DNA and led to the finding of several single nucleotide polymorphisms (SNPs) in proto-oncogenes like *RAS* (Orita et al. 1989), *APC* (Grodin et al. 1991), *p53* (Gaidano et al. 1991). These SNPs will turn the proto-oncogenes into oncogenes, driving the hallmarks of cancer. The phenotypic outcomes of genetic changes in cancer have led to a general classification of cancer genes as either tumor suppressors, which are involved in inhibition of cell growth and survival, or oncogenes which promote these effects (Hanahan and Weinberg 2000). The findings appeared to resolve a long debate issue – that cancer was predominantly a disease of genetics, thus downgrading the importance of epigenetics to a minor and/or non-existent role. With the completion of the Human Genome Project (HGP) in the early 2000s, the capacity to understand genetic variability has expanded exponentially and even more attention was attributed to the genetic causes of diseases. A direct consequence of the HGP was the genome wide association studies or GWAS. GWAS is a genome-wide set of genetic variants, or single-nucleotide

## Introduction

polymorphisms (SNPs), in different individuals to see if any variant or SNP is associated with a trait, like a major human disease (Chang et al. 2014). However, as it often happens in science when new methods are available, new data have changed this view. Cancer appeared to be a process that is fueled both by mutations in DNA and by epigenetic mechanisms. More surprisingly, these processes can interact and affect each other (Baylin and Herman 2000).

## 1.1. Epigenetic modifications

As every cell in a multicellular organism harbors the same DNA sequence, tissue specific regulation of genes is crucial. To ensure this process, cells have evolved pathways to modify the activation of certain genes, but not the genetic code sequence of DNA. Three prominent epigenetic mechanisms are described for cancers.

### 1.1.1. DNA methylation

Mammalian cells possess the capacity to epigenetically modify their genomes via the covalent addition of a methyl group to the 5-position of the cytosine ring within the context of the CpG dinucleotide. DNA methyltransferases (DNMTs) catalyze this reaction by the use of S-adenosyl methionine (SAM) as the methyl donor (Bird 1992). To establish *de novo* 5-methylcytosine (5mC), DNMT3A and DNMT3B are needed. These CpG methylation marks are set asymmetrically, meaning that just one DNA strand is methylated at a CpG motif (Lin et al. 2002). DNMT1 shows a strong preference for this asymmetrical (hemi-methylated) CpG methylation and methylates the CpG on the opposing strand (Okano et al. 1998). Symmetric CpG methylation is crucial for the somatic inheritance of DNA methylation. During S-phase, both parental DNA strands containing the epigenetic information are replicated, and DNMT1 establishes replication-coupled DNA methylation on the newly synthesized daughter strand. By this process, DNA methylation information is inherited to both daughter cells (Holliday and Pugh 1975).

CpG-rich regions are known as CpG islands (CGIs), which are mostly found adjacent to genes. The remaining genome is depleted for CpGs. The frequency of CpG dinucleotides in the human genome is about 1 %, less than one-quarter of the expected frequency. This deficiency was proposed to be due to an increased vulnerability of 5-methylcytosines (5mC) to spontaneously deaminate to thymine (T) leading to CG->TA transitions. By this process, CpGs got mostly eliminated from the genome during evolution (Scarano et al. 1967). More than thirty years later, it could be verified, that deamination of 5mC to T at CpG sites is probably the most important cause of spontaneous point mutations in humans, accounting for more than 20 % of all base substitutions that give rise to genetic diseases (Krawczak et al. 1998; Millar et al. 2002). In humans, over 70 % of all gene pro-

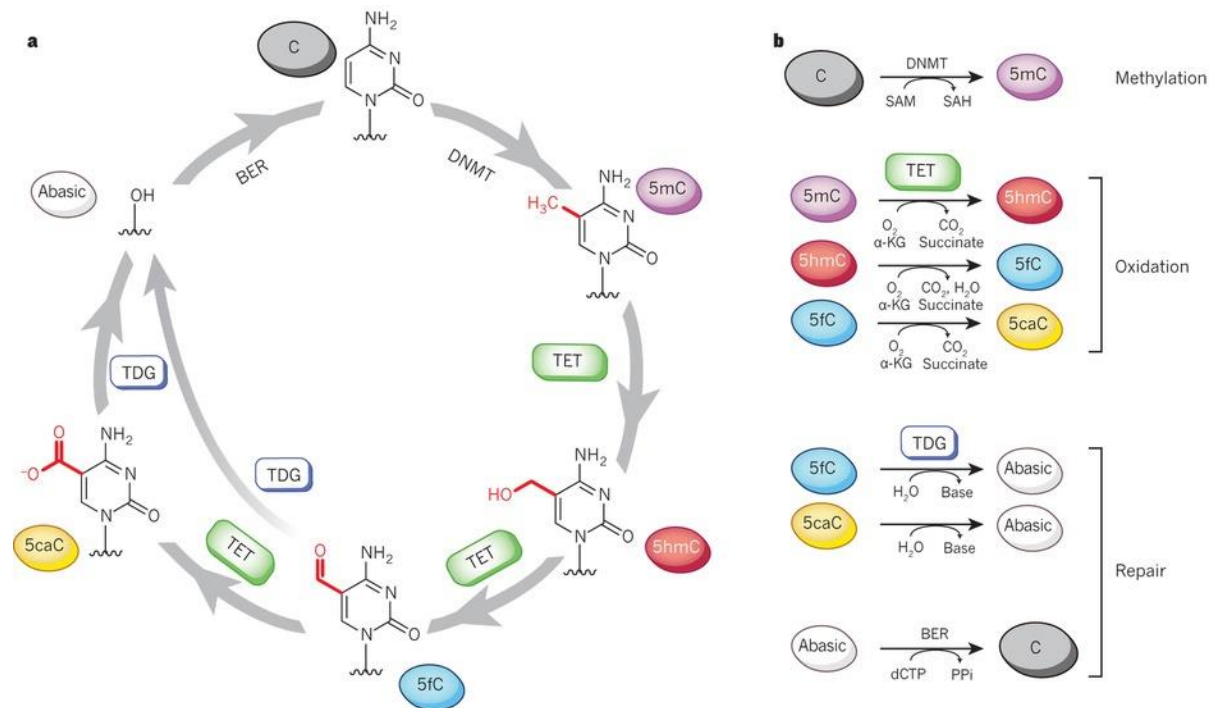
## Introduction

motors contain a CpG island (Deaton and Bird 2011). Promoters are located near the transcription start site of a gene and can range from less than 100 bp to several kb of length. A promoter consists of a certain consensus sequence that enables binding of transcription factors which then initiate or repress following gene expression. The transcriptional repressor CTCF, for example, binds to the 5'-CCGCGNGGNGGCAG-3' consensus sequence and represses transcription upon binding. CTCF's binding is abrogated by CpG methylation of the DNA it binds to and enables gene transcription (Bell and Felsenfeld 2000; Whitfield et al. 2012).

Although the enzymes that catalyze DNA methylation have been characterized, enzymes responsible for CpG demethylation have been elusive until 2007 (Barreto et al. 2007; Tahiliani et al. 2009; Ito et al. 2010). Before that time, passive CpG demethylation by downregulation of DNMT1 during cell division was believed to be the primary pathway of DNA demethylation (Reu et al. 2006). In animals, three mechanisms of active DNA demethylation have been proposed: DNA demethylation by i.) nucleotide excision repair (NER) (Barreto et al. 2007), ii.) base-excision repair (BER) upon 5mC deamination by Activation Induced Deaminase (AID) (Cortellino et al. 2011), and iii.) 5mC oxidation through the Ten-Eleven Translocation (TET) family enzymes followed by BER (Tahiliani et al. 2009; Ito et al. 2010; Li et al. 2015). The Growth Arrest and DNA-damage-inducible protein GADD45 alpha (GADD45a) was found to induce DNA demethylation together with enzymes belonging to DNA repair pathways, despite not having any enzymatic activity by itself (Schäfer et al. 2013). It was later found that GADD45a physically interacts and functionally cooperates with TET1 for 5mC processing (Kienhofer et al. 2015; Li et al. 2015).

Although 5hmC had previously been observed in mammalian genomes, these earlier observations did not receive attention until the discovery of TET enzymes. The TET family members (TET1, 2 and 3) each harbor a core catalytic domain, with a double-stranded  $\beta$ -helix fold that contains the crucial metal-binding residues found in the family of Fe(II)/ $\alpha$ -KG- dependent oxygenases (Loenarz and Schofield 2011). TET uses molecular oxygen to catalyze oxidative decarboxylation of  $\alpha$ -KG, thereby generating a reactive high-valent enzyme-bound Fe(IV)-oxo intermediate that converts 5mC to 5-hydroxymethylcytosine (5hmC). This pathway holds true for the even further oxidized 5-substituents, notably 5-formylcytosine (5fC) and 5-carboxycytosine (5caC) (**Figure 1**) (Iyer et al. 2009; Tahiliani et

al. 2009; Kohli and Zhang 2013). TET1 and TET3 contain chromatin-associated CXXC domain that is known to bind CpG sequences. Whereas the ancestral CXXC domain of TET2 is now encoded by a distinct gene, *IDAX* (*CXXC-type zinc finger protein 4*), so that these two proteins have to physically interact to oxidize 5- substituents (Ko et al. 2013).



**Figure 1: Pathway of TET regulated 5mC dynamics.** a) 5mC bases are caused by DNA methyltransferases (DNMTs). 5mC can be further oxidized by TET enzymes to 5hmC, 5fC, and 5caC. The latter are substrates for the thymine DNA glycosylase (TDG) leading to an abasic site, which is repaired by base excision repair (BER), resulting in an unmodified C. b) The individual reactions in the pathway are depicted.  $\alpha$ -KG,  $\alpha$ -ketoglutarate; SAM, S-adenosylmethionine; SAH, S-adenosylhomocysteine. Adapted and reprinted from Kohli and Zhang 2013 with permission.

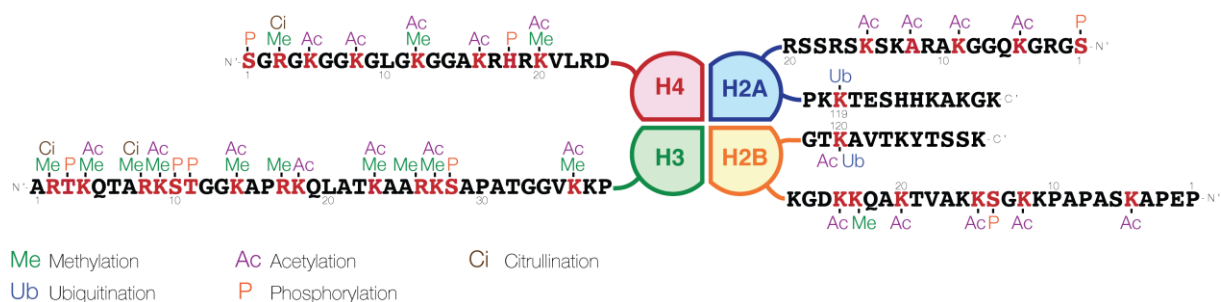
The epigenetic code is inherited through mitotic rounds of cell division, but at certain times in development (embryogenesis and gametogenesis) the epigenetic state is erased, changed and re-established (Monk et al. 1987). However, transgenerational inheritance of epigenetic marks has been observed in few endogenous gene loci including the dominant *agouti viable yellow* (*A<sup>vy</sup>*) and *axin-fused* alleles (Rakyan et al. 2003; Waterland and Jirtle 2003). The well-known “agouti mouse study” was the first to find a clear mechanism

## Introduction

for the effect of maternal nutrition on disease development in mammals without mutating the offspring's genes. All mice had a mutation in the *Agouti* gene, making them obese and yellow. When fed with methyl-donors like vitamin B12, folic acid, choline, and betaine before, during, and after pregnancy, the animals gave birth to thin, brown pups. Control animals' offspring were fat and yellow. The nutrients had silenced the mutated *Agouti* gene by increased promoter methylation, and this methylation status was inherited to the next generation (Waterland and Jirtle 2003).

### 1.1.2. Histone modification

Histones are alkaline proteins found in eukaryotic cell nuclei that package and order the DNA into structural units called nucleosomes. DNA is wrapped 1.65 times (147 bp) around a histone octamer that comprises two copies of each of the canonical histones: H3, H4, H2A and H2B (Kornberg 1974). The histone proteins are subject to numerous covalent modifications (**Figure 2**) that regulate biological processes that are associated with chromatin, such as gene expression.



**Figure 2: Possible histone modification patterns** in normal and cancer cells. Their protruding N-terminal tails, but also their C-terminal regions, amino acids are targets of post-translational modifications. In the right combination and translated by the right effectors, these modifications contribute to the establishing of global and local condensed (euchromatin) or decondensed (heterochromatin) chromatin states that can determine gene expression. (Image by Mariuswalter [CC BY-SA 4.0], via Wikimedia Commons).

The enzymes that add and remove modifications are, respectively, histone acetyltransferases (HATs) and deacetylases (HDACs and sirtuins), methyltransferases (HMTs) and demethylases (HDMs) (**Table 1**), phosphokinases and phosphatases, ubiquitin ligases and



deubiquitinases, and SUMO ligases and proteases (Kouzarides 2007). Various combinations of modification can lead to a more “open” (heterochromatin) or more “closed” (euchromatin) state of chromatin structure and therefore to the activation or repression of gene expression (Li et al. 2007).

**Table 1: Lysine (K) residues within the histone tails** get modified by methylation (me), demethylation (me2), trimethylation (me3), and acetylation (ac). This “code” determines to a large part gene activation or repression.

Gene activation		Gene repression	
Modification	Position	Modification	Position
me3	H3K4	me2 or me3	H3K9
	H3K36	me3	H3K27
	H3K79		
me	H4K20		
	H2BK5		
ac	H3K9		
	H3K14		

### 1.1.3. Other epigenetic mechanisms

Besides covalent modifications of either DNA or histones, additional epigenetic mechanisms have been described. Non-coding RNA (ncRNA) is a functional RNA that is transcribed from DNA but not translated into proteins. Epigenetic related ncRNAs include microRNA (miRNA), small interfering RNA (siRNA), piwi-interacting RNA (piRNA) (Yin and Lin 2007) and long non-coding RNA (lncRNA). NcRNAs in general function to regulate gene expression at the transcriptional and post-transcriptional level (Bartel 2004). miRNA expression is tissue specific and regulated by DNA methylation (Lujambio et al. 2007). miRNA function via base pairing with complementary sequences within mRNA molecules. As a result, these mRNA transcripts are silenced by either cleavage into two pieces, destabilization by poly (A) tail shortening, or blocking translation in ribosomes (Bartel 2009). lncRNAs are longer than 200 nt and often originate from introns during splicing (Louro et al. 2008)

## Introduction

During a meeting in December 2008, held at the Cold Spring Harbor Laboratory, a precise definition of epigenetics was proposed: “An epigenetic trait is a stably heritable phenotype resulting from changes in a chromosome without alterations in the DNA sequence.” (Berger et al. 2009).

As science moves further, many authors claim to have found new epigenetic gene-regulatory mechanisms. In 2017, the occurrence of 8-oxo-7,8-dihydroguanine (8-oxoG), an oxidative DNA base lesion induced by reactive oxygen species (ROS) was proposed to be “epigenetic”. The removal of 8-oxoG by BER (see 1.3.2) in guanine rich promoters lead to the active transcription of the adjacent genes (Fleming et al. 2017). This base modification is obviously not a heritable phenotype and does not comply with the definition of epigenetics. This is just one example to illustrate how excessive the word “epigenetics” is being used, and that adaption to the definition of epigenetics should be made to account for the newest scientific findings.

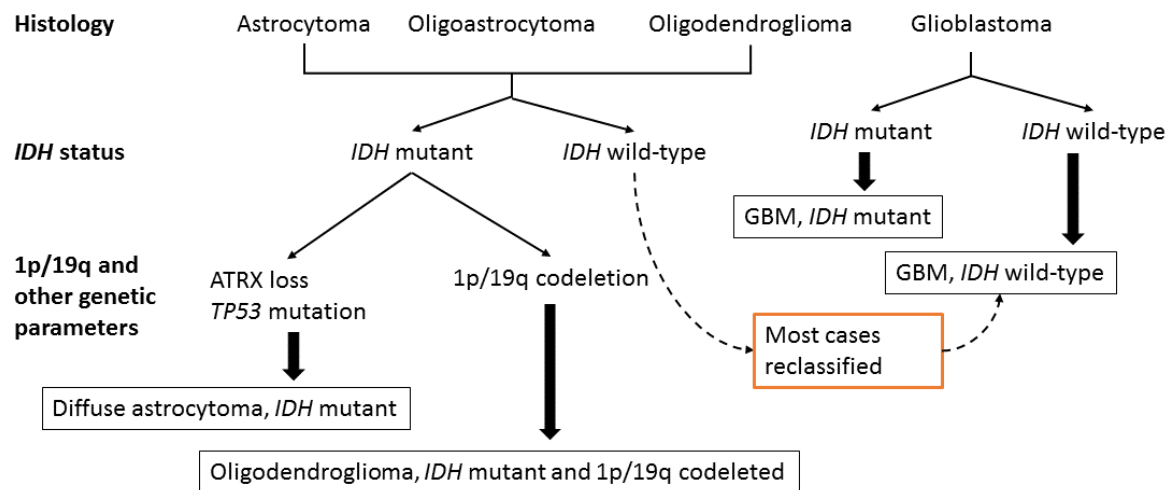
## 1.2. High-grade astrocytoma

High-grade astrocytoma (HGA), the most common subtype of primary brain tumors, are aggressive, highly invasive, and neurologically destructive tumors and considered to be among the deadliest of human cancers. The etiology of these tumors is not understood, although general risk factors as environmental toxins, family history and rare diseases with a higher risk of developing brain cancers (VHL-disease, Li-Fraumeni syndrome) were found (Ohgaki and Kleihues 2009; Watanabe et al. 2009b). HGA can be classified into anaplastic astrocytoma (AA, grade III) and glioblastoma multiforme (GBM, grade IV). For decades the WHO grading and diagnosis system of brain tumors was primarily based on light microscopic features in hematoxylin and eosin-stained sections, immunohistochemical expression of lineage-associated proteins, and ultrastructural characterization (Louis et al. 2007). In 2016, the CNS WHO classification system incorporated molecular parameters into the classification of CNS tumor entities (Louis et al. 2016). Important molecular diagnosis marker are mutations in isocitrate dehydrogenase 1 / 2 (IDH1 / IDH2; see 1.2.1), ATP-dependent helicase ATRX (ATRX), histone H3-K27M, and the 1p/19q chromosomal deletion. IDH mutations were found in around 70 % and 5 % of grade III and grade IV glioma, respectively. AA are now divided into IDH-mutated grade III and IDH-wild-type glioblastoma grade IV (Louis et al. 2016). Therefore, after introducing the new grading system in 2016, the incidence of glioblastoma increased, and anaplastic astrocytoma incidence declined.

The incidence for AA is 0.37 cases per 100,000 men and woman per year in the United states (Ostrom et al. 2013) and account for 8 % of all gliomas in adults. The incidence rate in Europe (0.44 in Austria, 0.60 in the Netherlands e.g.) does not differ much from the US one (Ostrom et al. 2013; Ho et al. 2014). Differences in diagnostic practices and completeness of reporting make all geographic comparisons difficult (Wrensch et al. 2002). AA may further progress to glioblastomas, also referred as secondary glioblastomas, which account for around 9 % of all GBM cases (Ohgaki and Kleihues 2013). The standard treatment for AA remains controversial, but typically includes radiotherapy and chemotherapy (Brandes et al. 2006; Cairncross et al. 2013), similar to the treatment of glioblastoma (Stupp et al. 2005; Pentsova et al. 2016).

## Introduction

Grade III AA that harbor either an *IDH1* or *IDH2* mutation (Louis et al. 2016) are further divided into two groups (see **Figure 3**). The first being tumors with the 1p/19q co-deletion, while the other group is defined by ATRX loss and *TP53* mutations (Louis et al. 2016).



**Figure 3: A simplified algorithm for classification** of grade III and IV based on histological and genetic features. Modified from (Louis et al. 2016).

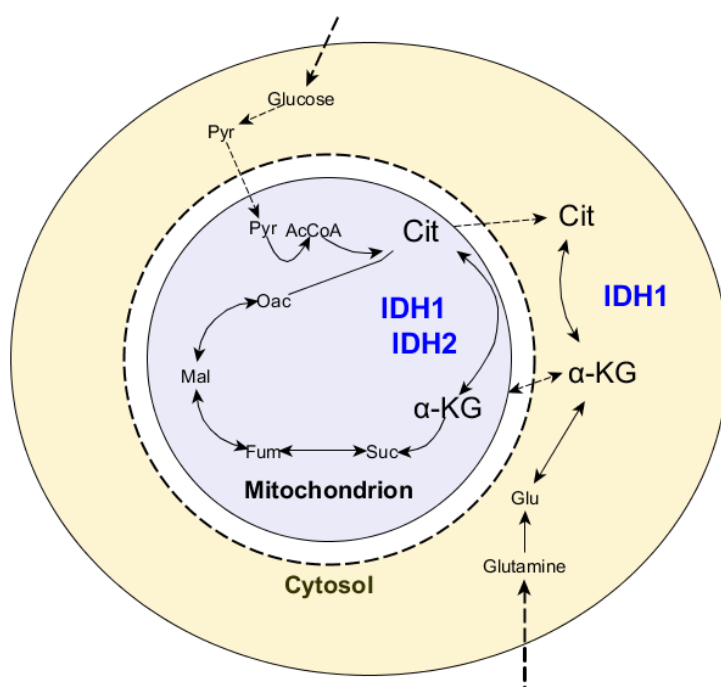
GBM is the most aggressive manifestation with a median survival of 14.6 months and a 2-year survival rate of 26 % (Hegi et al. 2005; Stupp et al. 2005). The incidence for GBM was 3.1 cases per 100,000 men and woman per year in the United states (Ostrom et al. 2013). GBM constitutes the major fraction of gliomas (50 %) (Ostrom et al. 2013). They originate from either oncogenic transformation of astrocytes or develop from lower grade astrocytomas (Ohgaki and Kleihues 2013), classified as so-called secondary GBM. In fact, most GBMs develop spontaneously *de novo* without any indications of primary lesions (primary GBM). Primary and secondary GBM share similar histological properties but can be differentiated by genetic means, as IDH mutations are exclusively found in secondary GBM (Ohgaki and Kleihues 2013). Copy number alterations of genes involved in the EGFR/PTEN/PI(3)K pathway frequently occur in primary GBMs, allowing the cell to efficiently activate proliferative pathways like protein kinase B (AKT) or MAPK (Parsons et al. 2008; Brennan et al. 2013). *MGMT* promoter methylation was found in about 50 % of all GBM tumor samples (Hegi et al. 2005; Quillien et al. 2012; Brennan et al. 2013), and the

likelihood of *MGMT* promoter methylation is higher in G-CIMP (glioma CpG island methylator phenotype) cases, but its status as a predictive marker is only given in the GBM classical subtype of GBM (non-proneural, non-neural, non-mesenchymal), but not other subtypes (Brennan et al. 2013). In other words, *MGMT* promoter methylation is a predictive marker for the combined TMZ chemotherapy and radiation treatment of HGA in IDH wild-type tumors (as IDH mutations are a key driver of G-CIMP (Turcan et al. 2012), that harbor an EGFR amplification/mutation and low expression of proapoptotic proteins (including cleaved caspase-7 and -9, Bid and Bak) (Brennan et al. 2013).

### 1.2.1. Isocitrate dehydrogenase 1 and Isocitrate dehydrogenase 2 mutations

In 2008 and 2009, two independent cancer genome sequencing projects identified mutations in *isocitrate dehydrogenase 1 (IDH1)* in GBM (Parsons et al. 2008) and acute myeloid leukemia (AML) (Mardis et al. 2009).

Further investigation revealed that mutations of the homologous enzyme isocitrate dehydrogenase 2 (IDH2) were present in other cases of these diseases (Yan et al. 2009). Wild-type IDH1/2 catalyze the oxidative decarboxylation of isocitrate to alpha ketoglutarate ( $\alpha$ -KG), also known as 2-oxoglutarate (Figure 4). Mutations of either *IDH1* or *IDH2* are always heterozygous.



**Figure 4: IDH1 exerts its enzymatic function** to convert isocitrate (Cit) to alpha ketoglutarate ( $\alpha$ -KG) in the cytoplasm and the mitochondrial matrix as part of the Krebs cycle. During this step,  $NAD^+$  is reduced to NADH. IDH2 is located in the mitochondrial matrix and catalyzes the same reaction as IDH1. Suc = succinate, Fum = fumarate, Mal = malate, Oac = oxaloacetate, AcCoa = acetyl coenzyme A, Pyr = Pyruvate, Glu = glutamine

## Introduction

IDH1 and IDH2, each form a homodimer (**Figure 5**) to exert their catalytic function. In a tumor cell, carrying an IDH mutation, theoretically, there will be 25 % each wild-type and mutant homodimers and 50% heterodimers (Zhao and Guan 2010). Nearly all identified mutations (**Table 2**) have been a single amino acid missense mutation in IDH1 at arginine 132 (R132) or the analogous residue in IDH2 (R172) (Cohen et al. 2013).

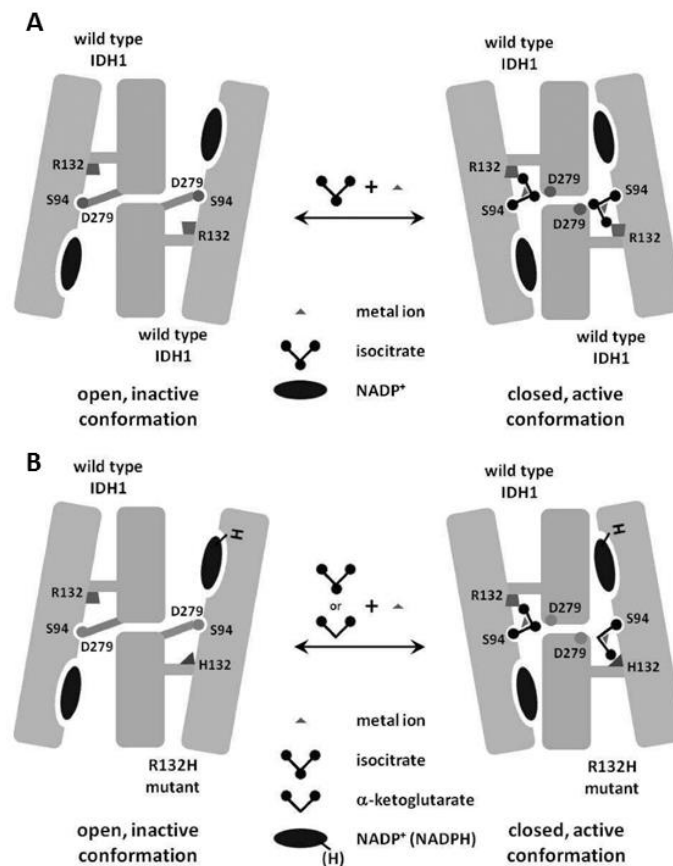
**Table 2: Summary of different IDH mutations found in glioma.** The frequency of IDH1 and IDH2 mutations in glioma is 33 % and 1.7 %, respectively. Frequency data were retrieved from the COSMIC database at cancer.sanger.ac.uk (Forbes et al. 2015). D-2-hydroxyglutarate (2-HG) levels of IDH mutation types differ and were determined *in vitro* for IDH1 (Pusch et al. 2014) and IDH2 (Jin et al. 2011) mutations, if not stated otherwise. The IDH1 R100Q mutation is not able to produce significant amounts of 2-HG.

Gene	Mutation	Base change	Distribution	2-HG production
<b>IDH1</b>	R132H	395G > A	87.6 %	+
	R132C	394C > T	2.9 %	++
	R132S	394C > A	1.8 %	++
	R132G	394C > G	2.3 %	+++
	R132L	395G > T	0.7 %	+++
	R100Q	299 G > A	0.15 %	-
<b>IDH2</b>	R172K	515G > A	58.2 %	++
	R172M	515G > T	19.1 %	++
	R172W	514A > T	8.2 %	++ (Borger et al. 2014)
	R172S	516G > C/T	3.6 %	+ (Churchill et al. 2015)
	R172G	514A > G	2.7 %	++

IDH1/2 mutations result in a loss of normal enzymatic function and the abnormal production of 2-HG instead of  $\alpha$ -KG. 2-HG was found to inhibit the enzymatic function of many  $\alpha$ -KG dependent dioxygenases, including histone (Jumonji domain-containing histone-lysine demethylases) and DNA demethylases (Ten-eleven translocation family), causing widespread changes in histone and DNA methylation and potentially promoting tumorigenesis (Chowdhury et al. 2011; Liu et al. 2015). The 2-HG concentration in patient derived IDH1 mutated tumor cells ranged from 5 to 35 mM (Dang et al. 2009; Andronesi et al. 2012). Patients suffering from an IDH mutated glioma have a prolonged progression free survival (50 months PFS), and overall survival (OS) compared to IDH wild-type glioma

(7.8 months PFS) patients (Hartmann et al. 2010; van den Bent et al. 2010; Cohen et al. 2013). However, some studies have proposed that IDH mutations act as an oncogene in glioma development (Dang et al. 2009; Watanabe et al. 2009a), which is inconsistent with its prognostic value. This inconsistency arises from the fact that IDH mutated tumors share similar histological properties, but their oncogenic transformation is distinct from IDH wild-type tumors. Analyses of multiple biopsies from the same patient (51 glioma cases) showed that there were no cases in which an *IDH1* mutation occurred after the acquisition of either a *TP53* mutation or loss of 1p/19q, suggesting that *IDH1* mutations are very early events in gliomagenesis (Watanabe et al. 2009a). *IDH* mutations are not one of many other mutations being acquired during gliomagenesis, but a key driver of the epithelial-mesenchymal transition through epigenetic and metabolic changes to promote tumorigenesis (Grassian et al. 2012; Grassian et al. 2014). Therefore, comparing IDH mutated tumors with IDH wild-type tumors as to their different consequences in glioma patients is meaningless.

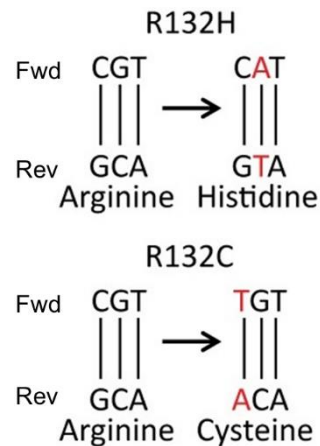
## Introduction



**Figure 5: A cartoon representation of IDH1 dimers** shifting between the inactive and active conformations. **(A)** The IDH1<sup>wt/wt</sup> homodimer binds NADP<sup>+</sup>, isocitrate, and Fe<sup>2+</sup> (metal ion). The R132 residue is in the catalytic pocket of the enzyme and catalyzes the oxidative decarboxylation of isocitrate to α-KG. **(B)** The IDH1R132H mutant subunit of the IDH1<sup>mt/wt</sup> heterodimer binds NADPH, α-KG, and Fe<sup>2+</sup>, leading to an NADPH-dependent reduction of α-KG which results in the generation of 2-HG (Dang et al. 2009). Adapted and reprinted from (Chang et al. 2011).

The question arises, why this SNP in the *IDH1* gene is so common in this highly evolutionary conserved R132 residue (Xu et al. 2004). Both *IDH1* R132H and R132C mutations involve a conversion of a CpG dinucleotide to TpG on opposite strands of the *IDH* R132 codon, which likely results from a spontaneous deamination event (see **Figure 6**) (Saha et al. 2014). Unrepaired deamination followed by replication leads to a CpG to TpG mutation.



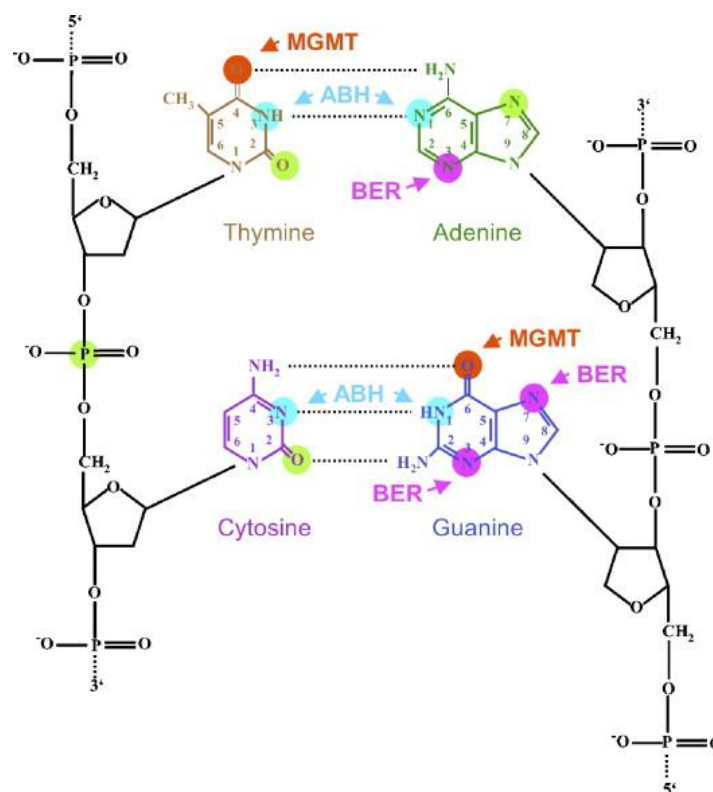


**Figure 6: The *IDH1*R132H mutation** seems to occur as a result of a spontaneous deamination of a CpG dinucleotide of the reverse strand yielding a TpG dinucleotide. Similarly, the R132C mutation appears to occur from the same spontaneous deamination event of a CpG to a TpG dinucleotide on the forward strand in the same codon. Adapted and reprinted from (Saha et al. 2014).

Since the discovery of the *IDH1/2* mutations, considerable efforts have been undertaken to exploit them for improved treatment. First, it was believed, that *IDH* mutated tumors are more sensitive to the applied chemotherapy (TMZ) (Houillier et al. 2010; Wang et al. 2014) or radiation therapy (Li et al. 2013b; Tran et al. 2014). However, the debate was even more confused by findings showing that mutant *IDH1* leads to TMZ resistance by upregulating homologous recombination (see 1.3.4.1) (Ohba et al. 2014), while other authors found that *IDH* mutations suppress homologous recombination (Sulkowski et al. 2017). Others could not find any differences between *IDH* mutations and their *IDH* wild-type counterparts as to TMZ sensitivity (Dubbink et al. 2009; Li et al. 2013b). Radiation decreased the viability of *IDH* mutated cells more than their wild-type counterparts did, and increased ROS levels were found in the mutated cells (Li et al. 2013b). ROS levels were always higher in *IDH* mutated cells after chemo and radiation treatment, even in untreated cells (Chaturvedi et al. 2013; Li et al. 2013b; Mohrenz et al. 2013; Gilbert et al. 2014; Shi et al. 2015). Increased ROS levels are now believed to be the cause for the observed phenotypes of these cells. *IDH* mutations are favorable predictive factors for patients suffering from a glioma.

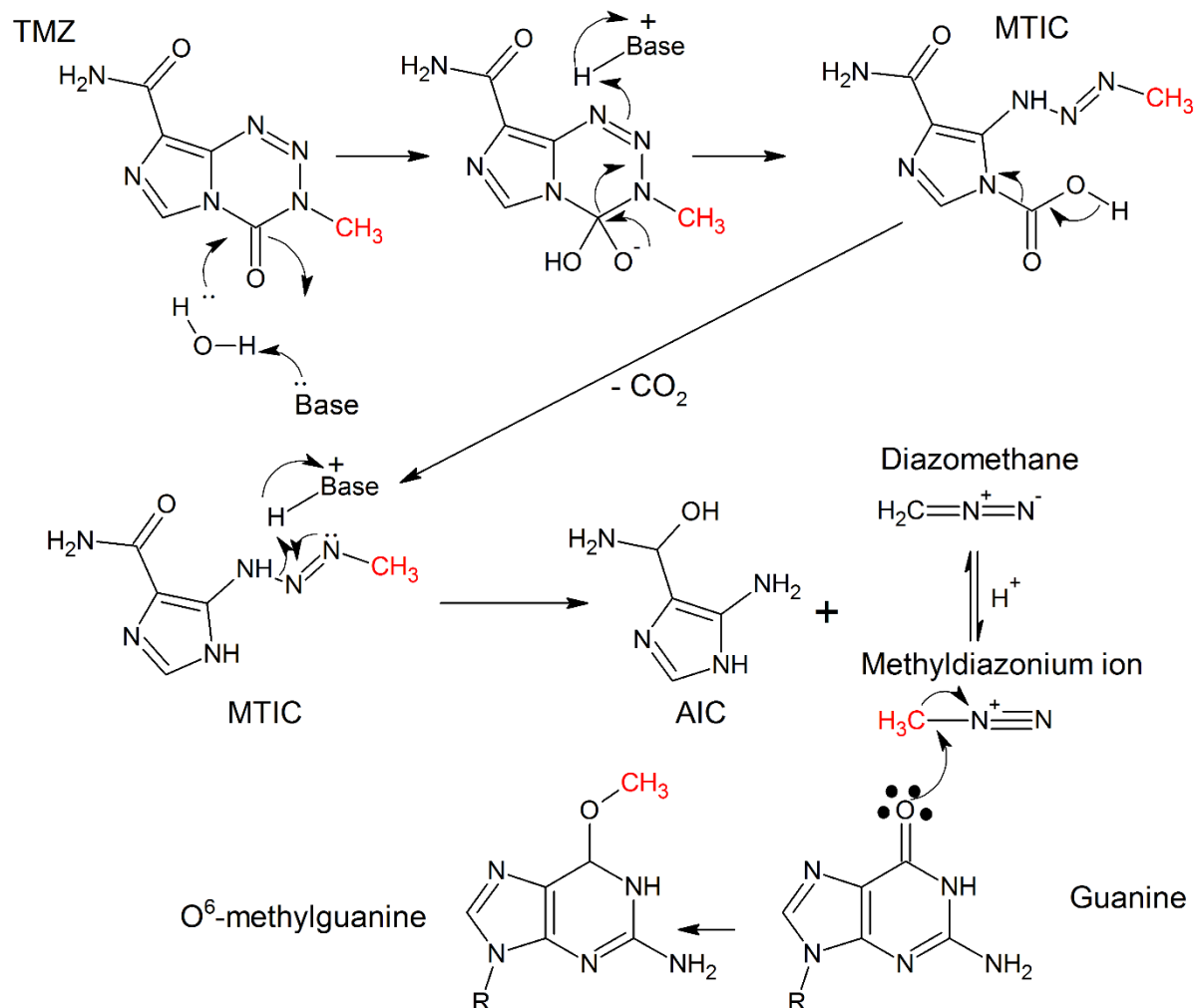
### 1.2.2. Alkylating agents in malignant glioma therapy

Standard treatment for HGA patients consists of surgical resection to the extent that is safely feasible, followed by radiotherapy plus concomitant daily TMZ, followed by adjuvant temozolomide (Stupp et al. 2005). The *MGMT* promoter methylation status plays a significant role in therapy outcome and is determined routinely by methylation specific PCR (see 2.7.4) (Stupp et al. 2014). For GBM patients, TMZ is administered independently from the MSP outcome. Whereas patients with a methylated *MGMT* promoter respond with a median survival of 23.4 months in the combination treatment compared to 15.3 months with radiation alone, combination treatment of tumors with unmethylated *MGMT* promoter results in a minimal increase in median survival from 11.8 months to 12.6 (Stupp et al. 2009). Relapses might be treated with chloroethylating agents such as CCNU (Stupp et al. 2014). TMZ as an alkylating agent induces various DNA lesions, which are repaired by MGMT, ALKBH2, ALKBH3, and BER (Kaina et al. 2007) (**Figure 7**).



**Figure 7: Overview of TMZ induced DNA methylation adducts.** MGMT, BER, and ABH (ALKBH2 and ALKBH3) are involved in the repair of these lesions. Adapted and reprinted from Kaina et al. 2007.

Among these,  $O^6$ -methylguanine (**Figure 8**), as the most cytotoxic lesion, results in continuous futile cycles of DNA base mismatch repair (MMR, see 1.3.3) with the eventual formation of DNA double-strand breaks, ultimately triggering cellular apoptosis (Li 2008; Quiros et al. 2010).



**Figure 8: Hydrolysis of TMZ to MTIC followed by its degradation and transfer of the methyl group to guanine.** Modified from (Newlands et al. 1997).

MGMT can remove the methyl group from the  $O^6$ -position of guanine, leading to cell survival and renders TMZ treatment ineffective. Mutational analysis of recurrent glioma has shown that TMZ induces hypermutation in the tumor genome, independently of the MGMT status. Overall, 97 % of these mutations are C->T/G->A transitions predominantly occurring at CpC and CpT dinucleotides, which was found to be a signature of TMZ-induced mutagenesis distinct from non-hypermethylated tumors. Through the acquisition of

## Introduction

new mutations, residual tumor cells can progress to a more aggressive state (Johnson et al. 2014). As only patients with a methylated *MGMT* status greatly benefit from TMZ treatment, the method of classification into responder and non-responder is crucial for preventing further mutational transformation of the tumor in a non-responder.

### 1.2.3. Ionizing radiation in malignant glioma therapy

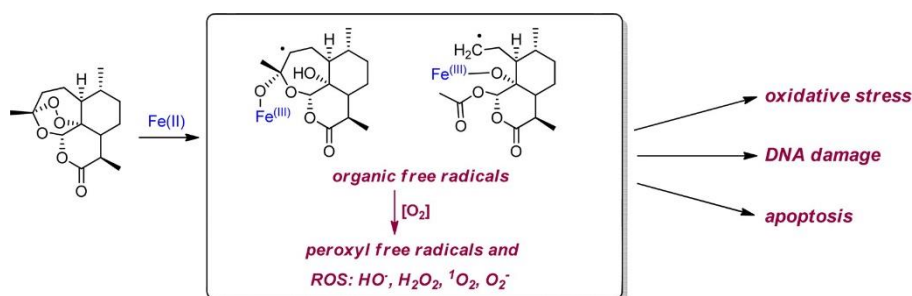
Ionizing radiation is used for the treatment of gliomas. IR has two modes of action. First, IR can hit DNA directly and break the sugar-phosphate backbone, and secondly, it ionizes water molecules which then attack DNA as highly nucleophilic radicals (OH•) (Maier et al. 2016). Free radicals can also be formed in the same manner, but their importance for the induction of toxic DNA lesions is neglectable (Herskind and Westergaard 1988). 1 Gray (Gy) is defined as 1 Joule absorbed dose per kg body weight. This dose leads approximately to 3000 damaged bases, 1000 SSBs, and 40 DSBs per cell (Hall and Giaccia 2006). DNA repair pathways of BER and NHEJ are of importance to process and repair SSBs and DSBs, respectively.

### 1.2.4. Artesunate in malignant glioma therapy

Artesunate (ART) is a semi-synthetic derivative of artemisinin, an ingredient of the *Artemisia annua* herb. Due to the very low solubility of the natural compound, some derivatives have been synthesized, including artesunate. Extracts of *Artemisia annua* were extensively used for centuries in traditional Chinese medicine (TCM). ART is currently being used as an antimalarial drug because of its potent activity against the chloroquine resistant pathogen *Plasmodium falciparum* (Klayman 1985). ART is a prodrug that is intracellularly rapidly converted to its active form dihydroartemisinin (Cui and Su 2009). *In vitro* off-label use of ART has shown to exert cytotoxic activity on cancer cells (Efferth et al. 2001), which was extensively studied in different experimental systems, making it a candidate for a cancer chemotherapeutic agent (Efferth et al. 2007; Berte et al. 2016). ART's modes of action against cancer cells were described as inhibition of metastasis (Rasheed et al. 2010), cancer-related signaling pathways (Konkimalla et al. 2009; Sertel et al. 2010a; Sertel et al. 2010b), angiogenesis (Dell'Eva et al. 2004; Soomro et al. 2011), and through the induction of DNA damage (Li et al. 2008; Berdelle et al. 2011).

For malaria treatment, ART is applied by two medication types, 40 mg/kg/day over three consecutive days for treatment, or 8 - 13 doses of 6 mg/kg/day over 2 - weeks intervals (Liu et al. 2011). The plasma level of ART after oral administration reaches its peak after 120 min. A dose of 500 mg ART leads to plasma levels of 0.25  $\mu\text{g}/\text{ml}$  after 120 min (Benakis et al. 1997). ART is rapidly transformed within minutes into dihydroartemisinin, the bio-active metabolite. This conversion occurs extracellularly by simple non-enzymatic gut pH hydrolysis, cleavage in blood influenced by esterases and by cytochrome P450 (CYP) 2A6 isoform (Li et al. 2003). Dihydroartemisinin disposition takes place in the liver and the gut by covalent attachment of glucuronic acid mediated by the UDP-glucuronosyltransferase 1A9 and 2B7 (Ilett et al. 2002).

ART is an endoperoxide that generates intracellular ROS (**Figure 9**) leading to 8-oxoG and other oxidative DNA damages. Furthermore, ART causes lipid peroxidation which gives rise to the formation of 1,  $N^6$ -ethenoadenine, 1,  $N^6$ -ethanoadenine, and 3,  $N^4$ -ethenocytosine, all being substrates for ALKBH2/3 (el Ghissassi et al. 1995; Delaney et al. 2005; Ringvoll et al. 2008; Berdelle et al. 2011).

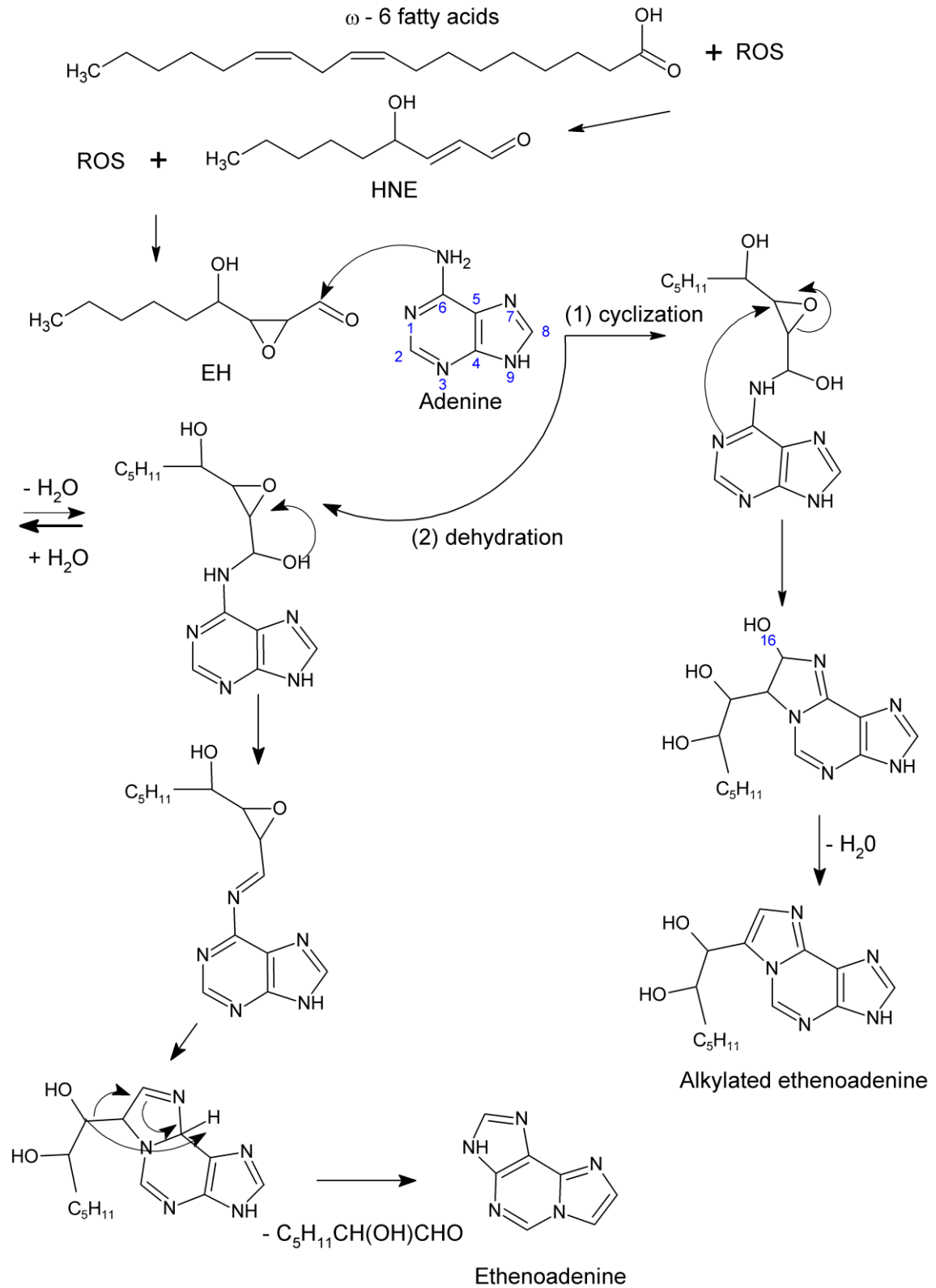


**Figure 9: Proposed pathway of dihydroartemisinin activation** by Fe(II). It involves cleavage of endoperoxide bridges by Fe(II), producing free radicals (hypervalent iron-oxo species, epoxides, aldehydes, and dicarbonyl compounds) which damage biological macromolecules causing oxidative stress in the cells. Adapted and reprinted from (Frohlich et al. 2016).

The exact pathway of etheno adduct formation *in vivo* is unclear, but it is accepted that this adducts may be generated by the exposure of DNA to lipid peroxides or certain environmental carcinogens like vinyl chloride or its metabolite, chloroacetaldehyde (CAA). The

## Introduction

lipid peroxide product that generates etheno adducts ( $\epsilon$ A,  $\epsilon$ C) with nucleobases is presumably trans-4-hydroxy-2-nonenal (HNE) (el Ghissassi et al. 1995; Winczura et al. 2014) (see **Figure 10**).



**Figure 10: Non-enzymatic lipid peroxidation** is an autocatalytic process, initiated by the attack of free radicals on membrane polyunsaturated fatty acids (PUFAs). The  $\alpha,\beta$ -unsaturated aldehyde trans-4-hydroxy-2-nonenal (HNE) is a major end product that is derived from the oxidation of  $\omega$ -6 PUFAs such as linoleic,  $\gamma$ -linolenic or arachidonic acids. Epoxidation of HNE with ROS leads to the generation of 2,3-epoxy-4-hydroxynonanal (EH). EH

## Introduction

reacts with deoxyadenosine, deoxycytidine, and deoxyadenosine (shown here). First, the carbonyl group of the EH attacks the exocyclic  $N^6$  amino group. Then, two reactions are possible: **(1)** Immediate ring closure at position N1 give rise to alkylated ethenoadenine after dehydration. **(2)** In an alternative pathway, dehydration into an imine takes place first. After ring closure, a retroaldol reaction induces the loss of the side chain of the aldehyde and yields ethenoadenine (Chung et al. 1993; Schaur 2003; Cadet et al. 2010; Petrova et al. 2011; Dalleau et al. 2013).

$\epsilon$ -lesions generate a broad spectrum of base substitutions (transitions and transversions) or frameshift mutations. It is estimated that in mammalian DNA, 14 % to 60 % of  $\epsilon$ -adducts give rise to mutations, while only 3 % of 8-oxoguanine residues are pro-mutagenic in cells with functional DNA repair (Zdzalik et al. 2015). These pro-mutagenic properties of  $\epsilon$ -lesions strongly underlie their contribution to carcinogenesis in mammals. Further, tumors with impaired DNA repair pathways that target  $\epsilon$ -lesions (ALKBHs and BER, see 1.3.1.2 and 1.3.2), could accumulate vast genetic alterations during tumor progression.



### 1.3. DNA repair pathways and their epigenetic regulation

Cellular DNA is constantly subject to modifications by intracellular and extracellular chemicals, which can result in covalent changes (Lindahl 1993). Most of the cells' damage arises from endogenous sources. Generation of ROS in mitochondria, falsely methylated nucleotides by S-adenosylmethionine (SAM), deamination of nucleotides, and replication errors are the primary source of spontaneous DNA damage. DNA damage induced by exogenous sources like UV radiation and chemical components of food or tobacco smoke only contribute to a minor part of all DNA damages in a cell (De Bont and van Larebeke 2004). These lesions are processed by a network of repair mechanisms, which are lesion specific and often backup each other. In cancers, DNA repair proteins or proteins involved in the DNA damage signaling pathways are often genetically mutated or epigenetically silenced, driving the oncogenic transformation of the tumor (Goode et al. 2002).

#### 1.3.1. Direct Reversal of DNA Alkylation Damage

Alkylation damage can be a result of exposure of DNA to experimental mutagens like *N*-methyl-*N'*-nitro-*N*-nitroso-guanidine (MNNG), *N*-methyl-*N*-nitrosourea (MNU), or methyl methanesulfonate (MMS), which all cause different O-alkylated and *N*-alkylated DNA adducts (Eker et al. 2009). *In vivo*, the most common source of DNA alkylation damage in humans results from *N*-nitroso compounds. *N*-nitroso-dimethylamine was the first identified *N*-nitroso compound in tobacco smoke, but several other compounds share the same DNA alkylation properties (Rhoades and Johnson 1972; Christmann and Kaina 2012). The sources of this compounds are smoked and cured fish and meat as well as in some beers (Lijinsky 1999). SAM is the primary endogenous reactive molecule causing DNA alkylation. SAM plays a central role in establishing epigenetically relevant cytosine methylation marks, by providing methyl groups for the DNMTs (see 1.1.1). Nevertheless, SAM non-enzymatically generates 4000 *N*<sup>7</sup>-methylguanine, 600 *N*<sup>3</sup>-methyladenine and 10 – 30 *O*<sup>6</sup>-methylguanine residues per day in a mammalian cell (Rydberg and Lindahl 1982). Other endogenous sources for DNA alkylation are betaine or choline (Barrows and Magee 1982; Rydberg and Lindahl 1982). Direct reversal of DNA alkylation is error-free, shows high substrate specificity, and does not involve incision of the sugar-phosphate backbone or base excision (De Bont and van Larebeke 2004).

## Introduction

### 1.3.1.1. $O^6$ -alkylguanine-DNA alkyltransferase – MGMT

In 1980 it was found that  $O^6$ -methylguanine residues disappear from alkylated DNA by an inducible repair process in *E. coli*. The authors could prove that the methyl group of  $O^6$ -methylguanine is transferred enzymatically to a protein cysteine residue (Olsson and Lindahl 1980). Two years later, the responsible methyltransferase was purified and characterized (Demple et al. 1982). Several years later, the cDNA was cloned in the laboratory of S. Mitra (Tano et al. 1990). The human *MGMT* gene is 300,800 bp long, contains six exons which result in an mRNA transcript of 1,372 bp, resulting in a 207 amino acid long and 21.6 kDa protein (Genome Reference Consortium Human Build 38 patch release 7) (Pruitt et al. 2014). It is located in the cytoplasm and translocates to the nucleus upon DNA alkylation damage as it contains a nuclear localization signal sequence (Lim and Li 1996). The human MGMT removes alkyl groups from the  $O^6$ - position of guanine and the  $O^4$ -position of thymine stoichiometrically (Demple et al. 1982) and is then modified by ubiquitin ligases, leading to its proteasomal degradation (Sassanfar et al. 1991; Srivenu-gopal et al. 1996). MGMT is referred to as a 'suicide enzyme', which has to be resynthesized to restore the DNA repair capacity of the cell. Inter-individual and tissue specific *MGMT* expression and MGMT enzyme activity could be found. High MGMT activity was found in liver, while the lowest was found in brain, lung tissue, and hematopoietic stem cells (Gerson et al. 1996; Margison et al. 2003; Christmann et al. 2011). Its role has emerged as a powerful determinant for alkylating agent based cancer therapy, as some tumors, especially high-grade glioma and metastatic melanoma, silence *MGMT* expression by promoter methylation.

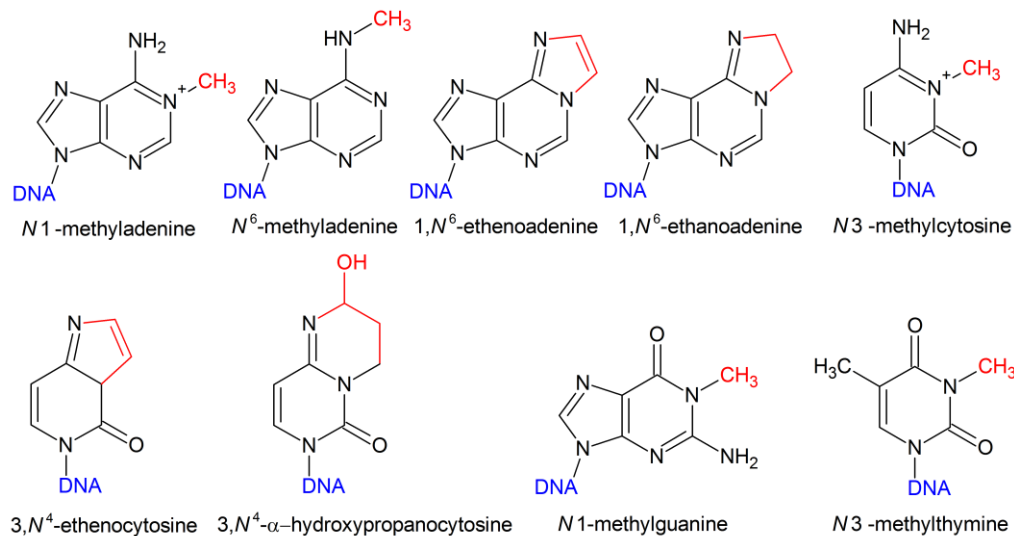
Since the determination of the MGMT activity usually relies on a radioactive assay, alternative techniques for detecting the MGMT status were established. These methods are based on the finding that the *MGMT* expression is highly regulated by *MGMT* promoter methylation (Costello et al. 1994a; Costello et al. 1994b). Most studies focused on methylation of two CpG islands positioned between -328 and -182 and between +28 and +117 relative to the ATG of the *MGMT* gene, which have been shown to provoke transcriptional silencing (Harris et al. 1991; Qian and Brent 1997). Methylation of individual CpG sites in these islands of the *MGMT* promoter was shown to correlate with loss of MGMT protein

expression in the tumor tissue (Esteller et al. 1999). *MGMT* promoter methylation is frequently analyzed via methylation specific PCR (MSP) for which primer pairs flanking different CpG sites within the *MGMT* promoter are being used (Esteller et al. 2000). Their utilization in a significant number of studies revealed epigenetic silencing of *MGMT* in about 45 % of the cases and established a correlation between *MGMT* promoter methylation and patient's overall survival (OS) and progression-free survival (PFS) (Esteller et al. 1999; Esteller et al. 2000; Hegi et al. 2004; Hegi et al. 2005; Everhard et al. 2006). *MGMT* promoter methylation is seen as an independent favorable prognostic factor of benefit from temozolomide based chemotherapy (Hegi et al. 2005).

#### 1.3.1.2. Oxidative Dealkylation by AlkB

In 2002, two separate groups revealed that Alpha-ketoglutarate-dependent dioxygenase AlkB (AlkB) in *E. Coli* directly reverses m<sup>1</sup>A and m<sup>3</sup>C to unmethylated bases in DNA through oxidative demethylation in the presence of Fe<sup>2+</sup>,  $\alpha$ -KG, and dioxygen (Falnes et al. 2002; Trewick et al. 2002). AlkB knock-down experiments showed extremely increased sensitivity towards MMS in *E. coli* (Falnes et al. 2002). The human genome encodes for nine proteins with AlkB dioxygenase motifs, consisting of eight AlkB homologs (ALKBH1 through ALKBH8) and the fat mass and obesity-associated (FTO) protein. Among these, ALKBH2 and ALKBH3 are the most similar to AlkB from *E. coli*. They function as DNA-repair proteins to protect the genomic integrity of mammalian cells. All ALKBH enzymes belong to the non-heme Fe<sup>2+</sup> /  $\alpha$ -KG dependent dioxygenase enzyme family. They have either DNA or RNA binding motifs, except for ALKBH7, which is believed to interact with proteins. ALKBH enzymes repair a broad spectrum of mutagenic and replication blocking DNA lesions, demethylate and modify different RNA variants, and demethylate proteins (see **Table 3** and **Figure 11**). ALKBH2 is solely present in the cell nucleus, where it localizes mainly to replication foci during the S phase of the cell cycle through interaction with proliferating cell nuclear antigen (PCNA) via an ALKBH2 PCNA-interacting motif (Aas et al. 2003; Fu et al. 2015). It has therefore been suggested that ALKBH2 may have a role in DNA repair close to the replication fork (Sundheim et al. 2008).

## Introduction

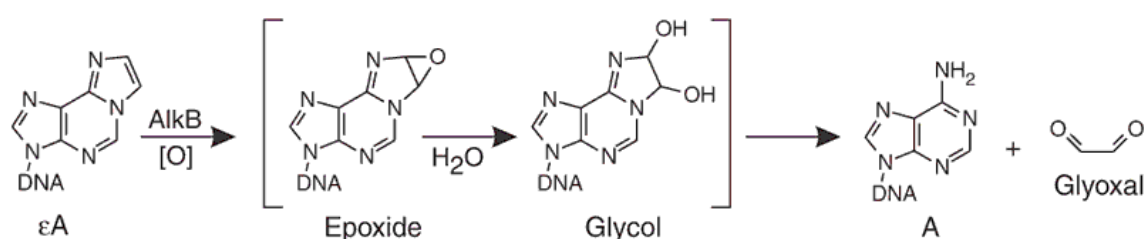


**Figure 11: DNA and RNA lesions that can be repaired by *E. coli* AlkB.** The nine mammalian AlkB homologs are less versatile and more specialized for certain DNA/RNA lesions. Nevertheless, all nine AlkB homologous together are responsible for the repair of a large spectrum of DNA/RNA lesions. Among these homologs, ALKBH2 and 3 are the most similar to *E. coli* AlkB. Adapted and reprinted from Zheng et al. 2014.

**Table 3: Properties of the mammalian AlkB homologs and their targets.** 1mA = 1-methyladenine, 3mC = N3-methylcytosine, 3EtC = N3-ethylcytosine, 1mG = N1-methylguanine, 3mT = N3-methylthymine, m<sup>6</sup>A = N<sup>6</sup>-methyladenine, EA = 1, N<sup>6</sup>-ethanoadenine, εA = 1, N<sup>6</sup>-ethenoadenine, εC = 3, N<sup>4</sup>-ethenocytosine, εG = 1, N<sup>2</sup>-ethenoguanine. m3U = N3-methyluracil

Homologue	Targets / binding properties / recognized lesions
ALKBH1	Lyase activity at abasic sites (Muller et al. 2013), demethylation of dsDNA: 1mA, 3mC (Zheng et al. 2014), histone H2A (Ougland et al. 2012)
ALKBH2	Demethylation of dsDNA: 1mA, 3mC, N3EtC, 1mG, 3mT, m <sup>6</sup> A, 1EA, εA, εC, εG (Ringvoll et al. 2008; Fu and Samson 2012; Zheng et al. 2014; Zdzalik et al. 2015)
ALKBH3	Demethylation of ssDNA, through ASSC3 (Dango et al. 2011) also dsDNA: 1mA, 3mC, m1T, εA (Zheng et al. 2014)
ALKBH4	Demethylation of actin (K84me1) (Li et al. 2013a)
ALKBH5	Possible demethylation of mRNA: m <sup>6</sup> A (Zheng et al. 2013)
ALKBH6	No documented function
ALKBH7	Mitochondrial location, triggers necrosis (Fu et al. 2013)
ALKBH8	Hypermethylation of tRNA: hydroxylation of mcm <sup>5</sup> U to (S)mchm <sup>5</sup> U in tRNA <sup>Gly</sup> (UCC); the only ALKBH enzyme not catalyzing demethylation, but instead mediates the process of hydroxylation (Fu et al. 2010; van den Born et al. 2011)
FTO	Demethylation of RNA: m <sup>3</sup> U; ssDNA: 3mT (Jia et al. 2008)

Exocyclic DNA adducts of 1,  $N^6$ -ethenoadenine ( $\epsilon$ A) and 3,  $N^4$ -ethenocytosine ( $\epsilon$ C) are generated by exposure to electrophilic vinyl chloride (VC) metabolites, chloroethylene oxide (CEO), or chloroacetaldehyde (CAA) from exogenous sources. Endogenously,  $\epsilon$ A and  $\epsilon$ C are generated as a result of the reaction of adenine and cytosine, with the breakdown products of oxidatively damaged unsaturated lipids from lipid peroxidation (Barbin et al. 1981; el Ghissassi et al. 1995). 1,  $N^6$ -ethenoadenine (EA) can be produced by the reaction of adenine with the anticancer drug 1,3-bis(2chloroethyl)-1-nitrosourea (BCNU) (Frick et al. 2007). 3,  $N^4$ - $\alpha$ -hydroxypropanocytosine is produced by lipid peroxidation (Maciejewska et al. 2013). Excision of etheno adducts is mainly established through the alkyl- $N$ -adenine-DNA glycosylase (APNG, also known as MPG, APG, and AAG) of the base excision repair pathway (see 1.3.2), leaving behind an abasic site. However, in AlkB-deficient *E. coli* but proficient in the APNG orthologue (DNA-3-methyladenine glycosylase I),  $\epsilon$ A showed to be 35 % mutagenic, yielding 25 % A->T, 5 % A->G and 5 % A->C mutations. The repair of etheno adducts by AlkB is established by cleaving the lipid-derived alkyl chain from DNA, causing  $\epsilon$ A and  $\epsilon$ C to revert to adenine and cytosine, respectively.  $\epsilon$ A is epoxidized at the etheno bond (**Figure 12**). The epoxide is putatively hydrolyzed to a glycol, and the glycol moiety is released as glyoxal (Delaney et al. 2005).



**Figure 12: Probable AlkB reaction mechanism for repair of etheno adducts.** The pathway of AlkB mediated  $\epsilon$ A and  $\epsilon$ C repair involves the formation of epoxide and glycol intermediates. Adapted and reprinted from Delaney et al. 2005.

Currently, there is no evidence of epigenetic downregulation of ALKBHs in cancers. Interestingly, overexpression of ALKBH2 was found in glioma cell lines and glioblastoma tissue samples (Murat et al. 2008; Johannessen et al. 2013).

## Introduction

### 1.3.2. Base excision repair – BER

Base excision repair (BER) is the primary repair mechanism for small base modifications that do not deform the helical structure of the DNA strand. These modifications result from alkylation, oxidation or deamination of DNA bases. BER is initiated by a DNA glycosylase that recognizes and removes the damaged base, leaving an abasic site, that is further processed by "short-patch" and "long-patch" repair (Krokan and Bjoras 2013).

11 mammalian DNA glycosylases were found, many of them having different substrate specificity and subcellular localization. Most of them are monofunctional (type 1 glycosylases), meaning, they solely remove the base, leaving an intact sugar-phosphate backbone. Glycosylases cleave the bond between the base and the deoxyribose, resulting in an abasic site (apurinic/apyrimidinic site or AP-site). After AP-site generation, AP endonuclease 1/2 (APE1/2) incise the sugar-phosphate backbone which results in 3'OH and 5' deoxyribose phosphate (5'dRP) ends. Bifunctional glycosylases (type 2 glycosylases) OGG1, NEIL1-3, and NTHL1 display an additional AP lyase activity allowing cleavage of the backbone is generating an unsaturated hydroxyaldehyde linked to the 3' end (3'dRP) and a phosphate at the 5'end. The 3'dRP is efficiently removed by APE1 that generates a 3'OH end, preparing the intermediate for the polymerase step. Depending on the actual cell cycle, either short patch (dominant in G1/G0) and long patch (dominant in S and G2) BER is initiated (Otterlei et al. 1999; Hegde et al. 2008). During short patch BER, polymerase  $\beta$  (POL $\beta$ ) removes the 5'dRP by its phosphodiester activity and uses dNTP to insert the appropriate nucleotide. During long patch BER, up to 10 nucleotides are inserted with the help of replication factor C (RFC) and proliferating cell nuclear antigen (PCNA). This leads to a displacement of the original strand by the newly synthesized strand, which is cleaved by flap endonuclease (FEN1). During the filling step, X-ray repair cross-complementing protein (XRCC1) participates in recruiting and stimulating factors like APE1 and POL $\beta$ . The last step is ligation of the nick after gap filling, which is fulfilled by DNA ligase 3 (LIG3) with its cofactor XRCC1 during short patch BER, and by DNA ligase 1 (LIG1) with its cofactor PCNA to complete long patch BER (Krokan and Bjoras 2013).

BER is involved in erasing epigenetic marks (see 1.1.1) during TET mediated DNA demethylation, but on the other hand, some key factors of BER are downregulated by promoter methylation in different cancers.

MBD4 (methyl-CpG-binding domain protein 4), a glycosylase which binds methylated CpGs and their deamination derivatives G-U and G-T base pairs, is downregulated by DNA promoter methylation in about 50 % of ovarian and 25 % of colorectal cancer cases (Bellacosa and Drohat 2015; Tricarico et al. 2015). The other BER enzyme being downregulated by DNA promoter methylation in tumors is NEIL1 (Endonuclease VIII-like 1) that belongs to the DNA glycosylases. NEIL1 recognizes and removes ROS damaged bases during DNA replication. A deficiency of NEIL1 leads to G->C and T->A transversion mutation at the site of an 8-oxoG. Methylation of the *NEIL1* promoter is found to a great extent in non-small cell lung cancers (NSCLC) and colorectal cancers (Do et al. 2014; Farkas et al. 2014). Recently, the function of NEIL1 and NEIL2 were extended, as they are both involved in the processing of AP sites during TET-mediated DNA demethylation. NEILs displace TDG from the AP site and initiate the sugar-backbone incision. NEIL1/2 knock-down experiments have shown that they are required for an efficient DNA demethylation (Schomacher et al. 2016).

### 1.3.3. DNA mismatch repair – MMR

Substrates that are processed by MMR are base pairings that do not follow Watson-Crick pairing (A-T/G-C). Base mismatches can be generated during S-phase, by incorrect nucleotide insertion by DNA polymerases or because of damaged nucleotides on the parental strand that mispair. For example, 8-oxoG on the parental strand will mispair with adenine during replication and *O*<sup>6</sup>mG with thymine. In order to begin repair, MMR has to distinguish the newly synthesized from the parental strand. This is mediated by nicks in the newly synthesized strand, but detailed knowledge how this occurs was not found until 2013 (Ghodgaonkar et al. 2013; Lujan et al. 2013; Williams et al. 2016). It is estimated that ribonucleotides are inserted into the newly synthesized strand at a rate of 1 in every 6500 deoxyribonucleotides. Falsely inserted ribonucleotides are removed by ribonucleotide excision repair (RER), which is initiated by RNase H2 –mediated recognition of ribonucleotides incorporated into DNA, followed by incision of the DNA backbone 5' of the ribonucleotide, creating a nick (Lujan et al. 2012; Ghodgaonkar et al. 2013; Williams et al. 2016). For the lagging strand, nicks are introduced between Okazaki fragments. Thus, by inserting wrong nucleotides (ribonucleotides), MMR can distinguish the newly synthesized mismatch-containing strand from the parental strand.

## Introduction

During G1/G0, spontaneous and enzyme catalyzed (AID and APOBEC3A<sup>1</sup>) deamination of cytosine forms uracil and deamination of 5meC forms thymine, yielding U:G and T:G mismatches, respectively (Wijesinghe and Bhagwat 2012). Subsequently, G->A transition mutation at the next round of DNA replication is established. U:G mispair arising through AID-catalyzed deamination of cytosines are substrates for both BER (Uracil glycosylase (UNG)) and MMR, the latter occasionally gives rise to DSB if multiple mismatches are closely situated on opposite strands. This mechanism is used in antigen-stimulated B-cells to rearrange their immunoglobulin constant heavy chain (C<sub>H</sub>) to generate antibodies with different effector functions. Similarly, chromosomal rearrangements occurring in cancers, are likely triggered by DSB arising through MMR- and BER mediated processing of AID-generated uracils (Bregenhorn et al. 2016). In *E. coli*, T:G mismatches resulting from 5meC deamination, are repaired by the very short patch (VSP) repair (Lieb and Bhagwat 1996). In *E.coli* it involves the binding and recognition of the T:G mismatch by MutS dimers, which are part of the MMR (Bhagwat and Lieb 2002). However, in eukaryotic cells, G:T mismatches resulting from deamination of 5meC are recognized the MMR, but unlike G:T mismatches that result from replication errors, this class of G:T mismatch cannot be accurately repaired by distinguishing between parental and daughter strand. Thymine-DNA glycosylase (TDG) and MBD4, both being BER glycosylases (see 1.3.2), repair this G:T mismatch in the context of a methylated CpG site (Bellacosa and Drohat 2015).

Deamination of cytosine occurs at a rate of about 100-500 bases per cell and day, and deamination of 5meC at a rate of about five bases per cell and day (Lindahl 1993; Shen et al. 1994; Nilsen et al. 2001). As 5meC is much less abundant than unmodified cytosine (only in CpGs), the risk of a spontaneous deamination of 5meC is 2-3 fold increased compared to the unmodified cytosine. Likewise, CpGs have long been known to be a hotspot for pathological mutations (Lutsenko and Bhagwat 1999; Cooper et al. 2010; Pena-Diaz et al. 2012).

The recognition of mismatches is performed by the MutS $\alpha$  heterodimer, consisting of the MSH2 and MSH6, and strand discrimination by RNase H2 generated nicks is accomplished

---

<sup>1</sup> AID: Activation-induced cytidine deaminase; APOBEC3A: Apolipoprotein B mRNA editing enzyme, catalytic polypeptide-like 3



by the MutL $\alpha$  heterodimer loading, consisting of MLH1 and PMS2. MSH2 and MSH6 exhibit ATPase function, which allows scanning of DNA substrates and is inhibited by the exchange of ADP $\rightarrow$ ATP upon substrate recognition. The heterodimer MutL $\alpha$  bears ATPase and endonuclease enzymatic activity. Exonuclease 1 (EXO1) is recruited to the site where MutL $\alpha$  and MutS $\alpha$  colocalize and resect up to several thousand nucleotides of the newly synthesized strand. As a final step, the replication machinery, including POL $\delta$ , RFC, and PCNA resynthesize the gap, which is then ligated by LIG1 (Li 2008; Jiricny 2013).

Transcription of *MLH1* and *MSH2* are affected by DNA methylation in several cancer types. MMR deficiency caused by promoter methylation of the *MLH1* gene was found in cancers of the stomach (Waki et al. 2002), esophagus (Chang et al. 2015), lung (Safar et al. 2005), and head and neck squamous cell carcinoma (HNSCC) (Tawfik et al. 2011). In sporadic colorectal cancers (CRC), *MLH1* is silenced due to promoter methylation in around 20 % of all cases (Li et al. 2013c). The Lynch syndrome (hereditary nonpolyposis colorectal cancer or HNPCC) is caused by autosomal dominant genetic mutations mostly affecting *MLH1* and *MSH2*, leading to a reduced or abolished MMR capacity. MMR defects resulting from genetic and epigenetic changes result in microsatellite instability (MSI), i.e. lead to genome wide CpG demethylation and mutations due to C $\rightarrow$ T transition mutations raising from deamination events and alteration in microsatellite length (Ellegren 2004; Poulos et al. 2017).

#### 1.3.4. DNA double-strand break repair

DNA double-strand breaks (DDSB) are among the most severe DNA damages. If not repaired, they ultimately lead to gene mutations, deletions, chromosomal aberrations, translocations, amplifications, cell death, or senescence. Cells have evolved two major repair DDSB pathways, which are active in different cell cycles (Bohgaki et al. 2010).

##### 1.3.4.1. Non-homologous end joining – NHEJ

Re-ligation of two DSB ends during G0/G1 is performed by NHEJ, which does not require homology, but it is error prone and can lead to deletions and translocations (Lieber 2010). Stabilization of the two DSB ends is initiated by the binding of Ku heterodimers (Ku70 and Ku80). KU70/80 bears an extraordinary binding affinity for DNA ends, targeting the sugar

## Introduction

backbone of the DNA, which makes this step sequence independent. Upon Ku70/80 binding, DNA-dependent protein kinase catalytic subunit (DNA-PKcs) is attracted to establish kinase activity of the complex, allowing autophosphorylation and phosphorylation of additional NHEJ proteins (Davis et al. 2014). Polynucleotide kinase 3-phosphatase (PNKP), X-ray repair cross-complementing protein 4 (XRCC4) and Artemis, are recruited to process the DNA ends. The XRCC4-LIG4 complex ligates the two ends (Lieber 2010). Besides its function in DNA repair, NHEJ is crucial for the antigen-specific immune system of vertebrates by processing endogenous DSB, which are generated during maturation of pre-B and pre-T cells. These DSB are generated during V(D)J recombination, and NHEJ is the rejoining pathway that generates the exon that encodes the variable domain of immunoglobulins and T-cell receptors. Immunodeficient animals like BALB/c mice are NHEJ deficient (Fabre et al. 2011).

Cells that are impaired in the classical NHEJ pathway (c-NHEJ) can use the alternative end joining (alt-EJ) repair pathway, which is even more error prone than NHEJ. PARP1 senses the damage and recruits XRCC1 and LIG3 (Iliakis 2009).

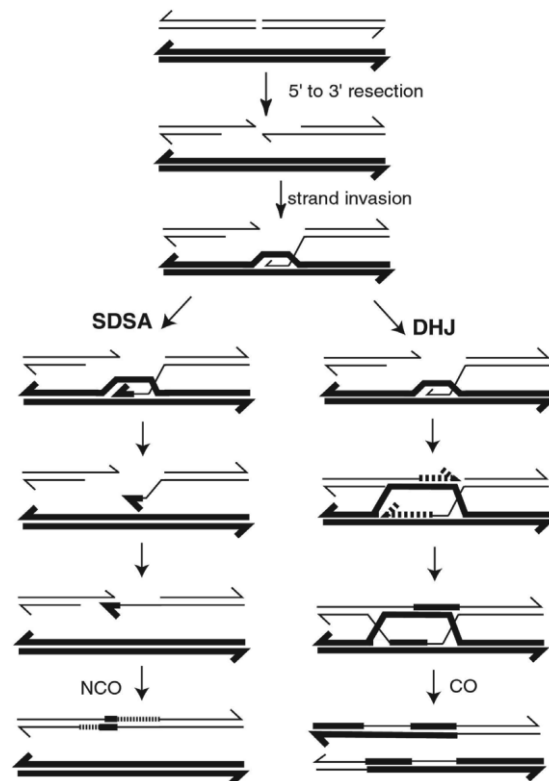
Downregulation due to promoter methylation of *XRCC5*, coding for the Ku80 enzyme, is found in 21 % of NSCLC cases, 32 % of oral squamous cell carcinoma (SCC), and 15 % of adenocarcinomas (Lee et al. 2007; Lahtz and Pfeifer 2011).

### 1.3.4.2. Homologous recombination – HR

HR is a complex repair process, the exact mechanism of which requires further elucidation. It is clear that during S- and G2-phase HR mediated repair of DSB is dominant over NHEJ. It makes use of homologous sequences on sister chromatids and is therefore regarded as error free. HR resolves stalled replication forks and DSB resulting from SSB in the DNA template strand during replication (Arnaudeau et al. 2001; Petermann and Helleday 2010). First, the MRN complex (MRE11, RAD50, NBS1) binds to the DSB and resection of the 5' ends around the break is performed by MRE11's 3'-5' exonuclease activity to create short 3' overhangs of ssDNA. Then, the MRN complex, which acts on 5' flaps and 5' branched structures, recruits the CtIP endonuclease (Sartori et al. 2007).

5'→3' resection is proceeded by EXO1 and the resulting 3' ssDNA ends are bound by replication protein A (RPA) to prevent it from rewinding on itself or forming secondary structures as well as from nucleolytic attacks. RAD51 then forms a filament on the RPA coated ssDNA and replaces RPA. This process is mediated by BRCA2. The resulting ssDNA - RAD51 nucleoprotein filament permits the search for homology sequences on the sister chromatid. Following homology finding, strand invasion is initiated resulting in the displacement-loop (D-Loop) (Qi et al. 2015). The 3' end of the RAD51 loaded strand serves as a primer for DNA synthesis by POL $\delta$  that uses the undamaged DNA strand as a template.

Currently, two primary models describe how this structure can be resolved. In the synthesis-dependent strand annealing (SDSA) pathway no crossover of the two strands is established. The double Holliday junction (DHJ) model involves a double crossover of the two strands. After resolution of the two crossovers involving the helicase Bloom syndrome protein (BLM) and topoisomerase TOP3 $\alpha$ , there is a high chance that a permanent crossover of the two chromosomes is established (**Figure 13**) (Helleday et al. 2007; Heyer et al. 2010). Template switching and interstrand crosslink repair during replication involve HR (good reviews are provided by (San Filippo et al. 2008; Branzei and Foiani 2010).



**Figure 13: Mechanisms of homologous recombination-mediated double-strand break repair.** First, a 5' to 3' resection by the MRN complex is initiated to generate 3' overhangs. After RPA and RAD51 coating of the ssDNA and homology finding, strand invasion is undertaken to form the D-loop. The resolution of this structure can either happen by synthesis-dependent strand annealing (SDSA) which leads to repair by non-crossover (NCO) or by the double Holliday junction (DHJ) model that repair the gap by crossover (CO) of the two strands. Adapted and reprinted from (Bernstein et al. 2011).

There exist five RAD51 paralogs, namely RAD51b, RAD51c, RAD51d, XRCC2, and XRCC3. The paralogs are all required of HR, and depletion of any paralog leads to decreased homologous recombination frequency (Chun et al. 2013). A downregulation of RAD51c due to promoter hypermethylation was found in more than 40 % of gastric cancer cases (Min et al. 2013).

#### 1.4. Aim of the work

Cancer therapies mainly rest on the simple scheme of damaging the DNA of the tumor to induce cell death, while sparing the healthy tissue of the body. Many DNA repair proteins are deregulated in cancer cells, which makes them vulnerable to certain toxins, while non-cancerous cells can repair these DNA lesions. MGMT is a cornerstone in the DNA repair process of DNA alkylation induced during therapy, and its expression is often silenced by promoter methylation in malignant gliomas. The method of classification into responder and non-responder is crucial for preventing further mutational transformation of the tumor in a non-responder as patients with a methylated MGMT status benefit more from TMZ-based treatment.

The first part of this work aimed at developing a method of DNA methylation quantification of the *MGMT* promoter that is superior to commonly used methods regarding speed, accuracy, costs, and predictive value. Therefore, high-resolution melt (HRM) analysis assays should be established and compared to assays based on pyrosequencing (PSQ) and methylation specific PCR (MSP). All three methods were applied on to analyzing DNA methylation from 83 HGA patient samples. The methylation results and their corresponding clinical data were compiled and compared using the Kaplan-Meier estimator method to clarify whether the determination of the *MGMT* promoter methylation status by HRM is better than the PSQ and MSP method in predicting progression free survival (PFS) and overall survival (OS) of high-grade glioma patients.

## Introduction

The second part of this work focused on a frequently mutated enzyme in HGA patients. Patients harboring a tumor that is mutated in the isocitrate dehydrogenase 1 (IDH1) gene display a PFS and OS that is remarkably different from *IDH1* wild-type glioma. It was assumed that either the *IDH1* mutated cells are more sensitive towards the applied TMZ therapy (predictive factor), or that an unknown pathway is affected by 2-hydroxyglutarate (2-HG), which is produced by the mutated IDH1 protein, resulting in decreased aggressiveness (prognostic factor). The working hypothesis was that IDH1mt leads to the production of 2-HG, which will affect the efficiency of the ALKBH2, which is inhibited by 2-HG. To proof or disproof this hypothesis, following questions will be addressed:

- Do IDH1mt cells display an increased sensitivity towards alkylating or oxidizing agents?
- Is this possible phenotype due to the accumulation of the 2-HG metabolite?
- Is this phenotype reproducible in ALKBH2 knock-out cells?
- Which DNA lesion leads to this phenotype?

## 2. Material and Methods

### 2.1. Chemicals and Consumables

Chemicals used for this work were obtained from Carl Roth GmbH & CoKG (Karlsruhe, Germany) and Sigma-Aldrich (Steinheim, Germany). Plastic ware was obtained from Greiner BioOne GmbH (Frickenhausen, Germany) and Eppendorf AG (Hamburg, Germany). Media and media supplements for cell culture were obtained from Gibco / ThermoFischerScientific (Paisley, UK).

### 2.2. Wet laboratory equipment

Description	Commercial Name	Supplier
<sup>137</sup> Cs source	Gammacell 2000	Molsgaard medical, Copenhagen, Denmark
<b>Analytical balances</b>	Sartorius analytical	Sartorius, Göttingen, Germany
<b>Blotting chamber</b>	TransBlot Cell	Biorad, Hercules, CA, USA
<b>Cell disruptor</b>	Sonifier cell disruptor	Branson Ultrasonics, Danbury, CT, USA
<b>Centrifuge</b>	Refrigerated, 5424 R	Eppendorf, Hamburg, Germany
	Hereaus Megafuge1.0	ThermoFisherScientific, Waltham, MA, USA
<b>CO<sub>2</sub> incubator</b>	HeraCell	ThermoFisherScientific, Waltham, MA, USA
<b>Electrophoresis chamber</b>	Tetra Vertical Electrophoresis Cell	Biorad, Hercules, CA, USA
<b>Flow cytometer</b>	FACS CANTO II	BD Biosciences, Heidelberg, Germany
	FACS Calibur	
<b>Heating block</b>	Thermomixer compact	Eppendorf, Hamburg, Germany
<b>Infrared imaging system</b>	Odyssey 9120	LI-COR, Bad Homburg, Germany
<b>Inverted microscope</b>	Axiovert 40 C	Carl Zeiss GmbH, Jena, Germany
<b>Laminar flow cabinet</b>	HERA safe	ThermoFisherScientific, Waltham, MA, USA
<b>Laser scanning microscope</b>	LSM 710	Carl Zeiss GmbH, Jena, Germany
<b>Liquid scintillation analyzer</b>	Tri-Carb 2100TR	Canberra-Packard, Dreieich, Germany
<b>Microplate reader</b>	Multiskan EX	ThermoFisherScientific, Waltham, MA, USA
	Sunrise Microplate Reader	Tecan, Grödig, Austria
	TriStar <sup>2</sup> LB 942	Berthold Technologies, Bad Wildbad, Germany

## Material and Methods

<b>Mini centrifuge</b>	Galaxy Mini	Merck eurolab, Leuven, Belgium
<b>Power supply</b>	PowerPac HC	Biorad, Hercules, CA, USA
<b>Refrigerator / Freezer</b>	Premium NoFrost	Liebherr, Ochsenhausen, Germany
<b>Thermal Cyclers</b>	CFX96 C1000 Real-Time PCR Detection System	Biorad, Hercules, CA, USA
	T100 Thermal Cyclers	
<b>Ultra-low temperature freezer</b>	DF8520GL	Skadi, WR Ede, Netherlands
<b>UV-Vis-Spectrophotometer</b>	NanoDrop 2000	ThermoFisherScientific, Waltham, MA, USA
<b>Vortex mixer</b>	VORTEX 1	VWR, Darmstadt, Germany
	Vortex-Genie	Bender & Hobein GmbH, Ismaning, Germany
<b>Water bath</b>	3044	Köttermann, Uetze/Hänigsen, Germany

### 2.3. Software

<b>Name and version</b>	<b>Source</b>
<b>Ascent Software Version 2.6</b>	Thermo Fisher Scientific, Waltham, MA USA
<b>BD FACSDiva Version 6</b>	BD Biosciences, Heidelberg, Germany
<b>Cell^A</b>	Olympus Soft Imaging Solutions, Münster, Germany
<b>CellQuest Pro</b>	BD Biosciences, Heidelberg, Germany
<b>CFX Manager software 3.1</b>	Biorad, Hercules, CA, USA
<b>ChemSketch</b>	ACD/Labs, Toronto, Canada
<b>EndNote Version X7</b>	Thomson Reuters, New York City, NY, USA
<b>Fiji</b>	
<b>Geneious 6.0</b>	Biomatters, Auckland, New Zealand
<b>GraphPad Prism Version 6</b>	GraphPad Software, La Jolla, CA, USA
<b>ICE software</b>	Berthold Technologies, Bad Wildbad, Germany
<b>Image Studio Lite 5.2</b>	LI-COR, Bad Homburg, Germany
<b>MS Office Version 2013</b>	Microsoft, Unterschleißheim, Germany



## 2.4. Solutions

Solution	Composition / Manufacturer
<b>20 % SDS</b>	20 g of sodium dodecyl sulfate to a final volume of 100ml with water
<b>1 M Tris/HCl</b>	60 g Tris, pH 6.8, add H <sub>2</sub> O to 500 ml (store at 4 C)
<b>1.5 M Tris/HCl</b>	90.83 g Tris, pH 8.8, add H <sub>2</sub> O to 500 ml (store at 4 C)
<b>20x SSC buffer</b>	3 M NaCl, 0.3 M Tri-sodium citrate (Na <sub>3</sub> C <sub>6</sub> H <sub>5</sub> O <sub>7</sub> )
<b>7.5 M NH<sub>4</sub>Ac</b>	28.9 g of Ammonium acetate to a final volume of 50 ml with water
<b>8:1 EtOH:NH<sub>4</sub>Ac</b>	35 ml EtOH (100 %) mixed with 5 ml 7.5 NH <sub>4</sub> Ac
<b>Annexin V PI binding buffer</b>	10 mM HEPES pH 7.4, 140 mM NaCl, 2.5 mM CaCl <sub>2</sub> , 0.1 % bovine serum albumin (BSA) (store at 4 C)
<b>APS 10 %</b>	1 g Ammonium persulfate, 10 ml H <sub>2</sub> O (store at - 20C)
<b>Artesunate</b>	Dafra Pharma, Turnhout, Belgium
<b>Blotting buffer (2.5 L)</b>	250 ml Laemmli stock buffer 5x, 500 ml MeOH, 1750 ml H <sub>2</sub> O
<b>Bradford reagent</b>	8.5 % phosphoric acid, 4.75 % ethanol, 1 % Coomassie Brilliant Blue G250
<b>BSA blocking buffer</b>	5 % nonfat dry milk in TBS-T (store at 4 C)
<b>Casein blocking buffer</b>	0.5 % casein in PBS-T (store at 4 C)
<b>Crack buffer</b>	62.5 mM Tris HCl pH 6.8, 10 % glycerol, 5 % β-mercaptoethanol, 2 % SDS and 0.01 % bromophenol blue (Roti®-Load 1, Roth)
<b>Laemmli stock buffer 5x (1 L)</b>	30 g Tris, 144 g Glycine, add H <sub>2</sub> O to 1 L
<b>LoTe</b>	3 mM Tris, 0.2 mM EDTA, pH 8.0
<b>Milk blocking buffer</b>	5 % bovine serum albumin (BSA) in TBS-T (store at 4 C)
<b>PBS high salt</b>	PBS, 0.4 M NaCl
<b>PBS-T</b>	PBS, 0.1 % Tween-20
<b>Ponceau</b>	0.1 % Ponceau, 5 % acetic acid
<b>RIPA buffer</b>	50 mM Tris-HCl pH 8, 150 mM NaCl, 0.1 % Triton Y-100, 0.5 % sodium deoxycholate, 0.1 % SDS, 1 mM NaVO <sub>3</sub> . 1mM NaF, 1x protease inhibitor cOmplete® (Roche)
<b>Running buffer (1 L)</b>	200 ml Laemmli stock buffer 5x, 5 ml 20 % SDS, add H <sub>2</sub> O to 1 L
<b>Sonication buffer</b>	20 mM Tris-HCl pH 8.5, 1 mM EDTA, 5 % glycerine, 1 mM β-Mercaptoethanol, 10 μM DTT, 1 x protease inhibitor cOmplete® (Roche)
<b>TBS-T</b>	20 mM Tris HCl pH 7.6, 150 mM NaCl, 0.1 % Tween-20

<b>TE buffer</b>	10 mM TRIS ph 8.0, 1 mM EDTA
<b>TE9 buffer</b>	50 mM Tris, 20mM EDTA, 10mM NaCl
<b>Temozolomid</b>	Schering-Plough, Kenilworth, New Jersey, USA
<b>Tris-NaCl buffer</b>	0.1 M TRIS HCl ph 7.5, 2 mM MgCl <sub>2</sub> , 1 M NaCl, 0.05 % Triton X-100

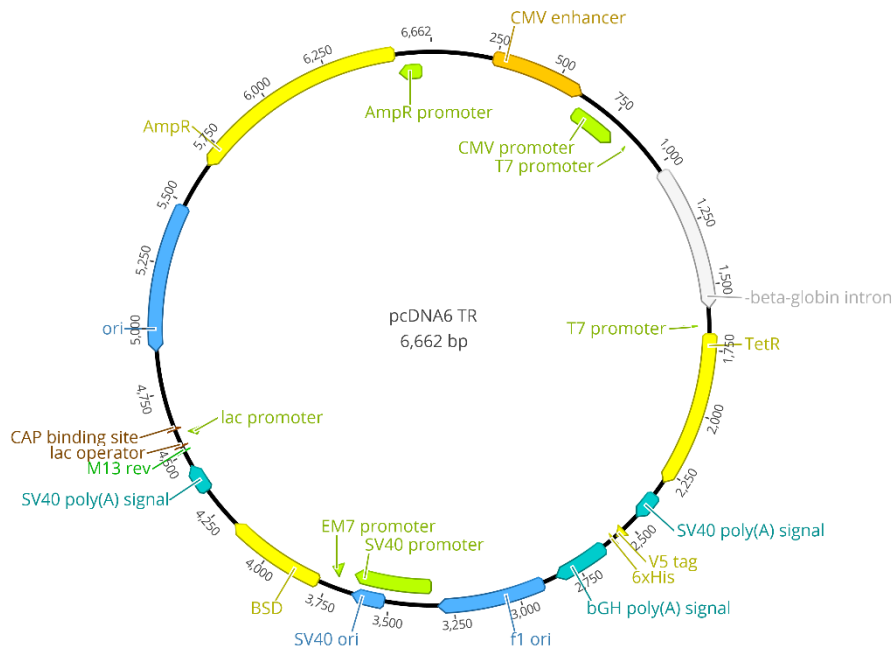
### 2.5. Cell culture

Human malignant glioblastoma cell lines used for the MGMT promoter methylation quantification project were all cultured in DMEM (Gibco) supplemented with 10 % fetal calf serum (Gibco) and grown at 37 °C, 5 % CO<sub>2</sub> and were the following: LN229, T98G, LN18, GBP44, GBP61, LN319, U87, U251, U373, U343MG, U138, LN308, A172, D247, and U118 (Table 4).

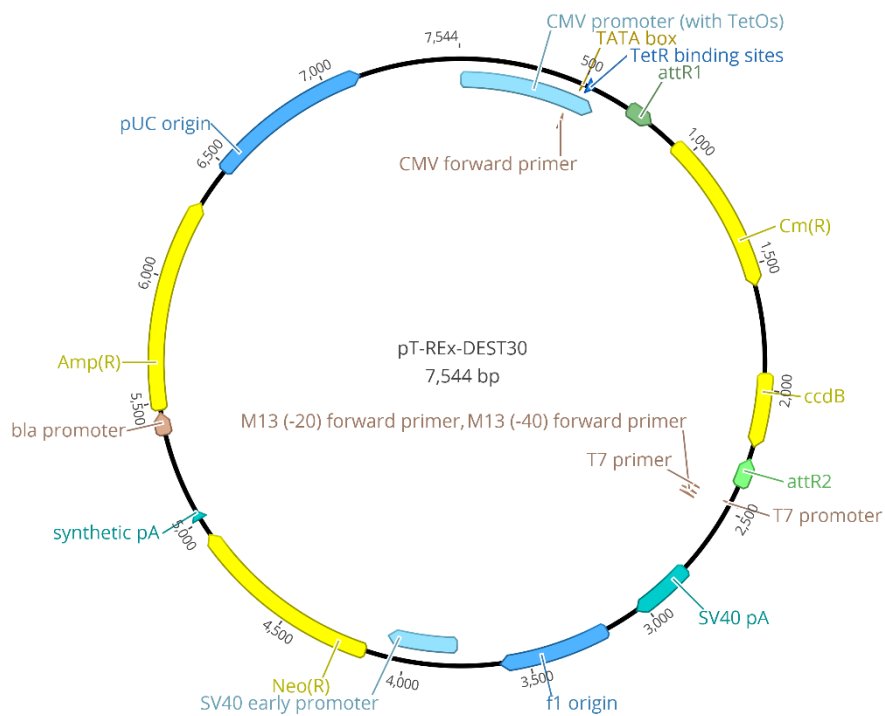
**Table 4** Characteristics of the parental cell lines used in this study.

<b>Cell line</b>	<b>Tissue origin</b>	<b>p53</b>	<b>PTEN</b>	<b>MGMT status</b>	<b>comment</b>
<b>LN229</b>	Glioblastoma	Functional	wild-type	deficient	
<b>T98G</b>	Glioblastoma	Mutant	mutant	proficient	
<b>LN18</b>	Glioblastoma	Mutant	wild-type	proficient	
<b>GBP44</b>	Glioblastoma	Unknown	unknown	proficient	
<b>GBP61</b>	Glioblastoma	Unknown	unknown	proficient	
<b>LN319</b>	Glioblastoma	Mutated	mutant	deficient	
<b>U87</b>	Glioblastoma	Functional	mutant	deficient	
<b>U251</b>	Glioblastoma	Mutant	mutant	deficient	
<b>U373</b>	Glioblastoma	Mutant	mutant	deficient	
<b>U343MG</b>	Glioblastoma	Functional	mutant	deficient	
<b>U138</b>	Glioblastoma	Mutant	mutant	deficient	
<b>LN308</b>	Glioblastoma	Mutant	mutant	deficient	
<b>A172</b>	Glioblastoma	Functional	mutant	deficient	
<b>D247</b>	Glioblastoma	Functional	mutant	deficient	
<b>U118</b>	Glioblastoma	Mutant	mutant	proficient	
<b>A375</b>	malignant melanoma	Functional	wild-type	proficient	BRAF V600E mutation
<b>HaCaT</b>	Keratinocyte	Mutant	wild-type	proficient	

The tet-inducible LN319 human glioblastoma cell lines, expressing either wt IDH1, R132H mt IDH1, or vector control were a kind gift of Dr. Stefan Pusch (DKFZ, Heidelberg, Germany) and were characterized previously (Birner et al. 2014). Briefly, the LN319 cell line was transfected with the tet-on vector pcDNA6/TR (ThermoFisher, **Figure 14**) which also expresses the Blastocidin resistance gene for selection purposes. The pcDNA6/TR vector expresses high levels of the tetracycline repressor (TetR) under the control of the human cytomegalovirus promoter (CMV). TetR binds to the tetracycline-responsive promoter (TRP) containing the tetracycline operator (TetO) of the second plasmid, followed by the transgene and suppresses its expression. In the presence of doxycycline (dox), TetR will bind to the freely available dox and will not bind to the promoter, permitting transcription (Hillen and Berens 1994). Wild-type *IDH1* (wt) and *IDH1*R132H (mt) were subcloned using the Gateway<sup>®</sup> system (Invitrogen) into the pt-Rex-DEST30 destination plasmid (**Figure 15**). The inserts are under control of a CMV promoter with TetO containing the TetR binding sites. LN319 cells (wt, mt) were maintained in DMEM (Gibco) supplemented with 5 % tet-system approved fetal bovine serum (Cloneteck) in the presence of Geneticin (4 mg/ml), and Blastocidin (80 µg/ml). LN319 mock cells only contain the pcDNA6/TR vector and were maintained only the presence of Geneticin (4 mg/ml). For experimental procedures, cells were always incubated with 1 µM dox (Sigma) unless otherwise stated.



**Figure 14: The tet-on pcDNA6/TR plasmid, which provides high expression of the tetra-cycline repressor (TetR) protein.**



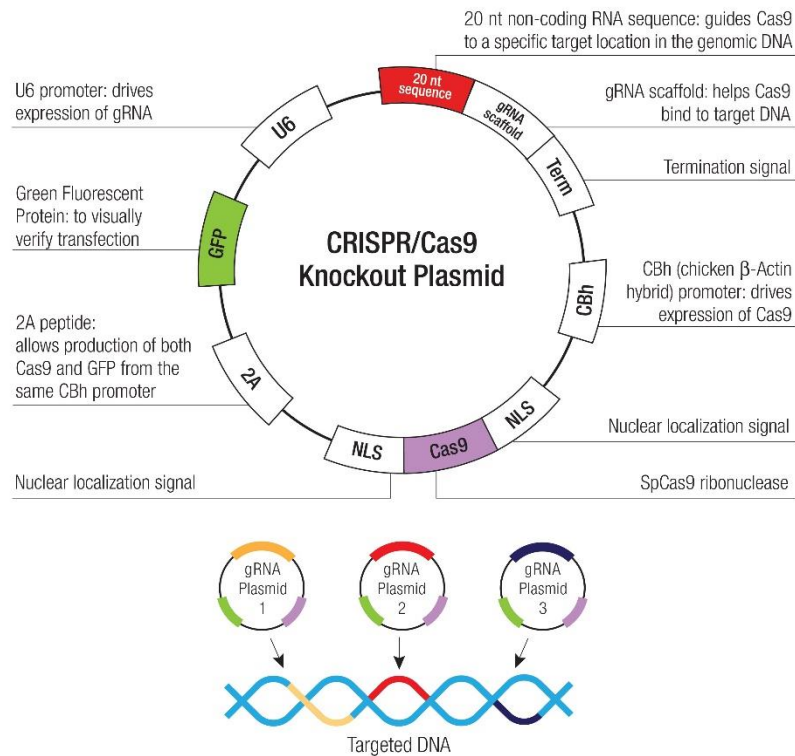
**Figure 15: The pT-Rex-DEST30 plasmid. *IDH1*wt and *IDH1*R132H were subcloned using the recombination sites (attR1 and attR2) that flank a gene for negative selection (*cccB*) whose product is lethal for bacterial cells.**

LN18, T98G, and the corresponding ALKBH2 knock-out clone cell lines (T98G D7, LN18 D11, LN18 G5, LN18 D7) were maintained in DMEM (Gibco) supplemented with 5 % fetal bovine serum (Gibco). ALKBH2 knock-out was performed using the ALKBH2 CRISPR/Cas9 KO Plasmids (**Figure 16**) (Santa Cruz Biotechnology) which consists of three plasmids, each harboring a different gRNA (**Table 5**) that targets the second or third exon of the ALKBH2 gene and a GFP marker. LN18 and T98G cells were transfected using Effectene (Qiagen) and collected after 48 h. GFP positive cells were single cell sorted on a FACS Aria III SORP CellSorter (BD Biosciences) and seeded into 96-well plates with 50  $\mu$ l complete medium and additional sodium pyruvate. Cell clones were expanded, and successful ALKBH2 knock-out was assayed by western blot.

**Table 5: The ALKBH2 CRISPR/Cas9 knock-out** sc-407363 (Santa Cruz) is performed with a pool of three different plasmids, each harboring different gRNAs

Plasmids	rRNA sequence 5'-3'
sc-407363A1:	CAGGCAACGTATGGCGACGC
sc-407363A2:	TGTGCCACTTCCCGAATACC
sc-407363A3:	TCCCACGGGAATCCTTATGC

## Material and Methods



**Figure 16: Cartoon of the ALKBH2 CRISPR/Cas9 knock-out plasmids (sc-407383; Santa Cruz).**

### 2.6. Patients and treatments

Paraffin-embedded tumor samples were studied from 83 high-grade (WHO grade III and IV) glioma patients treated at the Neurosurgical Center at the Medical University of Mainz, Germany. Tumor specimens were obtained before radio-chemotherapy, formalin fixed and paraffin embedded. DNA was extracted according to standard protocols. All patients provided written informed consent. The study was approved by the institutional ethics committee of the University Medical Center Mainz. Therapy regimen: All patients received combined radio-chemotherapy with temozolomide according to the EORTC regimen (Stupp et al. 2005; Stupp et al. 2009). In the case of tumor progression, second-line therapy was administered, e.g. dose-dense temozolomide, CCNU or bevacizumab. Two patients were lost to follow-up after the first progress.

## 2.7. Methylation quantification assays

### 2.7.1. DNA extraction

DNA from cell lines and FFPE patient tumor sections was extracted using the phenol/chloroform (Sambrook and Russell 2006) method. Briefly, 300  $\mu$ l of freshly prepared 1 % SDS-PK mix (16  $\mu$ l SDS 20 %, 304  $\mu$ l TE9 buffer, 8  $\mu$ l proteinase K (25 mg/ml)) was added to each sample and incubated over night at 48 °C at constant shaking (1100 rpm). 5  $\mu$ l of additional proteinase K was added and incubated at RT for 2 h. 700  $\mu$ l of PC (Roti®-Phenol/Chloroform/Isoamyl alcohol) was added to each sample and vortexed for 15 sec and centrifuged for 5 min at 14000 rpm. The upper aqueous phase is transferred to a new tube, and 700  $\mu$ l of PC is added, then vortexed and centrifuged, as described before. The upper aqueous phase is transferred to a new tube 750  $\mu$ l of 8:1 EtOH:NH<sub>4</sub>Ac mix is added. Tubes are inverted 4 times and left at RT for 1 h. Samples are centrifuged for 45 min at 14000 rpm at 4 °C. The supernatant is discarded by pipetting, and the pellet is washed with 1 ml 70 % Ethanol. Samples are centrifuged at 14000 rpm at RT for 15 min. The supernatant is discarded by pipetting. After drying for 10 min, the pellet is resuspended in 50  $\mu$ l LoTe or ddH<sub>2</sub>O, DNA content is measured spectrometrically (Nanodrop) and then stored at -20 °C.

### 2.7.2. DNA standards

Buccal swap DNA from a healthy female donor was used to generate DNA standards. 50 ng of DNA was used for whole genome amplification using the REPLI-g midi kit (Qiagen) to generate the unmethylated standard DNA. The reaction was performed according to the manufacturer's instructions. An aliquot of 100  $\mu$ g was in vitro methylated with 400 U SssI methylase and 640  $\mu$ M SAM (NEB) according to the manufacturer's instructions. After 4 h at 37 °C, additional SAM and 50 units of SssI methylase were added and incubated overnight at 37 °C to ensure complete methylation. Both methylated and unmethylated standard DNA were purified by phenol-chloroform extraction followed by ethanol precipitation, suspended in DNase-free water and stored at -80 °C.

## Material and Methods

### 2.7.3. Bisulfite treatment

500 ng of DNA underwent bisulfite treatment using the EZ DNA Methylation-kit (ZymoResearch) according to the manufacturer's protocol to convert all unmethylated cytosine to uracil while leaving 5-methylcytosine unaltered and was then eluted in 20 µl of DNase-free water. DNA methylation of the MGMT promoter was analyzed by MSP, pyrosequencing (PSQ) and HRM.

### 2.7.4. Analysis of the MGMT promoter methylation by MSP

For MSP of the MGMT promoter, we used primers previously described (Esteller et al. 2000). The method was carried out as described previously (Christmann et al. 2010). Briefly, The MSP reactions were routinely prepared in a total volume of 20 µl using Hot-StarTaqPlus® Master Mix Kit (Qiagen). For PCR, 2 µl of bisulfite-modified DNA (100 ng) was mixed with 2 µl Coraload (Qiagen) and both primers to a concentration of 500 nM and subjected to 37 PCR cycles with denaturation at 95 °C for 30 s, primer annealing at 59 °C for 30 s, extension at 72 °C for 15 s and a final extension for 10 min at 72 °C. PCR product were separated on an ethidium bromide stained 2 % agarose gel and visualized using a UV Transilluminator. The sample was classified as methylated when both bands or just the methylated band was visible. The classification was carried out binary, MGMT unmethylated and MGMT methylated, respectively. The investigator was blinded for all clinical information.

### 2.7.5. Analysis of the MGMT promoter methylation by high-resolution melt (HRM) curve analysis

A search for CpG islands in the *MGMT* promoter was performed using the Geneious 6 software (Biomatters). For the HRM of the *MGMT* promoter, we used methylation independent primers (r4 fwd: 5'-GGATATGTTGGGATAGTT- 3' and r4 rev: 5'-CCCAAACAC-TCACCAAAT-3') without a CpG site in it to avoid biased amplification (**Table 7**). Four sets of primers were designed using the Pyromark assay Designer 2.0 (Qiagen). Region r2 and r4 include the binding sites of the MSP primers published by Esteller et al. (Esteller et al. 2000). PCR amplification and HRM analyses were performed using a CFX96 real-time PCR system (BioRad). Each PCR was performed in a final volume of 15 µl, containing 7.5 µl precision melt supermix (BioRad), 400 nM of each primer, and 20 ng of bisulfite-converted DNA (theoretical concentration presuming no loss of DNA during bisulfite modification).



PCR amplification was performed with one step of 95 °C for 2 min, 45 cycles of 95 °C for 10 s, 54 °C for 30 s, and 72 °C for 15 s; followed by an HRM step of 95 °C for 30 s, 60 °C for 1 min, 70 °C for 10 s, and continuous acquisition to 90 °C at one acquisition per 0.2 °C. For cell lines, each reaction was performed in technical duplicates of biological triplicates, and in technical duplicates for the patient's samples. Fully methylated and unmethylated bisulfite-converted DNA was mixed to obtain the following ratios of methylation: 2.1, 24.3, 46.4, 68.6, and 90.8 % (theoretically 0, 25, 50, 75, and 100 %) and were included in duplicates in each assay, as well as a non-template control and a genomic DNA control. Commercially available bisulfite converted DNA standards (Qiagen) were analyzed together with our internal DNA standards. HRM data were analyzed using Bio-Rad Precision Melt Analysis software (BioRad), with output plots produced as normalized melting curves. Normalized relative fluorescence units (RFUs) were exported to Prism 6 (GraphPad). The area under the curve (AUC) was calculated, and the linear regression was used to interpolate the unknown samples from the standards.

#### 2.7.6. Analysis of the MGMT promoter methylation by pyrosequencing

Pyrosequencing is a method of sequencing based on the "sequencing by synthesis" principle. First, a regular endpoint PCR is performed to amplify the sequence, harboring the region of interest. The reverse primer used for PCR is biotinylated at the 5' end, which enables to bind the PCR products to Streptavidin Sepharose High-Performance beads (GE Healthcare). After the PCR, 3 µl of Streptavidin Sepharose High-Performance beads are added to each PCR well together with 40 µl of 2x Binding Buffer (Qiagen) and DNase free water. The plate is shaken for 5 min to maintain dispersion of the beads. 300 nM sequencing primer in 15 µl of 1x Annealing Buffer (Qiagen) is pipetted into wells of the pyrosequencing reaction plate and placed into the Vacuum Workstation (Qiagen) together with the PCR plate. The Vacuum prep tool is lowered into the PCR plate to aspirate all liquid. The bead bound PCR products remain on the surface of the filter tips. After washing with 70 % ethanol, denaturation buffer, and wash buffer, the now single stranded bead bound DNA is released into the prepared pyrosequencing plate (see above) which is then placed into the Pyrosequencer (Qiagen).

It differs from Sanger sequencing, as it does not rely on the chain termination with dideoxynucleotides, but rather on the detection of pyrophosphate released upon nucleotide

## Material and Methods

incorporation. The desired DNA sequence is able to be determined by light emitted upon incorporation of the next complementary nucleotide by the fact that only one out of four of the possible A/T/C/G nucleotides are added and available at a time so that only one base can be incorporated into the single stranded template (which is the sequence to be determined). The intensity of the light determines if there are more than one of these bases in a row. The previous nucleotide is degraded before the next nucleotide is added for synthesis. This process is repeated with each of the four nucleotides until the DNA sequence of the single stranded template is determined. The main limitations of this method are that the lengths of reads are rather short (200 bp is an excellent value) and the missing multiplex ability, as only one target sequence is analyzed.

The DNA methylation standards and patients DNA were analyzed by PSQ to quantify their methylation content. PCR was performed using the PyroMark Q96 CpG MGMT kit (Qiagen) according to manufacturer's instructions. The samples were then processed in the PyroMark Q96 ID instrument (Qiagen), and the obtained data were analyzed by PyroMark CpG Software. Patients were dichotomized upon a mean methylation level threshold of 8 % according to previous studies (Felsberg et al. 2011; Reifenberger et al. 2012; Berghoff et al. 2015). To further validate the methylation values of the HRM assay, we performed pyrosequencing for the whole HRM amplicon on a Pyromark Q24 advanced (Qiagen) for 38 patient samples and the DNA standards. The forward primer was also used as a sequencing primer (**Table 8**). The unmethylated DNA standard was methylated to the extent of 2.1 %, and the methylated DNA standard showed 90.8 % mean methylation at the MGMT promoter region. These values were taken for the linear regression analysis of data obtained by HRM (see above).

2.7.7. Analysis of the *ATM*, *BRCA1*, *BRCA2*, *EGFR*, *LINE1*, *MBD4*, *MLH1*, and *RAD51c* promoter methylation by high-resolution melt (HRM) curve analysis

A search for CpG islands in the promoter regions of this DNA repair enzyme coding genes was performed using the Geneious 6 software (Biomatters).

**Table 6: Eight gene promoter were analyzed by HRM assays** covering 25 regions in total.

Promoter of gene	Primer sets
<i>ATM</i>	2
<i>BRCA1</i>	2
<i>BRCA2</i>	3
<i>EGFR</i>	2
<i>LINE1</i>	3
<i>MBD4</i>	1
<i>MLH1</i>	5
<i>RAD51c</i>	7

The PCR reactions were analogous to the MGMT HRM assay. The exact primer sequences and annealing temperatures are listed in **Table 7**.

## 2.8. SNP detection by pyrosequencing

### 2.8.1. *IDH1* R132H mutation detection by pyrosequencing

The *IDH1* mutational status was determined by immunohistochemistry using an anti-*IDH1* R132H antibody (Dianova). We further validated the results by pyrosequencing in all samples using primers published previously on the Pyromark Q96 ID instrument (Cykowski et al. 2012). For PCR, 1 µl of genomic DNA (100 ng) was mixed with 2x Master Mix, Coraload, RNase-Free Water from the PyroMark PCR Kit (Qiagen) and primer (400 nM) (**Table 8**). The samples were subjected to 45 PCR cycles with denaturation at 95 °C for 15 min, primer annealing at 60 °C for 30 s, extension at 72 °C for 15 s and a final extension for 10 min at 72 °C. PCR product were separated on an ethidium bromide stained 2 % agarose gel and visualized using a UV Transilluminator.

## Material and Methods

### 2.8.2. BRAF V600E mutation detection by pyrosequencing

The BRAF V600E status of all glioma patients was analyzed by pyrosequencing. The cell line A375 was taken as a positive control for the mutational status. The BRAF V600E mutation is a heterozygous GTG->GAG SNP. For PCR, 1 µl of genomic DNA (100 ng) was mixed with 2x Master Mix, Coraload, RNase-Free Water from the PyroMark PCR Kit (Qiagen) and primer (400 nM) (**Table 7**). The samples were subjected to 45 PCR cycles with denaturation at 95 °C for 15min, primer annealing at 64 °C for 30 s, extension at 72 °C for 15 s and a final extension for 10 min at 72 °C. PCR product were separated on an ethidium bromide stained 2 % agarose gel and visualized using a UV Transilluminator.

For PCR, 1 µl of genomic DNA (100 ng) were mixed with 2x Master Mix, Coraload, RNase-Free Water from the PyroMark PCR Kit (Qiagen) and primer (400 nM). The samples were subjected to 45 PCR cycles with denaturation at 95 °C for 15 min, primer annealing at 64 °C for 30 s, extension at 72 °C for 15 s and a final extension for 10 min at 72 °C. PCR product were separated on an ethidium bromide stained 2 % agarose gel and visualized using a UV Transilluminator.

### 2.9. Primer sequences

**Table 7: Primers used for HRM analysis**

Name	Sequence 5'->3'	Ta C°	Amplicon length	CpGs	Location from ATG	successful primer set
hrmR1MGMTfwd	GGGTTATTTGG-TAAATTAAGGTA TAGA	54	392	50	-378 to -352	no
hrmR1MGMTrev	AAC-TATCCCAACAT-ATCC				-4 to +14	no
hrmR2MGMTfwd	GATTTGGTGAG-TGTTTGG	58	219	16	+76 to +93	no
hrmR2MGMTrev	CAAC-CTAATCCAAAAA CCCC				+275 to +294	no
hrmR3MGMTfwd	GGTTT-GGGGGTTTTT-GAT	56	199	21	-579 to -562	yes
hrmR3MGMTrev	ACCTTTTCC-TATCACAAAAA-TAATC				-405 to -381	yes
hrmR4MGMTfwd	GGATATGTTGG-GATAGTT	54	98	12	-4 to +14	yes

hrmR4MGMTrev	CCCAAACAC- TCACCAAAT				+77 to +94	yes
hrmR1MLH1fwd	AAGTATTTATTG GGTAG- GATGAGG	56	323	8	-7177 to -7154	no
hrmR1MLH1rev	TCTCCAC- TACAAC- CTCCTAAA- TAACT				-6855 to -6881	no
hrmR3MLH1fwd	GATA- GATTAGGTATA GGGTTTTAT	56	196	11	-597 to -574	yes
hrmR3MLH1rev	CTTCTCAAACCTC CTCCTCTC				-402 to -421	yes
hrmR4MLH1fwd	GGTATTTTT- GTTTTTATTGGT TGGATATT	56	186	11	-339 to -311	yes
hrmR4MLH1rev	AATAC- CAATCAAATTC TCAACTCTAT				-154 to -180	yes
hrmR5MLH1fwd	AG- GTGATTGGTT- GAAGGTATTT	56	182	13	-65 to -44	yes
hrmR5MLH1rev	CCAATTCTCAAT CATCTCTTTAA- TAACAT				+ 116 to +88	yes
hrmR7MLH1fwd	TTTTTAGGAG- TGAAGGAGGTT A	56	180	23	-755 to -733	yes
hrmR7MLH1rev	AAAACCCTATAC CTAATCTATC				-576 to -597	yes
hrmR2RAD51cfw d	ATGGTG- TA- TAAGTGAAAA	56	346	28	-171 to -143	no
hrmR2RAD51crev	ATAC- CTCAACTTAC- CATCAAAAATC				+174 to +150	no
hrmR3RAD51cfw d	GATTGTTGAG- GAATTTTA- GAGGTGAAATT	56	229	14	+98 to +127	no
hrmR3RAD51crev	ATTCTCCTAAC- CATTCAAACAAC T				+326 to +303	no
hrmR4RAD51cfw d	TAAGTTAGGTA GGTTATGAA- GAAATA	56	136	9	-689 to -664	no
hrmR4RAD51crev	AATTATAAAC- CAACCCCAAC				-554 to -574	no

## Material and Methods

hrmR5RAD51cfwd	GTTGGGGTT-GGTTTATAATT	56	119	14	-574 to -554	no
hrmR5RAD51crev	CTTTATAAAATT ACAATCTCTTAA CTCTTCC				-453 to -483	no
hrmR6RAD51cfwd	ATGGTG- TA- TAAGTGTGAAA	56	169	16	-171 to -143	yes
hrmR6RAD51crev	CAAACCTCAC- CTACTAACCC				-3 to -21	yes
hrmR1BRCA1fwd	GTATTTTGA- GAGGTTGTTGTT	56	148	11	-1374 to -1354	yes
hrmR1BRCA1rev	TAAAAAACCCCA CAACCTAT				-1246 to -1227	yes
hrmR1BRCA2fwd	TGGTTTGGGAT- TTTTAAGGGTTA	56	339	31	-1188 to -1166	no
hrmR1BRCA2rev	ATCACAAATCTA TCCCCTCAC				-850 to -870	no
hrmR4BRCA2fwd	GTGAGGGGA- TAGATTTGTGAT	56	97	5	-870 to -850	yes
hrmR4BRCA2rev	CCACTACCAC- CACCCTA				-774 to -791	yes
hrmR5BRCA2fwd	TGGGATGTTT- GATAAGGAATT	56	73	3	-1110 to -1090	yes
hrmR5BRCA2rev	AAAATCAAAC- CTAAATAAACC				-1038 to -1058	yes
hrmR2MBD4fwd	GGGAAAGTTA- GAAAAGTAG- TAAAAGTAATG	56	359	31	-147 to -171	yes
hrmR2MBD4rev	ATCCCCAAACT CAAACCTCTC				-671 to -695	yes
hrmR1ATMfwd	AGAGGGTGGGT GAGAGTT	56	126	13	-4812 to -4794	yes
hrmR1ATMrev	AAACAC- TACCCCAAACA TTC				-4686 to -4706	yes

**Table 8: Primers used for pyrosequencing analysis**

Name	Sequence 5'->3'	Ta C°	Amplicon length	CpGs	Location from ATG
hrmR4MGMTfwd_pyro	GGATATGTTGGGTAGTT	56	98	12	-4 to +14
hrmR4MGMTrev_pyro	CCCAAACACTCACAAAT -Biotin				+77 to +94
IDH1fwd_pyro	AAATATCCCCGGCTTG	60	88	SNP	+3113 to +3129
IDH1rev_pyro	TTGCCAACATGACTTACTTGATC- Biotin				+3178 to +3200
IDH1seq_pyro	GGGTAAAACCTATCATCATA				+3140 to +3159
BRAFfwd_pyro	TAGGTGATTTGGTCTAGC- TACAG	64		SNP	+171344 to +171367
BRAFrev_pyro	CTAGTAACTCAGCAG- CATCTCAGG				+ 171471 to +171494
BRAFseq_pyro	TGATTTTGGTCTAGCTACA				+ 171348 to +171366

## 2.10. Cell survival assays

### 2.10.1. Evaluation of cell viability using the MTT assay

Measurement of cell viability and proliferation forms the basis for numerous *in vitro* assays of a cell population's response to external factors. The reduction of tetrazolium salts is now widely accepted as a reliable way to examine cell proliferation. The yellow tetrazolium MTT [3-(4,5-dimethylthiazolyl-2)-2,5-diphenyltetrazolium bromide] is reduced by metabolically active cells, in part by the action of dehydrogenase enzymes, to generate reducing equivalents such as NADH and NADPH. The resulting intracellular purple formazan can be solubilized and quantified by spectrophotometric means.

For all MTT assays performed in this work, the following protocol has been applied. Cells were seeded at least 24 h before treatment in 96 well plates (Greiner) in 200 µl of appropriate medium in densities listed in **Table 9**.

**Table 9: Cell seeding densities** used for the MTT assay per well and for each incubation time. LN319 cells had to be seeded denser, as they are smaller compared to the other used cell lines.

Incubation time	LN319	All other cells
24 h	15000	12000
48 h	7000	6000
72 h	3500	3000
96 h	2000	1500
120 h	1200	800

For the measurement, cell culture medium was discarded and replaced with 100 µl DMEM without phenol red containing 0.5 mg/ml MTT and plates were incubated for 3.5 h. The medium was then discarded, and the formazan crystals were solubilized with 100 µl acidified isopropanol (0.04 N HCl). The plate was paced on a rocking shaker (400 rpm), and absorbance was measured at 570 nm on a TriStar2 LB 942 multimode reader (Berthold, Bad Wildbad, Germany). Viability was computed after normalization to control cells.

#### 2.10.2. Propidium iodide staining

Propidium iodide enters ethanol-fixed cells and intercalates into DNA, which multiplies its fluorescence and therefore allows measurement of a cell's DNA content by flow cytometry. A typical cell cycle profile of unperturbed cells shows a G1 (2n) and G2-peak (4n). The G2-peak shows double the fluorescence intensity of the G1 peak and S-phase cells show fluorescence intensities between the G1 and the G2 peaks. Cells with a sub-diploid DNA content are regarded as apoptotic due to DNA fragmentation and degradation during apoptosis (Krishan 1975; Nicoletti et al. 1991).

Cells were detached and combined with the cells in the supernatant medium and sedimented as described earlier. Then, cell sediments were resuspended in 20 µl PBS and fixed with ice-cold 80 % ethanol by adding 1 ml of the ethanol while vortexing. Samples were stored at -20 °C awaiting staining. To this end, 2 ml of PBS were added to the cell suspension and cells were sedimented by centrifugation (5 min, 1500 x g). Cells were resuspended in PBS containing RNase A (30 µg/ml working concentration, 10 mg/ml in H<sub>2</sub>O stock concentration stored at -20 °C). RNA digestion was performed for 30 min at room



temperature (RT). Propidium iodide (working concentration of 25  $\mu\text{M}$ , stock concentration 50  $\mu\text{g}/\text{ml}$  in PBS at 4  $^{\circ}\text{C}$ ) was added to the cell suspension and kept in the dark and on ice until analysis by flow cytometry (maximum 30 min). Apoptosis measurement by Sub-G1 content was analyzed using BD FACSDiva™ software, and cell cycle distribution was analyzed using ModFit LT™ software.

#### 2.10.3. Annexin V-FITC/Propidium iodide double-staining

An early event in apoptosis is flipping of phosphatidylserine from the inner cytoplasmic facing membrane to the outer cellular facing membrane, which marks the cell for phagocytosis by macrophages. AnnexinV binds to phosphatidylserine on the cell surface, but also to intracellular phosphatidylserine if the membrane integrity is lost. Membrane integrity is lost in cells undergoing necrosis or when apoptosis has progressed beyond the point where macrophages would have removed them from the cell population in a physiological environment. To discriminate between apoptotic cells and necrotic/late apoptotic cells, the DNA intercalator PI is added to the cells. PI is excluded from viable cells but not from dead cells and, therefore, marks late apoptotic or necrotic cells (Vermes et al., 1995).

Cells were detached and collected as described and washed with 1 ml PBS. For binding of AnnexinV-FITC, sedimented cells were resuspended in 50  $\mu\text{l}$  binding buffer (10 mM 4-(2-hydroxyethyl)-1-piperazineethanesulfonic acid [HEPES] pH 7.4, 140 mM NaCl, 2.5 mM  $\text{CaCl}_2$ , 0.1 % bovine serum albumin [BSA]) containing 2.4  $\mu\text{l}$  AnnexinV-FITC (Miltenyi, Bergisch Gladbach, Germany). After 20 min incubation on ice and in the dark, PI (in 430  $\mu\text{l}$  binding buffer) was added, yielding a final concentration of 1.5  $\mu\text{M}$  PI. Cells were kept in the dark and on ice until flow cytometry analysis. Data were analyzed using BD FACSDiva™ software. Double-negative cells were regarded as viable, FITC-only positives were regarded as apoptotic and FITC/PI double-positives were regarded as late apoptotic/necrotic.

#### 2.10.4. iCELLigence real-time cell analysis system

The real-time cell analysis (RTCA) iCELLigence instrument (Roche) together with two 8-well E-Plates (ACEA Biosciences) is an impedance-based system for cell-based assays, allowing for label-free and real-time monitoring of cellular processes such as cell growth,

## Material and Methods

proliferation, and cytotoxicity. The dimensionless parameter Cell Index (CI) represents the cell status and is directly proportional to number, proliferation, size, morphology, and attachment of cells. The iCELLigence RTCA Station was kept in an incubator at 37 °C and 7 % CO<sub>2</sub>.

### 2.11. Protein analysis

#### 2.11.1. Total protein extraction by sonication

Cells were washed with PBS, trypsinized and sedimented by centrifugation at 4 °C. The pellet was transferred to a 1.5 ml tube and flash frozen in liquid nitrogen. Pellets were stored at -20 °C (< 10 days) until protein extraction. For protein extraction, cells were resuspended in “sonication buffer” (20 mM TRIS-HCl pH 8.5, 1 mM EDTA, 5 % glycerine, 1 mM β-Mercaptoethanol, 10 μM DTT, 1 x protease inhibitor cOmplete® (Roche)). The suspension was sonicated on ice (2x 10 pulses at duty cycle 40 % and output control 5) and then centrifuged (10 min, 4 °C, 14000 rpm). The supernatant containing the dissolved proteins was stored at -20 °C.

#### 2.11.1. Protein extraction using RIPA buffer

Cells were washed with PBS, trypsinized and sedimented by centrifugation at 4 °C. The pellet was transferred to a 1.5 ml tube and flash frozen in liquid nitrogen. Pellets were stored at -20 °C (< 10 days) until protein extraction. For protein extraction, cells were resuspended in 100 -200 μl RIPA (Radio-Immunoprecipitation assay) lysis buffer (25 mM TRIS-HCl pH 8, 5 mM EDTA, 1 mM PMSF, 1 mM Na<sub>3</sub>VO<sub>4</sub>, 0.5 % NP40, 0.5 mM NaCl, 1 x protease inhibitor cOmplete® (Roche)) and were kept under constant agitation for 30 min at 4 °C and centrifuged for 20 min at 4 °C at 12.000 rpm. The supernatant containing the dissolved proteins was stored at -20 °C.

#### 2.11.2. Protein extraction using cracking buffer

For the analysis of large (> 200 kDa) or phosphorylated proteins, the cell monolayer was washed with PBS in the culture dish and the PBS was completely removed. Cells were lysed directly on the plate by addition of sodium dodecyl sulfate (SDS) sample loading buffer (62.5 mM TRIS HCl pH 6.8, 10 % glycerol, 5 % β-mercaptoethanol, 2 % SDS and 0.01 % bromophenol blue) with agitation and using a cell scraper. Lysates were

transferred into microfuge tubes, sonicated (2x 10 pulses at duty cycle 40 % and output control 5) and then centrifuged (10 min, 4 °C, 14000 rpm). The supernatant containing the dissolved proteins was stored at -20 °C.

#### 2.11.3. Protein concentration determination

The protein concentration in extracts was measured by the Bradford method, which is based on an adsorption shift of free Coomassie Brilliant Blue to protein bound Coomassie Brilliant Blue (Bradford 1976). A calibration curve of BSA (1 mg/ml in ddH<sub>2</sub>O) was pipetted into a 96 well plate ranging from 0-7 µg BSA per well. Likewise, 10 µl of pre-diluted protein samples (1:5 in ddH<sub>2</sub>O) were loaded on the plate and stained with 200 µl of Bradford reagent (8.5 % phosphoric acid, 4.75 % ethanol, 1 % Coomassie Brilliant Blue G250). Samples and calibration standards were performed in technical duplicates. After 10 min of incubation in the dark, adsorption was measured at 595 nm.

#### 2.11.4. Semi-quantitative measurement of protein concentration

Relative protein amounts of extracts obtained by direct lysis of cells in SDS-loading buffer (2.11.2) were determined by densitometry analysis of loading controls ( $\beta$ -Actin, GAPDH, or HSP90) as measured by SDS polyacrylamide gel electrophoresis (SDS-PAGE), western blotting and detection (2.11.5 and 2.11.6). After quantification of loading controls by densitometry, the volume loaded onto gels was adjusted to obtain equal relative protein amounts. The absence of regulation of the loading control proteins by the treatment was verified by blots performed with Bradford-quantified protein extracts.

#### 2.11.5. Sodium dodecyl sulfate polyacrylamide gel electrophoresis

SDS-PAGE allows separation of proteins by their size. SDS sample buffer was added to each sample (unless SDS sample buffer was used for cell lysis as described in section 2.11.2), denatured at 95 °C (for 5 min) or 56 °C (for 10 min) for proteins > 200 kDa. Depending on protein abundance, an amount of 30 - 100 µg of protein was loaded onto gels for electrophoresis. Proteins were firstly concentrated in the stacking gel (126 mM TRIS HCl pH 6.8, 4 % Acrylamide/Bisacrylamide, 0.1 % SDS, 0.1 % ammonium persulfate, 0.1 % TEMED) and then electrophoretically separated in the separating gel (375 mM TRIS HCl pH 8.8, 5 - 15 % Acrylamide/Bisacrylamide, 0.1 % SDS, 0.05 % ammonium persulfate, 0.05 % TEMED). Electrophoresis was performed between 50 and 120 V in running buffer

## Material and Methods

(50  $\mu$ M TRIS, 384 mM glycine, 0.1 % SDS). Protein ladders (protein-marker IV, Peqlab, Erlangen, Germany or Spectra™ Multicolor High Range Protein Ladder, ThermoFisherScientific, Waltham, MA, USA) were used in parallel to protein samples to allow size comparison after blotting.

### 2.11.6. Immunoblotting

Transfer of SDS-PAGE separated proteins onto a nitrocellulose membrane (Protran, Amersham, GE Healthcare, Dassel, Germany) was performed in blotting buffer (50  $\mu$ M TRIS, 384 mM glycine, 20 % methanol) at a current of 80 - 400 mA for 3 - 18 h at 4 °C. Transfer was verified by Ponceau staining (0.1 % Ponceau, 5 % acetic acid) for 2 min, which was removed by rinsing the membrane in ddH<sub>2</sub>O. Following ponceau removal, non-specific antibody binding to the membrane was blocked by incubation of the membrane with 5 % BSA or 5 % fat milk free in TRIS-buffered saline with Tween (TBS-T) (20 mM TRIS HCl pH 7.6, 150 mM NaCl, 0.2 % Tween-20) for 60 min. Primary antibodies (2.11.7) were diluted in 5 % BSA or fat-free milk in TBS-T and incubated with the membrane overnight at 4 °C. Unbound residual antibody was washed away by rinsing the membrane in TBS-T (three times for 5 min at RT). The appropriate secondary antibody (see 2.11.7) coupled to an infrared dye was diluted 1:10000 in TBS-T and incubated with the membrane for 3-5 h at RT in the dark. After binding of the secondary antibody to the primary antibody, the membrane was washed in the dark (three times for 5 min at RT) and the signal generated by the infrared dye coupled secondary antibody was detected with the Odyssey system (LI-COR) that measures infrared fluorescence. Relative protein levels were determined by densitometry analysis using Image Studio Lite (LI-COR).

## 2.11.7. Antibodies

Antigen	Host	Dilution	Supplier
<b>Western blot primary antibodies</b>			
<b>β-Actin</b>	Mouse	1:2000	Santa Cruz Biotechnology, Dallas, TX, USA
<b>HSP90</b>	Mouse	1:2000	
<b>ALKBH2</b>	Rabbit	1:250	SAB Biotech, MD, USA
<b>IDH1 R132H</b>	Mouse	1:250	Dianova, Hamburg, Germany
<b>pCHK1Ser345</b>	Rabbit	1:1000	Cell signaling technology, Danvers, MA, USA
<b>CHK1</b>	Mouse	1:1000	
<b>γH2AX Ser139</b>	Rabbit	1:2000	abcam, Cambridge, UK
<b>Western and south-western secondary antibodies</b>			
<b>IRDye anti mouse IgG 800CW</b>	Donkey	1:10000	LI-COR, Lincoln, NE, USA
<b>IRDye anti rabbit IgG 800CW</b>			
<b>IRDye anti mouse IgG 680RD</b>			
<b>IRDye anti rabbit IgG 680RD</b>			
<b>Anti-mouse peroxidase conjugated</b>	Goat	1:2000	Rockland Immunochemicals Inc.
<b>Anti-rabbit peroxidase conjugated</b>			
<b>Immunofluorescence primary antibody</b>			
<b>γH2AX (JBW301)</b>	Rabbit	1:1000	Millipore, Billerica, MA, USA
<b>Immunofluorescence secondary antibody</b>			
<b>Anti rabbit Alexa Fluor®488 coupled antibody,</b>	Goat	1:1000	LifeTechnologies, Carlsbad, CA, USA
<b>South-western slot-blot primary antibody</b>			
<b>3-Methylcytosine</b>	Rabbit	1:50	Sigma-Aldrich, Steinheim, Germany

## 2.11.8. Immunofluorescence

For detection of γH2AX foci, cells were seeded into 6-well plates with pretreated coverslips in each well (10 min in diethylether, 5 min in 100 % ethanol, 5 min in 70 % ethanol, 5 min in dH<sub>2</sub>O, 30 min in 1 M HCl and storage in 70 % ethanol at 4 °C). After treatment, cells were rinsed with PBS and fixed with Roti®-Histofix 4 % formaldehyde in PBS for 10 min. Coverslips were washed three times with PBS and then covered with ice cold 100 % methanol and incubated at -20 °C for 10 min. Cells were then washed three times

## Material and Methods

with PBS and stored in PBS at 4 °C until staining (maximum 5 days). Coverslips were placed in new 6-well plates. For the staining, coverslips were blocked with BSA (5 % in PBS with 0.3 % Triton-X-100) for 1 h at RT.  $\gamma$ H2AX antibody (see 2.11.7) was diluted 1:1000 in PBS with 0.3 % Triton-X-100 and 80  $\mu$ l were applied on each coverslip and incubated over night at 4 °C. After three PBS wash steps (5 min each), 100  $\mu$ l of secondary anti mouse Alexa Fluor<sup>®</sup>488 coupled antibody (1:1000 in PBS with 0.3 % Triton-X-100) was applied on each coverslip and incubated in the dark at RT for 1 h. After two PBS wash steps (5 min each), coverslips were rinsed with “high salt” PBS (NaCl 0.4 M) for 10 sec, followed by an additional PBS wash step. Nuclei were stained with TO-PRO<sup>®</sup>-3 in PBS with 0.3 % Triton-X-100 for 15 min, rinsed with PBS twice, rinsed with “high salt” PBS, followed by an additional PBS wash step. Coverslips were mounted with Vectashield (Vector Laboratories, Burlingame, CA, USA) and sealed with transparent nail polish. Images were acquired with laser scanning microscope. Foci per cell were counted using FIJI software.

### 2.11.9. MGMT enzyme activity assay

MGMT activity was measured for 14 GBM cell lines in triplicates using a protocol that has been published previously (Preuss et al. 1996). Briefly, the method is a radioactive assay in which tritium-labeled methyl group from the O<sup>6</sup>-position of guanine is transferred to the protein in the cell extract. Therefore <sup>3</sup>H-MNU treated calf thymus DNA (10  $\mu$ l, 80000 counts per minute) was incubated with 200  $\mu$ g of total protein extract (2.11.1) in reaction buffer (HEPES-KOH pH 7.8, 1 mM DTT, 5 mM EDTA) for 90 min at 37 °C. TCA (13 %) and 200  $\mu$ g BSA was added to stop the reaction. DNA was heat-denatured at 95 °C for 45 min. After precipitation of the protein (10 min, 14000 rpm), the pellet was washed three times with 5 % TCA and resuspended in 200  $\mu$ l NaOH (100 mM). The total volume was transferred to a scintillation vial, containing 5 ml scintillation fluid. The remaining radioactivity was measured in a liquid scintillation counter. Data were expressed as fmol of radioactivity transferred from <sup>3</sup>H-labelled DNA to protein per milligram of protein within the sample.

## 2.12. DNA adduct measurements

### 2.12.1. South-western slot-blot analysis

3-methylcytosine (3mC) content of cells treated with ART was measured by slot-blot analysis. Cells were trypsinized, and DNA was extracted (see 2.7.1). 500 ng DNA was transferred to a positively charged nylon membrane (Hybond plus, Amersham) by vacuum slot-blotting. 0.3 M NaOH was used for denaturation, followed by neutralization with 5x SSC and fixed by baking the membrane for 2 h at 80 °C. Antibody specific for 3-methylcytosine (Sigma) were used at a dilution of 1:50. The western blot procedure was performed as described above.

### 2.12.2. Fpg-modified alkaline comet assay

8-oxoG was measured by the formamidopyrimidine DNA glycosylase (FPG)-modified alkaline Comet Assay. Cells were trypsinized after 24 h and 48 h of ART treatment and embedded in 0.5 % low melting point agarose and transferred onto agarose-precoated slides. The slides were incubated in lysis buffer (2.5 M NaCl, 100 mM EDTA, 10 mM Tris, 10 % DMSO, 1 % Triton X, pH 10) for 55 min at 4°C. Slides were equilibrated 2 x 5 min in buffer F (40 mM HEPES, 0.1 M KCl, 0.5 mM EDTA, 0.2 % BSA, pH 8.0) at RT. FPG was diluted in buffer F and 50 µl was added to the slides and incubated in a humid chamber at 37 °C for 40 min. DNA unwound in electrophoresis buffer (300 mM NaOH, 1 mM EDTA, pH 13) for 20 min at 4 °C before electrophoresis was performed for 22 min at 0.74 V / cm and 300 mA. Slides were washed three times in neutralization buffer (0.4 M Tris, pH 7.5). The samples were fixed in 100 % ethanol for 10 min at RT, air-dried and stained with 50 µg/ml propidium iodide. Comets were analyzed by fluorescence microscopy using an Olympus BX50 equipped with a ColorView camera (Olympus, Münster, Germany). At least 100 cells were scored in each experiment using Comet IV software (Perceptive Instruments Ltd., Bury St Edmunds, UK).





### 3. Results

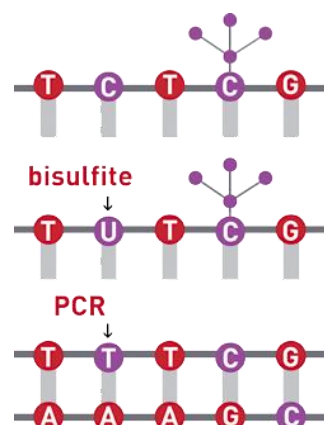
#### 3.1. Epigenetic regulation of DNA repair genes

##### 3.1.1. DNA methylation of the *MGMT* promoter

There are several methods available to determine the methylation status of DNA samples (Kurdyukov and Bullock 2016). Most methods for DNA methylation analysis involve the bisulfite conversion of DNA. In this step, all unmethylated cytosines become deaminated, which results in the conversion of cytosine to uracil. 5mC remains unaffected by this treatment and remains as cytosine. Following bisulfite treatment (**Figure 17**), the two converted strands are no longer complementary.

##### 3.1.1.1. Cell line based studies

Converted DNA (conDNA) was used for DNA methylation quantification by three methods, methylation specific PCR (MSP), high-resolution melt analysis (HRM), and pyrosequencing (PSQ). Primers for MSP are designed to target and assess the methylation status at specific CpG sites. One pair of primers binds specifically to the methylated conDNA, the other one binds to the unmethylated conDNA. For discrimination of methylated (M) and unmethylated (U) DNA, one or more CpG sites are included in each primer sequence. PCR reactions are performed using each primer pair, M and U primer pair. Successful amplification from the M primer pair is indicative of methylated DNA, while PCR products from U primers reflect unmethylated DNA (Herman et al. 1996).



**Figure 17: Treatment of DNA with bisulfite** converts cytosine residues to uracil but leaves 5-methylcytosine residues unaffected.

## Results

The promoter of the human *MGMT* gene harbors a CpG island of 762 bp (-531 to 231 from the ATG) and contains 98 CpG sites (Malley et al. 2011) (**Figure 18**). The GC content of this 762 bp long DNA stretch is 73.9 %.



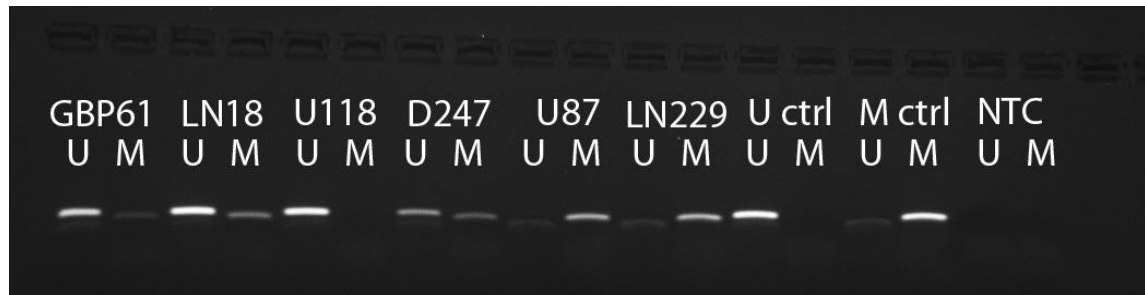
**Figure 18: The 762 bp long CpG island** (Malley et al.) of the *MGMT* promoter. The *MGMT* gene (green), and the *MGMT* CDS (coding DNA sequence; yellow), which starts with the ATG of the gene are shown. Primer binding sites for MSP, PSQ, and HRM are indicated.

Six GBM cell lines were analyzed as to their *MGMT* promoter methylation by MSP (**Figure 19 A**). GBP61, LN18, and U118 show no or only weak methylation, compared to D247, U87, and LN229, which show intermediate or high methylation (**Figure 19 B**).

A



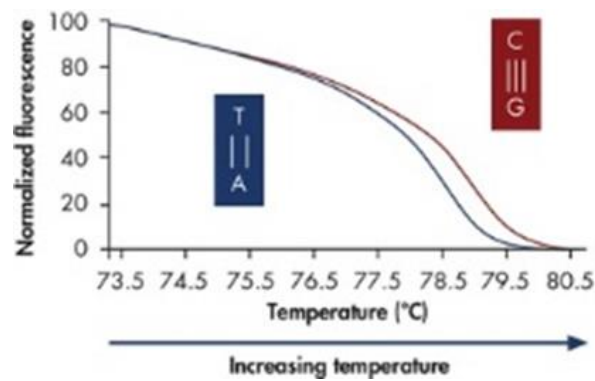
B



**Figure 19: *MGMT* promoter methylation determined by MSP.** (A) Location of the MSP primers either amplifying methylated (81 bp) or unmethylated (93 bp) conDNA of the first *MGMT* exon. Y = C or T, R = G or A (B) Series of six GBM cell lines has been analyzed by MSP together with unmethylated (U ctrl) and fully methylated control (M ctrl) DNA and a non-target control (NTC).

The results generated by the MSP method are only semi-quantitative, and although it lacks a threshold, classification is carried out binary, *MGMT* unmethylated and *MGMT* methylated, respectively. To overcome these limitations, high-resolution melt (HRM) analysis was applied, which reflects methylation levels in percent. This method relies on the fact that after bisulfite conversion an unmethylated C-G base pair will result in a T-A base pair, which now is bound to each other only by two H bonds, compared to three H bonds in the methylated context. An unmethylated CpG will result in a decreased melt temperature of the PCR amplicon compared to the methylated one (Figure 20).

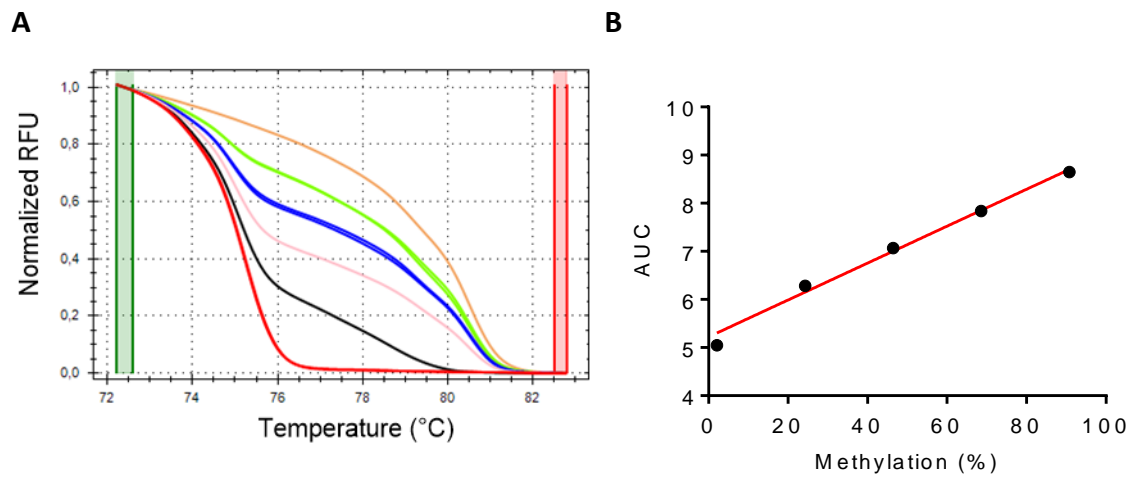
## Results



**Figure 20:** After bisulfite conversion, unmethylated DNA will result in a more thermolabile PCR amplicon, due to only two H-bonds between both opposing nucleosides compared to three H-bonds if the CpG was methylated.

An *in silico* search for CpG islands was conducted 8kb upstream and 1 kb downstream of the MGMT CDS start that could be used for methylation analysis by HRM. To avoid a PCR amplification bias, primers were placed outside of CpG sites to ensure equal amplification regardless of the methylation status. Four primer sets (**Table 7**) were found suitable for methylation analysis in MGMT proficient (HaCaT) and MGMT deficient (LN229) cells. Primer pair r1 generates a 392 bp amplicon producing several melt peaks. It was therefore unsuitable for HRM analysis. Using primer pair r2 (covering the MSP reverse primer binding site), only small differences in the methylation level between MGMT proficient versus deficient cells could be observed. The primer pair r3 and r4 revealed large differences in the MGMT promoter methylation level and, therefore, were suitable for further analysis.

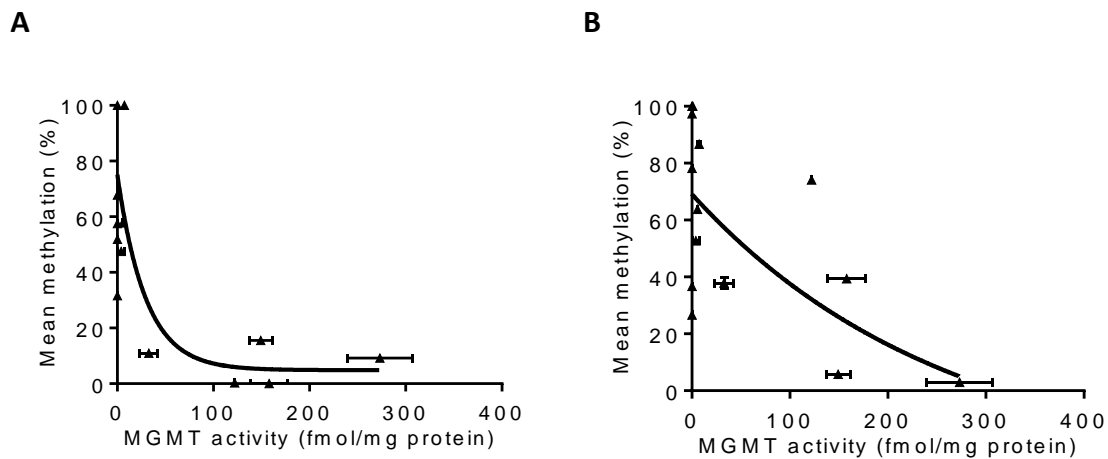
For cell lines, each reaction was performed in technical duplicates of biological triplicates, and in technical duplicates for the patient's samples. Fully methylated and unmethylated bisulfite-converted DNA was mixed to obtain the following ratios of methylation: 2.1, 24.3, 46.4, 68.6, and 90.8 % (theoretically 0, 25, 50, 75, and 100 %) and were included in duplicates in each assay, as well as a non-template control and a genomic DNA control. Commercially available bisulfite-converted DNA standards (Qiagen) were analyzed together with our internal DNA standards. HRM data were analyzed using Bio-Rad Precision Melt Analysis software (BioRad), with output plots produced as normalized melting curves (**Figure 21 A**). Normalized relative fluorescence units (RFUs) were exported to Prism 6 (GraphPad). The area under the curve (AUC) was calculated, and the linear regression was used to interpolate the unknown samples from the standards.  $R^2$  was  $> 0.98$  (**Figure 21 B**).



**Figure 21: Standard curve creation.** (A) Normalized melt curves in duplicates showing the melt behavior of methylation standards (red = 0 %, pink = 25 %, blue = 50 %, green = 75 %, orange = 100 %) and an unknown sample (black). (B) Regression model used for MGMT promoter methylation quantification. The area under the curve (AUC) from the normalized melt curves are used and regressed to the known methylation level of the standards. The linear regression model was chosen for quantification ( $R^2 > 0.98$ ).

MGMT protein activity was measured for 14 GBM cell lines, all covering a range from no measurable to very high activity. The regression analysis of promoter methylation determined by HRM and MGMT activity shows that the MGMT activity declines with increasing MGMT promoter methylation level (Figure 22).

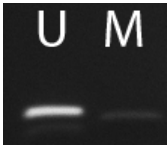
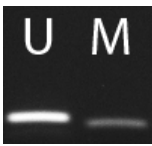

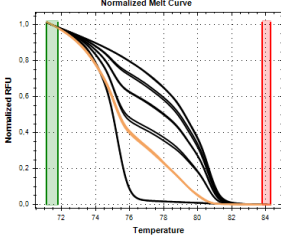
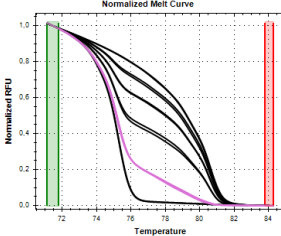
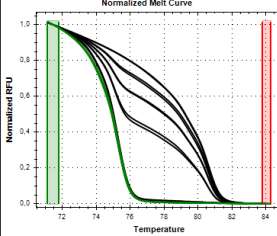
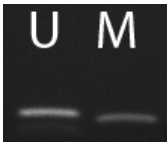


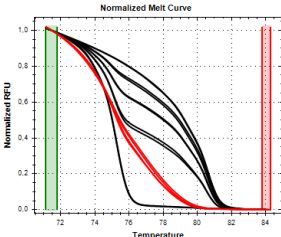
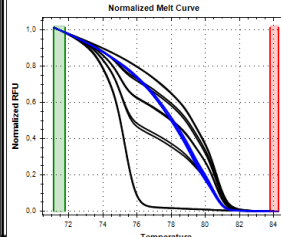
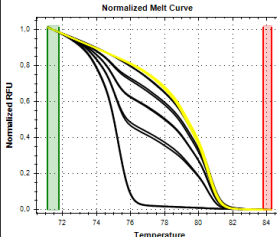
## Results



**Figure 22: Relationship between MGMT suicide-enzyme activity and level of promoter methylation determined by HRM using the (A) r4 primers and (B) r3 primers in 14 GBM cell lines.** A one-decay function between *MGMT* promoter methylation (r4) and *MGMT* protein activity could be found ( $R^2= 0.67$ ;  $r= -0.69$ ;  $p<0.01$ ). For r3, the relationship between the two variables was more linear, indicating that no threshold of methylation exists in this region.

The inverse “hockey-stick” relationship of promoter methylation of region r4 with *MGMT* activity indicates a possible methylation threshold for *MGMT* silencing. This pattern was not found in the region r3. Therefore, primer pair r4 covering 12 CpGs, including the region analyzed using the MSP and PSQ assay (Figure 18), was used for the further studies.

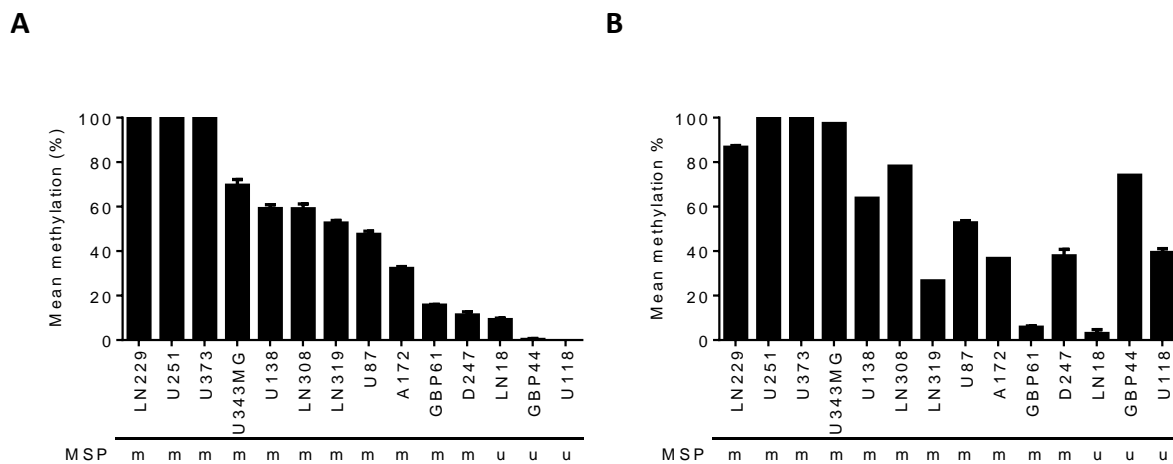
For the cell line studies, HRM was used to measure DNA methylation in technical duplicates and biological triplicates with a maximal deviance of 2 % (Figure 23).

Cell line	GBP61	LN18	U118
MSP			
HRM normalized plot			
HRM	15.33 % ± 0.409	8.06 % ± 0.740	0.00 % ± 0.000
MGMT activity	149.30 ± 11.951	273.17 ± 33.858	157.93 ± 19.107
Cell line	D247	U87	LN229
MSP			
HRM normalized plot			
HRM	10.37 % ± 1.547	51.25 % ± 1.632	100.00% ± 0.000
MGMT activity	32.68 ± 9.485	4.04 ± 3.711	7.33 ± 1.115

**Figure 23. MGMT promoter methylation was measured by MSP and HRM for three cell lines with high MGMT activity (top row) and and low MGMT activity (bottom row). For the HRM normalized plot, DNA methylation standards (0, 25, 50, 75, 100 %) are shown as black curves and the colored curve reflects the melt behavior of the sample. MGMT activity is given as fmol/mg total protein.**

## Results

The *MGMT* promoter methylation status was determined quantitatively by HRM in 14 GBM cell lines and compared with MSP (**Figure 24**). Interestingly, cell lines that are *MGMT* proficient and also do not show DNA methylation in the r4 region were highly methylated in the r3 region, indicating, that methylation in r3 does not affect *MGMT* transcription.

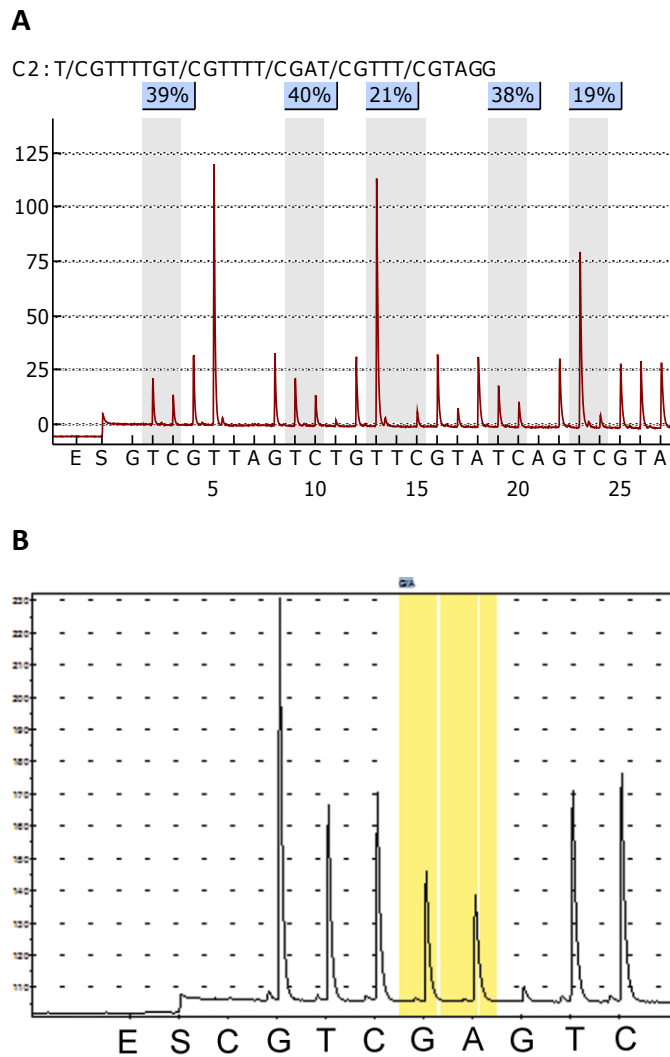


**Figure 24: *MGMT* promoter methylation of 14 GBM cell lines measured by HRM** (in triplicates) and the corresponding MSP categorization (m methylated; u unmethylated). **(A)** shows the mean methylation of region r4 and **(B)** shows the mean methylation of region r3.

### 3.1.1.2. *MGMT* promoter methylation in high-grade glioma samples

*MGMT* promoter methylation was analyzed in paraffinized tumor samples from 83 glioma patients whose *MGMT* promoter methylation has previously been assessed by MSP. The same tissue samples were subsequently analyzed by HRM and PSQ (**Figure 25**). *MGMT* promoter hypermethylation was identified by MSP in 37.3 % of the cases, whereas HRM showed promoter hypermethylation in 51.8 % and PSQ in 54.2 % of the samples. Thus, HRM was similar to PSQ in detecting promoter methylation. Methylation was not associated with the patient's age and sex (**Table 10**).





**Figure 25: Pyrogram of (A) the *MGMT* promoter of a patient tumor sample with a mean methylation of 31.4 %. (B) Typical pyrogram obtained from a grade III patient tumor sample indicating a heterozygous G-to-A point mutation of the *IDH1* gene resulting in a mutation at codon 132 (R132H). Agarose gel showing the *IDH1* PCR product is shown in **Supplementary Figure 1**.**

**Table 10: Characteristics of patients** and their MGMT promoter methylation status determined by HRM, MSP, and PSQ in 83 malignant gliomas, including 18 IDH1-mutated cases

Characteristics	n	HRM me (%)	MSP me (%)	PSQ me (%)	IDH1 mt (%)
<b>All patients</b>	83	51.8	37.3	54.2	21.7
<b>Woman</b>	28	50.0	39.3	53.6	21.4
<b>Man</b>	55	52.7	36.4	54.5	21.8
<b>Age ≥ 70</b>	27	44.4	25.9	44.4	0.0
<b>Age ≤ 70</b>	56	55.4	42.9	58.9	32.1
<b>Grade III</b>	23	73.9	56.5	69.6	69.6
<b>Grade IV</b>	60	43.3	30.0	48.3	3.3

Since IDH1-mutated tumors show a favorable patient survival and since the IDH1 status is considered to be an independent prognostic marker for WHO grade III gliomas (Weller et al. 2015), IDH1-mutated samples were excluded from further analysis. The IDH1 mutation was analyzed by immunohistochemistry using an anti-IDH1 R132H antibody (by Prof. Clemens Sommer, Neuropathology UM Mainz) and further confirmed by sequencing. The analysis revealed 18 of 83 analyzed tumors as IDH1 mutated. The IDH1 mutations were predominantly observed in grade III (88.9 %), but also in grade IV tumors (11.1 %) and a high correlation with MGMT promoter methylation was observed (**Table 12**), confirming data in the literature (Wick et al. 2009; SongTao et al. 2012).

To determine an optimal cut-off value for discriminating between methylated and unmethylated *MGMT* promoter, ROC curves were plotted for 15 methylation cut-off scores (1–15 %) to identify the optimum cut-off level for the prediction of PFS  $\geq$  12 months and OS  $\geq$  18 months. The cut-off value of 5 % showed the largest AUC for both PFS (0.705) and OS (0.637) (**Table 11**) confirming the suitability of a 5 % cut-off value for discriminating between the methylated and the unmethylated *MGMT* promoter.

**Table 11: ROC curves were plotted for 15 methylation cut-off scores (1-15 %) for predicting PFS  $\geq$  12 months and OS  $\geq$  18 months.**

Cut-off (%)	AUC PFS	AUC OS	Cut-off (%)	AUC PFS	AUC OS	Cut-off (%)	AUC PFS	AUC OS
1	0.677	0.635	6	0.664	0.614	11	0.631	0.604
2	0.677	0.635	7	0.622	0.591	12	0.641	0.616
3	0.686	0.647	8	0.622	0.591	13	0.608	0.570
4	0.686	0.647	9	0.622	0.591	14	0.608	0.570
5	0.705	0.637	10	0.631	0.604	15	0.608	0.570

The association between *MGMT* promoter methylation and clinical outcome (using a 5 % cut-off value) comparing HRM, MSP, and PSQ was analyzed in tumor material of 65 IDH1wt glioma patients (seven gliomas grade III and 58 grade IV). The data are shown in **Table 12** for all patients in the study (including IDH1 mutated) and in **Table 13** for IDH1 wild-type tumors only. In **Table 13**, the percentage of *MGMT*-methylated tumors upon sex, age, and tumor grade is compiled, indicating no differences to exist between these groups. Overall, the HRM values were again more comparable to PSQ than to the data obtained by MSP.

## Results

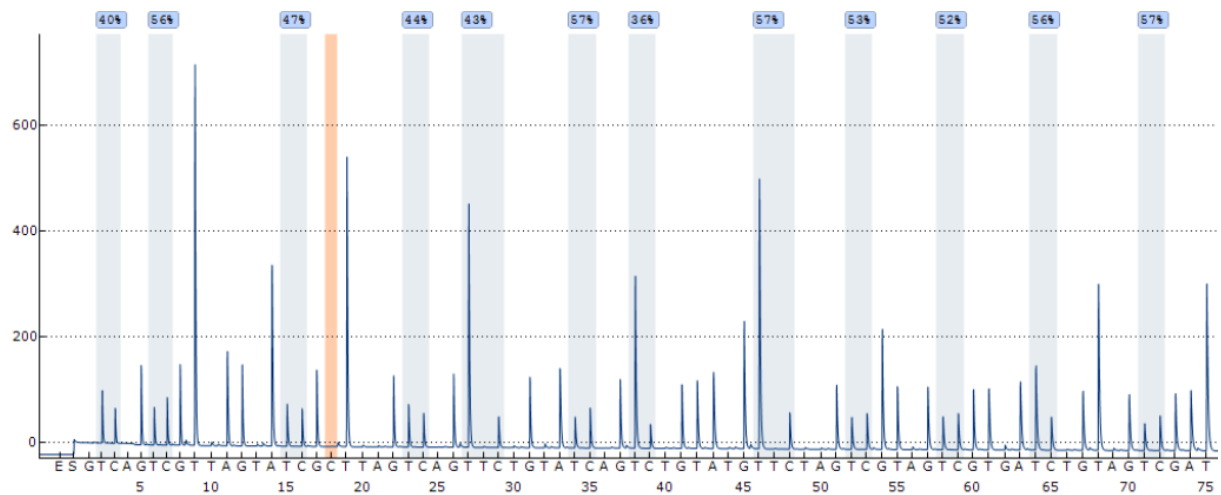
**Table 12: *MGMT* promoter methylation status** determined by HRM, MSP, and PSQ in dependence of the IDH1 status

Characteristics	n	HRM me (%)	MSP me (%)	PSQ me (%)	Grade III (%)	Grade IV (%)
All patients	83	51.8	37.3	54.2	27.7	72.3
IDH1wt	65	41.5	30.8	46.2	10.8	89.2
IDH1mt	18	88.9	61.1	83.3	88.9	11.1

**Table 13: Characteristics of patients** and their *MGMT* promoter methylation status determined by HRM, MSP, and PSQ in 65 IDH1wt malignant gliomas.

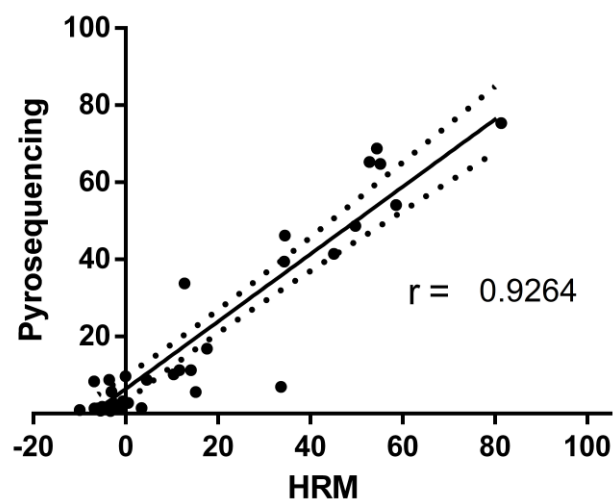
Characteristics	n	HRM me (%)	MSP me (%)	PSQ me (%)
All patients	65	41.5	30.8	46.2
Woman	22	40.9	31.8	40.9
Men	43	41.9	30.2	48.8
Age $\geq$ 70	27	44.4	25.9	44.4
Age $\leq$ 70	38	39.5	34.2	47.4
Grade III	7	42.9	42.9	42.9
Grade IV	58	41.4	29.3	46.6

To further validate the methylation data obtained by the HRM assay, pyrosequencing for the whole HRM amplicon on a Pyromark Q24 advanced (Qiagen) was performed for 38 patient samples and the DNA standards. The forward primer was also used as a sequencing primer (**Table 8; Figure 26**).



**Figure 26: Pyrogram of the whole HRM (R4) assay region from a patient sample.**

The 38 methylation scores determined by HRM and pyrosequencing showed a high correlation ( $r = 0.926$ ,  $p < 0.0001$ , **Figure 27**). The unmethylated DNA standard was methylated to the extent of 2.1 %, and the methylated DNA standard showed 90.8 % mean methylation at the *MGMT* promoter region. These values were taken for the linear regression analysis of data obtained by HRM (see above).

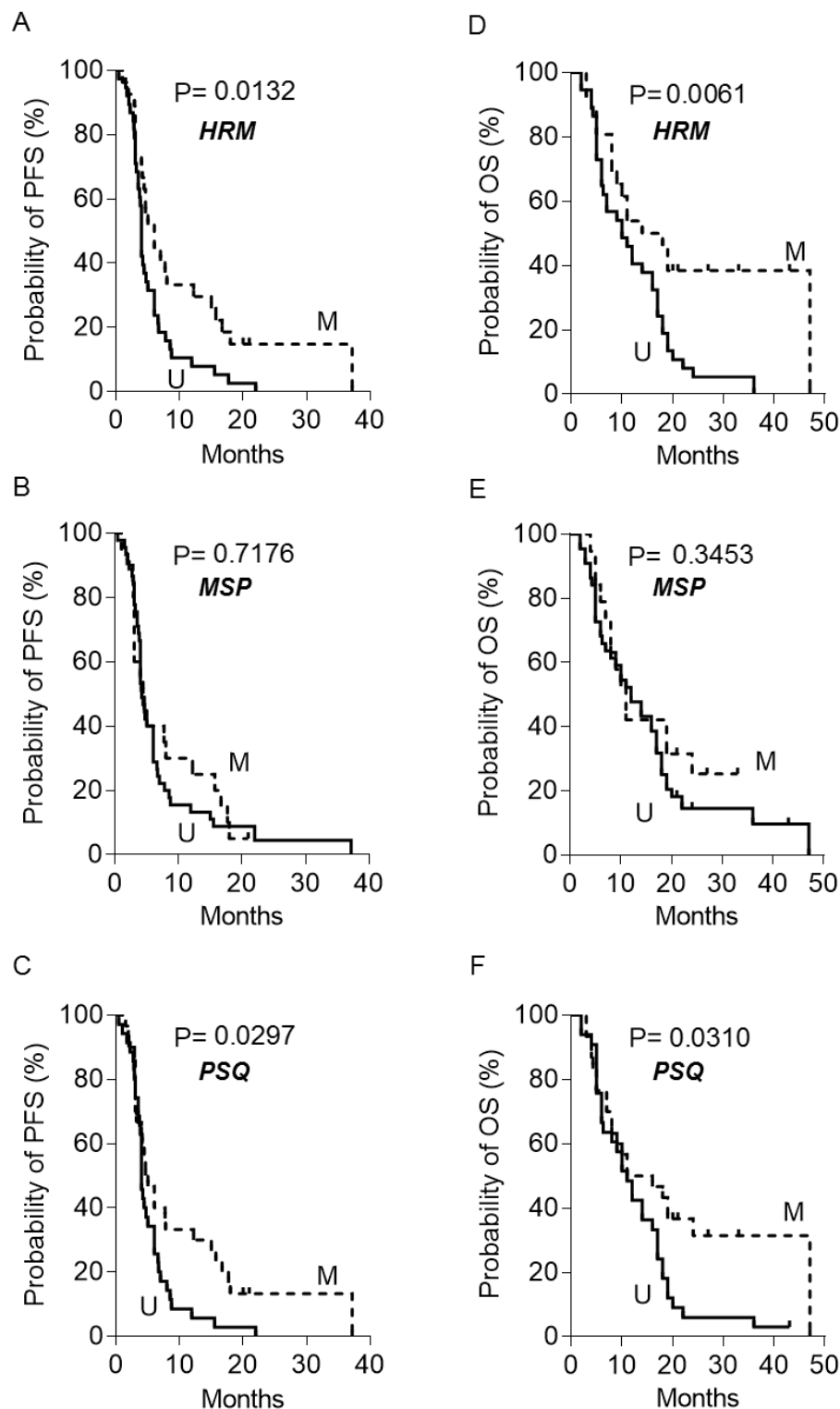


**Figure 27: Correlation of methylation quantification.** Dot-plot of the *MGMT* promoter methylation values obtained in a subsample by HRM and pyrosequencing showing a high correlation between these two methods. The dotted line indicates the 95% CI.

## Results

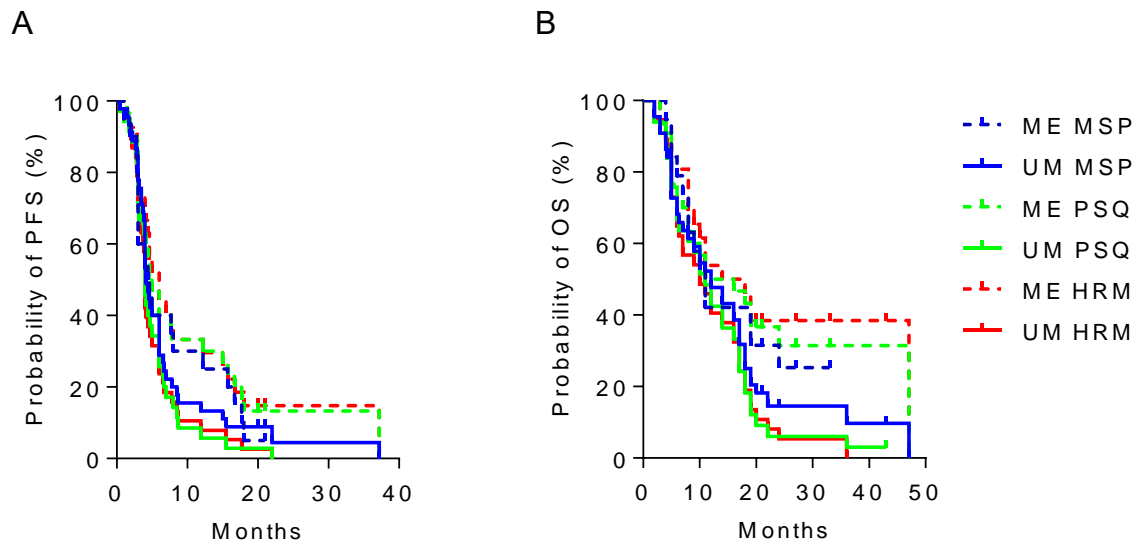
### 3.1.1.2.1. Univariate Kaplan-Meier survival analysis

A comparison of Kaplan–Meier estimates of progression-free survival (PFS) using the method of HRM, MSP, and PSQ is shown in **Figure 28** panels A, B, and C respectively. For HRM and PSQ, the difference in PFS was significant, whereas MSP did not show a significant difference. Kaplan–Meier estimates of overall survival (OS) of patients using the methods of HRM, MSP, and PSQ are shown in **Figure 28**, panels D, E, and F respectively. An overlay of all Kaplan–Meier curves is shown in **Figure 29**. The data for OS also revealed an enhanced predictive value when HRM or PSQ was used compared to MSP. In a bivariate analysis, the methylation status of the *MGMT* promoter was correlated with PFS ( $r = 0.252$ ,  $p = 0.042$ ) and Karnofsky score ( $r = 0.336$ ,  $p = 0.007$ ). In contrast, data obtained by MSP and PSQ failed to generate significance ( $p > 0.05$ ) both for PFS and OS.



**Figure 28: Kaplan–Meier estimates of PFS and OS** according to *MGMT* promoter methylation status determined by HRM, MSP, and PSQ. Kaplan–Meier estimates for PFS and OS of 65 high-grade glioma patients. PFS of patients with un-methylated and methylated *MGMT* status, determined by HRM (A), MSP (B), and PSQ (C). OS of patients with un-methylated and methylated *MGMT* status, determined by HRM (D), MSP (E), and PSQ (F). Significance levels were determined by the log-rank test. U un-methylated; M methylated *MGMT* promoter

## Results



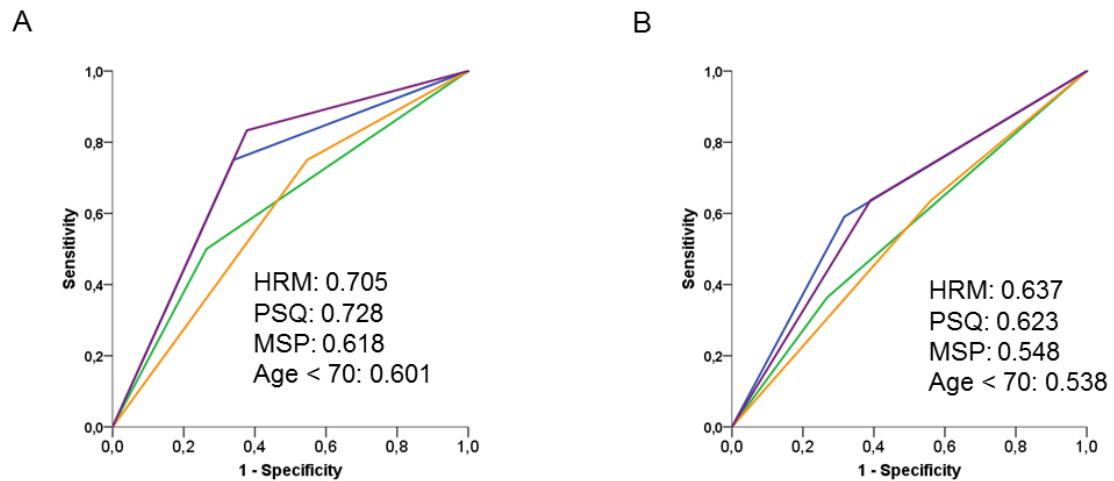
**Figure 29: Overlay of Kaplan-Meier estimates of PFS and OS** according to *MGMT* promoter methylation status. Kaplan-Meier estimates for (A) PFS and (B) OS of 65 high-grade glioma patients determined by HRM (red lines), MSP (blue) and PSQ (green). The solid and the dashed lines indicate the group as being categorized unmethylated (UM) or methylated (ME), respectively.

### 3.1.1.2.2. Accuracy of outcome prediction evaluated by receiver-operating characteristics (ROC) curve

The methods used for detection of *MGMT* promoter methylation were further compared by ROC analysis. The ROC methodology provides an unbiased method to define a threshold the highest possible true-positive rate (sensitivity) and a preferably low false-positive rate (1-specificity). ROC curves are used in different clinical setups to test variables with binary outputs for their suitability, e.g. as cancer risk factor, imaging biomarker, high-risk predictor, or other applications (Chopra et al. 2012; Hoggart et al. 2012).

ROC curves were generated to depict the sensitivity and specificity of *MGMT* promoter methylation status determined by HRM, MSP, PSQ as well as age <70 to predict PFS  $\geq 12$  months and OS  $\geq 18$  months. The AUC was larger for HRM than for MSP both for PFS and OS (Figure 30), supporting the notion that dichotomization of patients by HRM leads to less false positive and false negative results compared to MSP in predicting survival. The AUC for HRM and PSQ is nearly the same, indicating both methods provide the same discrimination accuracy.





**Figure 30: ROC curves for *MGMT* promoter methylation.** Receiver operator characteristics (ROC) curve calculated based on *MGMT* promoter methylation determined by MSP (orange line), HRM (blue line), PSQ (violet line), and age <70 (green line). ROC curves were calculated for (A) PFS  $\geq 12$  months and (B) OS  $\geq 18$  months. The area under the curve (AUC) corresponds to the prediction of survival, with a value of 1 indicating perfect discrimination, and a value of 0.5 no better than chance discrimination.

### 3.1.1.2.3. Multivariate Cox proportional hazards model

Furthermore, univariate and multivariate Cox regression analyses were performed with the factors HRM, MSP, PSQ, sex, age < 70 and grade, to determine independent factors for PFS and OS. In this model, HRM was found to be the only significant independent prognostic factor for OS (HR 0.473, 95 % CI 0.231 – 0.969,  $p = 0.041$ ) (Table 14). Overall, the study shows that for both PFS and OS, HRM was clearly superior to MSP in discriminating between responders and non-responders and equally effective as PSQ (data are summarized in Table 15).

**Table 14: Associations between MGMT promoter methylation status, demographic features, and grade of 65 IDH1wt glioma patients and PFS and OS, assessed by univariate (log-rank test) and multivariate (Cox-regression) analyses.**

	PFS			OS		
	univariate (p)	multivariate (HR, 95 CI, p)		univariate (p)	multivariate (HR, 95 CI, p)	
<b>MSP me</b>	0.718	1.456, 0.730 - 2.903, 0.286		0.345	1.270, 0.606 - 2.661, 0.527	
<b>PSQ me</b>	0.030	0.729, 0.358 - 1.482, 0.382		0.031	0.762, 0.376 - 1.544, 0.450	
<b>HRM me</b>	0.013	0.539, 0.278 - 1.045, 0.067		0.006	0.473, 0.231 - 0.969, 0.041	
<b>Sex = woman</b>	0.742	0.958, 0.545 - 1.684, 0.881		0.578	0.918, 0.494 - 1.705, 0.786	
<b>Age &lt; 70</b>	0.106	0.677, 0.389 - 1.178, 0.168		0.114	0.590, 0.331 - 1.052, 0.074	

**Table 15: MGMT promoter methylation status and progress and survival of patients. Promoter methylation was determined by HRM, MSP, and PSQ. mo = months.**

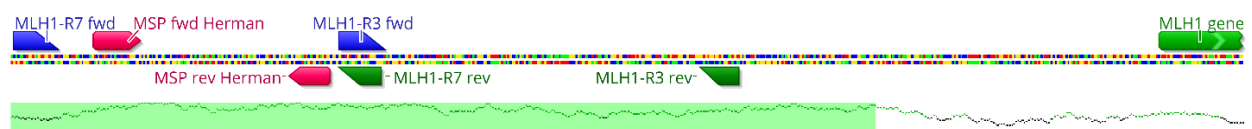
Promoter status	HRM	MSP	PSQ
<b>Methylated MGMT promoter</b>			
Progression-free survival			
Median duration (mo)	6.0 (3.64 – 8.36)	4.4 (3.09 – 5.72)	4.6 (2.88 – 6.32)
Rate at 6 mo (%)	51.9	40.0	46.7
Overall survival			
Median duration (mo)	14.0 (6.50 – 21.50)	11.0 (8.19 – 13.81)	11.0 (0.27 – 21.74)
Rate at 18 mo (%)	48.1	40.0	46.7
<b>Unmethylated MGMT promoter</b>			
Progression-free survival			
Median duration (mo)	4.0 (3.80 – 4.20)	4.2 (3.67 – 4.73)	4.0 (3.67 – 4.33)
Rate at 6 mo (%)	31.6	40.0	34.3
Overall survival			
Median duration (mo)	10.0 (5.03 – 14.97)	12.0 (7.36 – 16.64)	11.0 (7.62 – 14.38)
Rate at 18 mo (%)	23.7	31.1	22.9

### 3.1.2. DNA methylation of the *MLH1* promoter

The toxicity of the applied TMZ-based chemotherapy in high-grade astrocytoma (HGA) patients is mismatch repair (MMR, see 2.3.3). *MLH1* as one of the key players of the MMR is often silenced in cancers by promoter hypermethylation. If *MLH1* is silenced by promoter methylation, TMZ will not lead to the formation of DSB and subsequent apoptosis or senescence, but to TMZ resistance and survival at the expense of mutations.

#### 3.1.2.1. Cell line based studies

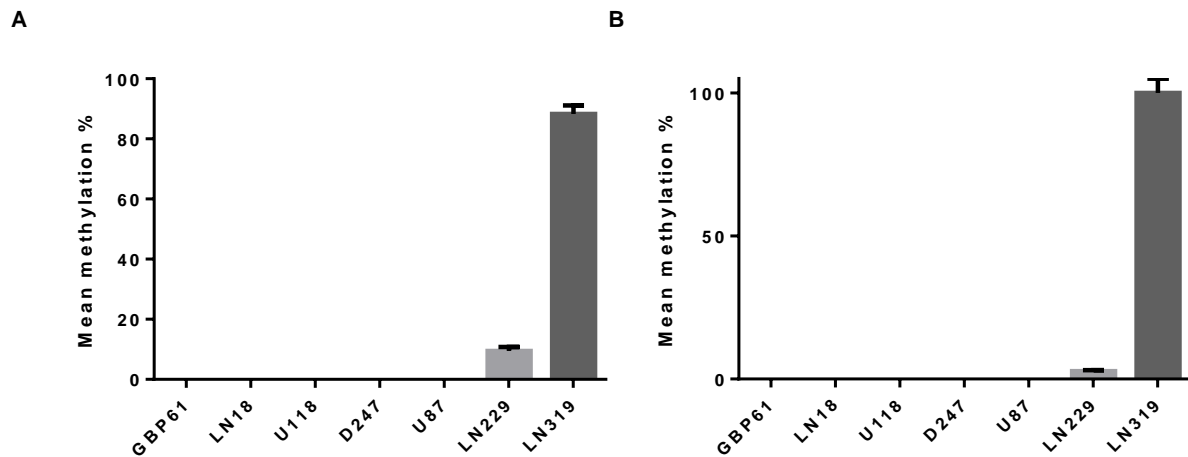
The promoter of the human *MLH1* gene consists of a CpG Island of about 1 kb around the TSS. This region in the proximal promoter was analyzed *in silico* and primers were designed to assess DNA methylation in regions known for their transcription silencing effects and further downstream (**Table 7**). Fully methylated and unmethylated DNA was used to determine successful amplification and meaningful (single distinct melt peak for each DNA standard) post-PCR melt behavior and two primer sets (R3 (-597 to -402 from ATG) and R7 (-755 to -579 from ATG); **Figure 31**) were then used for HRM based DNA methylation analysis in seven cell lines (see **Table 4**). Regions R4 (-339 to -154 from ATG) and R5 (-65 to +116 from ATG) were unmethylated in the seven tested glioma cell lines.



**Figure 31: Location of the *MLH1* HRM primers** relative to the TSS of the gene and the binding sites of the MSP primers routinely used for methylation studies (Herman et al. 1998). The green area below indicates the high density of CpGs, i.e. marks CpG islands.

For R3 and R7, LN229 shows only very low methylation levels, whereas LN319 is hypermethylated in both regions (**Figure 32**). Therefore, LN319 cells can be classified as *MLH1* deficient. This is consistent with survival results (see 3.2.2) in which LN319 cells have shown resistance to high doses of TMZ. These primer sets were then used for methylation analysis of the *MLH1* promoter in high-grade astrocytoma (HGA) patient samples.

## Results



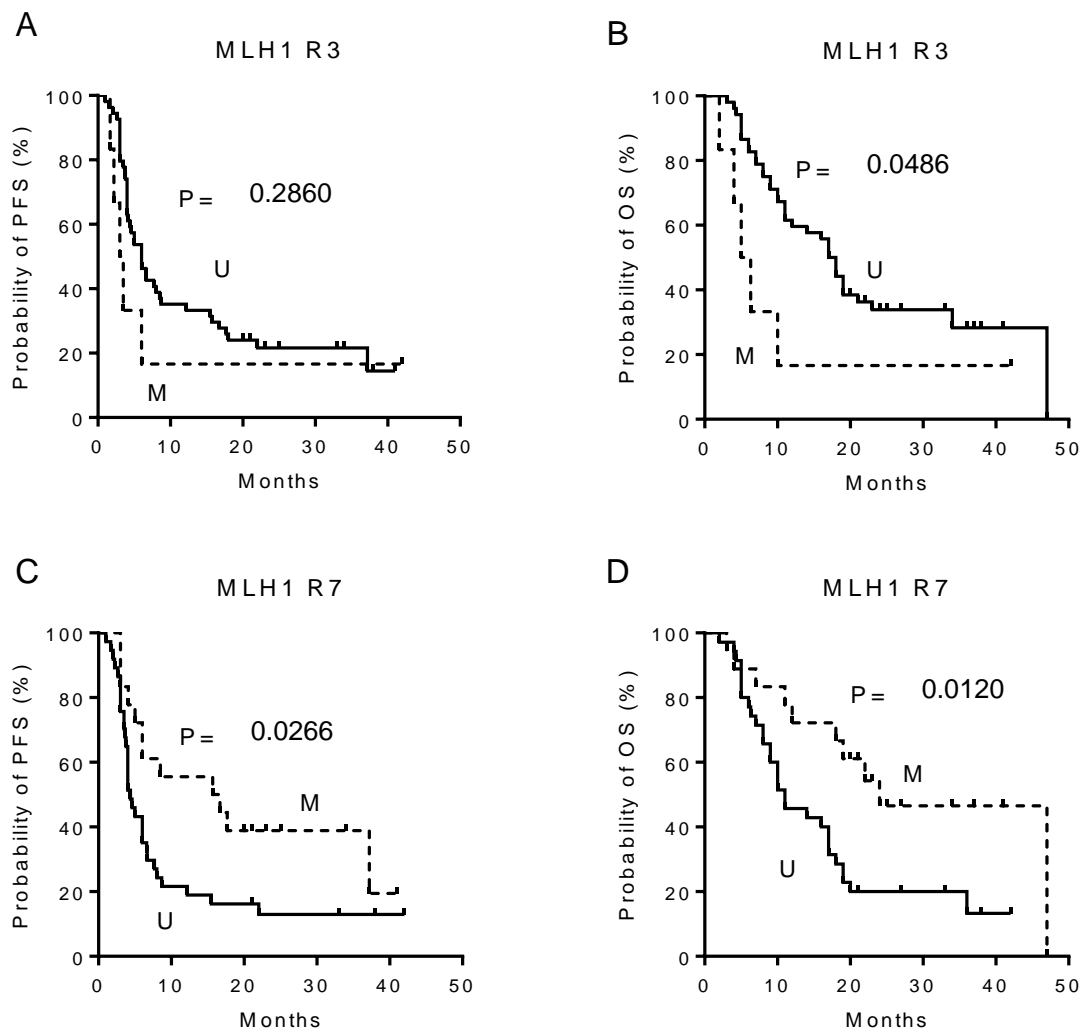
**Figure 32: *MLH1* promoter methylation** of 7 GBM cell lines measured by HRM (in triplicates). For the R3 region (**A**), LN229 shows a weak methylation, whereas LN319 is nearly fully methylated. (**B**) Likewise, in the R7 region, the methylation level is very low in LN229 and fully methylated in LN319 cells. All other cell lines are unmethylated in the analyzed *MLH1* promoter regions.

### 3.1.2.1. *MLH1* promoter methylation in high-grade glioma samples

Methylation in R3 and R7 of the *MLH1* promoter were analyzed in 60 HGA patients (including 10 IDH1 mutated patients) by HRM. Patients were declared as methylated if the methylation score was higher than 0 %. The mean methylation level in R3 for the patients being classified as methylated was 5.08 %  $\pm$  1.760 and for R7 4.03 %  $\pm$  4.095.

A comparison of Kaplan-Meier estimates of PFS for *MLH1* region R3 and R7 using the HRM method is shown in **Figure 33** panels A and C, respectively. For R3, no significant differences could be determined. For R7, patients with a methylated *MLH1* promoter showed a prolonged PFS compared to patients with an unmethylated methylation status ( $p = 0.0266$ ). Kaplan-Meier estimates of OS for *MLH1* region R3 and R7 using the HRM method is shown in **Figure 33** panels B and D, respectively. For both regions, significant differences between unmethylated and methylated *MLH1* promoter could be determined ( $p < 0.05$ ). For region R3, patients harboring a methylation, a poorer survival could be found, confirming data in the literature (Shinsato et al. 2013), since a reduction of *MLH1* leads to TMZ resistance (see 1.2.2), the latter leading to poorer survival. For the R7 region, the opposite effect was observed, where methylation of the *MLH1* promoter leads to

increased OS, contradicting the statement above. *MLH1* promoter methylation in region R7 was significantly correlated with the IDH1 mt status of the patients ( $p = 0.043$ ), which allows the conclusion that methylation in R7 is driven by the IDH1 mutation (see 1.2.1), i.e. reflecting the CIMP phenotype. Methylation in R3 was not correlated with the IDH1 mutational status of patients ( $p = 0.913$ ).



**Figure 33: Kaplan-Meier estimates of PFS and OS according to *MLH1* promoter methylation status determined by HRM in region R3 and R7 in 60 HGA patients.** PFS of patients with unmethylated and methylated *MLH1* promoter in the *MLH1* (A) R3 and (C) R7 region. OS of patients with unmethylated and methylated *MLH1* promoter in the *MLH1* (B) R3 and (D) R7 region. Significance levels were determined by the log-rank test. U unmethylated; M methylated *MLH1* promoter.

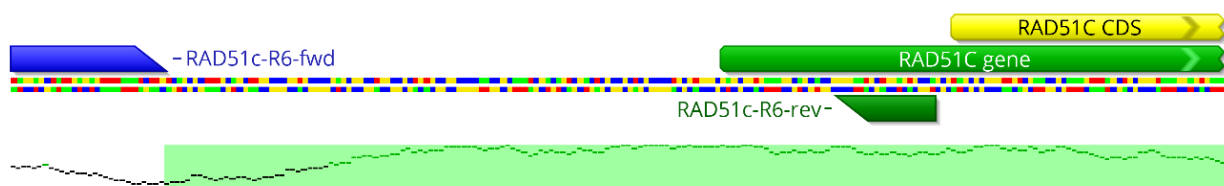
## Results

### 3.1.3. DNA methylation of the *RAD51c* promoter

The promoter of the human *RAD51c* gene harbors a CpG island of around 400 bp around the TSS (**Figure 34**). This region in the proximal promoter was analyzed *in silico* and primers were designed to assess DNA methylation.

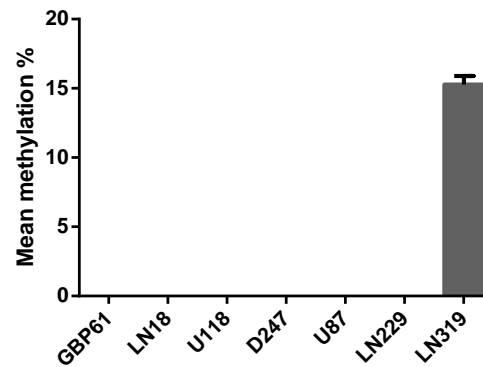
#### 3.1.3.1. Cell line based studies

The primer pair R6 passed the quality check (melt behavior, PCR efficiency, and single product) and was used to assess the *RAD51c* promoter methylation in seven GBM cell lines.



**Figure 34: Location of the *RAD51c* HRM primers** relative to the TSS of the gene. The green area below indicates the high density of CpGs, i.e. marks CpG islands. The yellow area indicates the coding DNA sequence.

In cell culture experiments, LN319 was methylated at the *RAD51c* promoter to a low extent. All other cell lines were unmethylated in this region (**Figure 35**). If a promoter methylation level of about 15 % is sufficient for gene silencing is unclear. However, it is rather unlikely to affect its expression, because 15 % methylation in this assay which spans 169 bp and covers 16 CpGs, i.e. 15 % reflects 1.5 CpGs. Methylation of one or two CpGs is unlikely to affect gene expression of *RAD51c*.



**Figure 35:** *RAD51c* promoter methylation of 7 GBM cell lines measured by HRM (in triplicates). LN319 shows a methylation of about 15 %, whereas other cell lines are unmethylated.

#### 3.1.3.1. *Rad51c* promoter methylation in high-grade glioma samples

Methylation of R6 in the *RAD51c* promoter was analyzed in 29 HGA patients by HRM. Although 16 out of 29 patient samples (55 %) displayed a *RAD51c* promoter methylation over 10 %, it had no impact on PFS and OS. Methylation was not correlated with any other variable. Kaplan-Meier estimates were not significantly different for the > 10 % methylation compared to the ≤ 10 % methylation group.

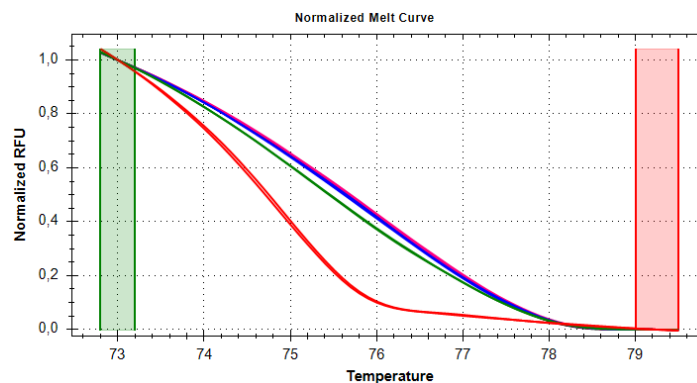
#### 3.1.4. DNA methylation of the *ATM*, *BRCA1*, *BRCA2*, and *MBD4* promoter

The promoters of *ATM*, *BRCA1*, *BRCA2*, and *MBD4* harbor a CpG island around the TSS, which spans 700, 400, 600, 2000, and 1000 bp, respectively. Seven GBM cell lines were analyzed as to their promoter methylation in the aforementioned promoters. All cell lines were unmethylated in the promoters of this study. 42 patient samples were analyzed with primer sets that passed the quality check (**Table 7**). *ATM* R1, *BRCA1* R1, *BRCA2* R4 *BRCA2* R5, and *MBD4* R2 were unmethylated in all 42 patient samples.

## Results

### 3.1.5. DNA methylation of the *LINE1* promoter

Long interspersed nuclear element 1 (*LINE-1*) are a group of transposons that make up around 20 % of the human genome. The *LINE1* promoter methylation is seen as a surrogate marker for estimating genome wide DNA methylation level. To analyze if *MGMT* promoter methylation is independent of genome wide methylation changes attempts to establish an HRM based *LINE1* promoter methylation assay was undertaken. Primers from literature (Tse et al. 2011) were taken and tested with fully methylated and unmethylated standard DNA. Although a clear separation of the two standards could be achieved, linearity of any mixture of the two standards (25, 50, 75 %) could not be reached (**Figure 36**). This assay was not further used for analysis. The failed reproduction of literature results might be caused by the use of different qPCR cyclers.

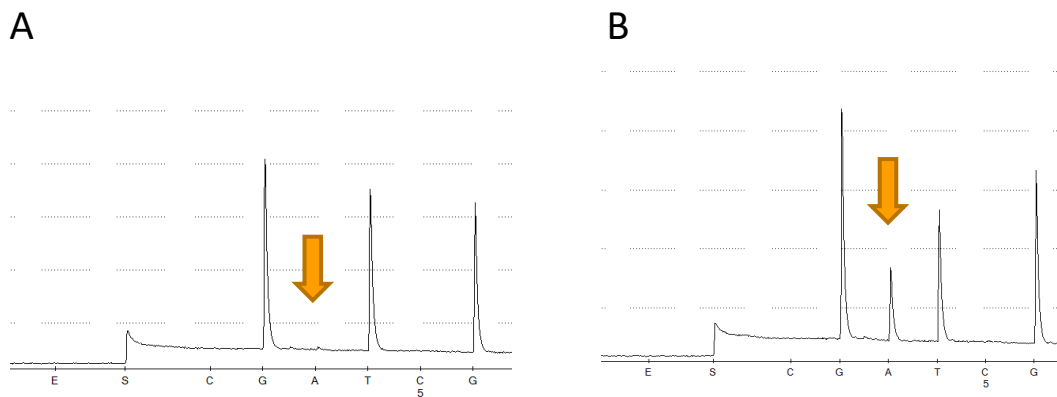


**Figure 36: Normalized *LINE1* melt curves** in duplicates showing melt behavior of methylation standards (red = 0%, green = 25%, blue = 50%, black = 75%, pink = 100%).

### 3.1.6. BRAFV600E mutational status in HGA patients

In 2002, BRAF V600 mutations were reported (Davies et al. 2002) for malignant melanoma and other cancers. The V600E mutation was also detected in a small fraction (5 %) of high-grade gliomas, but only in pediatric tumors (< 18 years) (Schindler et al. 2011). In adults, this mutation was only published in a case report in which one patient was suffering from a GBM harboring the V600E mutation survived longer compared to BRAF wt GBM (Takahashi et al. 2015). To elucidate whether the progress or survival of our HGA patient collective was affected by the V600E mutation, the mutational status of all 83 HGA patients was assessed by pyrosequencing (**Figure 37**).





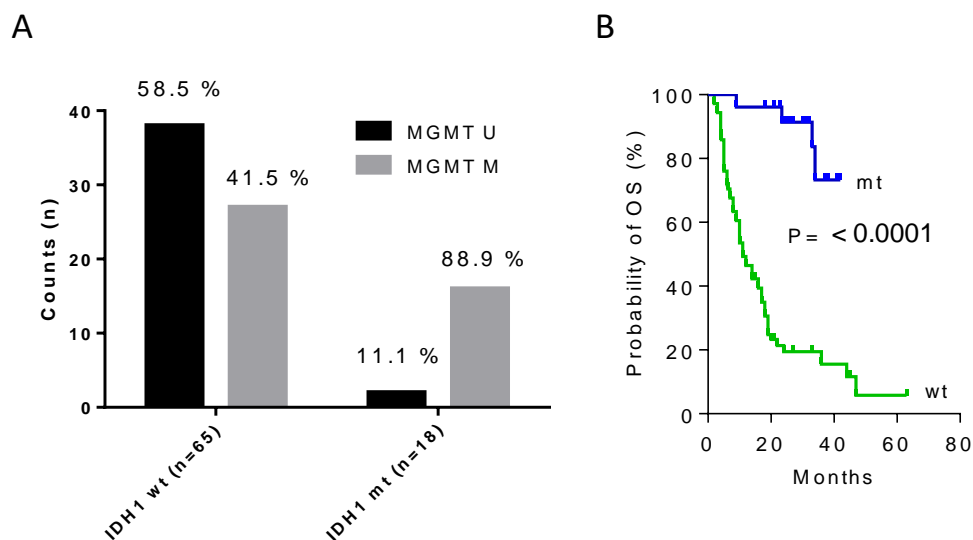
**Figure 37: *BRAF* V600E mutation detection by pyrosequencing.** Pyrogram obtained with (A) *BRAF* wild-type (G-T-G), and (B) V600E heterozygous mutation (G-A/T-G) in the A375 cell line. Agarose gel showing clear PCR products is shown in **Supplementary Figure 2**.

No V600E mutation could be found in any of the 83 HGA patient samples. This result might be due to the fact, that our HGA collective did not include any patient younger than 22 years. As a result, the survival of our HGA collective was not affected or biased by the BRAFV600E mutation.

## Results

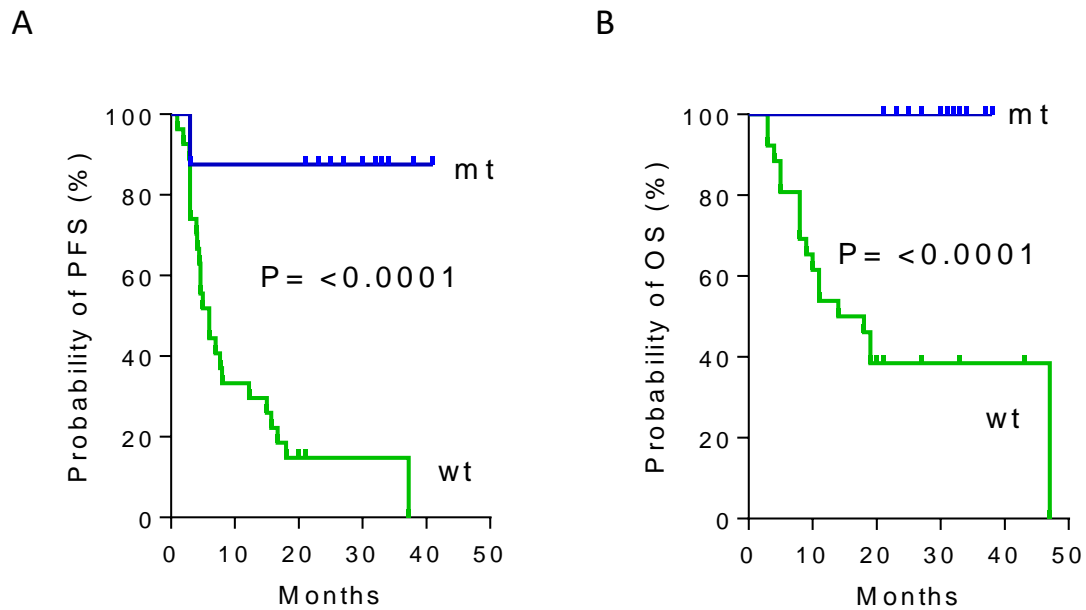
### 3.1.7. Association between *IDH1*R132H mutational status and *MGMT* promoter methylation in high-grade astrocytoma (HGA) patients

The HGA patients involved in this study comprised 18 *IDH1* mutated cases out of 83 (see **Table 12**). The *IDH1* mutation is one factor that increases the probability of *MGMT* promoter methylation but is not necessary to induce it, as *IDH1* wild-type tumors were *MGMT* promoter methylated in around 40 % of all cases (**Figure 38 A**). The likelihood of *MGMT* promoter methylation is higher in *IDH1* mutated HGA compared to *IDH1* wild-type HGA. *IDH1*mt HGA patients have a greatly increased OS compared to *IDH1*wt HGA patients (**Figure 38 B**). These results are in line with data from the literature (Wick et al. 2013; Zhang et al. 2016).



**Figure 38: *MGMT* promoter methylation in *IDH1*wt and *IDH1*mt patient glioma samples. (A)** In *IDH1*wt glioma samples (n=65), 41.5 % were *MGMT* promoter methylated. On the other hand, in *IDH1*mt samples (n=18) 88.9% were *MGMT* promoter methylated. **(B)** Kaplan-Meier estimates for *IDH1* mutated (mt) and *IDH1* wild-type (wt) HGA patients.

To overcome the different *MGMT* promoter methylation levels in *IDH1* wild-type and mutated patients, the patient collective was stratified, and only *MGMT* promoter methylated samples were processed. Patients with an *IDH1* mutation show a significantly favorable outcome for both PFS (**Figure 39 A**) and OS (**Figure 39 B**). Therefore, other factors that determine DNA repair might be affected by the *IDH1* mutation.



**Figure 39: Kaplan-Meier estimates for *MGMT* promoter methylated glioma samples.** 42 HGA patient samples were classified as *MGMT* promoter methylated. Although all samples display a methylated *MGMT* promoter, Kaplan-Meier estimates for IDH1 wild-type (wt) and IDH1 mutated (mt) are significantly different for **(A)** PFS and **(B)** OS.

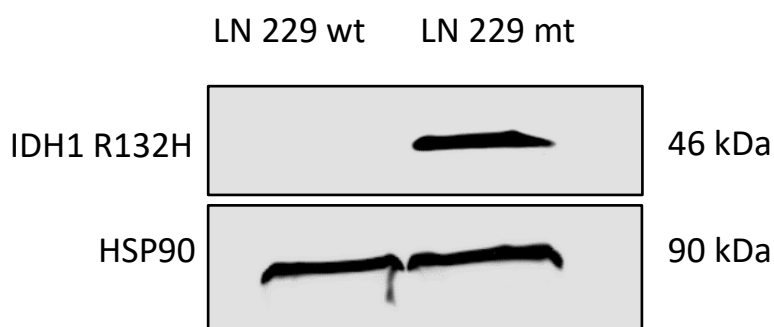
To answer the question if the IDH1 mutation by itself renders the tumor more sensitive to the applied chemo- and radiotherapy, a cell line based approach was chosen. This model allows to study the influence of the IDH1 mutation on cellular endpoints upon treatment with cytostatic drugs and ionizing radiation used for the treatment of gliomas.



### 3.2. Metabolic regulation of DNA repair enzymes

LN229 with stable expression of either IDH1wt or IDH1R132H were used to study the effects of different oxidizing and alkylating agents. They were obtained from the van Deimling group at the DKFZ in Heidelberg, Germany and were described and characterized previously (Mohrenz et al. 2013). Briefly, the generation of LN229 IDH1 wt overexpressing cells and LN229 IDH1 R132H overexpressing cells was done by Gateway® cloning. The *IDH1*wt ORF (open reading frame), in a pDONR221 plasmid, was obtained from the DKFZ Clone Repository and the *IDH1*R132H variant was generated by site directed mutagenesis. These ENTRY vectors were used for transfer of the cDNA in the destination vector pDEST26 (N-terminal 6x His Tag). LN229 cells were transfected with pDEST vectors by Fugene 6 (Promega, Madison, USA) followed by picking of single cell clones.

The expression of the mutated IDH1 protein was verified by western blot (**Figure 40**). The main question was, which enzymes involved in DNA repair are affected by the metabolite 2-HG, which is produced by the mutated IDH1 enzyme.



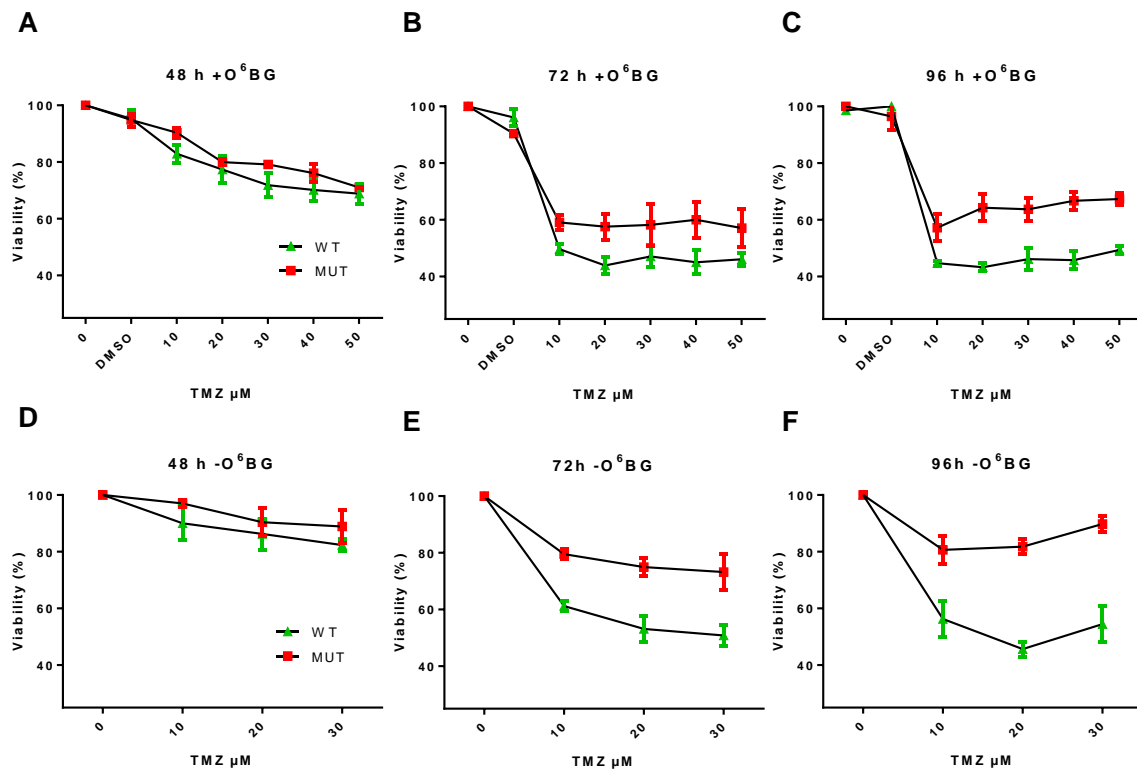
**Figure 40: Western blot analysis** and verification of LN229 glioma cells expressing either wild-type or mutant IDH1.

#### 3.2.1. Effect of DNA alkylation in LN229 IDH1wt and mt cells

LN229 cells are MGMT deficient and *MGMT* promoter methylated. Toxicity towards TMZ was assessed by MTT for LN229 cells either expressing IDH1wt or IDH1mt. TMZ exerts its cytotoxic effect after two replication rounds triggered by DNA DSBs. CCNU, however, leads to inter-strand crosslinks after 6 to 12 hours after treatment (Lemoine et al. 1991), resulting in cytotoxic stalled replication forks. Both, TMZ and CCNU, generate DNA adducts that are substrates for MGMT. *O*<sup>6</sup>-benzylguanine (*O*<sup>6</sup>BG) binds and inactivates MGMT.

## Results

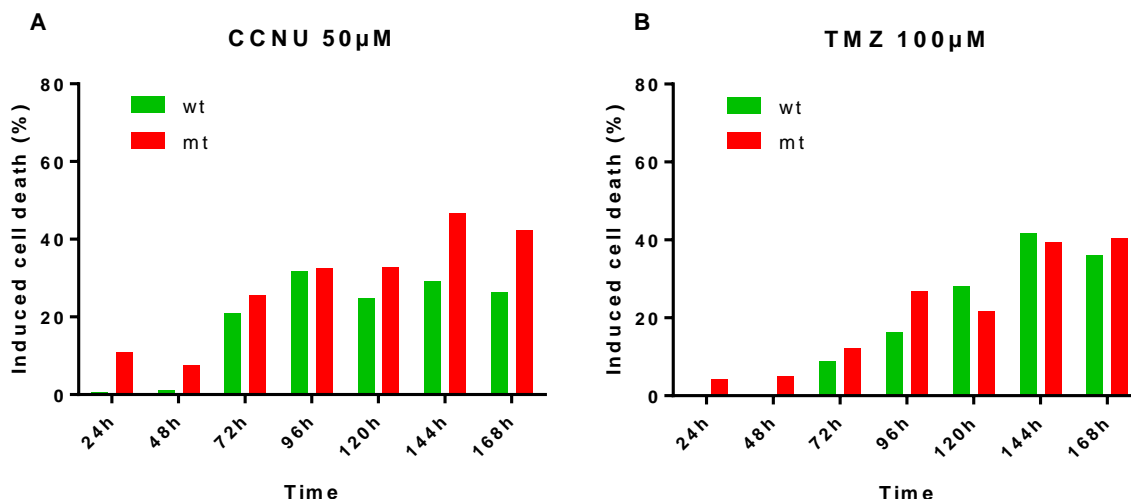
As the doubling time of these cells is around 24 h, DNA damages are induced after 48 h, followed by the induction of cell death. Cells were treated with increasing doses of TMZ together with or without 10  $\mu$ M  $O^6$ BG to be sure that MGMT is depleted. The results of this experiment are shown in **Figure 41**. The figure shows that for 48 h (A, D), 72 h (B, E), and 96 h (C, F).



**Figure 41: TMZ toxicity in LN229 cells assessed by the MTT assay.** LN229 IDH1wt and LN229 IDH1mt cells were treated with increasing doses of TMZ together with  $O^6$ BG for (A) 48 h, (B) 72 h, and (C) 96 h. Toxicity of TMZ treatment without  $O^6$ BG pretreatment was assessed after (D) 48 h, (E) 72 h, and (F) 96 h. Data are the mean of three independent experiments  $\pm$  SD.

After 72 h and 96 h, significant differences in cell survival could be detected, but IDH1 mt cells were more viable than IDH1wt cells after TMZ treatment. The results were not influenced by adding  $O^6$ BG, which was to be expected if no MGMT is present in the cells.

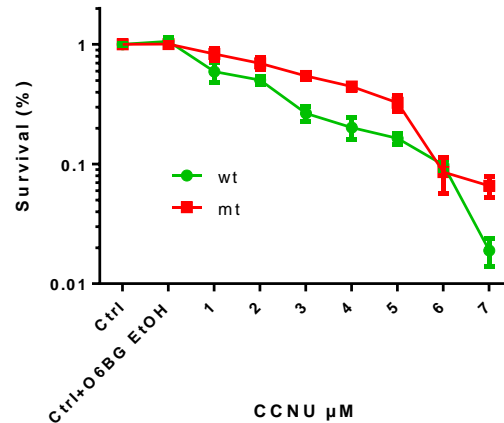
Annexin V/PI staining was then applied to quantify and qualify CCNU and TMZ induced cell death after different time points (**Figure 42 A, B**).



**Figure 42: CCNU and TMZ toxicity in LN229 cells assessed by Annexin V/PI staining and FACS analysis.** LN229 IDH1wt and LN229mt cells were treated with (A) 50  $\mu$ M CCNU or (B) 100  $\mu$ M TMZ for up to 168 h. The sum of apoptosis and necrosis is shown as induced cell death.

TMZ did not induce more cell death in IDH1 mt cells compared to their wild-type counterparts. For CCNU, up to 120 h following treatment, no striking differences in cell death were found. The cell death values obtained after 120 h should be considered with caution, as the number of seeded cells before treatment is very low to avoid confluence at the late time points. Small cell number differences during seeding have a strong influence on late time points. To assess the long-term toxicity of CCNU, a colony formation assay was performed. Colonies were fixed and counted after 17 days of incubation (Figure 43).

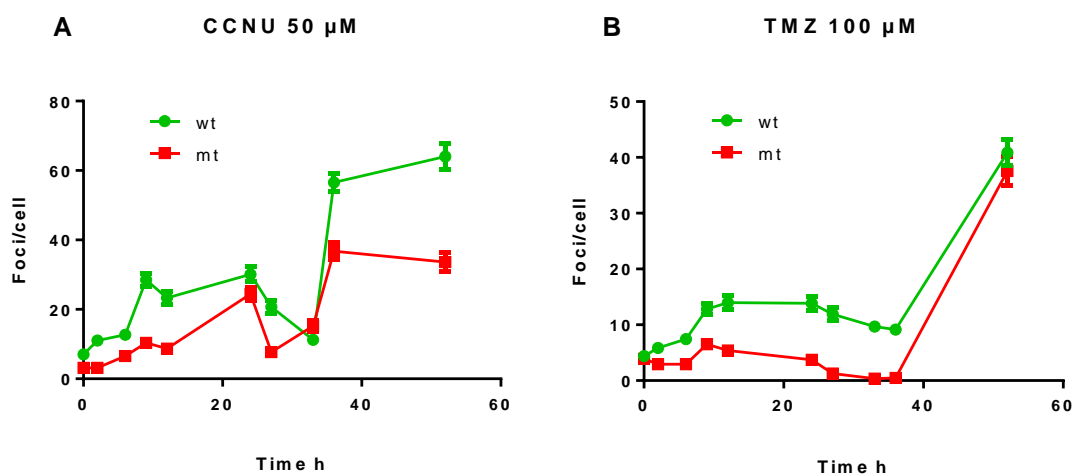
## Results



**Figure 43: Colony formation assay** performed with increasing doses of CCNU. Colonies were counted after 17 days and normalized to the untreated control. Data are the mean of three independent experiments  $\pm$  SD.

IDH1 mutated cells did not show increased toxicity towards CCNU in the colony formation assay compared with their wild-type counterparts.

Since CCNU and TMZ induce stalled replication forks and DNA DSBs, a time dependent quantification of  $\gamma$ H2AX foci formation, a classical DSB marker, was performed. For each time point at least 150 cells were analyzed (**Figure 44 A, B**).



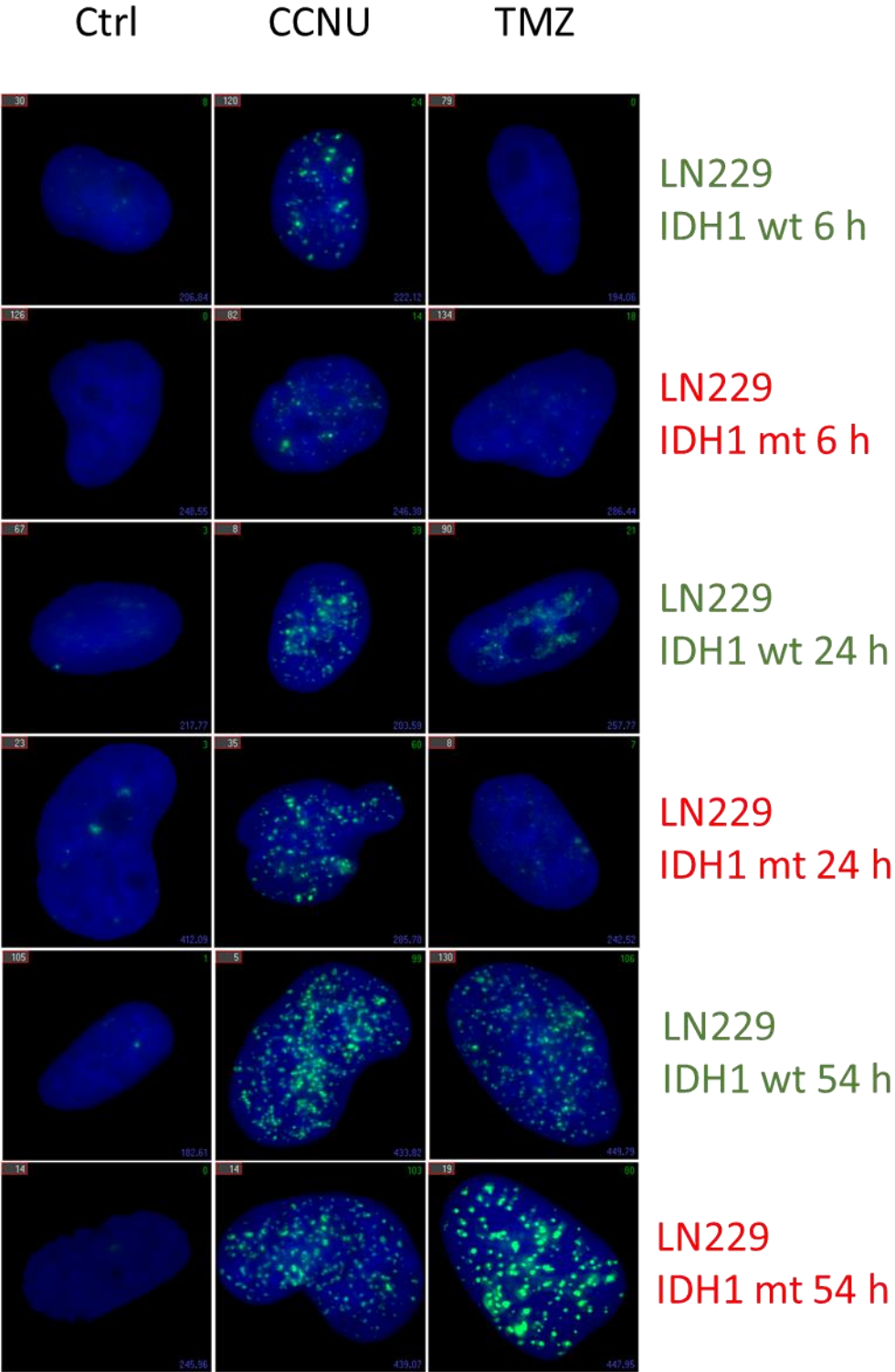
**Figure 44: Single cell  $\gamma$ H2AX foci quantification of LN229 IDH1wt and IDH1mt cells.** Cells were treated with 50  $\mu$ M CCNU (**A**) or 100  $\mu$ M TMZ (**B**). Cells were analyzed after 0, 2, 6, 9, 12, 24, 27, 30, 33, 36, and 54 hours. Data are the mean of three independent experiments  $\pm$  SEM.



As shown in **Figure 44 A**, CCNU led to the formation of more than 20  $\gamma$ H2AX foci per cell after 9 hours. For TMZ, an induction of over 20  $\gamma$ H2AX foci is reached after 54 hours of treatment (**Figure 44 B**). CCNU is much faster in  $\gamma$ H2AX foci formation compared to TMZ, because of its crosslinking ability that results in stalled replication forks. For TMZ induced DSBs, cells have to go through two replication rounds, which is reflected in the late  $\gamma$ H2AX foci formation. Representative single cell sections are shown in **Figure 45**.

Nevertheless, IDH1 mt cells did not show more  $\gamma$ H2AX after CCNU or TMZ treatment compared to their wild-type counterparts

Results



**Figure 45: Influence of CCNU and TMZ induced H2AX phosphorylation.** Cells were treated with 50 μM CCNU, 100 μM TMZ, or vehicle alone. Representative image sections are shown.

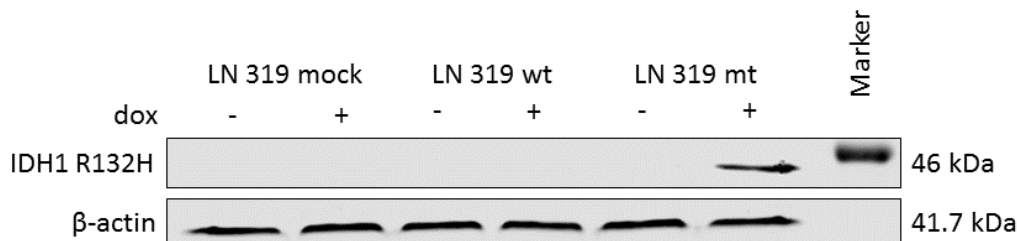
The two stably transfected LN229 cell lines express either IDH1wt or IDH1mt, which makes it possible that the constant production of 2-HG in the IDH1mt cell line has already induced epigenetic changes. These changes are reflected in higher DNA methylation and higher histone methylation, which leads to chromatin compaction (see 1.2.1). Especially histone demethylases (KDMs) are required for activation of pro-proliferative cell cycle genes and differentiation. 2-HG produced by the IDH1mt cells was shown to lead to a decrease of KDM activity (see 1.2.1), i.e. leads to a slower cell cycle progression that might influence their response towards alkylating agents.

To avoid such effects and to make the results better comparable to a suitable control cell line, a tetracycline (doxycycline (dox)) inducible cell system was chosen. Doxycycline is a preferred effector for tetracycline trans-regulation and is a member of the tetracycline antibiotics group. These cell lines are based on the LN319 glioblastoma cell line that was stably transfected with a TET-on vector and a second plasmid containing either *IDH1wt* or *IDH1mt*, together with a mock control (see 2.5.). In this cell system, the protein of interest is only expressed when dox is added. Therefore, long-term effects of 2-HG can be excluded. This cell line was a kind gift of Dr. Stefan Pusch from the van Deimling group (DKFZ, Heidelberg, Germany).



### 3.2.2. Effect of DNA alkylation in LN319 IDH1wt and mt cells

First, the induction of IDH1mt expression in LN319 cells after 24 h treatment with 1  $\mu$ M dox was verified by western blot (**Figure 46**).

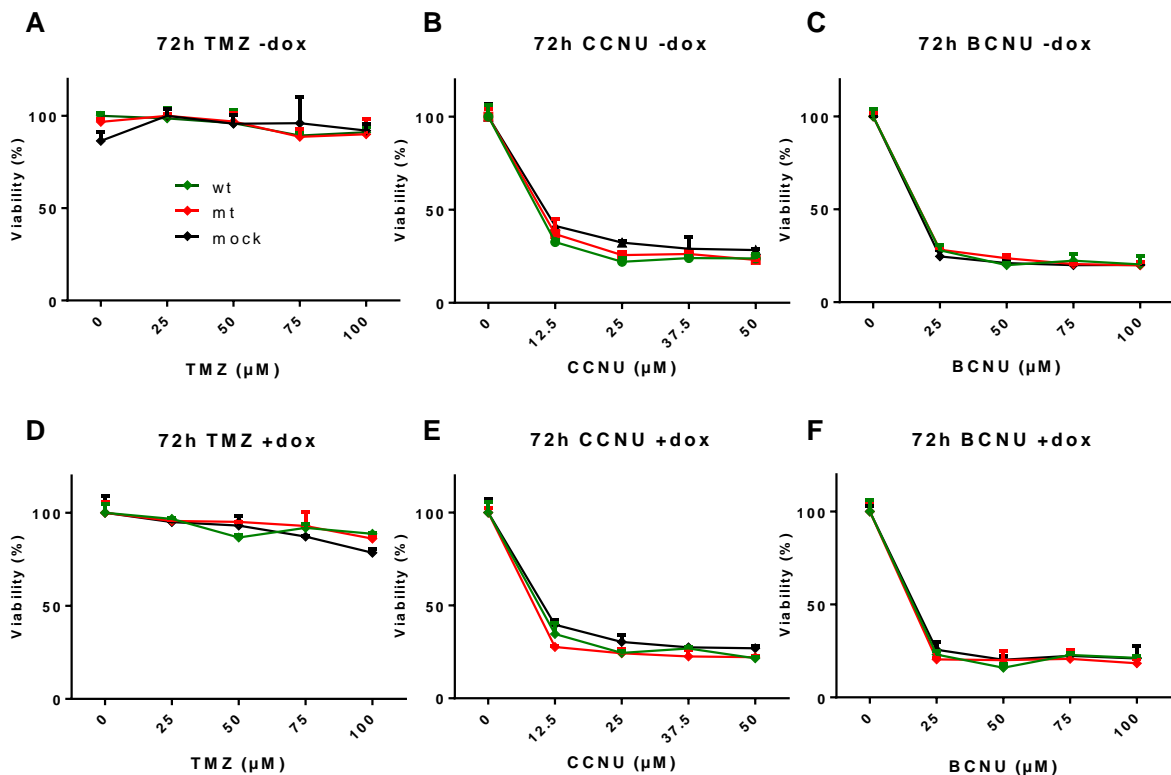


**Figure 46: Western blot analysis of LN319 glioma cells** expressing mutant IDH1 using a tetracycline-inducible system after 24 hours of doxycycline (dox) treatment. The first lane from the right shows a marker band (40 kDa).

LN319 cells are MGMT deficient and display *MGMT* promoter hypermethylation (see **Figure 24**). Further, LN319 cells are MMR deficient, as their *MLH1* promoter is hypermethylated (see **Figure 32**), making them TMZ resistant as no DSB can be generated. This cell system makes it possible to determine possible additional TMZ induced toxicity beyond the cytotoxic  $O^6$ meG DNA lesion in IDH1mt cells, therefore providing a rationale for the better survival of IDH1mt glioma patients.

The sensitivity towards alkylating and oxidizing agents of LN319 cells, either expressing IDH1wt, IDH1mt, or vector control was assessed by the MTT assay (**Figure 47**).

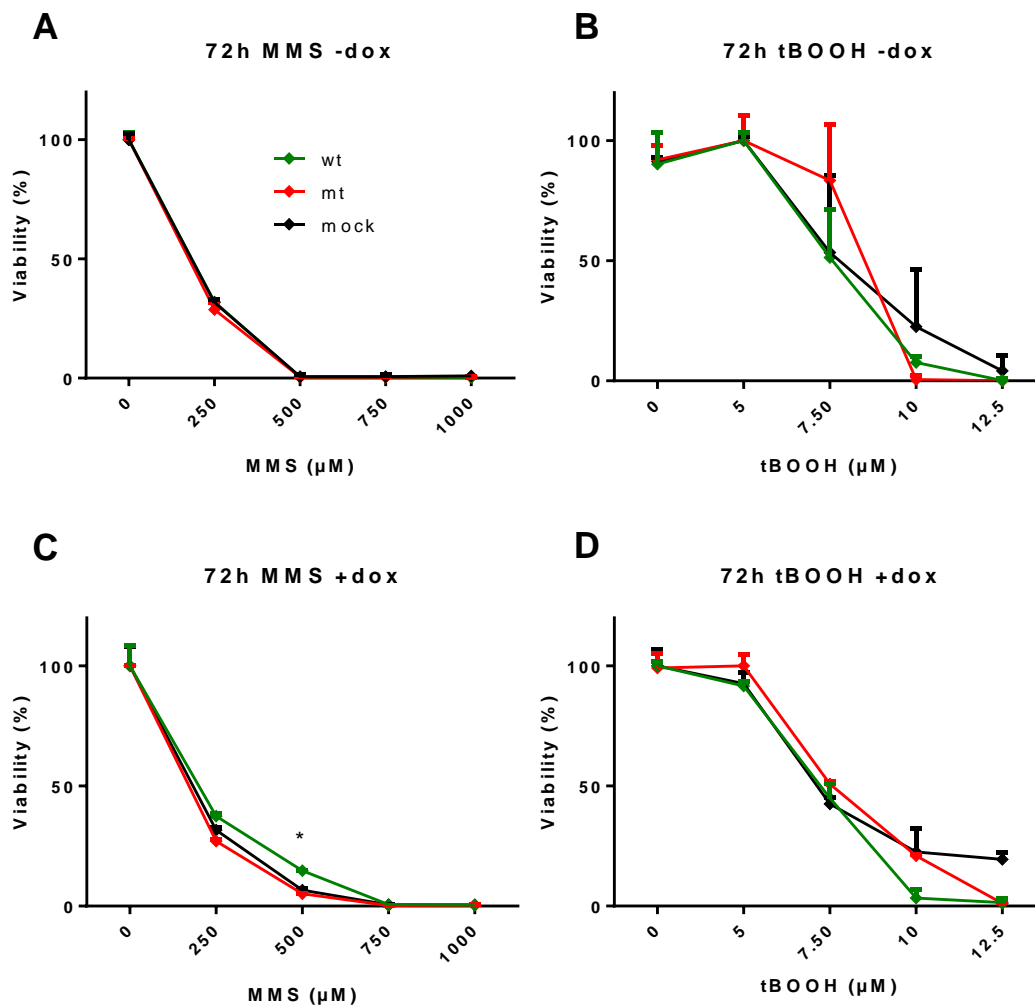
## Results



**Figure 47: Viability of LN319 cells assessed by the MTT assay after 72 h of prolonged treatment.** Panels **A**, **B**, and **C** show the viability of the three cell lines without the overexpression of the gene of interest (IDH1wt, IDH1mt). Panels **D**, **E**, and **F** show the viability after overexpression of IDH1wt or IDH1mt. Data are the mean of three independent experiments  $\pm$  SD.

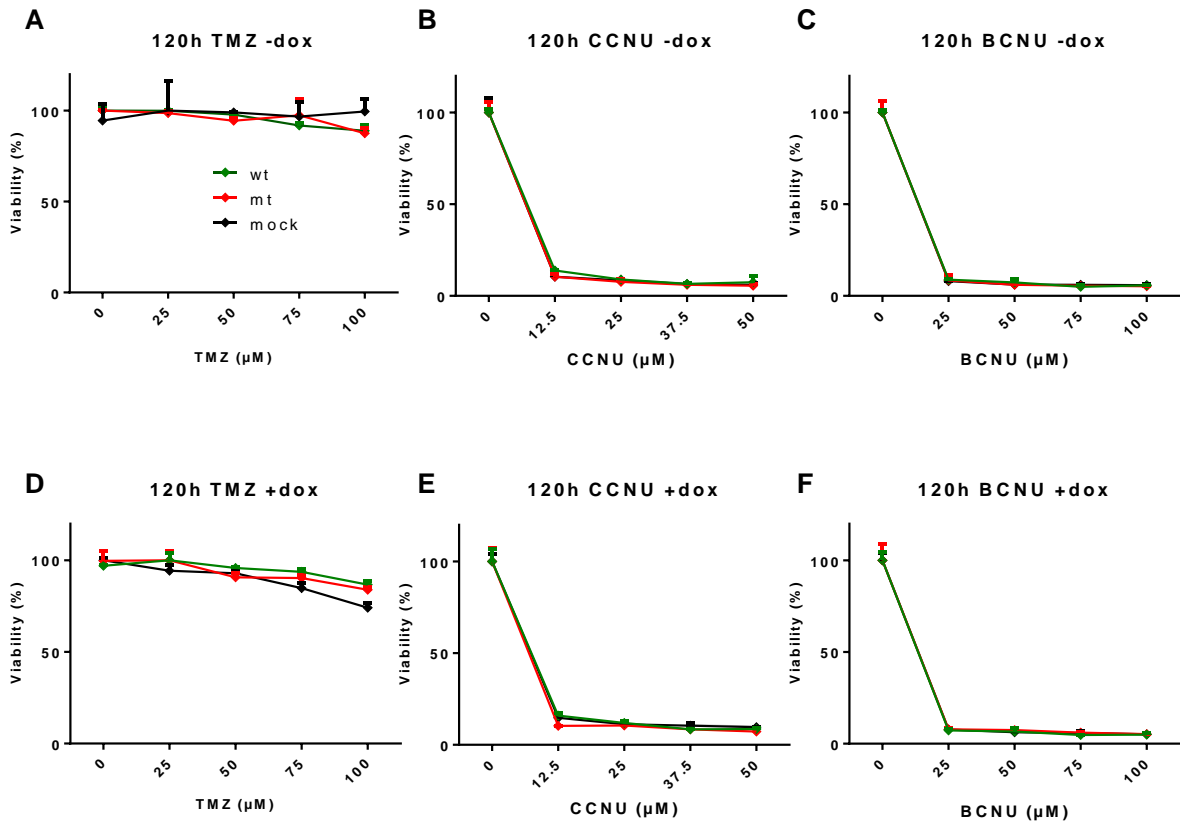
After 72 hours of continuous treatment with increasing doses of either TMZ (**Figure 47 A** and **D**), CCNU (**Figure 47 B** and **E**), and BCNU (**Figure 47 C** and **F**) no survival differences could be found between IDH1mt cells and the IDH1wt and control cell line. TMZ resistance of the LN319 cells due to their *MLH1* promoter methylation (see **Figure 32**) could be verified.

MMS leads to the formation of mutagenic and replication blocking DNA lesions and are widely used to study DNA repair processes, mainly homologous recombination and BER. Tert-Butyl hydroperoxide (tBOOH) is an organic peroxide, which induces a broad spectrum of oxidative damages on proteins and DNA, the latter being repaired by the BER DNA repair pathway. The cells were incubated with increasing doses of MMS and tBOOH for 72 h (**Figure 48 A-D**). IDH1wt cells with dox showed a survival benefit after MMS treatment, which was significant, compared to IDH1mt and vector control cells (**Figure 48 C**). For tBOOH, no significant differences in survival of the cell lines could be detected (**Figure 48 D**).



**Figure 48: Viability of LN319 cells assessed by the MTT assay after 72 h of prolonged treatment.** Panels **A** and **B** show the viability of the three cell lines without the overexpression of the gene of interest (IDH1wt, IDH1mt). Panels **C** and **D** show the viability after overexpression of IDH1wt or IDH1mt. Data are the mean of three independent experiments  $\pm$  SD.

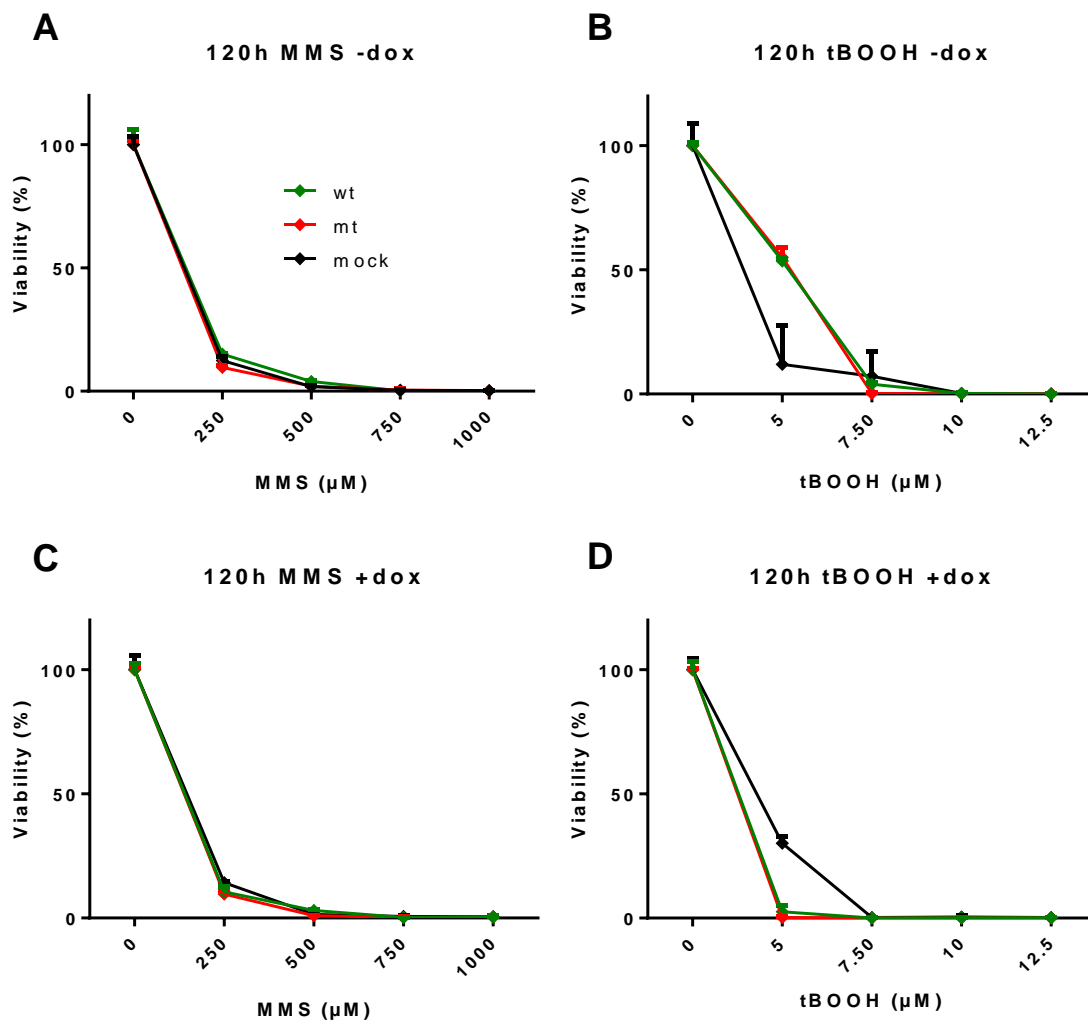
## Results



**Figure 49: Viability of LN319 cells assessed by the MTT assay** after 120 h of prolonged treatment. Panels **A**, **B**, and **C** show the viability of the three cell lines without the overexpression of the gene of interest (IDH1wt, IDH1mt). Panels **D**, **E**, and **F** show the viability after overexpression of IDH1wt or IDH1mt. Data are the mean of three independent experiments  $\pm$  SD.

Long-term TMZ treatment of LN319 cells expressing either IDH1wt or IDH1mt did not result in a different phenotype. TMZ resistance occurred irrespectively of the IDH1 status. That outcome is probably a result of the MLH1 deficiency. Interestingly, IDH1mt cells did not show any additional toxicity compared to IDH1wt and the control cell line (**Figure 49 A, D**). Neither CCNU (**Figure 49 B, E**) nor did BCNU (**Figure 49 C, F**) differently affected the survival of LN319 cells as to their IDH1 status.





**Figure 50: Viability of LN319 cells assessed by the MTT assay** after 120 h of prolonged treatment. Panels **A** and **B** show the viability of the three cell lines without the overexpression of the gene of interest (IDH1wt, IDH1mt). Panels **C** and **D** show the viability after overexpression of IDH1wt or IDH1mt with dox. Data are the mean of three independent experiments  $\pm$  SD.

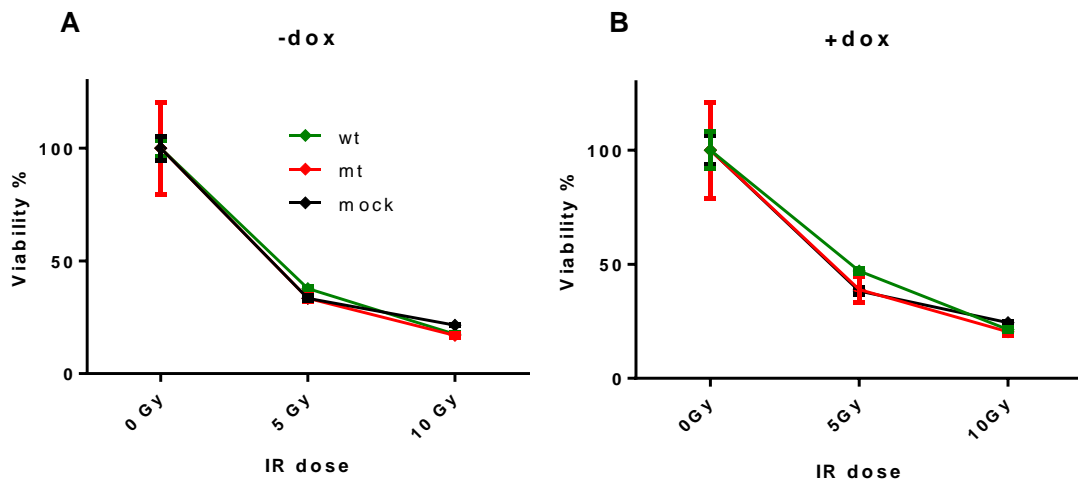
As shown by the viability dose-response curves in **Figure 50 A** and **Figure 50 C**, expression of the mutant IDH1 does not increase the sensitivity of the cells to MMS. Acute oxidative stress induced by tert-butyl-hydroperoxide (tBOOH) did not differently affect LN319 cell survival as to their IDH1 status as shown in **Figure 50 B, D**.

The DNA repair pathways of the homologous recombination and BER seems not affected by the IDH1 mutation.

## Results

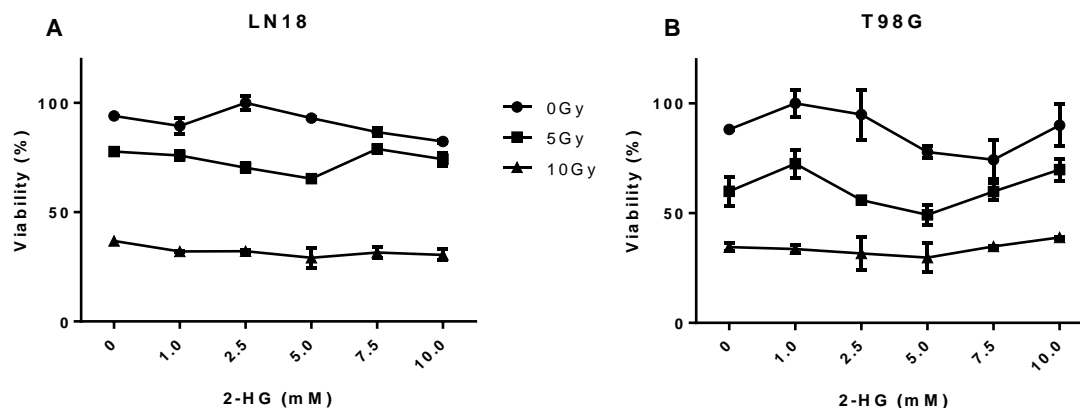
High-grade glioma patients receive concomitant radiation treatment with IR. The LN319 IDH1wt, IDH1mt, and mock control cell system was used to determine the effects of IR on to the survival of the three cell lines.

IDH1wt, mt and control cells were treated with 5 and 10 Gy, and the viability of the cells was determined after 96 h by the MTT assay (**Figure 51**).



**Figure 51: Viability of LN319 cells assessed by the MTT assay.** LN319 IDH1wt, mt, and control cells –dox (A) and +dox (B) were treated with 5 and 10 Gy or IR and viability was measured by the MTT assay after 96 h. Data are the mean of three independent experiments  $\pm$  SD.

Expression of the mutated IDH1 did not sensitize the cells to IR. To further prove that IR does not affect IDH1 mutated cells differently, the two glioma cell lines LN18 and T98G were pre-treated with increasing doses of 2-HG and exposed to 5 and 10 Gy and the viability was measured after 96 h by the MTT assay.



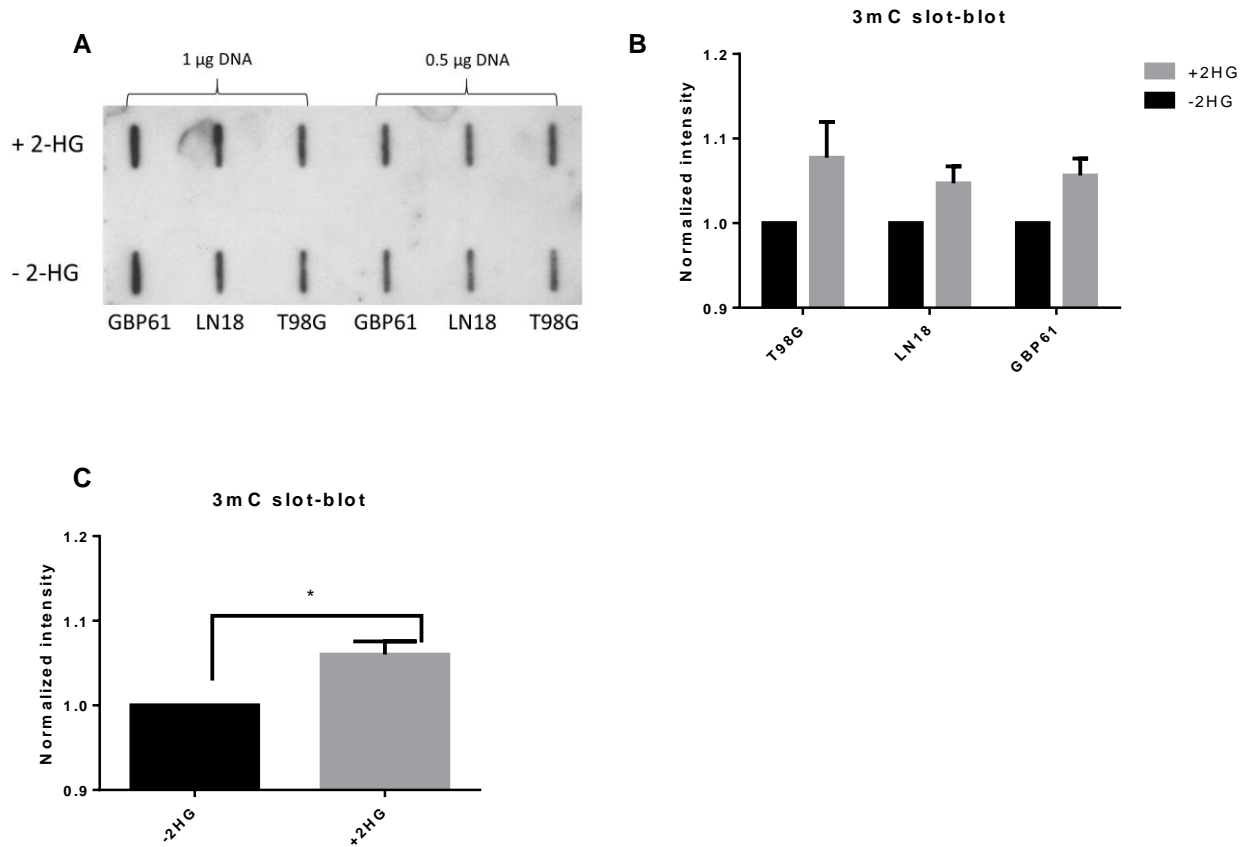
**Figure 52: Viability of LN319 cells assessed by the MTT assay.** Untransformed glioma cell lines (A) LN18 and (B) T98G were pretreated with increasing doses of 2-HG and exposed to 5 and 10 Gy IR. Viability was measured after 96 h by the MTT assay. Data are the mean of three independent experiments  $\pm$  SD.

Pretreatment with 2-HG did not increase the sensitivity to IR in LN18 (Figure 52 A) and T98G (Figure 52 B) cells.

As we could rule out that the better survival prognosis of IDH1 mutated HGA patients is not due to an increased sensitivity of the tumor to the applied chemotherapy or ionizing radiation treatment. Nevertheless, a literature research was undertaken to find possible targets of the 2-HG metabolite that are involved in DNA repair. ALKBH2/3 enzymes were found to be a potential target of 2-HG, as they are  $\alpha$ -KG dependent and act as DNA repair enzymes. ALKBH2/3 enzymes are crucial for the repair of a large spectrum of DNA adducts (see 1.3.1.2).

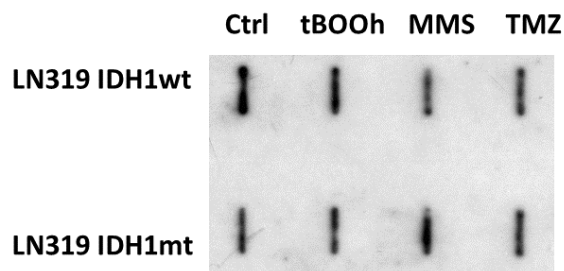
Because MMS leads to the formation of 3-methylcytosine (3mC) which is a known substrate for ALKBH2/3, three glioma cell lines (GBP61, LN18, and T98G) were pretreated with 5 mM 2-HG for 24 h and then exposed to 250  $\mu$ M MMS for another 24 h. DNA was extracted and 3mC was quantified by south-western slot blot (Figure 53 A, B). 2-HG was found to increase the 3mC levels after 250  $\mu$ M MMS in all three cell lines. Paired t-test statistics showed a significant cell line independent increase of 3mC after 2-HG and MMS treatment (Figure 53 C).

## Results



**Figure 53: 3mC quantification by south-western slot blot analysis.** (A) Three glioma cell lines (LN18, T98G, GBP61) were pretreated with or without 5 mM 2-HG for 24 h and then exposed to 250 µM MMS for another 24 h. The normalized band intensities are shown in panel B. 2-HG lead to a significant increase in 3mC after MMS treatment (C). Data are the mean of two independent experiments  $\pm$  SD.

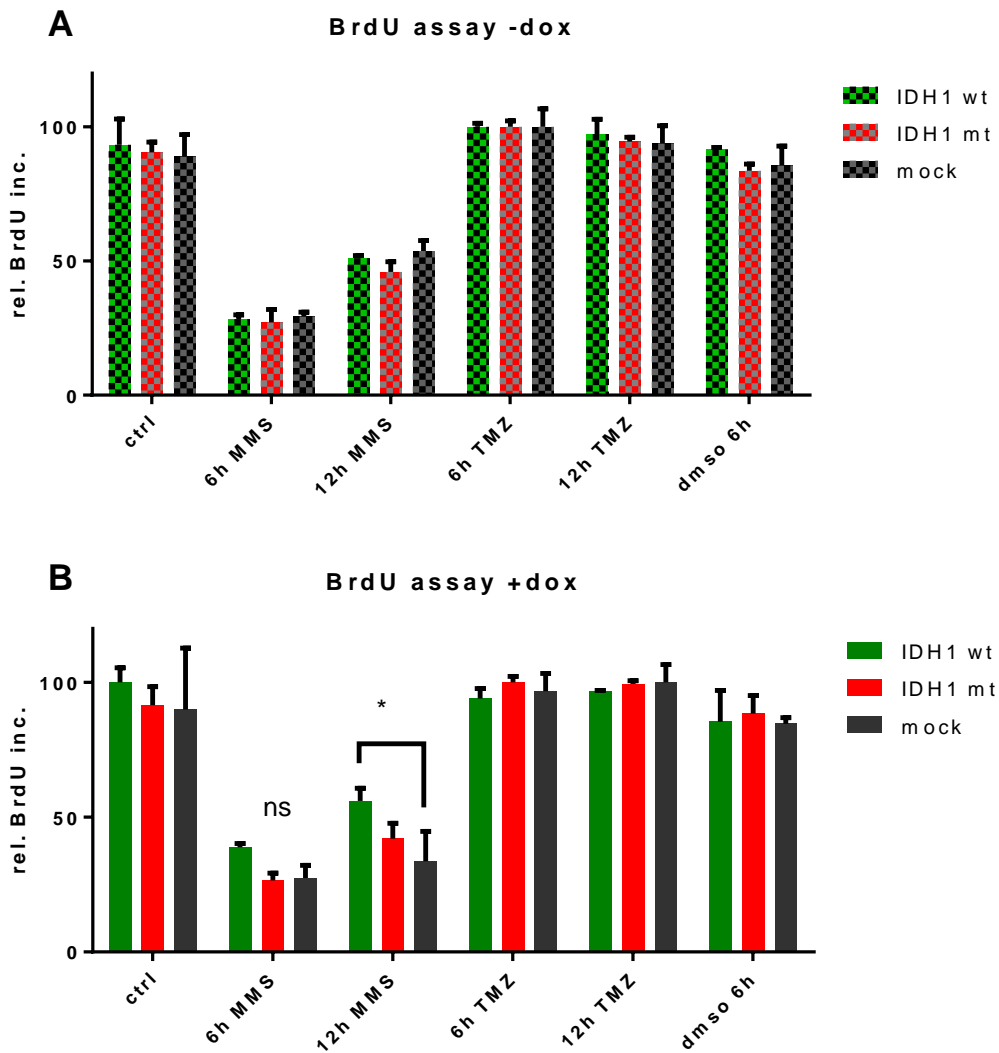
To assess whether MMS treatment together with 2-HG leads to higher 3mC levels can also be observed in IDH1 mutated cells, LN319 IDH1wt and mt cells +dox were treated with 250 µM MMS, 100 µM TMZ, and 50 µM tBOOH for 24 h.



**Figure 54: Slot-blot quantification of 3mC** in DNA of LN319 IDH1wt and mt cells after 24 h exposure to TMZ, MMS, tBOOH, and vehicle alone treatment (Ctrl.). 500 ng DNA were transferred onto the membrane.

As shown in **Figure 54**, the 3mC slot-blot showed a huge signal in the untreated samples, which was even higher than in MMS treated samples and could not be decreased, even after several attempts and repetitions. A BrdU incorporation assay was then chosen as an indirect way of 3mC quantification to quantify replication blockage by 3mC in LN319 IDH1wt, mt, and vector control cells (**Figure 55**).

## Results

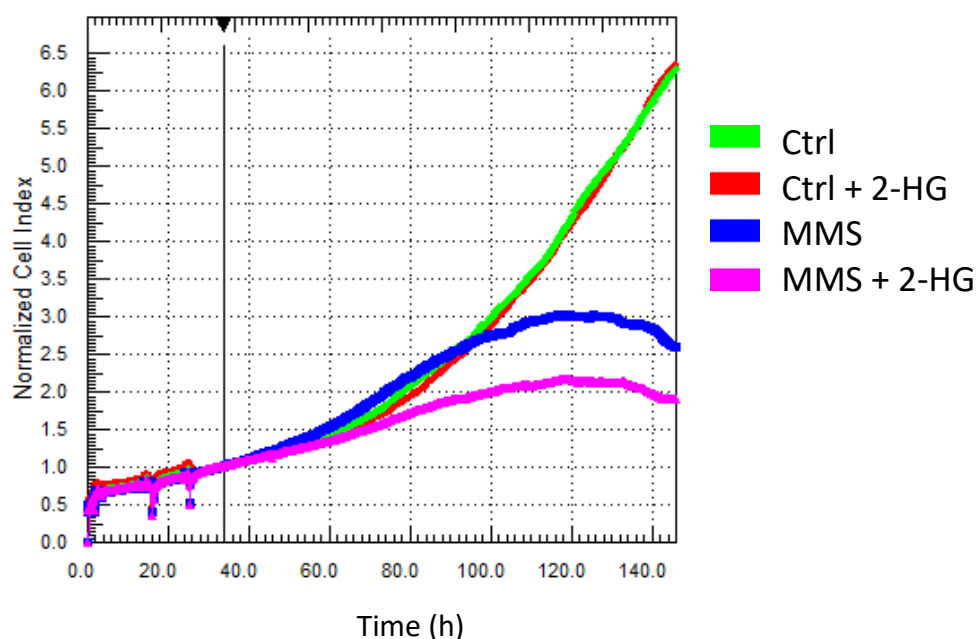


**Figure 55: BrdU incorporation assay** of LN319 IDH1wt, mt, vector control cells (A) without dox and (B) with dox after 6 and 12 of MMS (250  $\mu$ M) or TMZ (100  $\mu$ M) treatment. Data are the mean of two independent experiments  $\pm$  SD.

Without dox, no difference between the three cell lines could be observed. After adding dox, IDH1wt cells showed a significant increase in BrdU incorporation after 12 h of MMS treatment compared to IDH1mt and control, but IDH1mt did not show a higher S-phase blockage than the control cell line.

To further prove the point, that 2-HG produced by the IDH1 mutation leads to S-phase blockage and therefore a decreased proliferation rate, T98G cells were pretreated with 5 mM 2-HG for 24 h and then treated with 250 mM MMS. The cellular proliferation was analyzed by the iCELLigence real-time cell analysis (RTCA) system compared to the appropriate controls. The iCELLigence RTCA system uses noninvasive electrical impedance to quantify cell proliferation

and morphology change in a label-free, real-time manner. It measures the well coverage and spread of the cells in real-time. That system makes it possible to not only chose certain time points for viability measurements, but to analyze the coverage of the cell culture well every minute.



**Figure 56: iCELLigence real-time cell analysis of MMS treated T98G cells.** Pretreatment with 5 mM 2-HG was performed 18 h after seeding. 24 h after seeding, cells were treated with 250 mM MMS. 2-HG pretreatment alone did not affect cell grow over time. Cells were pre-treated with 2-HG and MMS treatment showed a reduced normalized cell index, indicating a reduced cell viability.

Cells were more sensitive towards MMS when pretreated with 2-HG (**Figure 56**). MTT assays were performed to validate this result. LN18 and T98G cells were pretreated with increasing doses of 2-HG (1-10 mM) and exposed to 100 and 250  $\mu$ M MMS. The viability of the cells was measured after 72 h, but no 2-HG dependent sensitization of the cells towards MMS could be observed (**Supplementary Figure 3**).

Despite of results shown here, that 2-HG leads to more MMS induced 3mC accumulation in the DNA and that viability measurements showed a decreased survival, the hypothesis that IDH1mt leads to higher sensitivity towards methylating agents was dropped due to unpersuasive and non-reproducible results.

## Results

This leads to the conclusion that the increased survival of patients suffering from an IDH1 mutated glioma is not due to the increased sensitivity of the tumor towards the applied treatment, including alkylating agents and irradiation. Therefore, the IDH1 mutation in HGA patients should not be seen as a predictive factor, but a prognostic factor.

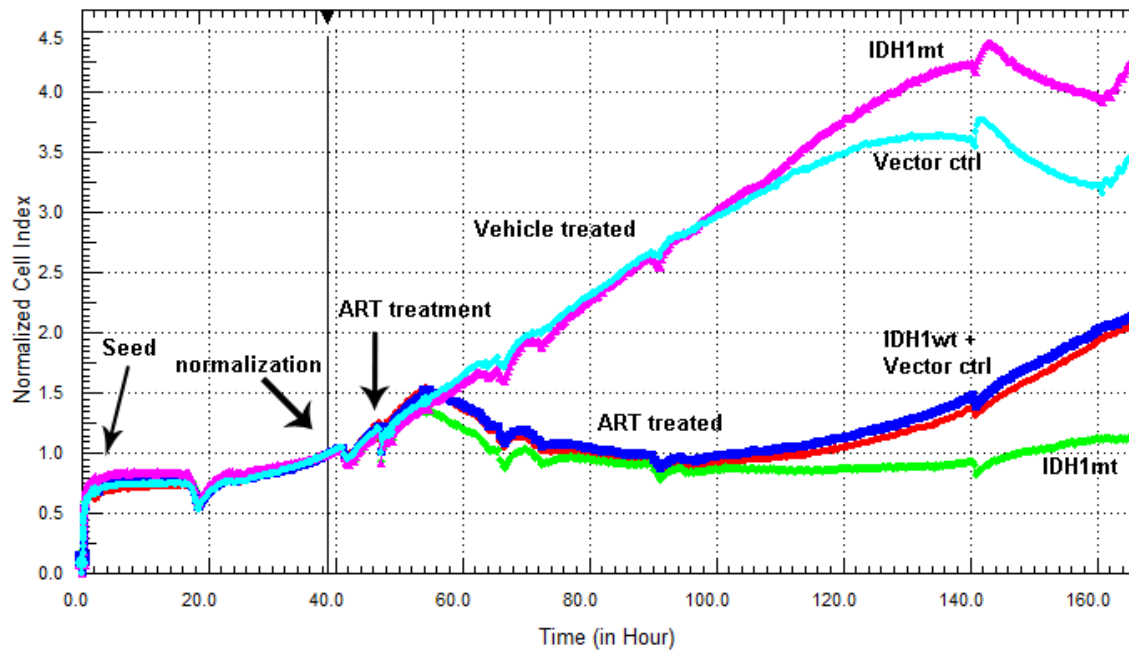
A literature research for each DNA lesion repaired by ALKBH2/3 was performed, and 1, *N*<sup>6</sup>-ethenoadenine ( $\epsilon$ A) and was chosen as a lesion that might be worth of studying deeper. Etheno adducts are highly mutagenic if left unrepaired. The repair of these lesions can be accomplished by the BER pathway leading to single strand breaks as repair intermediates, or by a direct reversal without DNA incision by ALKBH2/3. *In vivo*, etheno adducts are formed by ROS interacting with PUFAs derived from membrane phospholipids resulting in the production of reactive aldehydes as lipid peroxidation byproducts, such as trans-4-Hydroxy-2-nonenal (4-HNE) (see **Figure 10**). Unlike tBOOH that result in a high ROS peak within minutes, artesunate leads to a sustained release of ROS, reaching a maximum ROS level after 24 h (Berdelle et al. 2011). A sustained non-lethal level of ROS is a key driver of lipid peroxidation (Nair et al. 2006; Fritz and Petersen 2011). Artesunate (ART) was shown to produce  $\epsilon$ A adducts (see 1.2.4). As a result, the working hypothesis was changed, and ART treatment of IDH1 mutated and control cells was performed.

### 3.2.3. Cytotoxic effect of artesunate in LN319 IDH1wt and mt cells

As a first screening experiment, the cellular growth behavior of LN319 IDH1wt, mt, and vector control +dox was analyzed by the impedance-based iCELLigence system. Cells were treated 48 h after seeding with 2.5  $\mu$ g/ml ART or vehicle alone, and impedance was monitored every 15 min for over 160 h.

Although the chosen ART concentration was high and exhibited strong cytotoxic effects in all cell lines, IDH1wt and vector control cells recovered 60 h after ART treatment, whereas the IDH1mt cells did not. The cell density of IDH1wt and vector control cells was higher compared to IDH1mt cells at the end of the observation period (**Figure 57**).

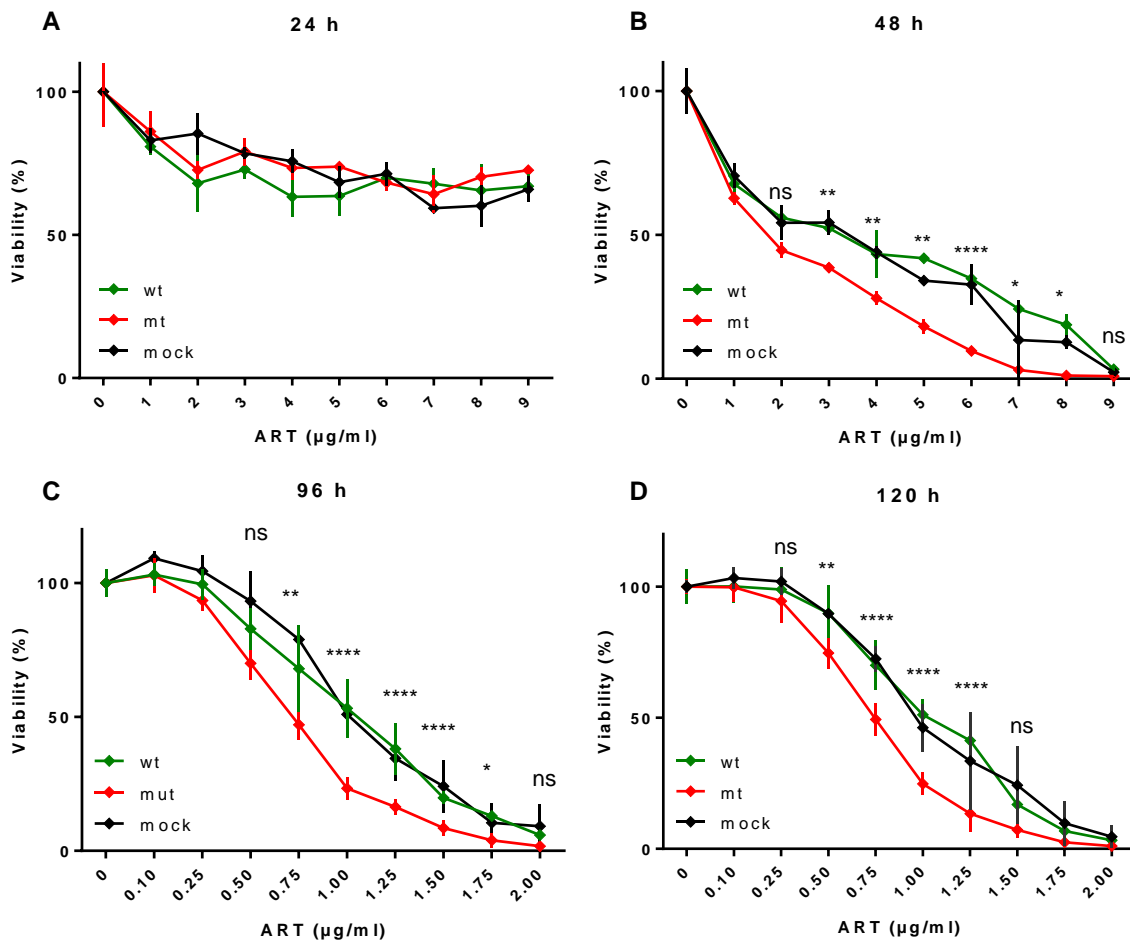




**Figure 57: iCELLigence in real-time monitoring of cell proliferation.** Cells were seeded and treated with 2.5  $\mu\text{g}/\text{ml}$  ART after 48 h of settlement. ART treated IDH1wt and vector control cells recovered around 60 h after treatment, whereas the IDH1mt cells did not recover as fast.

Because the iCELLigence system only provides 16 wells for analysis, further analysis was performed using the MTT assay in 96 well plates. LN319 cells were treated with increasing doses of ART and cell death was analyzed after 24, 48, 96, and 120 hours. Cell line sensitivity differences after ART treatment became apparent after 48 h (**Figure 58 A-D**). To assess long-term effects, the ART doses were reduced because of too high toxicity. After 96 and 120 h of ART treatment, IDH1mt cells were significantly less viable compared to the IDH1wt and control cell line (**Figure 58 C, D**). Short term and long term treatment with ART lead to more cell death in the IDH1 mutated cell line as measured by MTT assay, compared to IDH1wt and vector control.

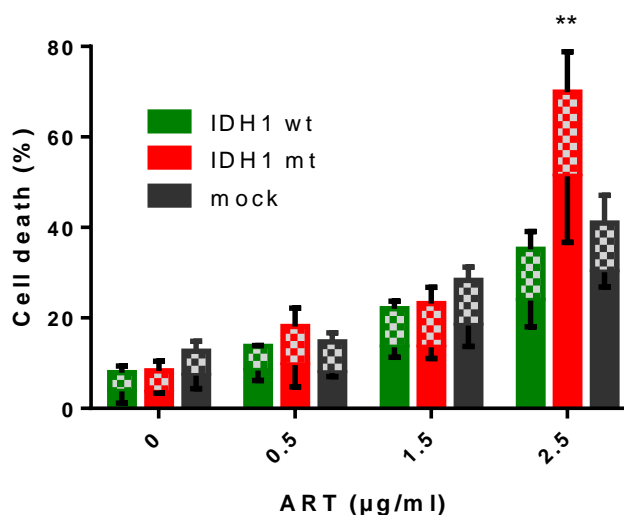
## Results



**Figure 58: Viability of LN319 cells assessed by the MTT assay.** Analysis of ART-induced cell death in LN319 IDH1 wt, mt, and mock control cells. Viability of the cells was measured after 24 h (A), 48 h (B), 96 h (C), and 120 h (D) of continuous ART treatment. Data are the mean of three independent experiments  $\pm$  SD. Data were analyzed by two-way ANOVA with Tukey post hoc test. ns = non-significant

The IDH1 mutation leads to a sensitization towards ART treatment, but the overexpression of IDH1wt does not increase viability compared to the control cell line. These results are consistent with the results obtained by the iCELLigence system.

As a third method of cell death measurement, the cells were stained with Annexin V/PI and cell death was qualified and quantified by FACS. LN319 cells +dox were treated for 120 h with increasing doses of ART and the amount of apoptotic and necrotic cells was quantified.



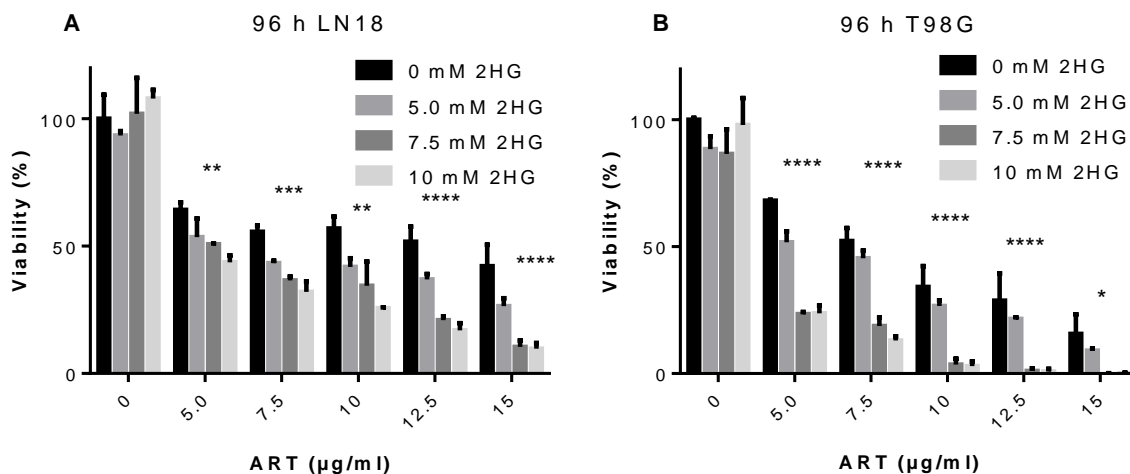
**Figure 59: Annexin V/PI staining and flow cytometry analysis** after 120 h of ART treatment indicated that IDH1 mutation leads to more apoptosis (solid bars) compared to overexpression of IDH1 wild-type or vector control. The level of necrosis (checked bars) was not significantly different. Data are the mean of three independent experiments  $\pm$  SD. Data were analyzed by two-way ANOVA with Tukey post hoc test.

The FACS analysis confirmed the results obtained from the iCELLigence and MTT assays. Cells expressing IDH1mt are more sensitive towards ART treatment compared to IDH1wt and vector control cells (**Figure 59**). The FACS analysis has shown, that the ART induced apoptosis is significantly higher in IDH1mt cells at a dose of 2.5  $\mu$ g/ml, but necrosis is not different between the three cell lines. The differences in cell death at a certain ART dose compared to the MTT assay results are caused because the ratio of cells per area and cells per media volume are not the same in both cell culture assays. For the FACS analysis, we used 6 cm culture dishes (21 cm<sup>2</sup> surface area) having 65 times the area of a 96-well surface area. The media volume was increased 20 fold in the 6 cm cell culture dishes (4 ml), and the cell amount was chosen to be 30 times larger than for the 96 well plate assays. In short, for each cell culture system the cytotoxic ART concentration to has to be determined empirically.

## Results

### 3.2.4. Influence of 2-HG on ART induced cell death

To test if 2-HG by itself is responsible for the increased sensitivity of IDH1 mutated cells to ART, LN18 and T98G glioblastoma cell lines were pretreated (1 h) with physiological 2-HG concentrations (5 to 35 mM; see 1.2.1) together with increasing doses of ART over 96 h and cell viability was measured by the MTT assay.

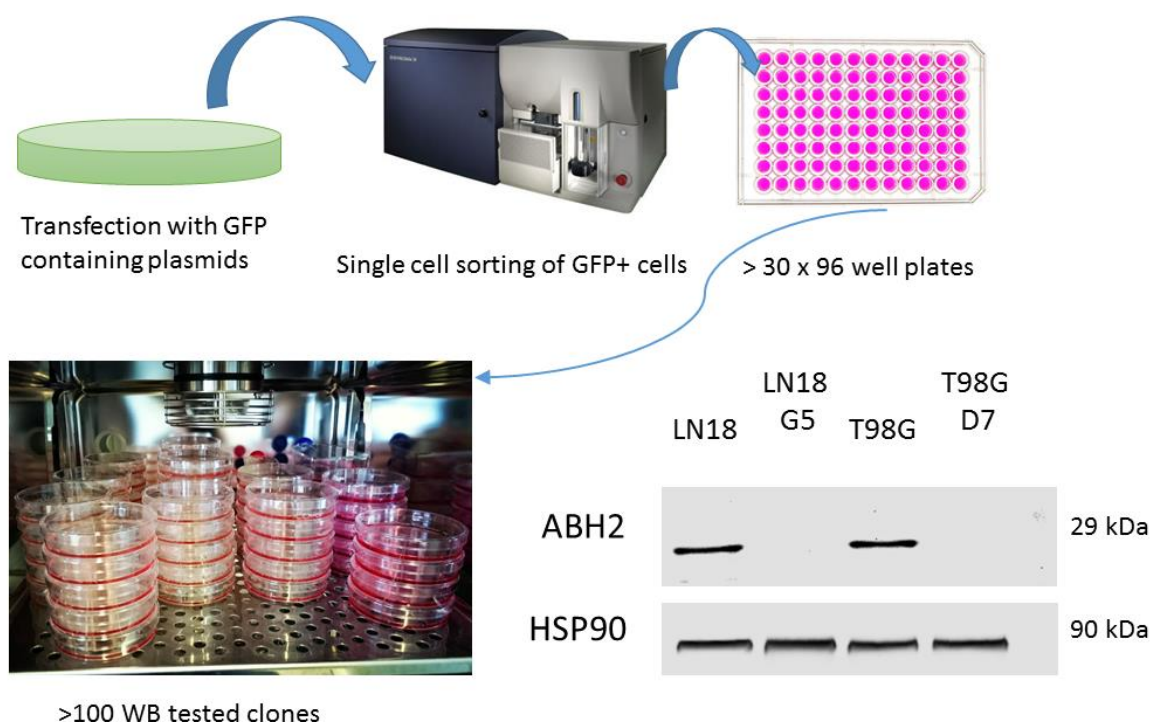


**Figure 60: Viability of 2-HG pretreated LN18 and T98G cells assessed by the MTT assay after 96 h of ART treatment.** 2-HG increases ART sensitivity in a dose depended manner in LN18 (A) and T98G (B) cell lines. Indicated significances represent the statistical comparison of 7.5 mM 2-HG vs. 0 mM 2-HG at a certain ART concentration. Data are the mean of three independent experiments  $\pm$  SD. Data were analyzed by two-way ANOVA with Tukey post hoc test.

The results presented in **Figure 60** show that 2-HG was able to sensitize both cell lines dose dependently towards ART treatment. The applied 2-HG concentrations alone did not affect cell growth. 7.5 mM of 2-HG sensitized LN18 (**Figure 60 A**) and T98G (**Figure 60 B**) cells to ART significantly. As a next step, the involvement of ALKBH2 in the ART mediated toxicity was assessed by knocking out ALKBH2 in LN18 and T98G cells.

### 3.2.5. Effect of DNA alkylation and ART in ALKBH2 knock-out cells

To determine if ALKBH2 is involved in the counteraction of ART induced cytotoxicity, the CRISPR/Cas9 method was used to knock out ALKBH2 in LN18 and T98G cells. The knock-out was performed with a pool of three different plasmids, each harboring different gRNAs with Cas9 and GFP expression (see 2.5). Transfection was performed with Effectene (Qiagen), and GFP positive cells were single cell sorted into 96 well plates. Over 100 clones were expanded, and the successful knock-out of ALKBH2 was verified by western blot. One successful ALKBH2 knock-out (KO) clone for each cell line could be generated as demonstrated by the lack of ALKBH2 protein expression (LN18 G5 and T98G D7) (**Figure 61**).

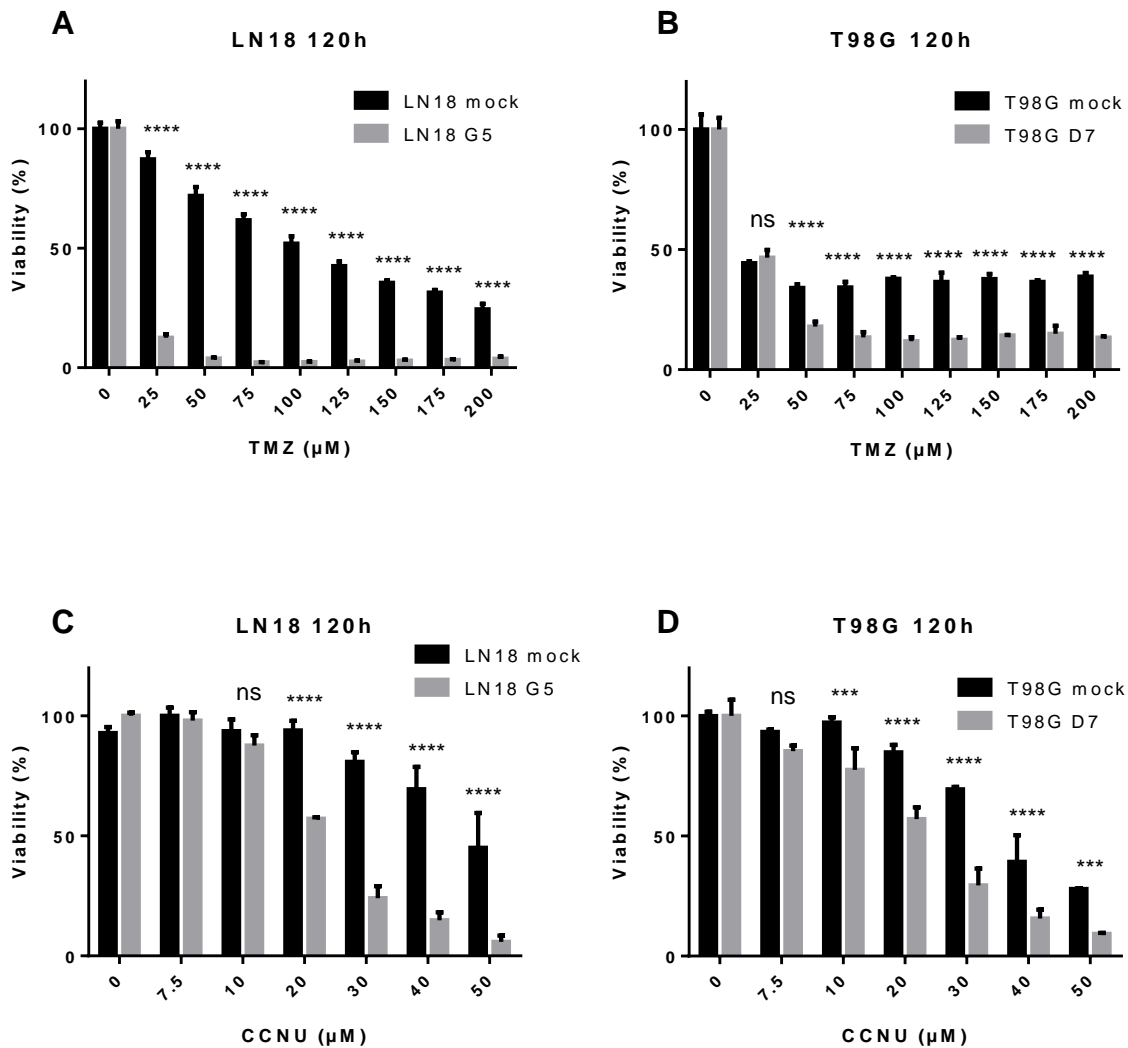


**Figure 61: Workflow of CRISPR/Cas9 knock-out of ALKBH2 in LN18 and T98G cell lines.** 24 h after transfection with GFP containing ALKBH2 or nonsense KO plasmids, cells were trypsinized. Single cell sorting of DAPI negative and GFP positive cells into 96 well plates was performed on an Aria III SORP CellSorter (BD Biosciences). After 10 days, cell clones were expanded in 24, 12, and later 6 well plates. After having obtained enough cells, Western blot analysis of successful ALKBH2 knock-out in LN18 and T98G glioma cell lines was performed for over 100 clones. One knock-out clone for each cell line could be established.

The genotype of these cells was further verified by phenotype verification. LN18, G5, T98G, and D7 cells were treated with increasing doses of TMZ and CCNU, as they induce different

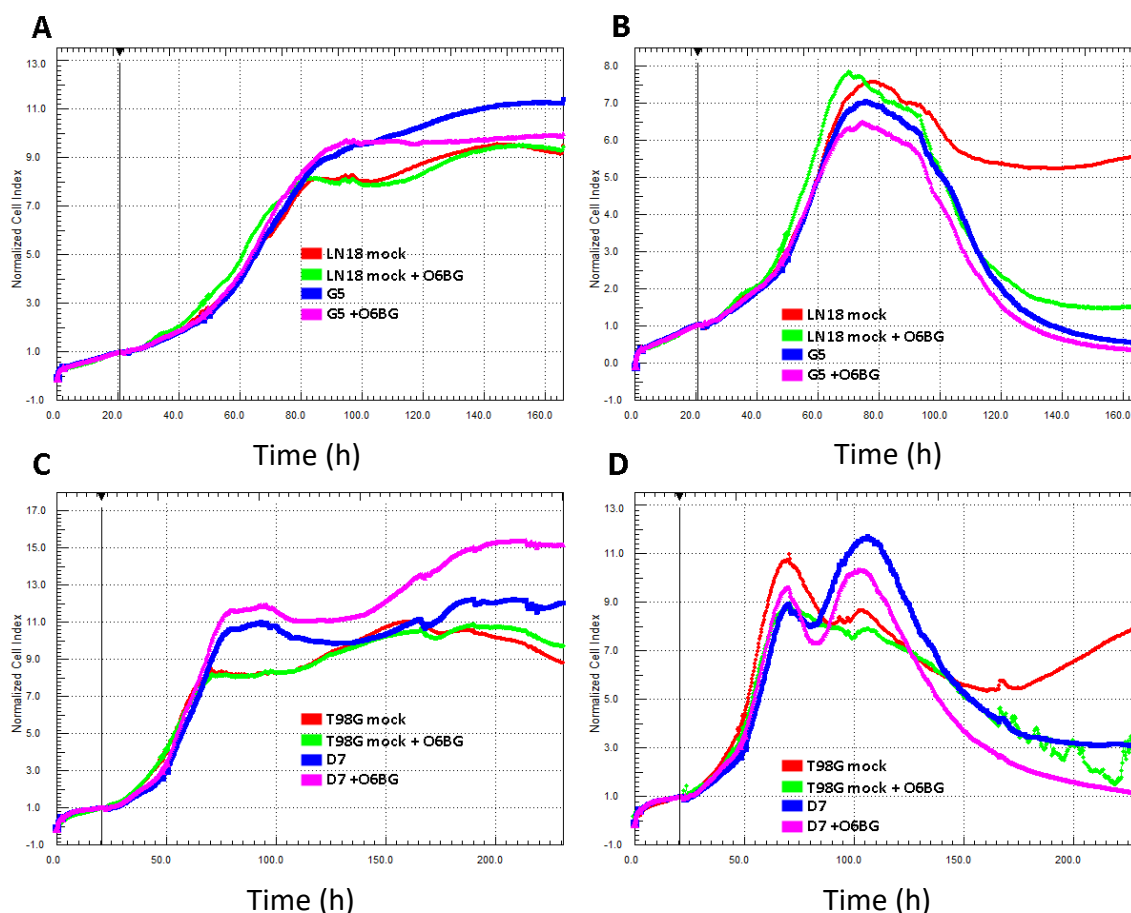
## Results

DNA alkylations (see **Figure 7**) that are a target of ALKBH2. ALKBH2 knock-out cells should therefore show an increased sensitivity towards TMZ, although all cells are MGMT proficient. After 120 h of treatment with TMZ and CCNU, cell viability was measured by the MTT assay. The ALKBH2 KO cells proved to be susceptible towards TMZ and CCNU treatment (**Figure 62**).



**Figure 62: Viability of ALKBH2 KO cells assessed by the MTT assay.** Survival of the parental LN18 (**A, C**) and T98G (**B, D**) cell lines was compared to their respective ALKBH2 KO (LN18 G5 and T98G D7) counterpart after increasing doses of TMZ (**A, B**) and CCNU (**C, D**) for 120 h. Data are the mean of two independent experiments  $\pm$  SD. Data were analyzed by two-way ANOVA with Tukey post hoc test. ns = non-significant

As a second method to verify this phenotype, ALKBH2 KO cells and their parental counterparts were treated with 50  $\mu\text{M}$  TMZ with or without  $O^6\text{BG}$  which inhibits MGMT, and their survival was quantified in real-time by the iCELLigence system.

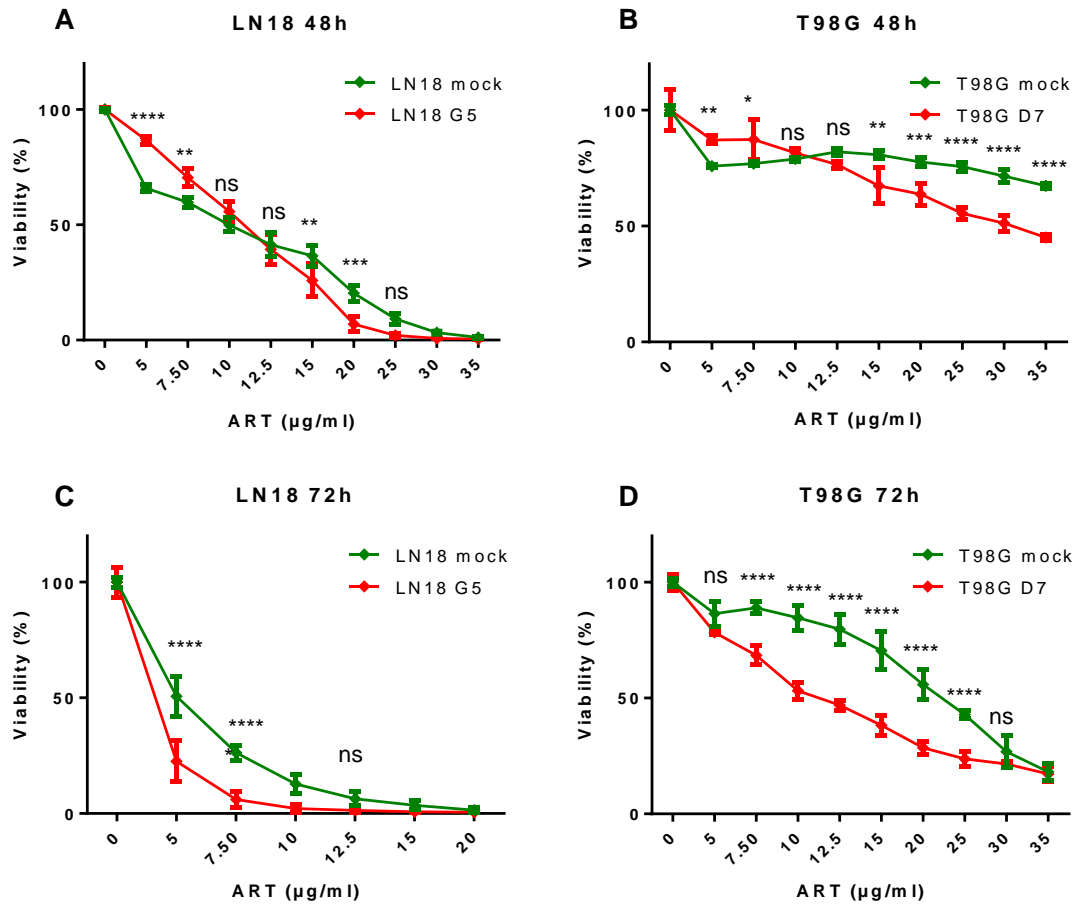


**Figure 63: TMZ induced cell death was assessed by the RTCA iCELLigence system.** All clones were tested with or without additional  $O^6BG$ . (A) shows untreated LN18 and G5 cells. (B) shows LN18 and G5 cells treated with 50  $\mu$ M TMZ. (C) shows untreated T98G and D7 cells. (D) shows T98G and D7 cells treated with 50  $\mu$ M TMZ.

The RTCA of the TMZ treatment of ALKBH2 KO cells and their parental cell lines clearly shows, that a lack of ALKBH2 leads to an immense sensitization of the cells, which is as prominent as the pretreatment of the parental cell line with  $O^6BG$  (Figure 63).

After the successful characterization of the cells, we tested if the ALKBH2 KO cells display in increased sensitivity to ART compared to their parental ALKBH2 wt counterpart. The cells were treated with increasing doses of ART, and their viability was measured by the MTT assay after 48 and 72 h.

## Results

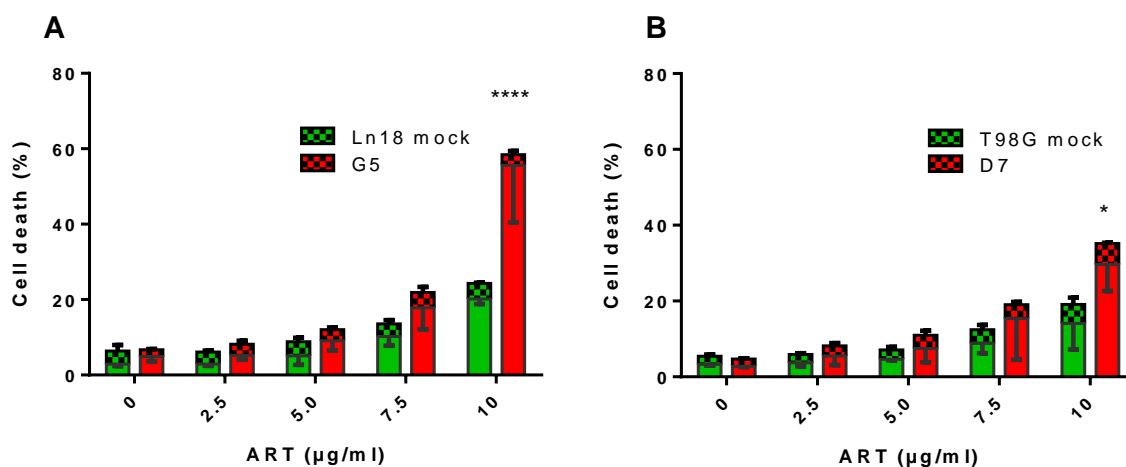


**Figure 64: Viability of ALKBH2 KO cells assessed by the MTT assay.** ALKBH2 knock-out (A, C) LN18 and (B, D) T98G cells and their mock transfected parental cell lines were treated with ART for (A, B) 48 h and (C, D) 72 h. After 72 h of ART treatment, ALKBH2 KO cells were significantly more sensitive towards ART, without exception. Data are the mean of three independent experiments  $\pm$  SD. Data were analyzed by two-way ANOVA with Tukey post hoc test. ns = non-significant

As shown in **Figure 64**, the MTT survival curves of the parental and KO cell line crossed each other at an ART concentration between 10 and 12.5  $\mu\text{g/ml}$  after 48 h of ART treatment. The reason for this might be the slightly different growth rate. The parental cell lines always showed a slightly higher growth rate than their KO counterparts (data not shown). This effect was evident during cell culturing, as the parental cell lines had to be split at a slightly higher ratio compared to the KO cells. Especially the T98G D7 cell line showed a notably slower growth rate compared to the parental cell line. After 72 h of ART treatment, ALKBH2 KO cells were significantly less viable than the parental cell lines, without exceptions (**Figure 64 C,D**).



To further confirm this result, staining with Annexin V/PI after ART treatment was performed and cell death was qualified and quantified by FACS.

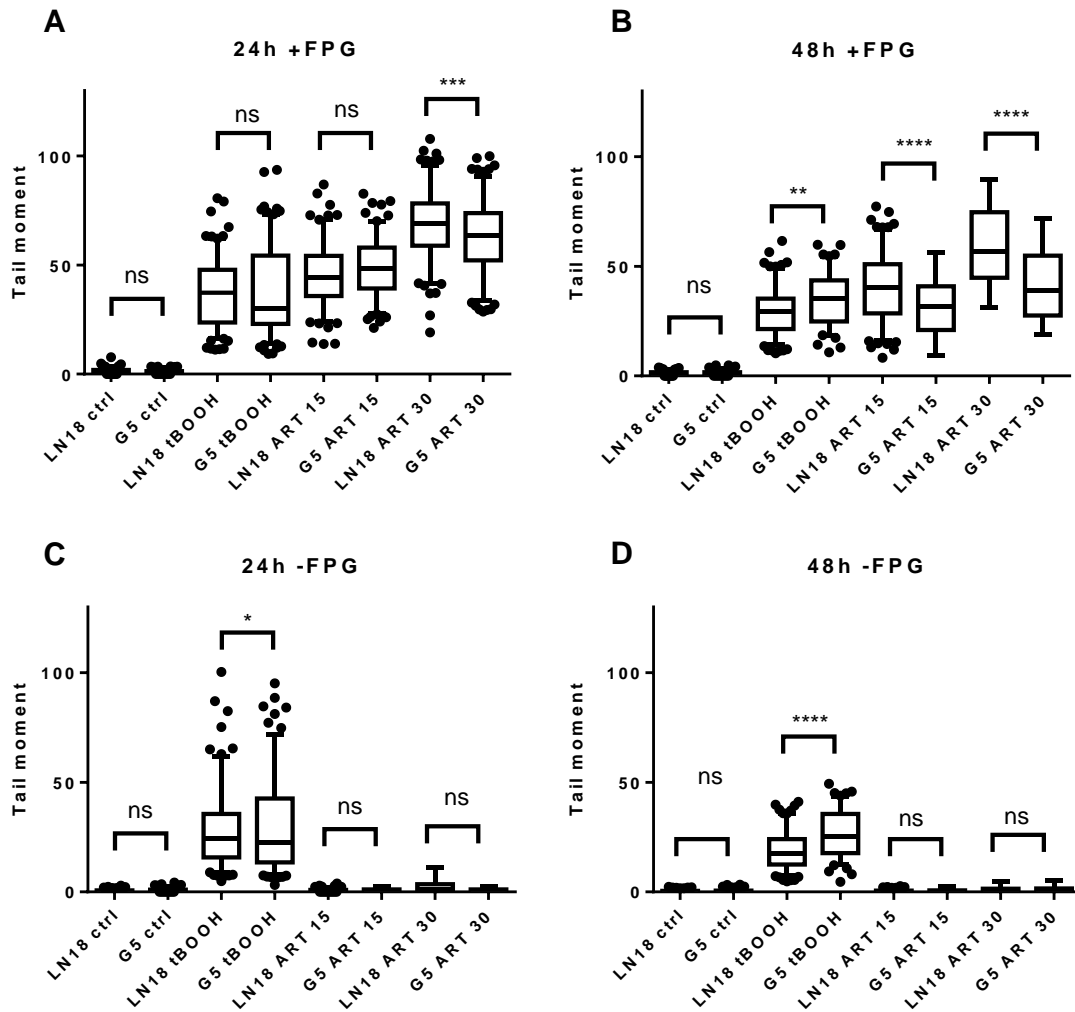


**Figure 65: Annexin V/PI staining and flow cytometry analysis** after 120 h of ART treatment indicates that ALKBH2 knock-out in (A) LN18 and (B) T98G leads to more apoptosis (solid bars) cells compared the parental cell lines. The level of necrosis (checked bars) was not significantly different. Data are the mean of two independent experiments  $\pm$  SD. Data were analyzed by two-way ANOVA with Tukey post hoc test.

As shown in **Figure 65**, the ART induced apoptosis was significantly higher in ALKBH2 KO cells. This result could be verified in LN18 ALKBH2 KO cells (**Figure 65 A**), as well as in T98G ALKBH2 KO cells (**Figure 65 B**). The level of necrosis was not differently affected by the genotype.

ART gives rise to 8-oxoG, which is a potent inducer of apoptosis. To exclude that the observed phenotype of the ALKBH2 KO cells (hypersensitivity to ART) is due to a higher amount of 8-oxoG, FPG-modified alkaline comet assay was performed after 24 and 48 h of ART treatment in ALKBH2 KO cells and their corresponding parental cell lines.

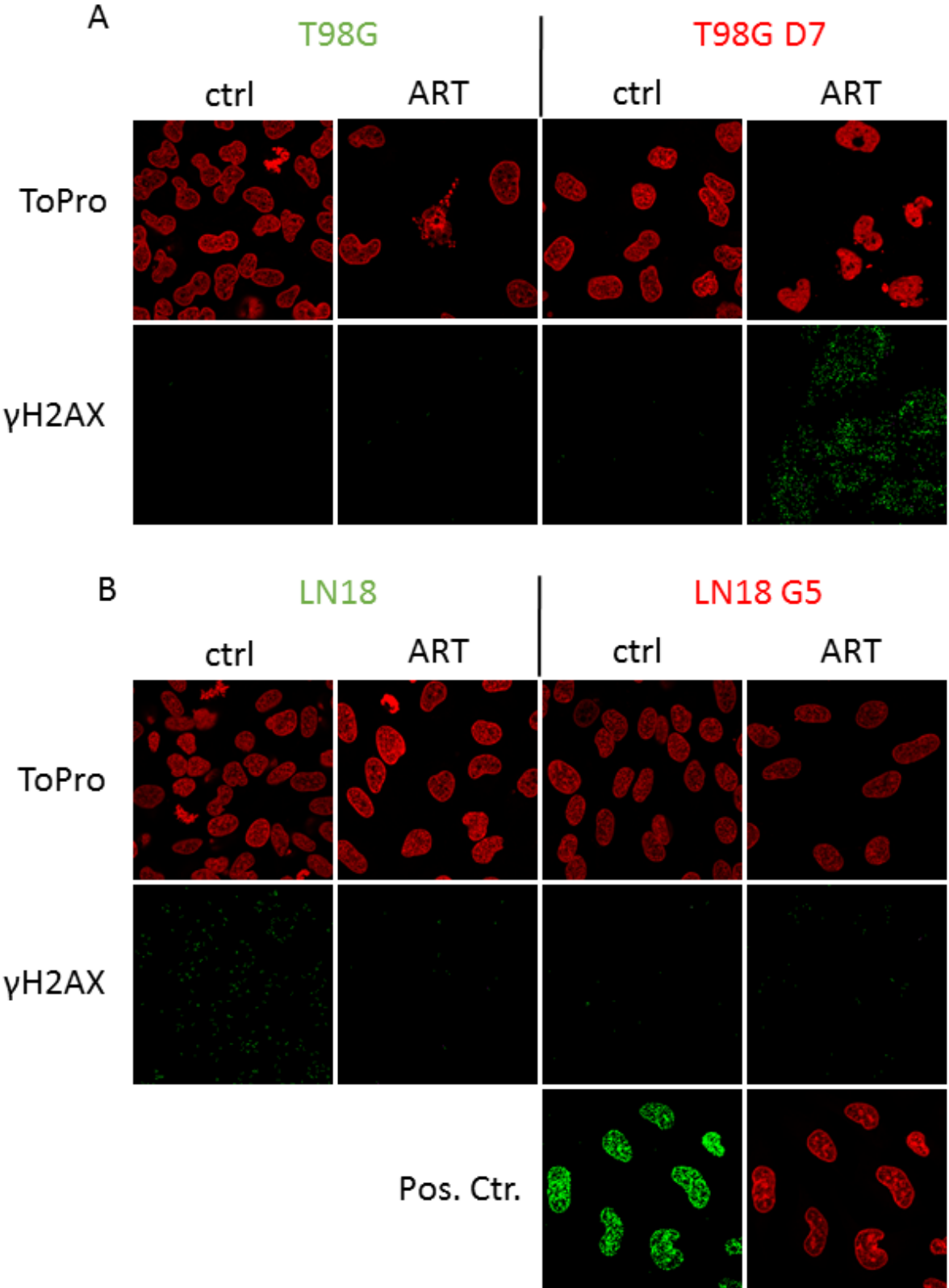
## Results



**Figure 66: FPG modified alkaline Comet assay** was performed for LN18 and G5 cells after 15 and 30  $\mu\text{g}/\text{ml}$  ART for either 24 h (A, C) or 48 h (B, D). (A) and (B) shows the tail moment after FPG cleavage of 8oxoG sites, (C) and (D) without the addition of FPG. Data are the mean of three independent experiments  $\pm$  SD. Data were analyzed by two-way ANOVA with Tukey post hoc test. ns = non-significant

As shown in **Figure 66** A to D, the amount of ART-induced 8-oxoG was not higher in the ALKBH2 KO cells. From this, it is concluded that the KO cells were not exposed to a higher ROS burden following ART treatment compared to the parental cell lines.

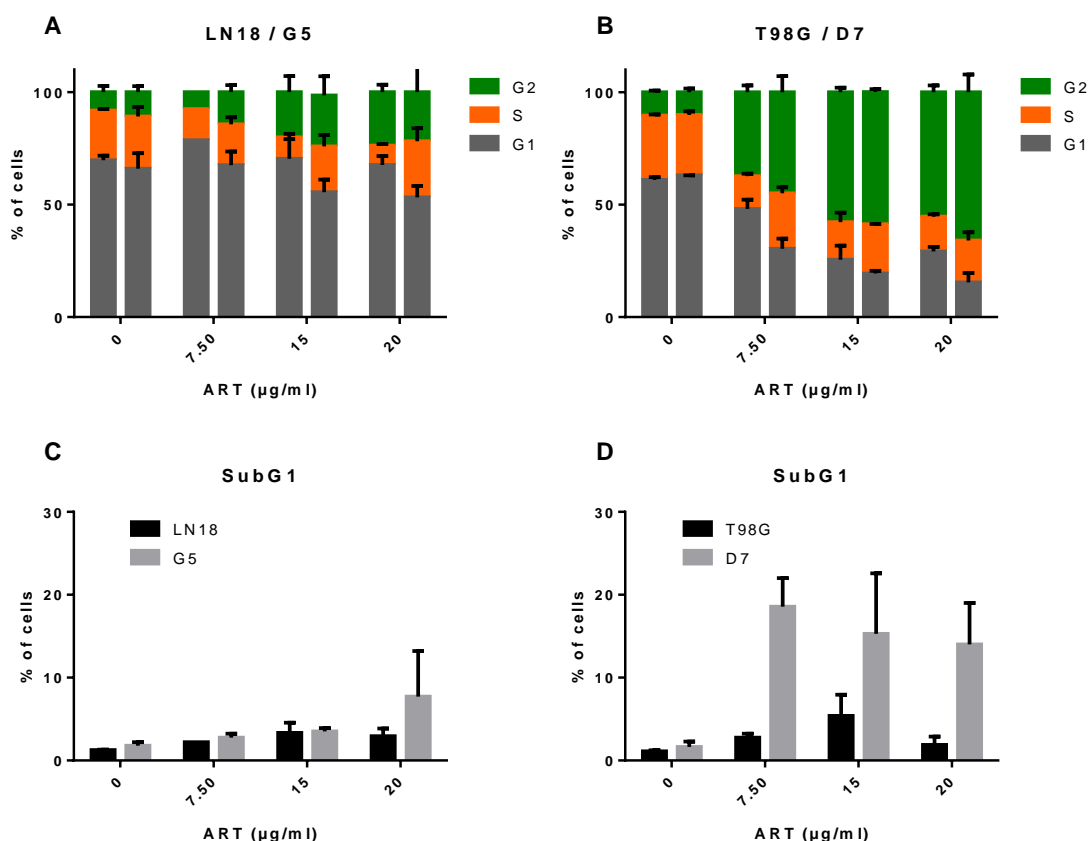
The mode of action of ART to induce apoptosis is under debate. As some papers (Li et al. 2008; Berdelle et al. 2011) have stated, that ART induces DSB, it is of interest to elucidate whether this is also true for the cell model used in this study. Therefore, LN18, LN18 G5, T98G, and T98G D7 cells were treated with 7.5  $\mu\text{g}/\text{ml}$  ART for 72 h and the amount of DSB was measured by  $\gamma\text{H2AX}$  staining. Images were generated on a confocal LSM. Representative image examples are shown in **Figure 67** A and B.



**Figure 67: Immunofluorescence images** showing (A) T98G and D7 ALKBH2 KO and (B) LN18 and G5 ALKBH2 KO cells after 72 h of 7.5 μg/ml ART treatment or vehicle alone. No induction of γH2AX could be measured. The positive control was treated with 50 μM TMZ + O<sup>6</sup>BG after 72 h in T98G cells.

The concentration of 7.5  $\mu\text{g/ml}$  ART, which was shown to decrease the cell number in an exponentially growing population significantly (see **Figure 64**) did not lead to the formation of DSB. As the  $\gamma\text{H2AX}$  signal was very low, the brightness and contrast of the images were enhanced so that some background staining is visible, resulting in weak perinuclear  $\gamma\text{H2AX}$  staining in the T98G D7 cell line. In conclusion, the cytotoxic effect of ART in LN18, G5, T98G, and D7 cells is not a consequence of DSB induction.

Next, a potential delay in the cell cycle progression resulting from ART treatment was quantified in LN18, G5, T98G, and D7 cells. Cells were treated with increasing doses of ART for 48 h and cell cycle analysis, as well as SubG1 measurements as a marker for apoptosis, were performed on a FACS. Cell cycle distribution was quantified and qualified by ModFit LT.

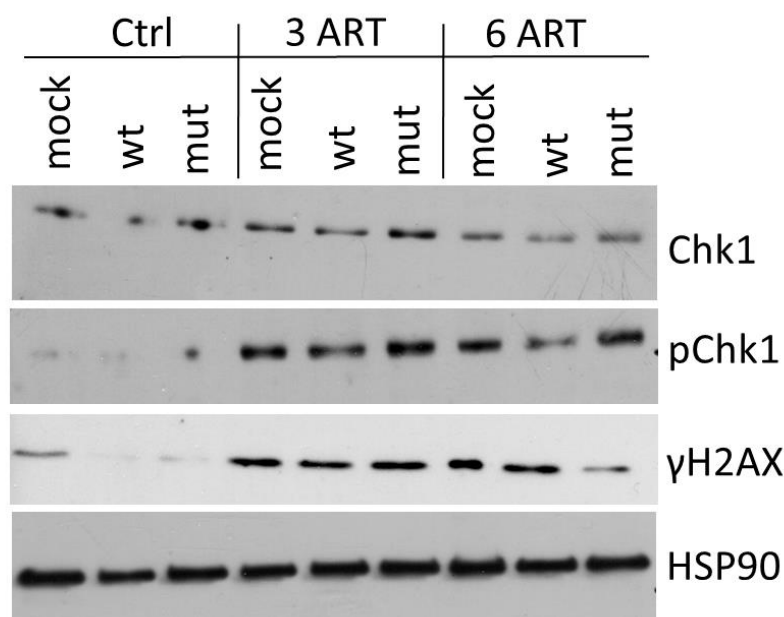


**Figure 68: Cell cycle distribution** was measured by PI staining and FACS analysis in (A) LN18 and G5 and (B) T98G and D7 cells after increasing doses of ART for 48 h. The left bar represents the parental and the right bar the ALKBH2 knock-out cell line. (C) Apoptosis was measured by SubG1 population quantification after increasing doses of ART in LN18 /G5 cell and in T98G/D7 cells (D). Data are the mean of two independent experiments  $\pm$  SD.

## Results

ART delayed the cell cycle of all cell lines. In LN18 cells, ART leads to an increased S-phase fraction when ALKBH2 is lacking (**Figure 68 A**). In T98G cells, ART leads to S-phase and G2 block, which was more prominent in ALKBH2 lacking cells (**Figure 68 B**). The induction of the SubG1 fraction was more notable in the ALKBH2 KO cells compared to their parental counterparts (**Figure 68 C, D**).

To confirm the S/G2 block, western blot analysis was performed for CHK1 and H2AX phosphorylation in LN319 cells, expressing IDH1 wt or mt.

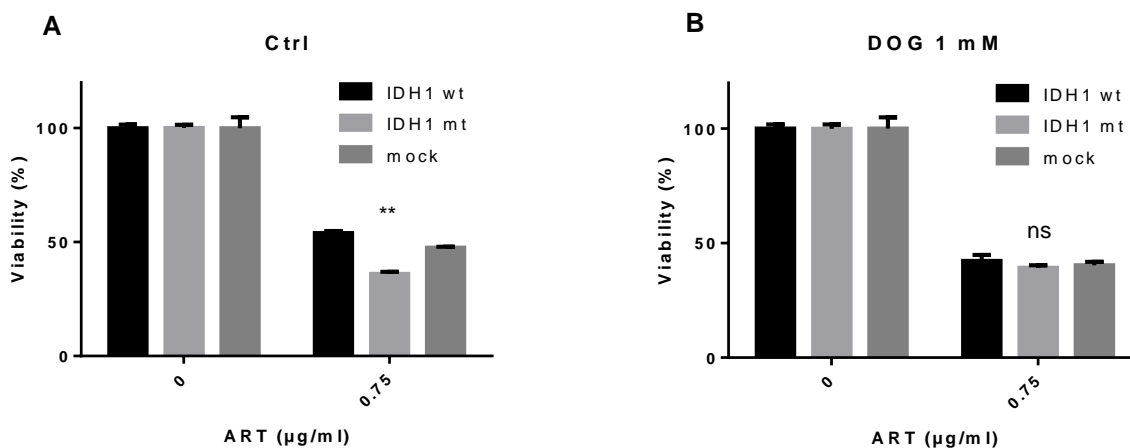


**Figure 69: Western blot analysis** after 48 h of ART treatment for dox pretreated LN319 expressing either IDH1wt, IDH1mt, or mock control. All cell lines undergo a phosphorylation of CHK1 (S345) and H2AX (S139) after ART treatment. 3 ART = 3  $\mu\text{g/ml}$  ART, 6 ART = 6  $\mu\text{g/ml}$  ART

As shown in **Figure 69**, LN319 cells expressing the mutated IDH1 protein show an increased CHK1 phosphorylation after 48 h of 3 and 6  $\mu\text{g/ml}$  ART treatment compared to the LN319 cells expressing IDH1wt. CHK1 and H2AX phosphorylation together are markers for stalled replication forks. CHK1 and H2AX are phosphorylated by the ataxia-telangiectasia-related (ATR) protein kinase in response to DNA damage or replication stress (Liu et al. 2000; Ward and Chen 2001). Artesunate leads to a DNA damage response resulting in a cell cycle arrest via CHK1 phosphorylation. This result is in accordance with the cell cycle analysis in the LN18/G5 and T98G/D7 ALKBH2 KO cell system, where ART led to an increased S and G2 cell cycle arrest, which was more pronounced in the ALKBH2 KO cell lines (G5, D7; see **Figure 68**).

### 3.2.1. Exogenous $\alpha$ -KG rescues higher ART induced toxicity in IDH1mt cells

To prove that lower  $\alpha$ -KG and higher 2-HG levels are responsible for the observed phenotype of higher cytotoxicity in IDH1 mutated cells, a rescue experiment was performed. LN319 expressing IDH1wt and IDH1mt were treated with dimethyl 2-oxoglutarate (DOG), a cell membrane-permeable precursor of a key metabolic intermediate  $\alpha$ -ketoglutarate ( $\alpha$ -KG).



**Figure 70: Viability of LN319 cells assessed by the MTT assay.** Cells were pretreated with (A) vehicle control (Ctrl) alone or (B) 1 mM dimethyl 2-oxoglutarate (DOG) 48 h after seeding. 56 h after seeding, cells were treated with 0.75  $\mu$ g/ml ART and cell viability was measured 72 h after ART treatment. Data are the mean of three independent experiments  $\pm$  SD. Data were analyzed by two-way ANOVA with Tukey post hoc test. ns = non-significant.

As shown in **Figure 70 A**, LN319 cells expressing the mutated IDH1 protein were significantly more sensitive to ART compared to cells expressing wt IDH1 or vector control. Pretreatment of the cells with 1 mM DOG (**Figure 70 B**) abolished this effect. DOG was able to rescue the IDH1mt specific phenotype by increasing the intracellular  $\alpha$ -KG levels.





## 4. Discussion

Since 1840, the average lifespan and the highest reported life expectancy of humans in developed countries is increasing almost linearly by 3 months per year. This came at a price of increased morbidity in the elderly population, characterized by a higher prevalence of chronic diseases and cancers. The total cancer incidence has been rising, mainly because of population aging, and also because of initially silent diseases that now get identified earlier by improved diagnostics (Christensen et al. 2009). Most cancer etiologies are related to lifestyle, behavior, and environmental exposures. Only 5 to 10 % of all cancers are due to inherited germline mutations (Nagy et al. 2004). Minimizing risk factors and screenings, if applicable, are powerful ways of cancer prevention.

The most consistent cancer decrease in developed countries was noted for gastric and cervical cancers, thanks to the availability of refrigerators and preventive gynecological examination, respectively (Howson et al. 1986; Arbyn et al. 2010). The vast majority of cancers are due to mutations acquired over time, most likely reflecting a chronic or acute overload of the DNA repair capacity, leading to persistent base changes in the genome. Similarly, aging itself is believed to be a consequence of the unrepaired accumulation of naturally occurring DNA damages (Freitas and de Magalhaes 2011). The DNA damage theory of aging proposes that the capacity of different mammalian species to carry out DNA repair increased systematically with species longevity. This striking correlation could be found in seven species and was later verified in other laboratories and species (Hart and Setlow 1974; Bernstein and Bernstein 1991; Diderich et al. 2011). Consequently, aging and cancer development are based on the same foundation. Given that the average lifespan increases, the same holds true for the cancer incidence, especially in the case of gliomas, where no exact causes or environmental risk factors besides age are known. Indeed, an increase in glioma incidence in developed countries in the last 50 years could be verified by different studies (Gurney and Kadan-Lottick 2001; Hess et al. 2004; Deltour et al. 2009). At the same time, the survival time of grade I-IV gliomas improved significantly in the last decade (deSouza et al. 2016; Dong et al. 2016). Although the survival of the patients did not increase by years turning glioma as well as all other cancers, into a chronic condition is a general trend. The basis to turn cancers into clinically manageable disease is improved diagnostics and advances in molecular biomarker discovery, hallmarks of personalized oncology.

### 4.1. Improved *MGMT* promoter methylation quantification by HRM

The therapy of high-grade gliomas is based on drugs that alkylate the DNA in the  $O^6$ -position of guanines such as temozolomide and the nitrosoureas lomustine, nimustine, and carmustine. For these drugs, MGMT is a key node in the repair of the major toxic lesion  $O^6$ -alkyl-guanine (Kaina et al. 2007), determining the level of drug resistance and being a decisive factor in identifying responders and non-responders (Hegi et al. 2005; Weller et al. 2012). The determination of MGMT activity requires native tissue while immunohistochemistry suffers from technical limitations and inter-observer differences (Preusser et al. 2008). In 1996, researchers found that the expression of the *MGMT* gene is tightly regulated by promoter methylation and that *MGMT* promoter methylation is a useful surrogate marker for the MGMT activity (Costello et al. 1994b; Qian and Brent 1997; Watts et al. 1997). Therefore, the method of choice for determination of the MGMT status is an analysis of the *MGMT* promoter methylation. Since pyrosequencing is cost-intensive, *MGMT* promoter methylation is usually determined by MSP in the clinical routine.

The human *MGMT* promoter is complex, harboring more than 90 CpG sites that are subject to cytosine methylation (Nakagawachi et al. 2003; Malley et al. 2011). For MSP, only a few of these sites in the *MGMT* promoter are being used. Although the methylation of the CpG sites appears to be highly variable in tumors, methylation of these target sites corresponds well with the therapeutic response, indicating that some CpG sites have a strong impact on epigenetic silencing of *MGMT* (Nakagawachi et al. 2003). Of note, >50 CpG sites in the promoter region of *MGMT* silenced tumors were found homogeneously methylated. The region commonly investigated by MSP was reported to show a concordance of about 85 % with the MGMT mRNA expression (Everhard et al. 2009). Although, the region encompassing the most often used MSP primers shows a strong concordance with *MGMT* silencing compared to other areas in the promoter (Malley et al. 2011), data obtained in different laboratories on this subject are quite heterogeneous (Nakagawachi et al. 2003; Preusser et al. 2008; Dunn et al. 2009; Everhard et al. 2009; Kitange et al. 2009). Also for MGMT activity, a correlation was found between *MGMT* promoter methylation determined by MSP, but also exceptions do exist (Christmann et al. 2010) indicating the importance of other methylation sites (and other regulatory mechanisms) in determining the *MGMT* expression status. It is evident that a method covering a larger area in the *MGMT* promoter than encompassed by the routinely

applied MSP is desirable. Another problem associated with MSP is the quality of the amplification product, which may arise due to inefficient PCR (Christmann et al. 2010; Hsu et al. 2015).

Further limitations in *MGMT* status determination are the heterogeneity of the tumor and contamination of the tumor sample with normal cells. Compared with grade II and grade III astrocytomas, glioblastoma cancer tissue is infiltrated with microglial cells (resident macrophage and immune cells of the brain) and tumor-associated macrophages (TAM). This poses the theoretical and practical challenge to isolate tumor cells from noncancerous cells. Tumor sample purity assessment is routinely performed by hematoxylin-eosin (H&E) staining (Aran et al. 2015). Genome-wide approaches like next-generation sequencing or allele-specific qPCR to quantify tumor specific noncoding mutations (telomerase promoter (pTERT)) are currently in development (Aran et al. 2015; Heidenreich et al. 2015; Schulze Heuling et al. 2017). However, this bias pertains to any PCR-based method.

HRM is an alternative method for the discrimination between 5-methylcytosine containing and non-containing DNA sequences, based on the difference in the melting curves between methylated and unmethylated templates. Compared to MSP, the HRM method relies on methylation standards that are analyzed with unknown samples, making the method investigator independent. Furthermore, HRM is a closed-tube technique that is less expensive, faster, and less laborious than methods based on DNA sequencing, including PSQ. The results obtained are quantitative. As HRM represents a real-time PCR-based method, the amplification and melting plot ensures quality control. The application of HRM for *MGMT* promoter methylation assessment has previously been proposed (Wojdacz and Dobrovic 2007; Quillien et al. 2012); however, a systematic comparison using a defined cut-off threshold was not undertaken, and DNA standards were not verified by other methods.

To elucidate whether HRM is a feasible and reasonable alternative to MSP in determining the *MGMT* promoter methylation status and predicting the high-grade glioma therapy response, we compared HRM and MSP systematically. In this study, PSQ was also included, which is regarded as the “gold standard” for methylation analysis (Karayan-Tapon et al. 2010). First, the data show that HRM correlates with the *MGMT* activity in glioblastoma cell lines. Then, we demonstrated that 51.8, 37.3, and 54.2 % of high-grade gliomas in our collection (including

## Discussion

IDH1-mutated tumors) were promoter methylated as determined by HRM, MSP, and PSQ, respectively, indicating HRM and PSQ provided comparable results. Finally, we compared the patient's response with the tumor methylation status, using Kaplan–Meier estimates. The data revealed a significant difference in PFS and OS between the methylated and unmethylated *MGMT* promoter when HRM and PSQ were used, while for MSP no significant difference was found (**Figure 28**). This indicates that HRM is superior to MSP and equal to PSQ in predicting PFS and OS of high-grade glioma patients. An additional statistical evaluation like a Cox regression model showed that HRM was the only significant independent prognostic factor for OS (HR 0.473, 95 % CI 0.231–0.969,  $p = 0.041$ ), and ROC analysis revealed that HRM and PSQ led to less false positive and false negative grouping compared to MSP in predicting survival. Overall, for both PFS and OS, HRM was superior to MSP in discriminating between responders and non-responders and equally effective to PSQ.

This is, to our best knowledge, the first study that compares in a well-defined tumor collection HRM, MSP, and PSQ, defining a distinct HRM promoter methylation cut-off level relevant for prediction of tumor progression and patient survival. Since the *MGMT* promoter methylation status analyzed by HRM is most precise in determining the patient's outcome, we recommend HRM as a feasible and reliable method for routine diagnostics of high-grade glioma patients.

### 4.2. Promoter methylation of other DNA repair genes

Besides *MGMT*, we analyzed the promoter methylation of *ATM*, *BRCA1/2*, *MBD4*, *RAD51c*, and *MLH1*. In cell line experiments, *MLH1* (**Figure 32**), and *RAD51c* (**Figure 35**) showed differentially methylated promoter sequences. These promoters were therefore analyzed in our HGA patient collective. For *MLH1*, two regions were analyzed, R3 and R7, with opposing results. For patients methylated in R3, a significantly poorer survival could be determined compared to patients unmethylated in R3, which is in accordance with reports by others, stating that *MLH1* is needed to process the TMZ induced DNA lesions into cytotoxic DSB by futile MMR cycles (Quiros et al. 2010; Shinsato et al. 2013). No patient was methylated at both regions, R3 and R7. This result was inverse for the R7 region, where patients with a methylated status show an improved PFS and OS compared to patients with an unmethylated *MLH1* R7 status, contradicting the statement above. *MLH1* promoter methylation in region R7 was significantly correlated with the IDH1 mt status of the patients ( $p=0.043$ ), which allows the statement, that methylation in R7 is driven by the IDH1 mutation (see 1.2.1), i.e. reflecting the CIMP

phenotype. Methylation in R3 was not correlated with the IDH1 mutational status of patients ( $p=0.913$ ). Taken together, *MLH1* promoter methylation at region R3 leads to a poorer survival of the patients due to *MLH1* silencing, and methylation at region R7 reflects the IDH1 mt dependent CIMP phenotype.



### 4.3. IDH1 mutation related 2-HG drives cells ART sensitive due to ALKBH2 impairment

In 2009, scientists discovered the IDH1 mutation in gliomas, which gives rise to elevated concentrations of 2-HG in the tumor tissue (Dang et al. 2009). Before that, 2-HG was known to accumulate in the inherited metabolic disorder 2-hydroxyglutaric aciduria, which is caused by a deficiency in the enzyme 2-hydroxyglutarate dehydrogenase that oxidizes 2-HG back to  $\alpha$ -KG (also known as 2-oxoglutarate (2-OG) (Struys et al. 2005). This enzyme is an example of a metabolite repair enzyme. Patients with mutations in the 2-hydroxyglutarate dehydrogenase accumulate 2-HG in the brain, as assessed by magnetic resonance imaging (MRI) and cerebrospinal fluid (CSF) analysis, develop leukoencephalopathy, and have an increased risk of developing brain tumors (Kölker et al. 2002a; Wajner et al. 2004; Aghili et al. 2009). Furthermore, high levels of 2-HG in the brain result in increased ROS levels, which might contribute to an increased risk of cancer development in this patients (Kölker et al. 2002b; Latini et al. 2003). The mode of action of 2-HG is manifold. First, 2-HG is able to act as an *N*-methyl-D-aspartate (NMDA) receptor agonist (Kölker et al. 2002b), resulting in an increased  $\text{Ca}^{2+}$  influx in neurons, which seems likely to be one of the most important mechanisms in NMDA receptor-mediated neurotoxicity (Hartley et al. 1993; Kölker et al. 2002b). Secondly, 2-HG competitively inhibits  $\alpha$ -KG using enzymes, mainly 2-oxoglutarate-dependent dioxygenases (2OGD), which might lead to a dysregulation of myriad pathways.

The total number of  $\alpha$ -KG-dependent oxygenases found in biology is immense. For example, mammals are thought to possess about 80 such enzymes (McDonough et al. 2010). The enzymes of this family can induce hydroxylation of proteins and demethylation of histones and DNA.  $\alpha$ -KG and oxygen are obligatory substrates, along with  $\text{Fe}^{2+}$  as their cofactor. These enzymes are cellular sensors for the changes in (i) energy metabolism through the availability of  $\alpha$ -KG, a Krebs cycle intermediate, (ii) oxygen level consequently inducing hypoxic responses, and (iii) the  $\text{Fe}^{2+}$  redox status indicating alterations in iron metabolism and oxidative stress (McDonough et al. 2010; Mole 2010; Kaelin and McKnight 2013; Ratcliffe 2013; Salminen et al. 2015). Activation of  $\alpha$ -KG-dependent oxygenases starts with binding of  $\alpha$ -KG- and  $\text{Fe}^{2+}$  into their specific sites in the catalytic domain of the enzyme.  $\text{O}_2$  binds to the  $\text{Fe}^{2+}$  ion, which initiates the oxidative decarboxylation

## Discussion

of  $\alpha$ -KG to succinate and  $\text{CO}_2$  and give rise to the formation of oxidized ferric ( $\text{Fe}^{3+}$ ) and ferryl ( $\text{Fe}^{4+}$ ) intermediates. These high-valent iron oxidant species hydroxylate the substrate molecules in the enzyme-substrate complex (Schofield and Zhang 1999; Hewitson et al. 2005; Ye et al. 2012). High ROS levels, as found in 2-HG accumulating cells, oxidize  $\text{Fe}^{2+}$  to  $\text{Fe}^{3+}$  (Cohen et al. 2013). It is still under debate if the reduced levels of  $\text{Fe}^{2+}$  and  $\alpha$ -KG in IDH1 mutated cells promote an accumulation of HIF-1 $\alpha$ , a transcription factor that target genes that affect angiogenesis and cell motility, as well as apoptosis, autophagy, and the metabolism (Fu et al. 2012; Cohen et al. 2013).

Several studies have shown that succinate and fumarate can bind to the  $\alpha$ -KG binding site of 2-oxoglutarate-dependent dioxygenase enzymes, but are unsuitable for the decarboxylation reaction, and thus are effective competitive inhibitors of these enzymes. Tissues with distinct mutations in the succinate dehydrogenase (SDH) enzyme provoke the accumulation of succinate, which increases the risk of carcinogenesis, probably due to the inhibition of TET enzymes since SDH mutations are associated with a robust hypermethylation of DNA (Killian et al. 2013; Letouze et al. 2013).

Taken together, 2-hydroxyglutarate dehydrogenase deficiency leading to higher 2-HG levels and SDH mutations that result in decreased 2OGD activity, share and display the same phenotypes that were found in IDH1/2 mutated gliomas. Gain of function mutations in IDH1 and IDH2 lead to a changed enzymatic function by converting  $\alpha$ -KG to 2-HG, instead of converting isocitrate to  $\alpha$ -KG. Therefore, on the one hand, the mutation depletes  $\alpha$ -KG levels, and on the other, it produces a metabolite that inhibits  $\alpha$ -KG dependent enzymes. Until now, no glioma has been diagnosed as IDH1/2 wild-type, which later acquired an IDH1/2 mutation during progression, leading to the conclusion that IDH1/2 mutations are early events in the development of astrocytomas (Watanabe et al. 2009a). IDH1/2 mutated cancer cells have to compensate for the loss of  $\alpha$ -KG, which is partly converted to 2-HG, by manufacturing  $\alpha$ -KG from glutamine, making them addicted to glutamine. Efforts have been undertaken, to exploit the glutamine addiction in IDH mutated cells by blocking the glutaminase enzyme, which hydrolyzes glutamine to produce glutamate that is subsequently converted to  $\alpha$ -KG. Glutaminase (GLS) inhibition was achieved by bis-2-(5-phenylacetamido-1,2,4-thiadiazol-2-yl)ethyl sulfide (BPTES) and anti-GLS siRNA. Both con-



ditions slowed down the growth of IDH1 mutated cells, showing the feasibility of this approach (Seltzer et al. 2010). However, the scientists involved in this study published no subsequent xenograft study, nor others groups, which makes this approach questionable.

Still, the better survival of IDH1 mutated HGA patients was unclear. Clinical glioma studies published after 2009 started to analyze and include the IDH1 status of the glioma patients. It became apparent, that the likelihood of a methylated *MGMT* promoter was much higher in IDH1 mutated tumors compared to wild-type tumors (Hartmann et al. 2010; van den Bent et al. 2010). We were also able to observe this uneven distribution of *MGMT* promoter methylation in our HGA patient collective (**Figure 38**).

It was believed that IDH1 mutated tumors are more sensitive to the applied chemotherapy (TMZ) (Houillier et al. 2010; Wang et al. 2014).  $O^6$ mG, if left unrepaired in a *MGMT* deficient cell background, is processed into DSB by futile MMR cycles. The cell system used in this work consists of IDH1wt, IDH1mt, and vector control in LN319 cells, which are *MGMT* deficient and MMR deficient due to the *MLH1* hypermethylation (**Figure 32**). All three cell line clones were resistant towards TMZ. The survival of IDH1mt cells was not worse than IDH1wt or vector control cells (**Figure 47**). This result underlines that mutated IDH1 by itself does not affect TMZ sensitivity.

In 2012, two consecutive Nature letters clarified the epigenetic changes of IDH1 mutated cells on both DNA methylation (Turcan et al. 2012) and histone modification (Lu et al. 2012) level. They showed that the IDH1 mutation is sufficient to establish the glioma CpG island methylator phenotype (G-CIMP), resulting in a large set of hypermethylated DNA regions with effects on the transcriptome. This was found to be a consequence of TET2 inhibition which is driven by 2-HG. The DNA demethylation process was slowed down, as expressed by decreased 5hmC levels and higher 5mC levels compared to IDH1wt cells. The differentially methylated DNA regions were not stochastically distributed. The authors identified 429 hypermethylated and downregulated gene sets and 176 hypomethylated and upregulated gene sets *in vitro* as well as in patient-derived IDH1mt tumor samples. Among these upregulated genes are those known to be involved in glioma initiation and outcome. Moreover, the introduction of mutant but not wild-type IDH1 into astrocytes resulted in the upregulation of nestin (and other genes associated with stem cell identity) at the time of DNA methylation increase and the adoption of a neurosphere/stem-like

## Discussion

phenotype (Turcan et al. 2012). As for the histones, large changes in histone methylation levels could be causally linked to the IDH1 mutation. H3K9me3, H3K27me3 and H3K79me2 levels increased dramatically over 27 cell line passages compared to the IDH1 wild-type cells. The histone demethylation by  $\alpha$ -KG-dependent Jumonji-C domain histone demethylases (JHDMs) is competitively inhibited by 2-HG, which leads to this IDH1-associated change in histone methylation (Lu et al. 2012). Because histone repressive marks can promote DNA methylation and *vice versa* (Esteve et al. 2006), the authors studied the temporal relationship of histone and DNA methylation in IDH1mt expressing astrocytes and found, that histone hypermethylation precedes DNA hypermethylation. Henceforth, the higher likelihood of *MGMT* promoter methylation in IDH1mt tumors could be explained. Still, IDH1 mutated patients with a methylated *MGMT* promoter showed a greatly improved survival compared to IDH1wt and *MGMT* methylated patients (Hartmann et al. 2010). We were also able to observe the same survival differences upon the IDH1 status in *MGMT* methylated HGA patients (**Figure 39**). Further, we could not see, that LN229 IDH1mt cells are more sensitive towards DNA alkylating agents compared to LN229 IDH1wt cells (**Figure 41- 44**). Also, in the tetracycline (dox) inducible LN319 cell system, IDH1mt cells did not show increased cytotoxicity compared to IDH1wt cells (**Figure 47-50**). Ionizing radiation did not differently affect IDH1mt and IDH1wt cells (**Figure 51**).

However, the finding, that mutated IDH1 leads to an inhibition of  $\alpha$ -KG-dependent enzymes (TETs, JHDMs) (Lu et al. 2012; Turcan et al. 2012) by 2-HG, let us to propose that DNA repair enzymes of the 2OGD enzyme family might also be affected in this tumor cells. ALKBH2 belongs to the 2OGD enzyme family and was first identified in humans in 2002 (Duncan et al. 2002). ALKBH2 removes a large variety DNA alkylation and oxidation damages from DNA, including ethenoadenine ( $\epsilon$ A) (Delaney et al. 2005) (**Figure 11**). We chose artesunate (ART) to induce  $\epsilon$ A adducts, according to previous studies (el Ghissassi et al. 1995; Berdelle et al. 2011). Indeed, IDH1mt cells were significantly less viable compared to IDH1wt and control cell line after ART treatment (**Figure 57-59**). To test if 2-HG by itself is accountable for the increased sensitivity of IDH1mt cells, different untransformed IDH1wt cell lines were exposed to ART doses together with increasing 2-HG concentrations. The chosen 2-HG doses alone were not toxic and were selected to be in a range that

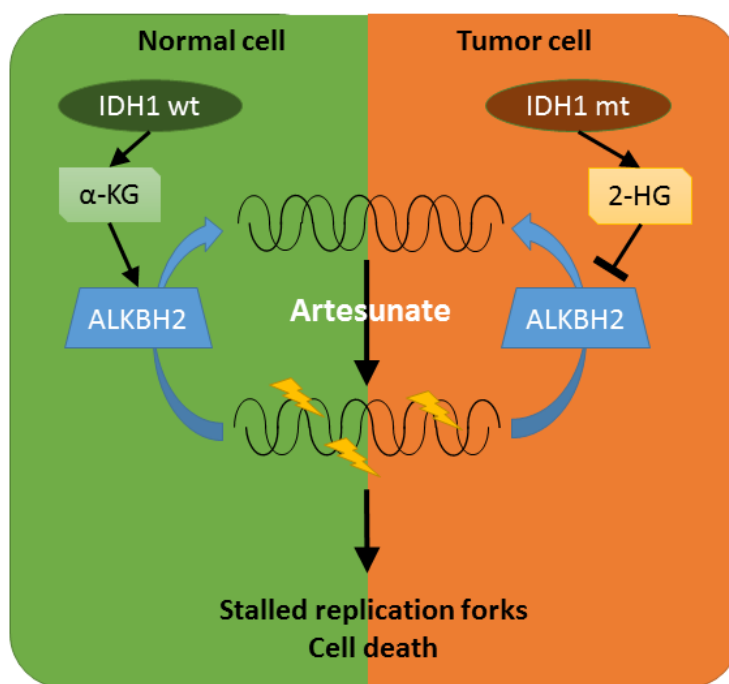
was previously measured in IDH1mt HGA patients (Andronesi et al. 2012). We observed that 2-HG sensitized glioma cell lines dose dependently towards ART treatment (**Figure 60**).

As a next step, the involvement of ALKBH2 in the ART mediated toxicity was assessed by knocking out ALKBH2 in IDH1wt LN18 and T98G cells, which was performed using the CRISPR/Cas9 method. ALKBH2 knock-out clones were verified by western blot analysis (**Figure 61**). Additionally, phenotype verification was carried out with DNA alkylating agents (TMZ, CCNU), resulting in an extreme sensitivity of ALKBH2 knock-out cells compared to their parental counterparts (**Figure 62**). After the successful characterization of the cells, the sensitivity of ALKBH2 knock-out cells towards ART treatment was compared to their parental counterparts, resulting in a significantly increased cell death when ALKBH2 was not available (**Figure 64**).

As the first results from ALKBH2 knock-out cells were obtained, a study was published, describing exactly the same model, i.e. that IDH1mt produced 2-HG inhibits ALKBHs (Wang et al. 2015). Their results and conclusions are mostly in line with ours, except that they were focusing on short-term (1 h) 1mA adduct generation by DNA alkylating agents. Our study is a substantial continuation of this work, in which we quantified long-term induced cell death by ART in the context of IDH1 mutation, exogenous 2-HG, and ALKBH2 knock-out.

The mode of action of ART to induce apoptosis is under debate. Our results could clarify that the induced oxidative stress and the formation of 8-oxoG was not responsible for the observed phenotypes (**Figure 66**). In ALKBH2 deficient cells, ART led to an S/G2 arrest that was more pronounced compared to the control cell lines (**Figure 68**). This was accompanied by a CHK1 and H2AX phosphorylation, accepted markers of an S/G2 cell cycle arrest (**Figure 69**). In a rescue experiment, we could prove that the increased sensitivity of LN319 IDH1mt cells to ART compared to IDH1wt and vector control cells can be abrogated by higher intracellular  $\alpha$ -KG levels (**Figure 70**).

Transferring these findings to the situation of IDH1 mutated high-grad glioma patients, it is most convincing that a co-treatment with ART lead to an increased cell death of tumor cells. Our proposed model is shown in **Figure 71** and **Figure 72**.

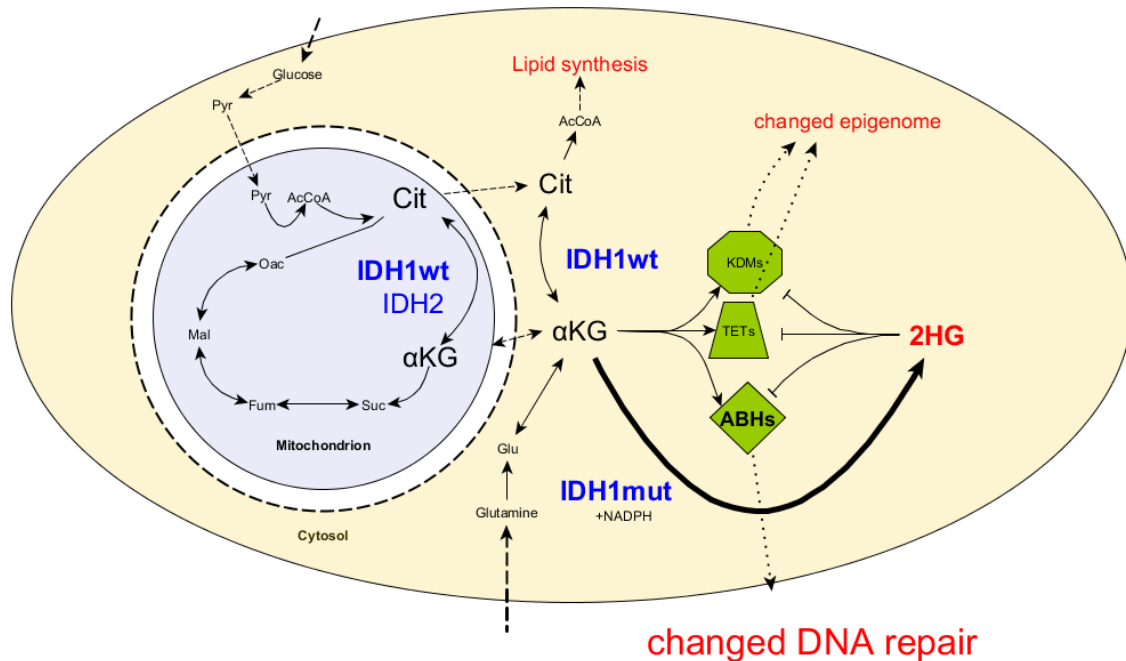


**Figure 71: Simplified model** of how the mutated IDH1 enzyme leads to an increased sensitivity to ART by the production of the oncometabolite 2-hydroxyglutarate (2-HG). Increased levels of 2-HG decrease the activity of ALKBH2, which is involved in the repair of ART, induced DNA damage. In IDH1 mutated cells, ART induced DNA lesions are not repaired as efficiently compared to IDH1 wt cells. (Adapted and modified from Wang et al. 2015)

This work has shown, that ALKBH2 is impaired in IDH1 mutated cells. Based on this, new models on how to exploit this phenomenon can be thought of.

Further experiments are needed to complete this model. First, ART induced etheno DNA lesions like  $\epsilon$ A,  $\epsilon$ C, and  $\epsilon$ G should be quantified in ALKBH2 KO cells, as well as in IDH1 mutated cells and compared to the appropriate controls. Second, 4-hydroxynonenal (4-HNE), which is the key substance to give rise to etheno DNA adducts, should be tested in the ALKBH2 KO and IDH1mt cell line systems. The outcome of this experiments would further substantiate the proposed model. Further, an *in vivo* xenograft study should be performed to complete this findings.

A detailed model for ALKBH2 inefficiency in IDH1 mutated cells is shown below (**Figure 72**).



**Figure 72: Detailed model** depicting the metabolic reprogramming of IDH1 mutated cells. 2-HG impairs the ALKBH (ABH) enzymes, leading to a decreased DNA repair capacity. In combination with ART that induces DNA lesions being substrates for ABHs, this leads to an increased cell death in IDH1 mutated tumor cells. The impairment of ABHs has not been studied so far and could open the door to new tailor-made therapies by exploiting this altered DNA repair pathway. KDM = Lysin specific histone demethylase, TET=Ten-eleven translocation enzymes, ABHs = ALKBH family enzymes, Glu = Glutamate, Cit = Citrate, Pyr = Pyruvate, Suc = Succinate, Fum = Fumarate, Mal = Malate, Oac = Oxaloacetate, AcCoa = Acetyl-CoA.



## 5. References

- Aas PA, Otterlei M, Falnes PO, Vagbo CB, Skorpen F, Akbari M, Sundheim O, Bjoras M, Slupphaug G, Seeberg E et al. 2003. Human and bacterial oxidative demethylases repair alkylation damage in both RNA and DNA. *Nature* **421**: 859-863.
- Aghili M, Zahedi F, Rafiee E. 2009. Hydroxyglutaric aciduria and malignant brain tumor: a case report and literature review. *Journal of neuro-oncology* **91**: 233-236.
- Andronesi OC, Kim GS, Gerstner E, Batchelor T, Tzika AA, Fantin VR, Vander Heiden MG, Sorensen AG. 2012. Detection of 2-hydroxyglutarate in IDH-mutated glioma patients by in vivo spectral-editing and 2D correlation magnetic resonance spectroscopy. *Science translational medicine* **4**: 116ra114.
- Aran D, Sirota M, Butte AJ. 2015. Systematic pan-cancer analysis of tumour purity. *Nat Commun* **6**: 8971.
- Arbyn M, Anttila A, Jordan J, Ronco G, Schenck U, Segnan N, Wiener H, Herbert A, von Karsa L. 2010. European Guidelines for Quality Assurance in Cervical Cancer Screening. Second edition--summary document. *Ann Oncol* **21**: 448-458.
- Arnaudeau C, Lundin C, Helleday T. 2001. DNA double-strand breaks associated with replication forks are predominantly repaired by homologous recombination involving an exchange mechanism in mammalian cells. *J Mol Biol* **307**: 1235-1245.
- Barbin A, Bartsch H, Leconte P, Radman M. 1981. Studies on the miscoding properties of 1,N6-ethenoadenine and 3,N4-ethenocytosine, DNA reaction products of vinyl chloride metabolites, during in vitro DNA synthesis. *Nucleic acids research* **9**: 375-387.
- Barreto G, Schäfer A, Marhold J, Stach D, Swaminathan SK, Handa V, Doderlein G, Maltry N, Wu W, Lyko F et al. 2007. Gadd45a promotes epigenetic gene activation by repair-mediated DNA demethylation. *Nature* **445**: 671-675.
- Barrows LR, Magee PN. 1982. Nonenzymatic methylation of DNA by S-adenosylmethionine in vitro. *Carcinogenesis* **3**: 349-351.
- Bartel DP. 2004. MicroRNAs: genomics, biogenesis, mechanism, and function. *Cell* **116**: 281-297.
- . 2009. MicroRNAs: target recognition and regulatory functions. *Cell* **136**: 215-233.
- Baylin SB, Herman JG. 2000. DNA hypermethylation in tumorigenesis: epigenetics joins genetics. *Trends Genet* **16**: 168-174.
- Bell AC, Felsenfeld G. 2000. Methylation of a CTCF-dependent boundary controls imprinted expression of the Igf2 gene. *Nature* **405**: 482-485.
- Bellacosa A, Drohat AC. 2015. Role of base excision repair in maintaining the genetic and epigenetic integrity of CpG sites. *DNA repair* **32**: 33-42.
- Benakis A, Paris M, Loutan L, Plessas CT, Plessas ST. 1997. Pharmacokinetics of artemisinin and artesunate after oral administration in healthy volunteers. *Am J Trop Med Hyg* **56**: 17-23.
- Berdelle N, Nikolova T, Quiros S, Efferth T, Kaina B. 2011. Artesunate induces oxidative DNA damage, sustained DNA double-strand breaks, and the ATM/ATR damage response in cancer cells. *Molecular cancer therapeutics* **10**: 2224-2233.
- Berger SL, Kouzarides T, Shiekhata R, Shilatifard A. 2009. An operational definition of epigenetics. *Genes & development* **23**: 781-783.

## References

- Berghoff AS, Kiesel B, Widhalm G, Rajky O, Ricken G, Wohrer A, Dieckmann K, Filipits M, Brandstetter A, Weller M et al. 2015. Programmed death ligand 1 expression and tumor-infiltrating lymphocytes in glioblastoma. *Neuro-oncology* **17**: 1064-1075.
- Bernstein C, Bernstein H. 1991. *Aging, sex, and DNA repair*. Academic Press.
- Bernstein H, Bernstein C, Michod RE. 2011. Meiosis as an Evolutionary Adaptation for DNA Repair. in *DNA repair* (ed. I Kruman). InTech.
- Berte N, Lokan S, Eich M, Kim E, Kaina B. 2016. Artesunate enhances the therapeutic response of glioma cells to temozolomide by inhibition of homologous recombination and senescence. *Oncotarget* **7**: 67235-67250.
- Bhagwat AS, Lieb M. 2002. Cooperation and competition in mismatch repair: very short-patch repair and methyl-directed mismatch repair in Escherichia coli. *Mol Microbiol* **44**: 1421-1428.
- Bird A. 1992. The Essentials of DNA Methylation. *Cell* **70**: 5-8.
- Birner P, Pusch S, Christov C, Mihaylova S, Toumangelova-Uzeir K, Natchev S, Schoppmann SF, Tchorbanov A, Streubel B, Tuettenberg J et al. 2014. Mutant IDH1 inhibits PI3K/Akt signaling in human glioma. *Cancer* **120**: 2440-2447.
- Bohgaki T, Bohgaki M, Hakem R. 2010. DNA double-strand break signaling and human disorders. *Genome Integr* **1**: 15.
- Borger DR, Goyal L, Yau T, Poon RT, Ancukiewicz M, Deshpande V, Christiani DC, Liebman HM, Yang H, Kim H et al. 2014. Circulating oncometabolite 2-hydroxyglutarate is a potential surrogate biomarker in patients with isocitrate dehydrogenase-mutant intrahepatic cholangiocarcinoma. *Clinical cancer research : an official journal of the American Association for Cancer Research* **20**: 1884-1890.
- Bradford MM. 1976. A rapid and sensitive method for the quantitation of microgram quantities of protein utilizing the principle of protein-dye binding. *Anal Biochem* **72**: 248-254.
- Brandes AA, Nicolardi L, Tosoni A, Gardiman M, Iuzzolino P, Ghimenton C, Reni M, Rotilio A, Sotti G, Ermani M. 2006. Survival following adjuvant PCV or temozolomide for anaplastic astrocytoma. *Neuro-oncology* **8**: 253-260.
- Branzei D, Foiani M. 2010. Maintaining genome stability at the replication fork. *Nature reviews Molecular cell biology* **11**: 208-219.
- Bregenhorn S, Kallenberger L, Artola-Boran M, Pena-Diaz J, Jiricny J. 2016. Non-canonical uracil processing in DNA gives rise to double-strand breaks and deletions: relevance to class switch recombination. *Nucleic acids research* **44**: 2691-2705.
- Brennan CW, Verhaak RG, McKenna A, Campos B, Nounshmehr H, Salama SR, Zheng S, Chakravarty D, Sanborn JZ, Berman SH et al. 2013. The somatic genomic landscape of glioblastoma. *Cell* **155**: 462-477.
- Cadet J, Douki T, Ravanat JL. 2010. Oxidatively generated base damage to cellular DNA. *Free Radic Biol Med* **49**: 9-21.
- Cairncross G, Wang M, Shaw E, Jenkins R, Brachman D, Buckner J, Fink K, Souhami L, Laperriere N, Curran W et al. 2013. Phase III trial of chemoradiotherapy for anaplastic oligodendroglioma: long-term results of RTOG 9402. *Journal of clinical oncology : official journal of the American Society of Clinical Oncology* **31**: 337-343.



- Chang C-M, Shu H-KG, Xu K, ed. 2011. *The role of isocitrate dehydrogenase mutations in glioma brain tumors*. INTECH Open Access Publisher.
- Chang CO, Yesupriya A, Rowell JL, Pimentel CB, Clyne M, Gwinn M, Khoury MJ, Wulf A, Schully SD. 2014. A systematic review of cancer GWAS and candidate gene meta-analyses reveals limited overlap but similar effect sizes. *Eur J Hum Genet* **22**: 402-408.
- Chang Z, Zhang W, Chang Z, Song M, Qin Y, Chang F, Guo H, Wei Q. 2015. Expression characteristics of FHIT, p53, BRCA2 and MLH1 in families with a history of oesophageal cancer in a region with a high incidence of oesophageal cancer. *Oncol Lett* **9**: 430-436.
- Chaturvedi A, Araujo Cruz MM, Jyotsana N, Sharma A, Yun H, Gorlich K, Wichmann M, Schwarzer A, Preller M, Thol F et al. 2013. Mutant IDH1 promotes leukemogenesis in vivo and can be specifically targeted in human AML. *Blood* **122**: 2877-2887.
- Chopra S, Verma A, Kundu S, Engineer R, Medhi S, Mahantshetty U, Gupta S, Shrivastava SK. 2012. Evaluation of diffusion-weighted imaging as a predictive marker for tumor response in patients undergoing chemoradiation for postoperative recurrences of cervical cancer. *J Cancer Res Ther* **8**: 68-73.
- Chowdhury R, Yeoh KK, Tian YM, Hillringhaus L, Bagg EA, Rose NR, Leung IK, Li XS, Woon EC, Yang M et al. 2011. The oncometabolite 2-hydroxyglutarate inhibits histone lysine demethylases. *EMBO reports* **12**: 463-469.
- Christensen K, Doblhammer G, Rau R, Vaupel JW. 2009. Ageing populations: the challenges ahead. *Lancet* **374**: 1196-1208.
- Christmann M, Kaina B. 2012. O(6)-methylguanine-DNA methyltransferase (MGMT): impact on cancer risk in response to tobacco smoke. *Mutation research* **736**: 64-74.
- Christmann M, Nagel G, Horn S, Krahn U, Wiewrodt D, Sommer C, Kaina B. 2010. MGMT activity, promoter methylation and immunohistochemistry of pretreatment and recurrent malignant gliomas: a comparative study on astrocytoma and glioblastoma. *International journal of cancer Journal international du cancer* **127**: 2106-2118.
- Christmann M, Verbeek B, Roos WP, Kaina B. 2011. O(6)-Methylguanine-DNA methyltransferase (MGMT) in normal tissues and tumors: enzyme activity, promoter methylation and immunohistochemistry. *Biochimica et biophysica acta* **1816**: 179-190.
- Chun J, Buechelmaier ES, Powell SN. 2013. Rad51 paralog complexes BCDX2 and CX3 act at different stages in the BRCA1-BRCA2-dependent homologous recombination pathway. *Molecular and cellular biology* **33**: 387-395.
- Chung FL, Chen HJ, Guttenplan JB, Nishikawa A, Hard GC. 1993. 2,3-epoxy-4-hydroxynonanal as a potential tumor-initiating agent of lipid peroxidation. *Carcinogenesis* **14**: 2073-2077.
- Churchill H, Naina H, Boriack R, Rakheja D, Chen W. 2015. Discordant intracellular and plasma D-2-hydroxyglutarate levels in a patient with IDH2 mutated angioimmunoblastic T-cell lymphoma. *Int J Clin Exp Pathol* **8**: 11753-11759.
- Cohen AL, Holmen SL, Colman H. 2013. IDH1 and IDH2 mutations in gliomas. *Current neurology and neuroscience reports* **13**: 345.

## References

- Cooper DN, Mort M, Stenson PD, Ball EV, Chuzhanova NA. 2010. Methylation-mediated deamination of 5-methylcytosine appears to give rise to mutations causing human inherited disease in CpNpG trinucleotides, as well as in CpG dinucleotides. *Hum Genomics* **4**: 406-410.
- Cortellino S, Xu J, Sannai M, Moore R, Caretti E, Cigliano A, Le Coz M, Devarajan K, Wessels A, Soprano D et al. 2011. Thymine DNA glycosylase is essential for active DNA demethylation by linked deamination-base excision repair. *Cell* **146**: 67-79.
- Costello JF, Futscher BW, Kroes RA, Pieper RO. 1994a. Methylation-related chromatin structure is associated with exclusion of transcription factors from and suppressed expression of the O-6-methylguanine DNA methyltransferase gene in human glioma cell lines. *Molecular and cellular biology* **14**: 6515-6521.
- Costello JF, Futscher BW, Tano K, Graunke DM, Pieper RO. 1994b. Graded methylation in the promoter and body of the O6-methylguanine DNA methyltransferase (MGMT) gene correlates with MGMT expression in human glioma cells. *The Journal of biological chemistry* **269**: 17228-17237.
- Cui L, Su XZ. 2009. Discovery, mechanisms of action and combination therapy of artemisinin. *Expert Rev Anti Infect Ther* **7**: 999-1013.
- Cykowski MD, Allen RA, Fung KM, Harmon MA, Dunn ST. 2012. Pyrosequencing of IDH1 and IDH2 mutations in brain tumors and non-neoplastic conditions. *Diagnostic molecular pathology : the American journal of surgical pathology, part B* **21**: 214-220.
- Dalleau S, Baradat M, Gueraud F, Huc L. 2013. Cell death and diseases related to oxidative stress: 4-hydroxynonenal (HNE) in the balance. *Cell Death Differ* **20**: 1615-1630.
- Dang L, White DW, Gross S, Bennett BD, Bittinger MA, Driggers EM, Fantin VR, Jang HG, Jin S, Keenan MC et al. 2009. Cancer-associated IDH1 mutations produce 2-hydroxyglutarate. *Nature* **462**: 739-744.
- Dango S, Mosammamarast N, Sowa ME, Xiong LJ, Wu F, Park K, Rubin M, Gygi S, Harper JW, Shi Y. 2011. DNA unwinding by ASCC3 helicase is coupled to ALKBH3-dependent DNA alkylation repair and cancer cell proliferation. *Molecular cell* **44**: 373-384.
- Davies H, Bignell GR, Cox C, Stephens P, Edkins S, Clegg S, Teague J, Woffendin H, Garnett MJ, Bottomley W et al. 2002. Mutations of the BRAF gene in human cancer. *Nature* **417**: 949-954.
- Davis AJ, Chen BP, Chen DJ. 2014. DNA-PK: a dynamic enzyme in a versatile DSB repair pathway. *DNA repair* **17**: 21-29.
- De Bont R, van Larebeke N. 2004. Endogenous DNA damage in humans: a review of quantitative data. *Mutagenesis* **19**: 169-185.
- Deaton AM, Bird A. 2011. CpG islands and the regulation of transcription. *Genes & development* **25**: 1010-1022.
- Delaney JC, Smeester L, Wong C, Frick LE, Taghizadeh K, Wishnok JS, Drennan CL, Samson LD, Essigmann JM. 2005. AlkB reverses etheno DNA lesions caused by lipid oxidation in vitro and in vivo. *Nature structural & molecular biology* **12**: 855-860.

- Dell'Eva R, Pfeffer U, Vene R, Anfosso L, Forlani A, Albini A, Efferth T. 2004. Inhibition of angiogenesis in vivo and growth of Kaposi's sarcoma xenograft tumors by the anti-malarial artesunate. *Biochem Pharmacol* **68**: 2359-2366.
- Deltour I, Johansen C, Auvinen A, Feychting M, Klæboe L, Schuz J. 2009. Time trends in brain tumor incidence rates in Denmark, Finland, Norway, and Sweden, 1974-2003. *Journal of the National Cancer Institute* **101**: 1721-1724.
- Demple B, Jacobsson A, Olsson M, Robins P, Lindahl T. 1982. Repair of alkylated DNA in *Escherichia coli*. Physical properties of O6-methylguanine-DNA methyltransferase. *The Journal of biological chemistry* **257**: 13776-13780.
- deSouza RM, Shaweis H, Han C, Sivasubramiam V, Brazil L, Beaney R, Sadler G, Al-Sarraj S, Hampton T, Logan J et al. 2016. Has the survival of patients with glioblastoma changed over the years? *British journal of cancer* **114**: 146-150.
- Diderich K, Alanazi M, Hoeijmakers JH. 2011. Premature aging and cancer in nucleotide excision repair-disorders. *DNA repair* **10**: 772-780.
- Do H, Wong NC, Murone C, John T, Solomon B, Mitchell PL, Dobrovic A. 2014. A critical re-assessment of DNA repair gene promoter methylation in non-small cell lung carcinoma. *Sci Rep* **4**: 4186.
- Dong X, Noorbakhsh A, Hirshman BR, Zhou T, Tang JA, Chang DC, Carter BS, Chen CC. 2016. Survival trends of grade I, II, and III astrocytoma patients and associated clinical practice patterns between 1999 and 2010: A SEER-based analysis. *Neuro-Oncology Practice* **3**: 29-38.
- Dubbink HJ, Taal W, van Marion R, Kros JM, van Heuvel I, Bromberg JE, Zonnenberg BA, Zonnenberg CB, Postma TJ, Gijtenbeek JM et al. 2009. IDH1 mutations in low-grade astrocytomas predict survival but not response to temozolomide. *Neurology* **73**: 1792-1795.
- Duncan T, Trewick SC, Koivisto P, Bates PA, Lindahl T, Sedgwick B. 2002. Reversal of DNA alkylation damage by two human dioxygenases. *Proceedings of the National Academy of Sciences of the United States of America* **99**: 16660-16665.
- Dunn J, Baborie A, Alam F, Joyce K, Moxham M, Sibson R, Crooks D, Husband D, Shenoy A, Brodbelt A et al. 2009. Extent of MGMT promoter methylation correlates with outcome in glioblastomas given temozolomide and radiotherapy. *British journal of cancer* **101**: 124-131.
- Efferth T, Dunstan H, Sauerbrey A, Miyachi H, Chitambar CR. 2001. The anti-malarial artesunate is also active against cancer. *International journal of oncology* **18**: 767-773.
- Efferth T, Li PC, Konkimalla VS, Kaina B. 2007. From traditional Chinese medicine to rational cancer therapy. *Trends Mol Med* **13**: 353-361.
- Eker AP, Quayle C, Chaves I, van der Horst GT. 2009. DNA repair in mammalian cells: Direct DNA damage reversal: elegant solutions for nasty problems. *Cell Mol Life Sci* **66**: 968-980.
- el Ghissassi F, Barbin A, Nair J, Bartsch H. 1995. Formation of 1,N6-ethenoadenine and 3,N4-ethenocytosine by lipid peroxidation products and nucleic acid bases. *Chemical research in toxicology* **8**: 278-283.
- Ellegren H. 2004. Microsatellites: simple sequences with complex evolution. *Nature reviews Genetics* **5**: 435-445.
- Esteller M, Garcia-Foncillas J, Andion E, Goodman SN, Hidalgo OF, Vanaclocha V, Baylin SB, Herman JG. 2000. Inactivation of the DNA-repair gene MGMT and the

## References

- clinical response of gliomas to alkylating agents. *The New England journal of medicine* **343**: 1350-1354.
- Esteller M, Hamilton SR, Burger PC, Baylin SB, Herman JG. 1999. Inactivation of the DNA repair gene O6-methylguanine-DNA methyltransferase by promoter hypermethylation is a common event in primary human neoplasia. *Cancer research* **59**: 793-797.
- Esteve PO, Chin HG, Smallwood A, Feehery GR, Gangisetty O, Karpf AR, Carey MF, Pradhan S. 2006. Direct interaction between DNMT1 and G9a coordinates DNA and histone methylation during replication. *Genes & development* **20**: 3089-3103.
- Everhard S, Kaloshi G, Criniere E, Benouaich-Amiel A, Lejeune J, Marie Y, Sanson M, Kujas M, Mokhtari K, Hoang-Xuan K et al. 2006. MGMT methylation: a marker of response to temozolomide in low-grade gliomas. *Annals of neurology* **60**: 740-743.
- Everhard S, Tost J, El Abdalaoui H, Criniere E, Busato F, Marie Y, Gut IG, Sanson M, Mokhtari K, Laigle-Donadey F et al. 2009. Identification of regions correlating MGMT promoter methylation and gene expression in glioblastomas. *Neuro-oncology* **11**: 348-356.
- Fabre KM, Ramaiah L, Dregalla RC, Desaintes C, Weil MM, Bailey SM, Ullrich RL. 2011. Murine Prkdc polymorphisms impact DNA-PKcs function. *Radiat Res* **175**: 493-500.
- Falnes PO, Johansen RF, Seeberg E. 2002. AlkB-mediated oxidative demethylation reverses DNA damage in Escherichia coli. *Nature* **419**: 178-182.
- Farkas SA, Vymetalkova V, Vodickova L, Vodicka P, Nilsson TK. 2014. DNA methylation changes in genes frequently mutated in sporadic colorectal cancer and in the DNA repair and Wnt/beta-catenin signaling pathway genes. *Epigenomics* **6**: 179-191.
- Felsberg J, Thon N, Eigenbrod S, Hentschel B, Sabel MC, Westphal M, Schackert G, Kreth FW, Pietsch T, Loffler M et al. 2011. Promoter methylation and expression of MGMT and the DNA mismatch repair genes MLH1, MSH2, MSH6 and PMS2 in paired primary and recurrent glioblastomas. *International journal of cancer Journal international du cancer* **129**: 659-670.
- Fleming AM, Ding Y, Burrows CJ. 2017. Oxidative DNA damage is epigenetic by regulating gene transcription via base excision repair. *Proceedings of the National Academy of Sciences of the United States of America* **114**: 2604-2609.
- Forbes SA, Beare D, Gunasekaran P, Leung K, Bindal N, Boutselakis H, Ding M, Bamford S, Cole C, Ward S et al. 2015. COSMIC: exploring the world's knowledge of somatic mutations in human cancer. *Nucleic acids research* **43**: D805-811.
- Freitas AA, de Magalhaes JP. 2011. A review and appraisal of the DNA damage theory of ageing. *Mutation research* **728**: 12-22.
- Frick LE, Delaney JC, Wong C, Drennan CL, Essigmann JM. 2007. Alleviation of 1,N6-ethanoadenine genotoxicity by the Escherichia coli adaptive response protein AlkB. *Proceedings of the National Academy of Sciences of the United States of America* **104**: 755-760.
- Fritz KS, Petersen DR. 2011. Exploring the biology of lipid peroxidation-derived protein carbonylation. *Chemical research in toxicology* **24**: 1411-1419.
- Frohlich T, Capci Karagoz A, Reiter C, Tsogoeva SB. 2016. Artemisinin-Derived Dimers: Potent Antimalarial and Anticancer Agents. *J Med Chem* **59**: 7360-7388.

- Fu D, Brophy JA, Chan CT, Atmore KA, Begley U, Paules RS, Dedon PC, Begley TJ, Samson LD. 2010. Human AlkB homolog ABH8 Is a tRNA methyltransferase required for wobble uridine modification and DNA damage survival. *Molecular and cellular biology* **30**: 2449-2459.
- Fu D, Jordan JJ, Samson LD. 2013. Human ALKBH7 is required for alkylation and oxidation-induced programmed necrosis. *Genes & development* **27**: 1089-1100.
- Fu D, Samson LD. 2012. Direct repair of 3,N(4)-ethenocytosine by the human ALKBH2 dioxygenase is blocked by the AAG/MPG glycosylase. *DNA repair* **11**: 46-52.
- Fu D, Samson LD, Hubscher U, van Loon B. 2015. The interaction between ALKBH2 DNA repair enzyme and PCNA is direct, mediated by the hydrophobic pocket of PCNA and perturbed in naturally-occurring ALKBH2 variants. *DNA repair* **35**: 13-18.
- Fu Y, Zheng S, Zheng Y, Huang R, An N, Liang A, Hu C. 2012. Glioma derived isocitrate dehydrogenase-2 mutations induced up-regulation of HIF-1 $\alpha$  and beta-catenin signaling: possible impact on glioma cell metastasis and chemoresistance. *Int J Biochem Cell Biol* **44**: 770-775.
- Gaidano G, Ballerini P, Gong JZ, Inghirami G, Neri A, Newcomb EW, Magrath IT, Knowles DM, Dalla-Favera R. 1991. p53 mutations in human lymphoid malignancies: association with Burkitt lymphoma and chronic lymphocytic leukemia. *Proceedings of the National Academy of Sciences of the United States of America* **88**: 5413-5417.
- Gerson SL, Phillips W, Kastan M, Dumenco LL, Donovan C. 1996. Human CD34+ hematopoietic progenitors have low, cytokine-unresponsive O6-alkylguanine-DNA alkyltransferase and are sensitive to O6-benzylguanine plus BCNU. *Blood* **88**: 1649-1655.
- Ghodgaonkar MM, Lazzaro F, Olivera-Pimentel M, Artola-Boran M, Cejka P, Reijns MA, Jackson AP, Plevani P, Muzi-Falconi M, Jiricny J. 2013. Ribonucleotides misincorporated into DNA act as strand-discrimination signals in eukaryotic mismatch repair. *Molecular cell* **50**: 323-332.
- Gilbert MR, Liu Y, Neltner J, Pu H, Morris A, Sunkara M, Pittman T, Kyprianou N, Horbinski C. 2014. Autophagy and oxidative stress in gliomas with IDH1 mutations. *Acta neuropathologica* **127**: 221-233.
- Goode EL, Ulrich CM, Potter JD. 2002. Polymorphisms in DNA repair genes and associations with cancer risk. *Cancer Epidemiol Biomarkers Prev* **11**: 1513-1530.
- Grassian AR, Lin F, Barrett R, Liu Y, Jiang W, Korpai M, Astley H, Gitterman D, Henley T, Howes R et al. 2012. Isocitrate dehydrogenase (IDH) mutations promote a reversible ZEB1/microRNA (miR)-200-dependent epithelial-mesenchymal transition (EMT). *The Journal of biological chemistry* **287**: 42180-42194.
- Grassian AR, Parker SJ, Davidson SM, Divakaruni AS, Green CR, Zhang X, Slocum KL, Pu M, Lin F, Vickers C et al. 2014. IDH1 mutations alter citric acid cycle metabolism and increase dependence on oxidative mitochondrial metabolism. *Cancer research* **74**: 3317-3331.
- Groden J, Thliveris A, Samowitz W, Carlson M, Gelbert L, Albertsen H, Joslyn G, Stevens J, Spirio L, Robertson M et al. 1991. Identification and characterization of the familial adenomatous polyposis coli gene. *Cell* **66**: 589-600.
- Gurney JG, Kadan-Lottick N. 2001. Brain and other central nervous system tumors: rates, trends, and epidemiology. *Curr Opin Oncol* **13**: 160-166.

## References

- Hall EJ, Giaccia AJ. 2006. *Radiobiology for the Radiologist*. Lippincott Williams & Wilkins.
- Hanahan D, Weinberg RA. 2000. The hallmarks of cancer. *Cell* **100**: 57-70.
- Harris LC, Potter PM, Tano K, Shiota S, Mitra S, Brent TP. 1991. Characterization of the promoter region of the human O6-methylguanine-DNA methyltransferase gene. *Nucleic acids research* **19**: 6163-6167.
- Hart RW, Setlow RB. 1974. Correlation between deoxyribonucleic acid excision-repair and life-span in a number of mammalian species. *Proceedings of the National Academy of Sciences of the United States of America* **71**: 2169-2173.
- Hartley DM, Kurth MC, Bjerkness L, Weiss JH, Choi DW. 1993. Glutamate receptor-induced  $^{45}\text{Ca}^{2+}$  accumulation in cortical cell culture correlates with subsequent neuronal degeneration. *J Neurosci* **13**: 1993-2000.
- Hartmann C, Hentschel B, Wick W, Capper D, Felsberg J, Simon M, Westphal M, Schackert G, Meyermann R, Pietsch T et al. 2010. Patients with IDH1 wild type anaplastic astrocytomas exhibit worse prognosis than IDH1-mutated glioblastomas, and IDH1 mutation status accounts for the unfavorable prognostic effect of higher age: implications for classification of gliomas. *Acta neuropathologica* **120**: 707-718.
- Hegde ML, Theriot CA, Das A, Hegde PM, Guo Z, Gary RK, Hazra TK, Shen B, Mitra S. 2008. Physical and functional interaction between human oxidized base-specific DNA glycosylase NEIL1 and flap endonuclease 1. *The Journal of biological chemistry* **283**: 27028-27037.
- Hegi ME, Diserens AC, Godard S, Dietrich PY, Regli L, Ostermann S, Otten P, Van Melle G, de Tribolet N, Stupp R. 2004. Clinical trial substantiates the predictive value of O-6-methylguanine-DNA methyltransferase promoter methylation in glioblastoma patients treated with temozolomide. *Clinical cancer research : an official journal of the American Association for Cancer Research* **10**: 1871-1874.
- Hegi ME, Diserens AC, Gorlia T, Hamou MF, de Tribolet N, Weller M, Kros JM, Hainfellner JA, Mason W, Mariani L et al. 2005. MGMT gene silencing and benefit from temozolomide in glioblastoma. *The New England journal of medicine* **352**: 997-1003.
- Heidenreich B, Rachakonda PS, Hosen I, Volz F, Hemminki K, Weyerbrock A, Kumar R. 2015. TERT promoter mutations and telomere length in adult malignant gliomas and recurrences. *Oncotarget* **6**: 10617-10633.
- Helleday T, Lo J, van Gent DC, Engelward BP. 2007. DNA double-strand break repair: from mechanistic understanding to cancer treatment. *DNA repair* **6**: 923-935.
- Herman JG, Graff JR, Myohanen S, Nelkin BD, Baylin SB. 1996. Methylation-specific PCR: a novel PCR assay for methylation status of CpG islands. *Proceedings of the National Academy of Sciences of the United States of America* **93**: 9821-9826.
- Herman JG, Umar A, Polyak K, Graff JR, Ahuja N, Issa JP, Markowitz S, Willson JK, Hamilton SR, Kinzler KW et al. 1998. Incidence and functional consequences of hMLH1 promoter hypermethylation in colorectal carcinoma. *Proceedings of the National Academy of Sciences of the United States of America* **95**: 6870-6875.
- Herskind C, Westergaard O. 1988. Variable protection by OH scavengers against radiation-induced inactivation of isolated transcriptionally active chromatin: the influence of secondary radicals. *Radiat Res* **114**: 28-41.
- Hess KR, Broglio KR, Bondy ML. 2004. Adult glioma incidence trends in the United States, 1977-2000. *Cancer* **101**: 2293-2299.

- Hewitson KS, Granatino N, Welford RW, McDonough MA, Schofield CJ. 2005. Oxidation by 2-oxoglutarate oxygenases: non-haem iron systems in catalysis and signalling. *Philos Trans A Math Phys Eng Sci* **363**: 807-828; discussion 1035-1040.
- Heyer WD, Ehmsen KT, Liu J. 2010. Regulation of homologous recombination in eukaryotes. *Annu Rev Genet* **44**: 113-139.
- Hillen W, Berens C. 1994. Mechanisms underlying expression of Tn10 encoded tetracycline resistance. *Annu Rev Microbiol* **48**: 345-369.
- Ho VK, Reijneveld JC, Enting RH, Bienfait HP, Robe P, Baumert BG, Visser O, Dutch Society for N-O. 2014. Changing incidence and improved survival of gliomas. *European journal of cancer* **50**: 2309-2318.
- Hoggart C, Brennan P, Tjonneland A, Vogel U, Overvad K, Ostergaard JN, Kaaks R, Canzian F, Boeing H, Steffen A et al. 2012. A risk model for lung cancer incidence. *Cancer Prev Res (Phila)* **5**: 834-846.
- Holliday R, Pugh JE. 1975. DNA modification mechanisms and gene activity during development. *Science* **187**: 226-232.
- Houillier C, Wang X, Kaloshi G, Mokhtari K, Guillevin R, Laffaire J, Paris S, Boisselier B, Idbaih A, Laigle-Donadey F et al. 2010. IDH1 or IDH2 mutations predict longer survival and response to temozolomide in low-grade gliomas. *Neurology* **75**: 1560-1566.
- Howson CP, Hiyama T, Wynder EL. 1986. The decline in gastric cancer: epidemiology of an unplanned triumph. *Epidemiol Rev* **8**: 1-27.
- Hsu CY, Ho HL, Lin SC, Chang-Chien YC, Chen MH, Hsu SP, Yen YS, Guo WY, Ho DM. 2015. Prognosis of glioblastoma with faint MGMT methylation-specific PCR product. *Journal of neuro-oncology* **122**: 179-188.
- Ilett KF, Ethell BT, Maggs JL, Davis TM, Batty KT, Burchell B, Binh TQ, Thu le TA, Hung NC, Pirmohamed M et al. 2002. Glucuronidation of dihydroartemisinin in vivo and by human liver microsomes and expressed UDP-glucuronosyltransferases. *Drug Metab Dispos* **30**: 1005-1012.
- Iliakis G. 2009. Backup pathways of NHEJ in cells of higher eukaryotes: cell cycle dependence. *Radiotherapy and oncology : journal of the European Society for Therapeutic Radiology and Oncology* **92**: 310-315.
- Ito S, D'Alessio AC, Taranova OV, Hong K, Sowers LC, Zhang Y. 2010. Role of Tet proteins in 5mC to 5hmC conversion, ES-cell self-renewal and inner cell mass specification. *Nature* **466**: 1129-1133.
- Iyer LM, Tahiliani M, Rao A, Aravind L. 2009. Prediction of novel families of enzymes involved in oxidative and other complex modifications of bases in nucleic acids. *Cell Cycle* **8**: 1698-1710.
- Jia G, Yang CG, Yang S, Jian X, Yi C, Zhou Z, He C. 2008. Oxidative demethylation of 3-methylthymine and 3-methyluracil in single-stranded DNA and RNA by mouse and human FTO. *FEBS Lett* **582**: 3313-3319.
- Jin G, Reitman ZJ, Spasojevic I, Batinic-Haberle I, Yang J, Schmidt-Kittler O, Bigner DD, Yan H. 2011. 2-hydroxyglutarate production, but not dominant negative function, is conferred by glioma-derived NADP-dependent isocitrate dehydrogenase mutations. *PloS one* **6**: e16812.
- Jiricny J. 2013. Postreplicative mismatch repair. *Cold Spring Harb Perspect Biol* **5**: a012633.

## References

- Johannessen TC, Prestegarden L, Grudic A, Hegi ME, Tysnes BB, Bjerkvig R. 2013. The DNA repair protein ALKBH2 mediates temozolomide resistance in human glioblastoma cells. *Neuro-oncology* **15**: 269-278.
- Johnson BE, Mazar T, Hong C, Barnes M, Aihara K, McLean CY, Fouse SD, Yamamoto S, Ueda H, Tatsuno K et al. 2014. Mutational analysis reveals the origin and therapy-driven evolution of recurrent glioma. *Science* **343**: 189-193.
- Kaelin WG, Jr., McKnight SL. 2013. Influence of metabolism on epigenetics and disease. *Cell* **153**: 56-69.
- Kaina B, Christmann M, Naumann S, Roos WP. 2007. MGMT: key node in the battle against genotoxicity, carcinogenicity and apoptosis induced by alkylating agents. *DNA repair* **6**: 1079-1099.
- Karayan-Tapon L, Quillien V, Guilhot J, Wager M, Fromont G, Saikali S, Etcheverry A, Hamlat A, Loussouarn D, Champion L et al. 2010. Prognostic value of O6-methylguanine-DNA methyltransferase status in glioblastoma patients, assessed by five different methods. *Journal of neuro-oncology* **97**: 311-322.
- Kienhofer S, Musheev MU, Stapf U, Helm M, Schomacher L, Niehrs C, Schafer A. 2015. GADD45a physically and functionally interacts with TET1. *Differentiation* **90**: 59-68.
- Killian JK, Kim SY, Miettinen M, Smith C, Merino M, Tsokos M, Quezado M, Smith WI, Jr., Jahromi MS, Xekouki P et al. 2013. Succinate dehydrogenase mutation underlies global epigenomic divergence in gastrointestinal stromal tumor. *Cancer discovery* **3**: 648-657.
- Kitange GJ, Carlson BL, Schroeder MA, Grogan PT, Lamont JD, Decker PA, Wu W, James CD, Sarkaria JN. 2009. Induction of MGMT expression is associated with temozolomide resistance in glioblastoma xenografts. *Neuro-oncology* **11**: 281-291.
- Klayman DL. 1985. Qinghaosu (artemisinin): an antimalarial drug from China. *Science* **228**: 1049-1055.
- Ko M, An J, Bandukwala HS, Chavez L, Aijo T, Pastor WA, Segal MF, Li H, Koh KP, Lahdesmaki H et al. 2013. Modulation of TET2 expression and 5-methylcytosine oxidation by the CXXC domain protein IDAX. *Nature* **497**: 122-126.
- Kohli RM, Zhang Y. 2013. TET enzymes, TDG and the dynamics of DNA demethylation. *Nature* **502**: 472-479.
- Kölker S, Mayatepek E, Hoffmann GF. 2002a. White matter disease in cerebral organic acid disorders: clinical implications and suggested pathomechanisms. *Neuropediatrics* **33**: 225-231.
- Kölker S, Pawlak V, Ahlemeyer B, Okun JG, Horster F, Mayatepek E, Kriegelstein J, Hoffmann GF, Kohr G. 2002b. NMDA receptor activation and respiratory chain complex V inhibition contribute to neurodegeneration in d-2-hydroxyglutaric aciduria. *Eur J Neurosci* **16**: 21-28.
- Konkimalla VB, McCubrey JA, Efferth T. 2009. The role of downstream signaling pathways of the epidermal growth factor receptor for Artesunate's activity in cancer cells. *Curr Cancer Drug Targets* **9**: 72-80.
- Kornberg RD. 1974. Chromatin structure: a repeating unit of histones and DNA. *Science* **184**: 868-871.
- Kouzarides T. 2007. Chromatin modifications and their function. *Cell* **128**: 693-705.



- Krawczak M, Ball EV, Cooper DN. 1998. Neighboring-nucleotide effects on the rates of germ-line single-base-pair substitution in human genes. *Am J Hum Genet* **63**: 474-488.
- Krishan A. 1975. Rapid flow cytofluorometric analysis of mammalian cell cycle by propidium iodide staining. *The Journal of cell biology* **66**: 188-193.
- Krokan HE, Bjoras M. 2013. Base excision repair. *Cold Spring Harb Perspect Biol* **5**: a012583.
- Kurdyukov S, Bullock M. 2016. DNA Methylation Analysis: Choosing the Right Method. *Biology (Basel)* **5**.
- Lahtz C, Pfeifer GP. 2011. Epigenetic changes of DNA repair genes in cancer. *Journal of molecular cell biology* **3**: 51-58.
- Latini A, Scussiato K, Rosa RB, Llesuy S, Bello-Klein A, Dutra-Filho CS, Wajner M. 2003. D-2-hydroxyglutaric acid induces oxidative stress in cerebral cortex of young rats. *Eur J Neurosci* **17**: 2017-2022.
- Lee MN, Tseng RC, Hsu HS, Chen JY, Tzao C, Ho WL, Wang YC. 2007. Epigenetic inactivation of the chromosomal stability control genes BRCA1, BRCA2, and XRCC5 in non-small cell lung cancer. *Clinical Cancer Research* **13**: 832-838.
- Lemoine A, Lucas C, Ings RM. 1991. Metabolism of the chloroethylnitrosoureas. *Xenobiotica* **21**: 775-791.
- Letouze E, Martinelli C, Lorient C, Burnichon N, Abermil N, Ottolenghi C, Janin M, Menara M, Nguyen AT, Benit P et al. 2013. SDH mutations establish a hypermethylator phenotype in paraganglioma. *Cancer cell* **23**: 739-752.
- Li B, Carey M, Workman JL. 2007. The role of chromatin during transcription. *Cell* **128**: 707-719.
- Li GM. 2008. Mechanisms and functions of DNA mismatch repair. *Cell Res* **18**: 85-98.
- Li MM, Nilsen A, Shi Y, Fusser M, Ding YH, Fu Y, Liu B, Niu Y, Wu YS, Huang CM et al. 2013a. ALKBH4-dependent demethylation of actin regulates actomyosin dynamics. *Nat Commun* **4**: 1832.
- Li PC, Lam E, Roos WP, Zdzienicka MZ, Kaina B, Efferth T. 2008. Artesunate derived from traditional Chinese medicine induces DNA damage and repair. *Cancer research* **68**: 4347-4351.
- Li S, Chou AP, Chen W, Chen R, Deng Y, Phillips HS, Selfridge J, Zurayk M, Lou JJ, Everson RG et al. 2013b. Overexpression of isocitrate dehydrogenase mutant proteins renders glioma cells more sensitive to radiation. *Neuro-oncology* **15**: 57-68.
- Li X, Yao X, Wang Y, Hu F, Wang F, Jiang L, Liu Y, Wang D, Sun G, Zhao Y. 2013c. MLH1 promoter methylation frequency in colorectal cancer patients and related clinicopathological and molecular features. *PLoS one* **8**: e59064.
- Li XQ, Bjorkman A, Andersson TB, Gustafsson LL, Masimirembwa CM. 2003. Identification of human cytochrome P(450)s that metabolise anti-parasitic drugs and predictions of in vivo drug hepatic clearance from in vitro data. *Eur J Clin Pharmacol* **59**: 429-442.
- Li Z, Gu TP, Weber AR, Shen JZ, Li BZ, Xie ZG, Yin R, Guo F, Liu X, Tang F et al. 2015. Gadd45a promotes DNA demethylation through TDG. *Nucleic acids research* **43**: 3986-3997.
- Lieb M, Bhagwat AS. 1996. Very short patch repair: reducing the cost of cytosine methylation. *Mol Microbiol* **20**: 467-473.

## References

- Lieber MR. 2010. The mechanism of double-strand DNA break repair by the nonhomologous DNA end-joining pathway. *Annual review of biochemistry* **79**: 181-211.
- Lijinsky W. 1999. N-Nitroso compounds in the diet. *Mutation research* **443**: 129-138.
- Lim A, Li BF. 1996. The nuclear targeting and nuclear retention properties of a human DNA repair protein O6-methylguanine-DNA methyltransferase are both required for its nuclear localization: the possible implications. *EMBO J* **15**: 4050-4060.
- Lin IG, Han L, Taghva A, O'Brien LE, Hsieh CL. 2002. Murine de novo methyltransferase Dnmt3a demonstrates strand asymmetry and site preference in the methylation of DNA in vitro. *Molecular and cellular biology* **22**: 704-723.
- Lindahl T. 1993. Instability and decay of the primary structure of DNA. *Nature* **362**: 709-715.
- Liu Q, Guntuku S, Cui XS, Matsuoka S, Cortez D, Tamai K, Luo G, Carattini-Rivera S, DeMayo F, Bradley A et al. 2000. Chk1 is an essential kinase that is regulated by Atr and required for the G(2)/M DNA damage checkpoint. *Genes & development* **14**: 1448-1459.
- Liu R, Dong HF, Guo Y, Zhao QP, Jiang MS. 2011. Efficacy of praziquantel and artemisinin derivatives for the treatment and prevention of human schistosomiasis: a systematic review and meta-analysis. *Parasit Vectors* **4**: 201.
- Liu Y, Hu H, Zhang C, Wang Z, Li M, Zhang W, Jiang T. 2015. Methylation associated genes contribute to the favorable prognosis of gliomas with isocitrate dehydrogenase 1 mutation. *Am J Cancer Res* **5**: 2745-2755.
- Loenarz C, Schofield CJ. 2011. Physiological and biochemical aspects of hydroxylations and demethylations catalyzed by human 2-oxoglutarate oxygenases. *Trends Biochem Sci* **36**: 7-18.
- Louis DN, Ohgaki H, Wiestler OD, Cavenee WK, Burger PC, Jouvet A, Scheithauer BW, Kleihues P. 2007. The 2007 WHO classification of tumours of the central nervous system. *Acta neuropathologica* **114**: 97-109.
- Louis DN, Perry A, Reifenberger G, von Deimling A, Figarella-Branger D, Cavenee WK, Ohgaki H, Wiestler OD, Kleihues P, Ellison DW. 2016. The 2016 World Health Organization Classification of Tumors of the Central Nervous System: a summary. *Acta neuropathologica* **131**: 803-820.
- Louro R, El-Jundi T, Nakaya HI, Reis EM, Verjovski-Almeida S. 2008. Conserved tissue expression signatures of intronic noncoding RNAs transcribed from human and mouse loci. *Genomics* **92**: 18-25.
- Lu C, Ward PS, Kapoor GS, Rohle D, Turcan S, Abdel-Wahab O, Edwards CR, Khanin R, Figueroa ME, Melnick A et al. 2012. IDH mutation impairs histone demethylation and results in a block to cell differentiation. *Nature* **483**: 474-478.
- Lujambio A, Ropero S, Ballestar E, Fraga MF, Cerrato C, Setien F, Casado S, Suarez-Gauthier A, Sanchez-Cespedes M, Git A et al. 2007. Genetic unmasking of an epigenetically silenced microRNA in human cancer cells. *Cancer research* **67**: 1424-1429.
- Lujan SA, Williams JS, Clausen AR, Clark AB, Kunkel TA. 2013. Ribonucleotides are signals for mismatch repair of leading-strand replication errors. *Molecular cell* **50**: 437-443.

- Lujan SA, Williams JS, Pursell ZF, Abdulovic-Cui AA, Clark AB, Nick McElhinny SA, Kunkel TA. 2012. Mismatch repair balances leading and lagging strand DNA replication fidelity. *PLoS Genet* **8**: e1003016.
- Lutsenko E, Bhagwat AS. 1999. Principal causes of hot spots for cytosine to thymine mutations at sites of cytosine methylation in growing cells. A model, its experimental support and implications. *Mutation research* **437**: 11-20.
- Maciejewska AM, Poznanski J, Kaczmarek Z, Krowisz B, Nieminuszczy J, Polkowska-Nowakowska A, Grzesiuk E, Kusmierk JT. 2013. AlkB dioxygenase preferentially repairs protonated substrates: specificity against exocyclic adducts and molecular mechanism of action. *The Journal of biological chemistry* **288**: 432-441.
- Maier P, Hartmann L, Wenz F, Herskind C. 2016. Cellular Pathways in Response to Ionizing Radiation and Their Targetability for Tumor Radiosensitization. *Int J Mol Sci* **17**.
- Malley DS, Hamoudi RA, Kocalkowski S, Pearson DM, Collins VP, Ichimura K. 2011. A distinct region of the MGMT CpG island critical for transcriptional regulation is preferentially methylated in glioblastoma cells and xenografts. *Acta neuropathologica* **121**: 651-661.
- Mardis ER, Ding L, Dooling DJ, Larson DE, McLellan MD, Chen K, Koboldt DC, Fulton RS, Delehaunty KD, McGrath SD et al. 2009. Recurring mutations found by sequencing an acute myeloid leukemia genome. *The New England journal of medicine* **361**: 1058-1066.
- Margison GP, Povey AC, Kaina B, Santibanez Koref MF. 2003. Variability and regulation of O6-alkylguanine-DNA alkyltransferase. *Carcinogenesis* **24**: 625-635.
- McDonough MA, Loenarz C, Chowdhury R, Clifton IJ, Schofield CJ. 2010. Structural studies on human 2-oxoglutarate dependent oxygenases. *Curr Opin Struct Biol* **20**: 659-672.
- Millar CB, Guy J, Sansom OJ, Selfridge J, MacDougall E, Hendrich B, Keightley PD, Bishop SM, Clarke AR, Bird A. 2002. Enhanced CpG mutability and tumorigenesis in MBD4-deficient mice. *Science* **297**: 403-405.
- Min A, Im SA, Yoon YK, Song SH, Nam HJ, Hur HS, Kim HP, Lee KH, Han SW, Oh DY et al. 2013. RAD51C-deficient cancer cells are highly sensitive to the PARP inhibitor olaparib. *Molecular cancer therapeutics* **12**: 865-877.
- Mohrenz IV, Antonietti P, Pusch S, Capper D, Balss J, Voigt S, Weissert S, Mukrowsky A, Frank J, Senft C et al. 2013. Isocitrate dehydrogenase 1 mutant R132H sensitizes glioma cells to BCNU-induced oxidative stress and cell death. *Apoptosis : an international journal on programmed cell death* **18**: 1416-1425.
- Mole DR. 2010. Iron homeostasis and its interaction with prolyl hydroxylases. *Antioxid Redox Signal* **12**: 445-458.
- Monk M, Boubelik M, Lehnert S. 1987. Temporal and regional changes in DNA methylation in the embryonic, extraembryonic and germ cell lineages during mouse embryo development. *Development* **99**: 371-382.
- Muller TA, Andrzejak MM, Hausinger RP. 2013. A covalent protein-DNA 5'-product adduct is generated following AP lyase activity of human ALKBH1 (AlkB homologue 1). *The Biochemical journal* **452**: 509-518.
- Murat A, Migliavacca E, Gorlia T, Lambiv WL, Shay T, Hamou MF, de Tribolet N, Regli L, Wick W, Kouwenhoven MC et al. 2008. Stem cell-related "self-renewal"

## References

- signature and high epidermal growth factor receptor expression associated with resistance to concomitant chemoradiotherapy in glioblastoma. *Journal of clinical oncology : official journal of the American Society of Clinical Oncology* **26**: 3015-3024.
- Nagy R, Sweet K, Eng C. 2004. Highly penetrant hereditary cancer syndromes. *Oncogene* **23**: 6445-6470.
- Nair J, Gansauge F, Beger H, Dolara P, Winde G, Bartsch H. 2006. Increased etheno-DNA adducts in affected tissues of patients suffering from Crohn's disease, ulcerative colitis, and chronic pancreatitis. *Antioxid Redox Signal* **8**: 1003-1010.
- Nakagawachi T, Soejima H, Urano T, Zhao W, Higashimoto K, Satoh Y, Matsukura S, Kudo S, Kitajima Y, Harada H et al. 2003. Silencing effect of CpG island hypermethylation and histone modifications on O6-methylguanine-DNA methyltransferase (MGMT) gene expression in human cancer. *Oncogene* **22**: 8835-8844.
- Newlands ES, Stevens MF, Wedge SR, Wheelhouse RT, Brock C. 1997. Temozolomide: a review of its discovery, chemical properties, pre-clinical development and clinical trials. *Cancer treatment reviews* **23**: 35-61.
- Nicoletti I, Migliorati G, Pagliacci MC, Grignani F, Riccardi C. 1991. A rapid and simple method for measuring thymocyte apoptosis by propidium iodide staining and flow cytometry. *J Immunol Methods* **139**: 271-279.
- Nilsen H, Haushalter KA, Robins P, Barnes DE, Verdine GL, Lindahl T. 2001. Excision of deaminated cytosine from the vertebrate genome: role of the SMUG1 uracil-DNA glycosylase. *EMBO J* **20**: 4278-4286.
- Ohba S, Mukherjee J, See WL, Pieper RO. 2014. Mutant IDH1-driven cellular transformation increases RAD51-mediated homologous recombination and temozolomide resistance. *Cancer research* **74**: 4836-4844.
- Ohgaki H, Kleihues P. 2009. Genetic alterations and signaling pathways in the evolution of gliomas. *Cancer science* **100**: 2235-2241.
- . 2013. The definition of primary and secondary glioblastoma. *Clinical cancer research : an official journal of the American Association for Cancer Research* **19**: 764-772.
- Okano M, Xie S, Li E. 1998. Cloning and characterization of a family of novel mammalian DNA (cytosine-5) methyltransferases. *Nature genetics* **19**: 219-220.
- Olsson M, Lindahl T. 1980. Repair of alkylated DNA in Escherichia coli. Methyl group transfer from O6-methylguanine to a protein cysteine residue. *The Journal of biological chemistry* **255**: 10569-10571.
- Orita M, Suzuki Y, Sekiya T, Hayashi K. 1989. Rapid and sensitive detection of point mutations and DNA polymorphisms using the polymerase chain reaction. *Genomics* **5**: 874-879.
- Ostrom QT, Gittleman H, Farah P, Ondracek A, Chen Y, Wolinsky Y, Stroup NE, Kruchko C, Barnholtz-Sloan JS. 2013. CBTRUS statistical report: Primary brain and central nervous system tumors diagnosed in the United States in 2006-2010. *Neuro-oncology* **15 Suppl 2**: ii1-56.
- Otterlei M, Warbrick E, Nagelhus TA, Haug T, Slupphaug G, Akbari M, Aas PA, Steinsbekk K, Bakke O, Krokan HE. 1999. Post-replicative base excision repair in replication foci. *EMBO J* **18**: 3834-3844.

- Ougland R, Lando D, Jonson I, Dahl JA, Moen MN, Nordstrand LM, Rognes T, Lee JT, Klungland A, Kouzarides T et al. 2012. ALKBH1 is a histone H2A dioxygenase involved in neural differentiation. *Stem Cells* **30**: 2672-2682.
- Parsons DW, Jones S, Zhang X, Lin JC, Leary RJ, Angenendt P, Mankoo P, Carter H, Siu IM, Gallia GL et al. 2008. An integrated genomic analysis of human glioblastoma multiforme. *Science* **321**: 1807-1812.
- Pena-Diaz J, Bregenhorn S, Ghodgaonkar M, Follonier C, Artola-Boran M, Castor D, Lopes M, Sartori AA, Jiricny J. 2012. Noncanonical mismatch repair as a source of genomic instability in human cells. *Molecular cell* **47**: 669-680.
- Pentsova EI, Reiner AS, Panageas KS, DeAngelis LM. 2016. Anaplastic astrocytoma and non-1p/19q co-deleted anaplastic oligoastrocytoma: long-term survival, employment, and performance status of survivors. *Neuro-Oncology Practice* **3**: 71-76.
- Petermann E, Helleday T. 2010. Pathways of mammalian replication fork restart. *Nature reviews Molecular cell biology* **11**: 683-687.
- Petrova KV, Stec DF, Voehler M, Rizzo CJ. 2011. Synthesis of the four stereoisomers of 2,3-epoxy-4-hydroxynonanal and their reactivity with deoxyguanosine. *Org Biomol Chem* **9**: 1960-1971.
- Poulos RC, Olivier J, Wong JWH. 2017. CpG methylation accounts for genome-wide C>T mutation variation and cancer driver formation across cancer types. *bioRxiv*.
- Preusser M, Charles Janzer R, Felsberg J, Reifenberger G, Hamou MF, Diserens AC, Stupp R, Gorlia T, Marosi C, Heinzl H et al. 2008. Anti-O6-methylguanine-methyltransferase (MGMT) immunohistochemistry in glioblastoma multiforme: observer variability and lack of association with patient survival impede its use as clinical biomarker. *Brain pathology* **18**: 520-532.
- Pruitt KD, Brown GR, Hiatt SM, Thibaud-Nissen F, Astashyn A, Ermolaeva O, Farrell CM, Hart J, Landrum MJ, McGarvey KM et al. 2014. RefSeq: an update on mammalian reference sequences. *Nucleic acids research* **42**: D756-763.
- Pusch S, Schweizer L, Beck AC, Lehmler JM, Weissert S, Balss J, Miller AK, von Deimling A. 2014. D-2-Hydroxyglutarate producing neo-enzymatic activity inversely correlates with frequency of the type of isocitrate dehydrogenase 1 mutations found in glioma. *Acta neuropathologica communications* **2**: 19.
- Qi Z, Redding S, Lee JY, Gibb B, Kwon Y, Niu H, Gaines WA, Sung P, Greene EC. 2015. DNA sequence alignment by microhomology sampling during homologous recombination. *Cell* **160**: 856-869.
- Qian XC, Brent TP. 1997. Methylation hot spots in the 5' flanking region denote silencing of the O6-methylguanine-DNA methyltransferase gene. *Cancer research* **57**: 3672-3677.
- Quillien V, Lavenu A, Karayan-Tapon L, Carpentier C, Labussiere M, Lesimple T, Chinot O, Wager M, Honnorat J, Saikali S et al. 2012. Comparative assessment of 5 methods (methylation-specific polymerase chain reaction, MethyLight, pyrosequencing, methylation-sensitive high-resolution melting, and immunohistochemistry) to analyze O6-methylguanine-DNA-methyltransferase in a series of 100 glioblastoma patients. *Cancer* **118**: 4201-4211.

## References

- Quiros S, Roos WP, Kaina B. 2010. Processing of O6-methylguanine into DNA double-strand breaks requires two rounds of replication whereas apoptosis is also induced in subsequent cell cycles. *Cell Cycle* **9**: 168-178.
- Rakyan VK, Chong S, Champ ME, Cuthbert PC, Morgan HD, Luu KV, Whitelaw E. 2003. Transgenerational inheritance of epigenetic states at the murine Axin(Fu) allele occurs after maternal and paternal transmission. *Proceedings of the National Academy of Sciences of the United States of America* **100**: 2538-2543.
- Rasheed SA, Efferth T, Asangani IA, Allgayer H. 2010. First evidence that the antimalarial drug artesunate inhibits invasion and in vivo metastasis in lung cancer by targeting essential extracellular proteases. *International journal of cancer Journal international du cancer* **127**: 1475-1485.
- Ratcliffe PJ. 2013. Oxygen sensing and hypoxia signalling pathways in animals: the implications of physiology for cancer. *J Physiol* **591**: 2027-2042.
- Reifenberger G, Hentschel B, Felsberg J, Schackert G, Simon M, Schnell O, Westphal M, Wick W, Pietsch T, Loeffler M et al. 2012. Predictive impact of MGMT promoter methylation in glioblastoma of the elderly. *International journal of cancer Journal international du cancer* **131**: 1342-1350.
- Reu FJ, Bae SI, Cherkassky L, Leaman DW, Lindner D, Beaulieu N, MacLeod AR, Borden EC. 2006. Overcoming resistance to interferon-induced apoptosis of renal carcinoma and melanoma cells by DNA demethylation. *Journal of clinical oncology : official journal of the American Society of Clinical Oncology* **24**: 3771-3779.
- Rhoades JW, Johnson DE. 1972. N-dimethylnitrosamine in tobacco smoke condensate. *Nature* **236**: 307-308.
- Riggs AD. 1975. X inactivation, differentiation, and DNA methylation. *Cytogenet Cell Genet* **14**: 9-25.
- Ringvoll J, Moen MN, Nordstrand LM, Meira LB, Pang B, Bekkelund A, Dedon PC, Bjelland S, Samson LD, Falnes PO et al. 2008. AlkB homologue 2-mediated repair of ethenoadenine lesions in mammalian DNA. *Cancer research* **68**: 4142-4149.
- Rydberg B, Lindahl T. 1982. Nonenzymatic methylation of DNA by the intracellular methyl group donor S-adenosyl-L-methionine is a potentially mutagenic reaction. *EMBO J* **1**: 211-216.
- Safar AM, Spencer H, 3rd, Su X, Coffey M, Cooney CA, Ratnasinghe LD, Hutchins LF, Fan CY. 2005. Methylation profiling of archived non-small cell lung cancer: a promising prognostic system. *Clinical cancer research : an official journal of the American Association for Cancer Research* **11**: 4400-4405.
- Saha SK, Parachoniak CA, Bardeesy N. 2014. IDH mutations in liver cell plasticity and biliary cancer. *Cell Cycle* **13**: 3176-3182.
- Salminen A, Kauppinen A, Kaarniranta K. 2015. 2-Oxoglutarate-dependent dioxygenases are sensors of energy metabolism, oxygen availability, and iron homeostasis: potential role in the regulation of aging process. *Cell Mol Life Sci* **72**: 3897-3914.
- Sambrook J, Russell DW. 2006. Purification of nucleic acids by extraction with phenol:chloroform. *CSH Protoc* **2006**.
- San Filippo J, Sung P, Klein H. 2008. Mechanism of eukaryotic homologous recombination. *Annual review of biochemistry* **77**: 229-257.

- Sartori AA, Lukas C, Coates J, Mistrik M, Fu S, Bartek J, Baer R, Lukas J, Jackson SP. 2007. Human CtIP promotes DNA end resection. *Nature* **450**: 509-514.
- Sassanfar M, Dosanjh MK, Essigmann JM, Samson L. 1991. Relative efficiencies of the bacterial, yeast, and human DNA methyltransferases for the repair of O6-methylguanine and O4-methylthymine. Suggestive evidence for O4-methylthymine repair by eukaryotic methyltransferases. *The Journal of biological chemistry* **266**: 2767-2771.
- Scarano E, Iaccarino M, Grippo P, Parisi E. 1967. The heterogeneity of thymine methyl group origin in DNA pyrimidine isostichs of developing sea urchin embryos. *Proceedings of the National Academy of Sciences of the United States of America* **57**: 1394-1400.
- Schäfer A, Karaulanov E, Stapf U, Doderlein G, Niehrs C. 2013. Ing1 functions in DNA demethylation by directing Gadd45a to H3K4me3. *Genes & development* **27**: 261-273.
- Schaur RJ. 2003. Basic aspects of the biochemical reactivity of 4-hydroxynonenal. *Mol Aspects Med* **24**: 149-159.
- Schindler G, Capper D, Meyer J, Janzarik W, Omran H, Herold-Mende C, Schmieder K, Wesseling P, Mawrin C, Hasselblatt M et al. 2011. Analysis of BRAF V600E mutation in 1,320 nervous system tumors reveals high mutation frequencies in pleomorphic xanthoastrocytoma, ganglioglioma and extra-cerebellar pilocytic astrocytoma. *Acta neuropathologica* **121**: 397-405.
- Schofield CJ, Zhang Z. 1999. Structural and mechanistic studies on 2-oxoglutarate-dependent oxygenases and related enzymes. *Curr Opin Struct Biol* **9**: 722-731.
- Schomacher L, Han D, Musheev MU, Arab K, Kienhofer S, von Seggern A, Niehrs C. 2016. Neil DNA glycosylases promote substrate turnover by Tdg during DNA demethylation. *Nature structural & molecular biology* **23**: 116-124.
- Schulze Heuling E, Knab F, Radke J, Eskilsson E, Martinez-Ledesma E, Koch A, Czabanka M, Dieterich C, Verhaak RG, Harms C et al. 2017. Prognostic Relevance of Tumor Purity and Interaction with MGMT Methylation in Glioblastoma. *Molecular cancer research : MCR* **15**: 532-540.
- Seltzer MJ, Bennett BD, Joshi AD, Gao P, Thomas AG, Ferraris DV, Tsukamoto T, Rojas CJ, Slusher BS, Rabinowitz JD et al. 2010. Inhibition of glutaminase preferentially slows growth of glioma cells with mutant IDH1. *Cancer research* **70**: 8981-8987.
- Sertel S, Eichhorn T, Sieber S, Sauer A, Weiss J, Plinkert PK, Efferth T. 2010a. Factors determining sensitivity or resistance of tumor cell lines towards artesunate. *Chem Biol Interact* **185**: 42-52.
- Sertel S, Eichhorn T, Simon CH, Plinkert PK, Johnson SW, Efferth T. 2010b. Pharmacogenomic identification of c-Myc/Max-regulated genes associated with cytotoxicity of artesunate towards human colon, ovarian and lung cancer cell lines. *Molecules* **15**: 2886-2910.
- Shen JC, Rideout WM, 3rd, Jones PA. 1994. The rate of hydrolytic deamination of 5-methylcytosine in double-stranded DNA. *Nucleic acids research* **22**: 972-976.
- Shi J, Sun B, Shi W, Zuo H, Cui D, Ni L, Chen J. 2015. Decreasing GSH and increasing ROS in chemosensitivity gliomas with IDH1 mutation. *Tumour biology : the journal of the International Society for Oncodevelopmental Biology and Medicine* **36**: 655-662.

## References

- Shih C, Weinberg RA. 1982. Isolation of a transforming sequence from a human bladder carcinoma cell line. *Cell* **29**: 161-169.
- Shinsato Y, Furukawa T, Yunoue S, Yonezawa H, Minami K, Nishizawa Y, Ikeda R, Kawahara K, Yamamoto M, Hirano H et al. 2013. Reduction of MLH1 and PMS2 confers temozolomide resistance and is associated with recurrence of glioblastoma. *Oncotarget* **4**: 2261-2270.
- Slack JM. 2002. Conrad Hal Waddington: the last Renaissance biologist? *Nature reviews Genetics* **3**: 889-895.
- SongTao Q, Lei Y, Si G, YanQing D, HuiXia H, XueLin Z, LanXiao W, Fei Y. 2012. IDH mutations predict longer survival and response to temozolomide in secondary glioblastoma. *Cancer science* **103**: 269-273.
- Soomro S, Langenberg T, Mahringer A, Konkimalla VB, Horwedel C, Holenya P, Brand A, Cetin C, Fricker G, Dewerchin M et al. 2011. Design of novel artemisinin-like derivatives with cytotoxic and anti-angiogenic properties. *J Cell Mol Med* **15**: 1122-1135.
- Srivenugopal KS, Yuan XH, Friedman HS, Ali-Osman F. 1996. Ubiquitination-dependent proteolysis of O6-methylguanine-DNA methyltransferase in human and murine tumor cells following inactivation with O6-benzylguanine or 1,3-bis(2-chloroethyl)-1-nitrosourea. *Biochemistry* **35**: 1328-1334.
- Struys EA, Salomons GS, Achouri Y, Van Schaftingen E, Grosso S, Craigen WJ, Verhoeven NM, Jakobs C. 2005. Mutations in the D-2-hydroxyglutarate dehydrogenase gene cause D-2-hydroxyglutaric aciduria. *Am J Hum Genet* **76**: 358-360.
- Stupp R, Brada M, van den Bent MJ, Tonn JC, Pentheroudakis G, Group EGW. 2014. High-grade glioma: ESMO Clinical Practice Guidelines for diagnosis, treatment and follow-up. *Ann Oncol* **25 Suppl 3**: iii93-101.
- Stupp R, Hegi ME, Mason WP, van den Bent MJ, Taphoorn MJ, Janzer RC, Ludwin SK, Allgeier A, Fisher B, Belanger K et al. 2009. Effects of radiotherapy with concomitant and adjuvant temozolomide versus radiotherapy alone on survival in glioblastoma in a randomised phase III study: 5-year analysis of the EORTC-NCIC trial. *The Lancet Oncology* **10**: 459-466.
- Stupp R, Mason WP, van den Bent MJ, Weller M, Fisher B, Taphoorn MJ, Belanger K, Brandes AA, Marosi C, Bogdahn U et al. 2005. Radiotherapy plus concomitant and adjuvant temozolomide for glioblastoma. *The New England journal of medicine* **352**: 987-996.
- Sulkowski PL, Corso CD, Robinson ND, Scanlon SE, Purshouse KR, Bai H, Liu Y, Sundaram RK, Hegan DC, Fons NR et al. 2017. 2-Hydroxyglutarate produced by neomorphic IDH mutations suppresses homologous recombination and induces PARP inhibitor sensitivity. *Science translational medicine* **9**.
- Sundheim O, Talstad VA, Vagbo CB, Slupphaug G, Krokan HE. 2008. AlkB demethylases flip out in different ways. *DNA repair* **7**: 1916-1923.
- Tahiliani M, Koh KP, Shen Y, Pastor WA, Bandukwala H, Brudno Y, Agarwal S, Iyer LM, Liu DR, Aravind L et al. 2009. Conversion of 5-methylcytosine to 5-hydroxymethylcytosine in mammalian DNA by MLL partner TET1. *Science* **324**: 930-935.



- Takahashi Y, Akahane T, Sawada T, Ikeda H, Tempaku A, Yamauchi S, Nishihara H, Tanaka S, Nitta K, Ide W et al. 2015. Adult classical glioblastoma with a BRAF V600E mutation. *World J Surg Oncol* **13**: 100.
- Tano K, Shiota S, Collier J, Foote RS, Mitra S. 1990. Isolation and structural characterization of a cDNA clone encoding the human DNA repair protein for O6-alkylguanine. *Proceedings of the National Academy of Sciences of the United States of America* **87**: 686-690.
- Tawfik HM, El-Maqsoud NM, Hak BH, El-Sherbiny YM. 2011. Head and neck squamous cell carcinoma: mismatch repair immunohistochemistry and promoter hypermethylation of hMLH1 gene. *Am J Otolaryngol* **32**: 528-536.
- Taylor SM, Jones PA. 1979. Multiple new phenotypes induced in 10T1/2 and 3T3 cells treated with 5-azacytidine. *Cell* **17**: 771-779.
- Tran AN, Lai A, Li S, Pope WB, Teixeira S, Harris RJ, Woodworth DC, Nghiemphu PL, Cloughesy TF, Ellingson BM. 2014. Increased sensitivity to radiochemotherapy in IDH1 mutant glioblastoma as demonstrated by serial quantitative MR volumetry. *Neuro-oncology* **16**: 414-420.
- Trewick SC, Henshaw TF, Hausinger RP, Lindahl T, Sedgwick B. 2002. Oxidative demethylation by Escherichia coli AlkB directly reverts DNA base damage. *Nature* **419**: 174-178.
- Tricarico R, Cortellino S, Riccio A, Jagmohan-Changur S, Van der Klift H, Wijnen J, Turner D, Ventura A, Rovella V, Percesepe A et al. 2015. Involvement of MBD4 inactivation in mismatch repair-deficient tumorigenesis. *Oncotarget* **6**: 42892-42904.
- Tse MY, Ashbury JE, Zwingerman N, King WD, Taylor SA, Pang SC. 2011. A refined, rapid and reproducible high resolution melt (HRM)-based method suitable for quantification of global LINE-1 repetitive element methylation. *BMC research notes* **4**: 565.
- Turcan S, Rohle D, Goenka A, Walsh LA, Fang F, Yilmaz E, Campos C, Fabius AW, Lu C, Ward PS et al. 2012. IDH1 mutation is sufficient to establish the glioma hypermethylator phenotype. *Nature* **483**: 479-483.
- van den Bent MJ, Dubbink HJ, Marie Y, Brandes AA, Taphoorn MJ, Wesseling P, Frenay M, Tijssen CC, Lacombe D, Idbaih A et al. 2010. IDH1 and IDH2 mutations are prognostic but not predictive for outcome in anaplastic oligodendroglial tumors: a report of the European Organization for Research and Treatment of Cancer Brain Tumor Group. *Clinical cancer research : an official journal of the American Association for Cancer Research* **16**: 1597-1604.
- van den Born E, Vagbo CB, Songe-Moller L, Leihne V, Lien GF, Leszczynska G, Malkiewicz A, Krokan HE, Kirpekar F, Klungland A et al. 2011. ALKBH8-mediated formation of a novel diastereomeric pair of wobble nucleosides in mammalian tRNA. *Nat Commun* **2**: 172.
- Wajner M, Latini A, Wyse AT, Dutra-Filho CS. 2004. The role of oxidative damage in the neuropathology of organic acidurias: insights from animal studies. *J Inherit Metab Dis* **27**: 427-448.
- Waki T, Tamura G, Tsuchiya T, Sato K, Nishizuka S, Motoyama T. 2002. Promoter methylation status of E-cadherin, hMLH1, and p16 genes in nonneoplastic gastric epithelia. *Am J Pathol* **161**: 399-403.

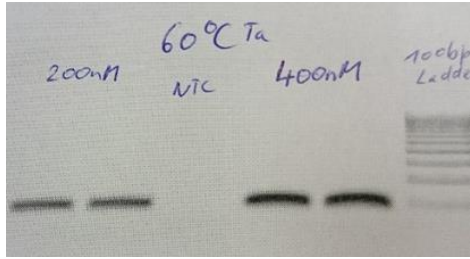
## References

- Wang JB, Dong DF, Wang MD, Gao K. 2014. IDH1 overexpression induced chemotherapy resistance and IDH1 mutation enhanced chemotherapy sensitivity in Glioma cells in vitro and in vivo. *Asian Pac J Cancer Prev* **15**: 427-432.
- Wang P, Wu J, Ma S, Zhang L, Yao J, Hoadley KA, Wilkerson MD, Perou CM, Guan KL, Ye D et al. 2015. Oncometabolite D-2-Hydroxyglutarate Inhibits ALKBH DNA Repair Enzymes and Sensitizes IDH Mutant Cells to Alkylating Agents. *Cell reports* **13**: 2353-2361.
- Ward IM, Chen J. 2001. Histone H2AX is phosphorylated in an ATR-dependent manner in response to replicational stress. *The Journal of biological chemistry* **276**: 47759-47762.
- Watanabe T, Nobusawa S, Kleihues P, Ohgaki H. 2009a. IDH1 mutations are early events in the development of astrocytomas and oligodendrogliomas. *Am J Pathol* **174**: 1149-1153.
- Watanabe T, Vital A, Nobusawa S, Kleihues P, Ohgaki H. 2009b. Selective acquisition of IDH1 R132C mutations in astrocytomas associated with Li-Fraumeni syndrome. *Acta neuropathologica* **117**: 653-656.
- Waterland RA, Jirtle RL. 2003. Transposable elements: targets for early nutritional effects on epigenetic gene regulation. *Molecular and cellular biology* **23**: 5293-5300.
- Watts GS, Pieper RO, Costello JF, Peng YM, Dalton WS, Futscher BW. 1997. Methylation of discrete regions of the O6-methylguanine DNA methyltransferase (MGMT) CpG island is associated with heterochromatinization of the MGMT transcription start site and silencing of the gene. *Molecular and cellular biology* **17**: 5612-5619.
- Weller M, Stupp R, Hegi ME, van den Bent M, Tonn JC, Sanson M, Wick W, Reifenberger G. 2012. Personalized care in neuro-oncology coming of age: why we need MGMT and 1p/19q testing for malignant glioma patients in clinical practice. *Neuro-oncology* **14 Suppl 4**: iv100-108.
- Weller M, Weber RG, Willscher E, Rieher V, Hentschel B, Kreuz M, Felsberg J, Beyer U, Loffler-Wirth H, Kaulich K et al. 2015. Molecular classification of diffuse cerebral WHO grade II/III gliomas using genome- and transcriptome-wide profiling improves stratification of prognostically distinct patient groups. *Acta neuropathologica* **129**: 679-693.
- Whitfield TW, Wang J, Collins PJ, Partridge EC, Aldred SF, Trinklein ND, Myers RM, Weng Z. 2012. Functional analysis of transcription factor binding sites in human promoters. *Genome biology* **13**: R50.
- Wick W, Hartmann C, Engel C, Stoffels M, Felsberg J, Stockhammer F, Sabel MC, Koeppen S, Ketter R, Meyermann R et al. 2009. NOA-04 randomized phase III trial of sequential radiochemotherapy of anaplastic glioma with procarbazine, lomustine, and vincristine or temozolomide. *Journal of clinical oncology : official journal of the American Society of Clinical Oncology* **27**: 5874-5880.
- Wick W, Meisner C, Hentschel B, Platten M, Schilling A, Wiestler B, Sabel MC, Koeppen S, Ketter R, Weiler M et al. 2013. Prognostic or predictive value of MGMT promoter methylation in gliomas depends on IDH1 mutation. *Neurology* **81**: 1515-1522.

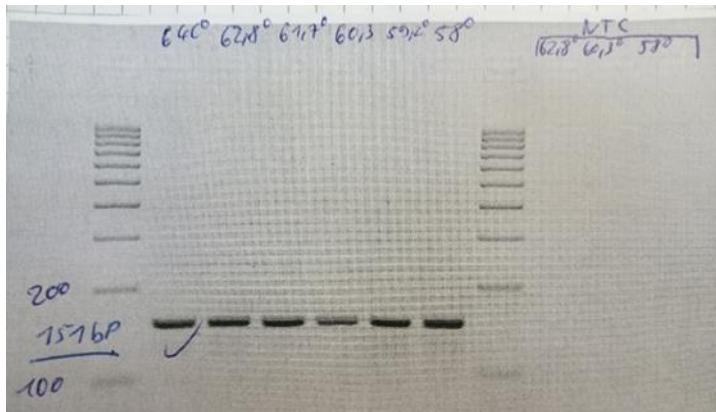
- Wijesinghe P, Bhagwat AS. 2012. Efficient deamination of 5-methylcytosines in DNA by human APOBEC3A, but not by AID or APOBEC3G. *Nucleic acids research* **40**: 9206-9217.
- Williams JS, Lujan SA, Kunkel TA. 2016. Processing ribonucleotides incorporated during eukaryotic DNA replication. *Nature reviews Molecular cell biology* **17**: 350-363.
- Winczura A, Czuby A, Winczura K, Maslowska K, Nalecz M, Dudzinska DA, Saparbaev M, Staron K, Tudek B. 2014. Lipid peroxidation product 4-hydroxy-2-nonenal modulates base excision repair in human cells. *DNA repair* **22**: 1-11.
- Wojdacz TK, Dobrovic A. 2007. Methylation-sensitive high resolution melting (MS-HRM): a new approach for sensitive and high-throughput assessment of methylation. *Nucleic acids research* **35**: e41.
- Wrensch M, Minn Y, Chew T, Bondy M, Berger MS. 2002. Epidemiology of primary brain tumors: current concepts and review of the literature. *Neuro-oncology* **4**: 278-299.
- Xu X, Zhao J, Xu Z, Peng B, Huang Q, Arnold E, Ding J. 2004. Structures of human cytosolic NADP-dependent isocitrate dehydrogenase reveal a novel self-regulatory mechanism of activity. *The Journal of biological chemistry* **279**: 33946-33957.
- Yan H, Parsons DW, Jin G, McLendon R, Rasheed BA, Yuan W, Kos I, Batinic-Haberle I, Jones S, Riggins GJ et al. 2009. IDH1 and IDH2 mutations in gliomas. *The New England journal of medicine* **360**: 765-773.
- Ye S, Riplinger C, Hansen A, Krebs C, Bollinger JM, Jr., Neese F. 2012. Electronic structure analysis of the oxygen-activation mechanism by Fe(II)- and alpha-ketoglutarate (alphaKG)-dependent dioxygenases. *Chemistry* **18**: 6555-6567.
- Yin H, Lin H. 2007. An epigenetic activation role of Piwi and a Piwi-associated piRNA in *Drosophila melanogaster*. *Nature* **450**: 304-308.
- Zdzalik D, Domanska A, Prorok P, Kosicki K, van den Born E, Falnes PO, Rizzo CJ, Guengerich FP, Tudek B. 2015. Differential repair of etheno-DNA adducts by bacterial and human AlkB proteins. *DNA repair* **30**: 1-10.
- Zhang J, Yang JH, Quan J, Kang X, Wang HJ, Dai PG. 2016. Identification of MGMT promoter methylation sites correlating with gene expression and IDH1 mutation in gliomas. *Tumour biology : the journal of the International Society for Oncodevelopmental Biology and Medicine* **37**: 13571-13579.
- Zhao S, Guan KL. 2010. IDH1 mutant structures reveal a mechanism of dominant inhibition. *Cell Res* **20**: 1279-1281.
- Zheng G, Dahl JA, Niu Y, Fedorcsak P, Huang CM, Li CJ, Vagbo CB, Shi Y, Wang WL, Song SH et al. 2013. ALKBH5 is a mammalian RNA demethylase that impacts RNA metabolism and mouse fertility. *Molecular cell* **49**: 18-29.
- Zheng G, Fu Y, He C. 2014. Nucleic acid oxidation in DNA damage repair and epigenetics. *Chem Rev* **114**: 4602-4620.



## 6. Supplementary information

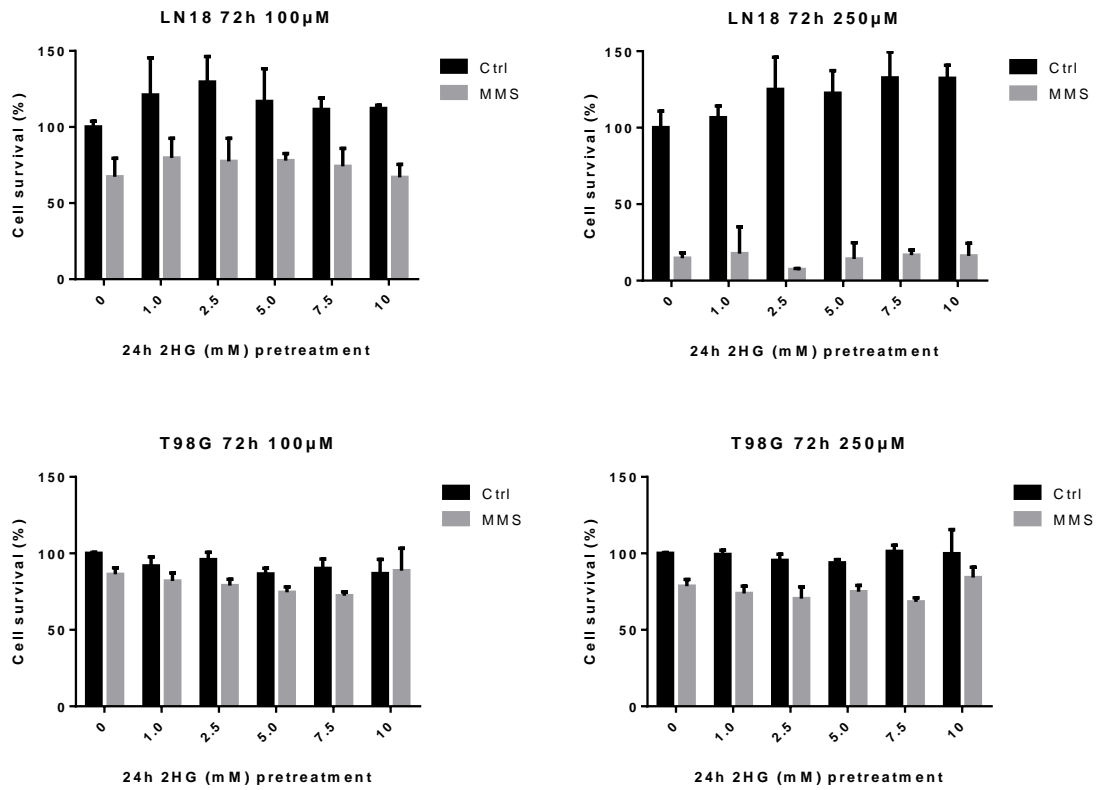


**Supplementary Figure 1** Agarose gel showing a clear IDH1 PCR product (88bp) at 200nM and 400nM primer concentration at 60°C Ta with no byproducts and clean NTC.



**Supplementary Figure 2** Agarose gel showing clear products from 58°C to 64°C Ta and clear NTCs.

## Supplementary information



**Supplementary Figure 3** LN18 and T98G cells were pretreated with increasing doses of 2-HG and then exposed to 100 µM or 250 µM MMS. Cell survival was measured after 72 h by the MTT assay. No 2-HG dose dependent sensitization towards MMS treatment could be observed.

## 7. Abbreviations

3mC	3-methylcytosine
μ	micro
3mA	3-Methyladenine
8oxoG	8-oxo-7,8-dihydroguanine
AA	Anaplastic astrocytoma
AAG	<i>3-alkyladenine DNA glycosylase (aka APNG, MPG)</i>
ABH	<i>ALKBH / alkB homolog</i>
ACNU	Nimustine
AP	Apurinic/Apyrimidinic site
APE1	Human AP Endonuclease
APS	Ammoniumpersulfat
ART	Artesunate
ATM	<i>ataxia-telangiectasia mutated</i>
ATP	Adenosine triphosphate
ATR	<i>ataxia telangiectasia and Rad3-related</i>
BCNU	Carmustine
BER	Base excision repair
bp	base pair
BSA	Bovine serum albumin
CCNU	Lomostine
CFA	Colony formation assay
DMSO	Dimethylsulfoxide
DNA	Deoxyribonucleic acid
DSB	DNA double-strand break
DTIC	5-(3,3-Dimethyl-1-triazenyl)imidazole-4-carboxamide (Dacarbazine)
DTT	Dithiothreitol
EDTA	Ethylenediaminetetraacetic acid
EtOH	Ethanol
FITC	Fluorescein-isothiocyanate
GBM	Glioblastoma
GFP	Green fluorescent protein
Gy	Gray
h	hours
HAT	<i>Histone acetyl transferase</i>
HDAC	Histone deacetylase
HEPES	4-(2-hydroxyethyl)-1-piperazineethanesulfonic acid
HGA	High-grade astrocytoma
HJ	Holiday junction

## Abbreviations

HR	Homologous recombination
HSP90	<i>heat shock protein 90</i>
ICL	Interstrand crosslink
IDH	<i>Isocitrate dehydrogenase</i>
IR	Ionizing radiation
kcps	kilo counts per second
kDa	kilo dalton
KDM	<i>Lysine-specific histone demethylase</i>
KO	Knock-out
Ku70	<i>X-ray repair cross-complementing 6 (XRCC6)</i>
Ku80	<i>X-ray repair cross-complementing 5 (XRCC5)</i>
LIG1	<i>DNA-Ligase I</i>
LIG3	<i>DNA-Ligase III</i>
M	Molar
m	<i>milli</i>
MeOH	Methanol
MGMT	<i>O<sup>6</sup>-methylguanine-DNA methyltransferase</i>
min	Minute
MITC	Monomethyl-triazenoimidazol-carboxamid
MLH1	<i>MutL homolog 1</i>
MMR	Mismatch repair
MMS	Methyl methanesulfonate
MNNG	N-methyl-N'-nitro-N-nitrosoguanidine
MNU	N-methyl-N-nitrosourea
MPG	see AAG
MRE11	meiotic recombination 11 homolog 1
MSH2	<i>MutS homolog 2</i>
MSH6	<i>MutS homolog 6</i>
mt	Mutant
n	nano
NaCl	Sodium chloride
NaOH	Sodium hydroxide,
NER	Nucleotide excision repair
NHEJ	Non-homologous end joining
NP40	Nonidet P-40 (Octoxinol 9)
<i>O<sup>6</sup>BG</i>	<i>O<sup>6</sup>-benzylguanine</i>
<i>O<sup>6</sup>mG</i>	<i>O<sup>6</sup>-methylguanine</i>
ORF	Open reading frame
p	pico
PARP1	<i>Poly [ADP-ribose] polymerase 1</i>
PBS	Phosphate-buffered saline
PCR	Polymerase chain reaction



PI	Propidium Iodide
PMS2	postmeiotic segregation increased 2
PMSF	Phenylmethylsulfonylfluoride
POL	<i>DNA-Polymerase</i>
PTEN	<i>Phosphatase and Tensin homolog</i>
RAD51	<i>RAD51 homolog</i>
RAD51c	<i>RAD51 homolog C</i>
RNA	Ribonucleic acid
rpm	rounds per minute
RT	room temperature
SAM	S-Adenosylmethionin
SD	standard deviation
SDS	Sodium dodecyl sulphate
SDS-PAGE	Sodium dodecyl sulphate-Polyacrylamide gel electrophoresis
sec	seconds
SNP	Single nucleotide polymorphism
SSB	Single strand break
ssDNA	Single stranded DNA
Sub-G1	sub-diploid DNA content
TBS	Tris-buffered saline
TCA	Trichloroacetic acid
TEMED	Tetramethylethylenediamin
TET	Ten-eleven translocation enzymes
TLS	Translesion synthesis
TMZ	Temozolomide
TRIS	Tris(hydroxymethyl)aminomethane
TSS	Transcription start site
U	unit
wt	Wild-type
XRCC	<i>X-ray repair cross-complimenting protein</i>



## 8. Summary

**Background** Both genetic and epigenetic changes contribute to the development of human cancer. Malignant brain tumors (WHO grade III - IV) account for about 60 % of all gliomas. Median survival is 12-20 months from the time of diagnosis. Patients undergo surgical resection and concomitant treatment with radiotherapy plus temozolomide (TMZ). Two molecular markers have been found to increase the progression free survival (PFS) and the overall survival (OS) of patients. The first marker is the promoter hypermethylation of *O*<sup>6</sup>-methylguanine-DNA methyltransferase (*MGMT*), a well-established predictive marker. The current state of the art for determining the *MGMT* promoter methylation status is methylation specific PCR (MSP), which has limits in specificity and sensitivity. We developed a high-resolution melt (HRM) analysis assay and compared it with MSP and pyrosequencing regarding its predictive value. The second molecular marker is a somatic mutation in the *isocitrate dehydrogenase 1 (IDH1)* gene, an important prognostic marker. It is a gain of function mutation that produces the oncometabolite 2-hydroxyglutarate (2-HG) by NADPH-dependent reduction of alpha-ketoglutarate ( $\alpha$ -KG). 2-HG is a competitive inhibitor of  $\alpha$ -KG dependent enzymes (ten-eleven translocation methylcytosine dioxygenases (TETs), histone lysine demethylases (KDMs), AlkB homologs (ALKBHs), e.g.). This is reflected in a general DNA and histone hypermethylation in mutated IDH1 tumor cells. The impairment of the DNA repair enzymes belonging to the ALKBH family has not been studied so far and could open the door to new tailor-made therapies, by exploiting this altered DNA repair pathway. To determine whether the IDH1 mutation can be exploited for targeted therapy, a cell line based approach was chosen. Artesunate causes lipid peroxidation and generates intracellular ROS that gives rise to the formation of 1, *N*<sup>6</sup>-ethenoadenine which is a substrate for ALKBH2. We tested whether the impairment of ALKBH2 in IDH1 mutated cells leads to an increased sensitivity to artesunate. Further, ALKBH2 knock-out cells were generated to test if the cytotoxicity of artesunate is depended on the ALKBH2 functionality.

**Results** The *MGMT* promoter of 14 glioblastoma cell lines with known *MGMT* activity and 83 formalin-fixed samples from high-grade glioma patients treated with radiation and temozolomide was analyzed by HRM, MSP, and pyrosequencing. The data were compared as to PFS and OS of patients exhibiting the methylated and unmethylated *MGMT* status. A promoter methylation cut-off level relevant for PFS and OS was determined. In a multivariate Cox regression model, methylation of *MGMT* promoter of high-grade gliomas analyzed by HRM, but not MSP, was found to be an independent predictive marker for OS. Univariate Kaplan–Meier analyses revealed for PFS and OS a significant and better discrimination between methylated and unmethylated tumors when HRM was used instead of MSP.

To determine whether the *IDH1* mutation can be exploited for targeted therapy, a doxycycline inducible TET-on system in LN319 glioma cells was chosen. Upon doxycycline treatment, either IDH1 mt or IDH1 wt were overexpressed. Cells expressing the mutated IDH1 enzyme were more sensitive to artesunate compared to cells expressing the wild-type IDH1 enzyme, which was reflected in higher apoptosis levels. To test if the oncometabolite 2-HG is the key metabolite responsible for the observed phenotype in IDH1 mutated cells, LN18 and T98G glioma cell lines were exposed to exogenous 2-HG together with increas-

## Summary

ing doses of artesunate. 2-HG was able to sensitize both cell lines dose dependently towards artesunate treatment. To confirm that ALKBH2 is involved in the counteraction and repair of ART induced cytotoxicity and DNA damage, CRISPR/Cas9 ALKBH2 knock-out clones of LN18 and T98G glioma cell lines were generated, and their sensitivity to ART was compared to their parental counterparts. ALKBH2 knock-out cells showed increased levels of apoptosis compared to the wild-type counterparts. The increased sensitivity of IDH1 mt cells to artesunate could be rescued by exogenous  $\alpha$ -KG.

*IDH1* mutated cells and cells with defective ALKBH2 were both characterized by an increased DNA damage response and increased S/G2 cell cycle fraction compared to the appropriate controls when treated with artesunate.

**Conclusion** This is, to our best knowledge, the first study that compares in a well-defined tumor collection HRM, MSP, and PSQ, defining a distinct HRM promoter methylation cut-off level relevant for prediction of tumor progression and patient survival. Compared to MSP and pyrosequencing, the HRM method is simple, cost effective, highly accurate and fast. HRM is at least equivalent to pyrosequencing in quantifying the methylation level. It is superior in predicting PFS and OS of high-grade glioma patients compared to MSP and, therefore, can be recommended being used routinely for determination of the MGMT status of gliomas.

Further, this work has shown that ALKBH2 plays a major role in the DNA repair of DNA damage induced by artesunate. Strong evidence has been found to claim that the IDH1 mutation leads to an impairment the functionality of ALKBH2 by the production of 2-HG. This metabolic attenuation of ALKBH2 in cancer cells can be exploited to increase apoptosis by drugs, which induce DNA lesions being substrates of ALKBH2.

## 9. Curriculum Vitae

### Education

- 01/2013 – 08/2017 **PhD - University Medical Center of the Johannes Gutenberg University Mainz**, Institute of Toxicology, Supervisor: Prof. Bernd Kaina  
*Epigenetic and metabolic regulation of DNA repair proteins in malignant glioma.*  
Enrolled in the international PhD program from the Institute of Molecular Biology (IMB) in Mainz.
- 03/2010 – 06/2012 **Master thesis - University of Vienna, Austria**, Department of Nutritional Sciences, Supervisor: Dr. Alexander Haslberger  
*Changes of DNA mismatch repair MLH1 promoter methylation in DMT2 patients after a dietary intervention.*
- 03/2010 – 06/2012 **Master studies** – Public Health Nutrition - University of Vienna, Austria
- 06/2009 – 02/2010 **Bachelor thesis - University of Vienna, Austria**, Department of Nutritional Sciences, Supervisor: Dr. Alexander Haslberger  
*Epigenetics in plants - considerations for the Risk Assessment of Gene modified Plants.*
- 10/2004 – 02/2010 **Bachelor studies** – Nutritional Sciences – University of Vienna, Austria
- 10/2003 – 02/2005 **Study of medicine** – Medical University of Vienna, Austria  
Discontinued after 18 months and focused on Nutritional Sciences studies.
- 09/1992 – 07/2002 **High School** – BG Blumenstraße, Bregenz, Austria  
Student representative in the statutory elected panel of teachers, parents and pupils (SGA).

## Curriculum Vitae

### Teaching activities

- 01/2013 – 08/2017     **Teaching assistant** - University Medical Center of the Johannes Gutenberg University Mainz, Institute of Toxicology
- 10/2010 – 06/2012     **Teaching assistant** - University of Vienna, Dept. of Nutritional Sciences

### Awards & Grants

- **Academic excellence scholarship** – University of Vienna, 2012
- **Co-author for a FWF grant proposal** - Epigenetics of DNA repair after ROS damage in obesity (284.109 €; project leader: Dr. A. Haslberger), 2012
- **3-year PhD fellowship 01/2013 – 12/2015** - Institute of Molecular Biology Mainz - Boehringer Ingelheim Foundation

### Employments

- 05/2017 – 08/2017     **University Medical Center of the Johannes Gutenberg University Mainz, Germany**  
Research assistant, Institute of Toxicology
- 01/2016 – 12/2016     **University Medical Center of the Johannes Gutenberg University Mainz, Germany**  
Research assistant, Institute of Toxicology
- 10/2010 – 06/2012     **University of Vienna, Austria**  
Research assistant, Dept. of Nutritional Sciences
- 07/2006 – 08/2007     **Table Service Team GmbH, Vienna, Austria**  
Part-time employee as a catering waiter. Job sites were fairs, congresses, and the Austrian presidential office
- 04/2005 – 02/2006     **DialogDirect PR GmbH, Vienna, Austria**  
Part-time employee as a face-to-face fund-raiser for NGOs (Amnesty international, WWF, e.g.). Promoted as team leader after 4 months. Worked with teams from 3 to 5 persons. Key duties were motivation of the team and support for the individual sales talks.
- 08/2003 – 09/2003     **doX Applied Technology, Vienna, Austria**  
Secretary for the manager. Planning business trips, reorganizing the archives.
- 11/2002 – 07/2003     **Military service, Bregenz, Austria**  
Received paramedic training and had 8 weeks of practical training as a paramedic at the Austrian Red Cross.
- 1997 – 2001             **Holiday laborer, Austria**  
Summer jobs as laborer, postal worker, promoter for cellphone plans, and secretary

**Internships**

- 03/2010 – 07/2010 **University of Vienna, Dept. of Nutritional Sciences**, Vienna, Austria  
Introduction to lab methods and co-working on different peer reviewed publications and poster. *Supervisor*: Dr. Alexander Haslberger
- 02/2010 – 03/2010 **University of Vienna, Dept. of Nutritional Sciences**, Vienna, Austria  
Literature research, drawing up and evaluation of food questionnaires, cooperation with a health promotion program. *Supervisor*: Dr. Petra Rust

**Research skills**

PCR, RT-PCR, MSP, COBRA, pyrosequencing, cell culture, FACS (Annexin V/PI, subG1, cell cycle analysis, GFP-sorting) MTT, MTS, colony formation assay, western blot, dot blot, BrdU assay, confocal microscopy, transfection, bacterial transformation, CRISPR/CAS, tetracycline-controlled transcriptional activation, cloning, HRM; SPSS, Origin, R, Graphpad, Sigmaplot, Ugene, Geneious, ImageJ, Photoshop, MS Office, Linux

**Language Skills**

German (native), French (native), English (fluent)

**Leisure activities**

Cooking, hiking, and mountain bike tours with friends.

**Memberships**

Deutsche Gesellschaft für DNA-Reparaturforschung (German DNA Repair Association)

**Review Duties for**

**Scientific Journals** Journal of Veterinary Science